The impact on mechanical properties and corrosion resistance of silica nanoparticles on a sol-gel based coating

Laura Vivar Mora

Submitted in accordance with the requirements for the degree of

Doctor of Philosophy

The University of Leeds

School of Mechanical Engineering

January, 2018

The candidate confirms that the work submitted is her own, except where work which has formed part of jointly-authored publications has been included. The contribution of the candidate and the other authors to this work has been explicitly indicated below. The candidate confirms that appropriate credit has been given within the thesis where reference has been made to the work of others.

Sections 6.1.5, 6.1.6, 7.2 and 7.3 contains work published in:

L. Vivar Mora, S. Naik, S. Paul, R. Dawson, A. Neville, R. Barker, Influence of silica nanoparticles on corrosion resistance of sol-gel based coatings on mild steel, Surf. Coatings Technol. 2017, 324, 368-375

All the work in the paper mentioned above is a contribution of the candidate, under the supervision of the co-authors.

This copy has been supplied on the understanding that it is copyright material and that no quotation from the thesis may be published without proper acknowledgement.

© 2017 The University of Leeds and Laura Vivar Mora

Acknowledgements

First, I would like to express my gratitude to the Lloyd's Register Foundation for sponsoring this PhD and giving me the opportunity to carry out this research. I am deeply grateful to Dr Alan Taylor, Dr Shiladitya Paul, Dr Sanjeev Naik, Prof Anne Neville and Dr Richard Barker for their guidance, encouragement and motivation. It has been a real pleasure to work under their supervision. I am also very grateful to Richard Dawson for his mentoring and professional advice during all the stages of this research.

Massive thank you to all my friends and colleagues at TWI: Gillian Dixon-Payne, Dr Anna Wojdyla-Cieslak, Marta Alvarez, Maria Linzoain, Nadia Sid, Angelo La-Rosa, Aurelie Rexach, Marion Bourebrab, Chris Graham and Dr Geraldine Durand. I would like to thank also Steve Mycock, Alexander Russell, Jacob Greenwood and Mike Bennet for their help.

I would like to thank Dr Chun Wang for her help and guidance with AFM and nanoindentation testing, John Harrington and Dr Zabeada Aslam for their help with FIB-TEM analysis, and Dr Wassim Taleb and Josh Owen for their help with erosion testing and profilometry analysis.

Last but not least, I would like to thank my family, my parents, my sister, my fiancé and friends for their infinite support, patience and encouragement.

Abstract

Corrosion has a huge impact on metallic structures which not just affect the economy but also assets, environment and society. Finding measures to reduce and prevent corrosion damage is crucial. Organic coatings (epoxies), and inorganic coatings (polysiloxanes), have long been used to mitigate corrosion. Combining the best features of both organic and inorganic coatings to create high performance protective coatings is still a challenge.

Many studies have reported increased corrosion protection and durability through the use of these hybrid coatings which could be further enhanced with the incorporation of nanoparticles. Many nanoadditives are now commercially available and many more in the development stage, but integration into coatings is a key challenge since modifies its physical and mechanical properties.

The purpose within this investigation was to identify preliminary design rules by studying the effect and impact of these key materials in order to start establishing a materials by design approach which can be further developed and will help the integration of novel materials into industrial applications.

A sol-gel based coating was created to modify it with unfunctionalised and functionalised silica nanoparticles and study both their interaction with the coating matrix and their influence on coating morphology and mechanical durability. It was found that non-functionalised silica led to improved barrier properties, however, when the same silica was surface treated the corrosion resistance was further enhanced. Following that line of investigation, three

functionalisation levels as well as three loading levels of functionalised silica were examined. This study showed that the highest loading (20 wt.%) of the lowest functionalised silica (T0.1) led to coatings with improved properties and durability. This functionalised silica was homogeneously distributed within the polysiloxane-based matrix with no signs of agglomeration, highlighting the importance of the relation between nanoparticles, matrix and nanoparticle distribution as a key factor to improve coating performance.

Table of Contents

List of Tables

List of Figures

Chapter 1. Introduction

1.1 Project background

This project was carried out under a PhD programme with the Institute of Functional Surfaces at Leeds University in partnership with TWI Ltd and NSIRC and was sponsored by the Lloyd's Register Foundation.

The National Structure Integrity Research Centre (NSIRC) is a state-of-the-art postgraduate engineering facility established and managed by TWI, working closely with leading academic partners. Its mission is to train the next generation of engineers and scientists to support the UK's R&D and accelerate uptake of research. The PhD programmes under NSIRC are a new model of postgraduate research driven by the needs of industry.

Lloyd's Register Foundation (LRF) is a charitable foundation, helping to protect life and property by supporting engineering-related education, public engagement and the application of research. The Foundation is a Founder Sponsor and Board member of the Structural Integrity Research Foundation (SIRF), responsible for industrial support of NSIRC. The collaboration between the Lloyd's Register Foundation and TWI, through SIRF, aims to inspire and engage the next generation of engineers by providing fundamental science and industry-driven research with a postgraduate education programme.

Over last fifteen years, TWI has developed expertise in functional and high performance coatings through European and UK Government funded

projects and the sponsorship of PhDs. The focus has been on the development and fabrication of advanced and novel materials, which is in line with the research carried out in this thesis.

1.2 Research need

Corrosion is an issue of prime importance which has impact not just economically but also environmentally on almost all the world's metallic infrastructure. The corrosion of steel, which is one of the most widely used building materials, can compromise the materials integrity and lead to catastrophic failure.

The corrosion rate of unprotected steel in most steel structures placed inland are estimated at 25-50 µm per year, while in offshore areas the corrosion rate is in the range of 80-200 µm per year [1]. There are conventional protection methods to overcome corrosion and the problems associated with it, with the use of coatings being the most common way to protect steel. Coatings can be suited to different steel products depending on the end-use application. The high corrosion rates for offshore structures are caused by long-term exposure to high humidity and high concentrations of chlorides that accelerate corrosion, and another factor is the influence of UV light, which can have a degrading effect on the protective coatings.

The use of nanoadditives in coatings is a promising route which can aid corrosion protection as well as lead to more durable coatings. However, many challenges remain in the processing of nanostructured bulk/coating materials. Although some nanoadditives have been shown to have potential and promising developments are expected in the near future, there is much

room for further development of this line of research and more work is needed in order to be able to provide improved solutions to withstand longer periods of time. Understanding of structure property relationships, design rules, synthesis and formulation guidelines are needed to accomplish this.

The aim of this PhD project was to design, synthesise and test new nanoenabled coatings in order to obtain a wider understanding of the influence and interactions of nanoadditives as well as their influence on coating characteristics. This line of research can make a significant contribution to knowledge in different ways, for protection of steel structures and reducing the impact on the environment. The acquired know-how will generate advances in engineering contributing to advances in nanoenabled coatings.

1.3 Objectives of the research

Research of environmentally friendly protective coatings is a growing market that is getting more and more attention as industry is trying to comply with REACH (Registration, Evaluation, Authorisation and Restriction of Chemicals). The focus of this work is to investigate the possible advantages of the addition of nanoadditives to enhance the anticorrosion performance and mechanical durability of a coating system.

The main objectives of this study are:

- Identify the different nanoadditives and resins used currently in commercially available corrosion protection sector and in

development and look for an environmental and friendly alternative to be developed

- Formulate new coating systems to exploit the role of nanoadditives
- Assess the role of these nanoadditives when added to coating formulations according to the current literature and study its impacts on coating microstructure, corrosion performance and mechanical durability
- Provide insight on the functionalisation of nanoadditives to understand the benefits and impact on the final performance of coatings
- Develop a materials by design approach which can be further used for other studies

1.4 Thesis layout

The work presented in this thesis is organised in 10 chapters:

Chapter 2 presents the basic theory and principles of corrosion, coatings and nanomaterials. This chapter aims to provide a basic understanding on these subjects before going for a more detailed description of the state-of-the-art technology.

Chapter 3 presents a the literature review on the subjects described in chapter 2, and a more detailed description of the nanoparticles and coatings which will be studied within this project, together with its impact not just on coating microstructure but also on corrosion performance and mechanical durability.

Chapter 4 presents the experimental techniques used to characterise coating microstructure, the set-up used for the tests and the procedures used for the corrosion and mechanical examination of the specimens.

Chapter 5 presents the formulation of the coatings developed for this study, with the materials and methods used to prepare them and the synthesis procedure.

Chapter 6 presents the results obtained for the characterisation of the coating microstructure, looking at understanding the impact of nanoparticles on coating structure and properties.

Chapter 7 presents the experimental results obtained after corrosion testing to understand the impact on the corrosion performance of nanoparticles incorporated in the matrix.

Chapter 8 presents the experimental results obtained after mechanical characterisation of the coatings in order to provide understanding of the consequences on coating durability and mechanical performance of the addition of nanoparticles.

Chapter 9 presents a detailed discussion of the experimental results, describing and establishing the contributions of this study.

Chapter 10 presents the conclusions drawn from this research and also explains the contribution of this research to the existing knowledge and includes suggestions for further work.

Chapter 2. Background

2.1 Overview

Corrosion has a significant impact both economically and environmentally on almost all the world's metallic infrastructure. Steel is one of the most widely used building materials in infrastructure, mainly because of its versatility, durability and affordability. The corrosion of steel as a result of chemical or electrochemical reactions with its service environment is a spontaneous process, which can compromise the material's integrity and impact assets, environment, and people if no measures are taken to prevent or control it.

A study on corrosion costs conducted by NACE in 2016 indicated that the annual estimated cost of corrosion in the U.S. alone was $2.5 trillion per year [2]. These costs are expected to rise year on year. There is no doubt that the impact of corrosion and environmental degradation on the economies of the developed nations is considerable.

Thus, corrosion protection is an issue of prime importance and a number of strategies have been developed in an effort to prevent corrosion. The most common way in which steel is treated to prevent corrosion and the problems associated with its effects is via the use of specialised coatings. Different types of coatings are best suited to different steel products depending on the end-use application.

One of the most promising routes to develop high performance anticorrosion systems is the use of nanotechnology in coatings. The use of nanoadditives

can aid corrosion protection as well as lead to more durable coatings. This chapter looks at providing a general background on corrosion, coatings and nanomaterials which can then leads to a materials by design methodology to design coatings for corrosion protection of carbon steel with improved properties via the use of nanoadditives.

2.2 Corrosion

2.2.1 Definition of corrosion

By definition, corrosion is the “physicochemical interaction between a metal and its environment that results in changes in the properties of the metal, and which may lead to significant impairment of the function of the metal, the environment, or the technical system, of which these form a part” (ISO 8044-1999).

2.2.2 Thermodynamics and kinetics

Thermodynamic and electrochemical principles play a major role in determining the corrosion behaviour of materials. Thermodynamics indicates the spontaneous direction of a chemical reaction. It is used to determine whether or not corrosion is theoretically possible.

For a reaction to be occurred spontaneously there must be a negative change in the Gibbs free energy, ΔG. Thus, corrosion takes place spontaneously when there is a decrease of free energy, $\Delta G < 0$. When ΔG is positive, the metal is stable and will not react spontaneously and when ΔG is zero the system is at equilibrium.

The differences in free energy are measurable as electrical potentials and current flow. The electrical potential and the free energy change are related by the following equation [3]:

$$\Delta G = -n F E \qquad (2.1)$$

where ΔG is the free energy change, n is the number of electrons transferred in the half-cell reaction, F is the Faraday constant, which is equal to the charge transported by 1 mole of electrons and has the value of 9.6×10^4 coulombs/mole, and E is the measured potential in volts.

In the same way:

$$\Delta G^0 = -n F E^0 \qquad (2.2)$$

where ΔG° is the standard free energy change, n and F are defined as above and E° is the standard electrode potential which can be defined as the electrode potential of a reversible electrode at 298 K, an effective concentration of 1mol/l and a gas pressure of $1 \cdot 10^5$ Pa against standard hydrogen electrode (SHE) with E^0=0 V and can be obtained from thermodynamic tables [3].

For the dissolution reaction of a metal [Red] -> [Ox] + ne^-, free energy can be calculated as:

$$\Delta G = \Delta G° + RT ln \frac{[Ox]}{[Red]} \qquad (2.3)$$

which in combination with equation (2.2) gives:

$$E = E° - \frac{RT}{nF} ln \frac{[Ox]}{[Red]} \qquad (2.4)$$

Equation (2.4) is called the Nernst equation and can be used to calculate the energy of an electrochemical reaction and the feasibility of the reaction can be predicted on the basis of electrochemical potentials. Also it can be seen from this equation that the concentration of the oxidized species, [Ox], increases as electrode potential E becomes more positive.

Almost all metals and alloys in service are actually in an unstable thermodynamic state. There is a fundamental thermodynamic tendency for them to return to a stable state through corrosion processes. Thermodynamics can predict whether a corrosion reaction will take place, but it does not provide an indication of the rate of corrosion reactions. The rate of corrosion reactions is described by kinetics. The analysis of thermodynamic data alone is not a sufficient criterion to decide about a possible corrosive threat. Even if a reaction can proceed spontaneously it may be hindered by a kinetic barrier and the reaction rate will be slowed down or even inhibited and no measurable change will occur.

Taking into account that thermodynamic data provides information about the possibility of a spontaneous reaction, it is also important to take into consideration the kinetic effects since the practical susceptibility to corrosion can only be estimated by the kinetics.

Therefore, once it is established that corrosion can occur, the next step will be to determine the corrosion rate, which is achieved by measuring and calculating the corrosion kinetics. The corrosion rate (mm yr^{-1}) can be measured by electrochemical methods and correlated to corrosion current density, i_{corr}, as [4]:

$$corrosion\ rate = \frac{dW}{dt} = \frac{Mi_{corr}}{nF} \qquad (2.5)$$

where dW/dt is the weight loss of a metal with time, M is the atomic mass of metal (g/mol), i_{corr} is the corrosion current density (μA/cm^2), n is the number of electrons in the reaction equation and F is the Faraday's constant (9.6·10^4 coulombs/mole).

The corrosion current density is not directly measurable because a corroding metal does not show any net current flow. Therefore, to determine this parameter, the Butler-Volmer equation or its approximation, the Tafel equation, can be used.

The Butler-Volmer equation describes how the electrical current in an electrochemical reaction depends on the electrode potential, considering that both anodic and cathodic reactions occur on the same electrode, and is represented as follows:

$$i_{net} = i_0 exp^{\frac{(1-\propto)n\eta F}{RT}} - i_0 exp^{-\frac{\alpha n\eta F}{RT}} \qquad (2.6)$$

where i_{net} is the net current density (A m^{-2}), i_0 is the equilibrium exchange current density (A m^{-2}), α is the transfer coefficient and η is the activation overpotential (V).

As can be seen, the Butler-Volmer equation relates the net current density to the change in potential experienced by the electrode. The equilibrium exchange current density i_0 is the current density in each direction when the electrode reactions are at equilibrium. The potential change is the potential by which the electrode is polarised away from the equilibrium potential and its value depends on the reaction rate of electron transfer. The slower this

step the greater is η. The transfer coefficient α is related to an energy barrier which the reacting species must overcome for the electron transfer to occur.

The Butler-Volmer equation has also simplified forms, depending of the η value:

- For small overpotentials, equation (2.6) reduces to:

$$i_{net} = \frac{i_0 F \eta}{RT} \qquad (2.7)$$

and depending on whether the electrode acts as an anode or as a cathode, the last equation can be rewritten as:

$$\eta_a = i_a \frac{RT}{i_0 F} \qquad (2.8)$$

or

$$\eta_c = -i_c \frac{RT}{i_0 F} \qquad (2.9)$$

These relationships are linear with the slope dependent on i_0.

- For large overpotentials, the second term on equation (2.6) is negligible and taking logarithms and rearranging:

$$\eta_a = \left[\frac{2.3RT}{(1-\alpha)nF}\log i\right] - \left[\frac{2.3RT}{(1-\alpha)nF}\log i_0\right] \qquad (2.10)$$

A similar equation can be written if η is large and negative, which in this case the first term on equation (2.6) is the one negligible:

$$\eta_c = -\left[\frac{2.3RT}{\alpha nF}\log i\right] + \left[\frac{2.3RT}{\alpha nF}\log i_0\right] \qquad (2.11)$$

Equations (2.10) and (2.11) are straight line relationships with the form:

$$|\eta| = a + b \log i \quad (2.12)$$

and are called the Tafel equations. According to these equations, the value of either the anodic or the cathodic current at the intersection is i_{corr}, which suggests that i_{corr} can be determined by extrapolating the linear portions of the Tafel plot back to their intersection, where the overpotential ($\eta = E - E_{corr}$) is zero. This can be seen in Figure 2.1.

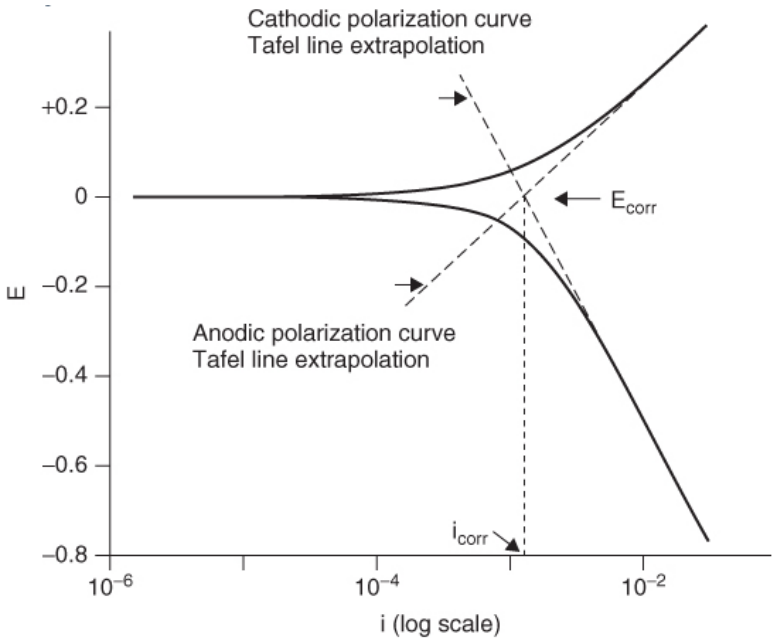

Figure 2.1. Typical Tafel plot [5].

In summary, Tafel plots can be used to estimate Tafel slopes and the corrosion current density which is then converted to a corrosion rate as a thickness loss per unit time. This test is destructive, causing some degree of surface roughening.

Polarisation methods such as potentiodynamic polarisation are often used for laboratory corrosion testing. The technique has the potential to provide useful information regarding the corrosion mechanisms, corrosion rate and susceptibility of specific materials to corrosion in designated environments.

2.2.3 Types of corrosion

There are various mechanisms which can result in different forms of corrosion, depending on the nature of corrosion (galvanic corrosion and crevice corrosion) and on the effect of the corrosion on surface morphology (general corrosion and pitting corrosion) or to its effect on bulk properties (intergranular corrosion and stress corrosion cracking) [6, 7].

Uniform corrosion

Uniform corrosion, also known as general corrosion, is the simplest form of corrosion which occurs over the entire surface area or large areas of the metal or alloy surface.

There is no localised attack and corrosion does not penetrate very deep inside. This form of corrosion if represents the greatest destruction of the metal, it is not of great concern since it can be approximately estimated with simple tests.

Intergranular corrosion

Intergranular corrosion is a form of attack occurring in the vicinity of the grain boundaries of a metal or alloy. Grains are “crystals” usually on a microscopic scale which constitute the microstructure of the metal and alloys.

Corrosion occurs at the grain boundaries due to a potential difference between the anodic grain boundaries and the cathodic grains, resulting in the flow of electrons from the anodic to the cathodic area, causing rapid attack of the metal.

Galvanic corrosion

This form of corrosion results from one metal being in electrical contact with another where both are in an electrically conducting environment. A potential difference exists between the two since different elements with different compositions have different chemical and electrochemical properties in the same environment. This potential difference produces the flow of electrons between the metals. One metal (the cathode) is protected, whilst the other metal (the anode) develops pits and grooves in the surface.

Microbial corrosion

It refers to the degradation of metals (as well as non-metals) caused by the presence and activity of living microorganisms. This type of corrosion, which is also called Microbiologically Influenced Corrosion (MIC), does not produce a unique form of localised corrosion but it can result in pitting and crevice corrosion.

Stress corrosion cracking

Stress Corrosion Cracking (SCC) is the cracking induced from the combined influence of tensile stress and a corrosive medium. It is one of the most dangerous forms of corrosion, since the detection of fine cracks can be very difficult and the damage not easy to predict.

It is usually associated with other types of corrosion that create a stress concentrator that leads to cracking failure. For SCC to take place three factors are needed: a susceptible metallic material, a crack-promoting environment and the presence of tensile stress.

Crevice corrosion

Crevice corrosion is a form of localised attack that occurs in narrow spaces or gaps between metal-to-metal or non-metal-to-metal components. It is initiated by a difference in concentration of some chemical constituents, usually oxygen, which establishes an electrochemical cell. The material within the crevice is low in oxygen and acts as the anode, which creates a high corrosive environment inside the crevice. The area low in oxygen corrodes (anode) while the exterior material which has a high oxygen concentration is protected and acts as the cathode.

Pitting corrosion

Pitting corrosion is a localised corrosion attack which generally creates small holes or pits that penetrates the metal surface. It is considered more dangerous than uniform corrosion since it is more difficult to detect and thus also to design against. The mechanism of pitting corrosion is hypothesised to be similar to crevice corrosion. The area within the pit acts as the anode, where the oxidation of metal occurs, while the reduction takes place at the area around the pit, which acts as the cathode.

2.2.4 Corrosion mechanisms

Corrosion reactions are of electrochemical nature, involving the transfer of charged ions across the surface between a metal and the electrolyte solution in which it is immersed. There are two types of electrode reaction occurring simultaneously at the metal surface: anodic and cathodic. Reactions that involve oxidation of the metal and areas where oxidation occurs are called

anodes, and those reactions are anodic. When electrochemical reduction occurs these reactions are cathodic and the locations are called cathodes.

There are four conditions that must exist before electrochemical corrosion can occur [7, 8]:

- Presence of a metal (anode) that corrodes
- Presence of a conductive material (cathode) with less tendency to corrode
- Presence of a continuous conductive liquid (electrolyte, usually condensate and salt or other contaminations)
- Electrical contact to carry the flow of electrons between the anode and cathode (usually in the form of metal-to-metal contact)

The elimination of any one of these four conditions will stop corrosion [7].

The corrosion process produces a new and less desirable material from the original metal and can result in a loss of function of the component or system. It is difficult to prevent reactions from occurring, and there are lots of electrochemically active species that cause corrosion. Water is one of them, it is electrochemically active and can cause corrosion of many important metals. Other electrochemically active species are oxygen (O_2), carbon dioxide (CO_2) dissolved in water, inorganic acids such as hydrochloric acid (HCl), hydrogen sulphide (H_2S), and strong organic acids.

In the case of steel, iron oxide is formed on the surface by the reaction of iron to ferrous hydroxide and ferric oxide. The corrosion mechanism of iron, which is the major component of steel, is described in Figure 2.2. Firstly, the

iron atom can lose electrons as represented in equation (2.13); this equation represents the anodic reaction.

$$Fe \rightarrow Fe^{+2} + 2e^{-} \qquad (2.13)$$

Then, the electrons released flow through the iron metal to the cathodic area where they react with oxygen:

$$O_2 + H_2O + 4e^{-} \rightarrow 4OH^{-} \qquad (2.14)$$

The hydroxyl ions, OH^-, from the cathode combined with the ferrous ions, Fe^{2+}, from the anode, form ferrous hydroxide, as shown in equation (2.15). In presence of oxygen and water, this reacts forming ferric oxide, (equation (2.16)), which finally turns into hydrated ferric oxide or rust (equation (2.18)):

$$Fe^{2+} + 2OH^{-} \rightarrow \mathrm{Fe(OH)_2} \qquad (2.15)$$

$$4Fe(OH)_2 + \mathrm{O_2} + 2\mathrm{H_2O} \rightarrow 4\mathrm{Fe(OH)_3} \qquad (2.16)$$

$$4Fe(OH)_3 \rightarrow \mathrm{Fe_2O_3.H_2O(red\ colour)} + 2\mathrm{H_2O} \qquad (2.17)$$

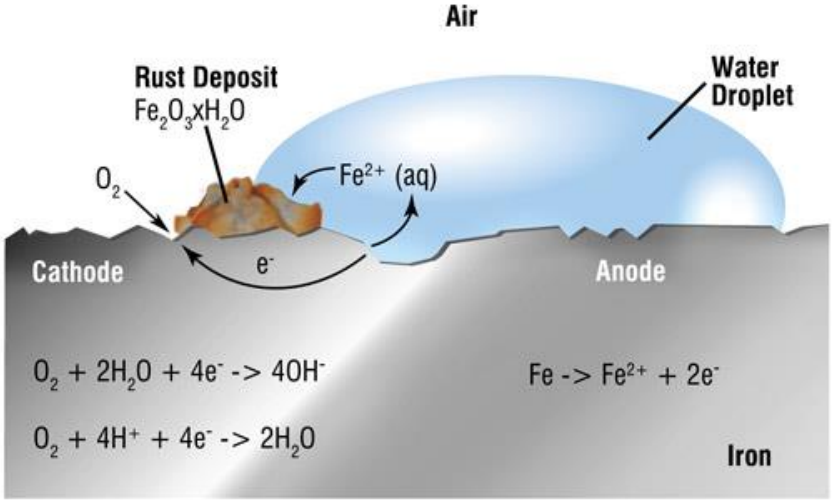

Figure 2.2. Corrosion mechanism of iron [9].

2.2.5 Methods of corrosion prevention

Over the last two decades, significant advancements have been made to improve the management of steel corrosion. Figure 2.3 gives an overview of the different corrosion protection mechanisms.

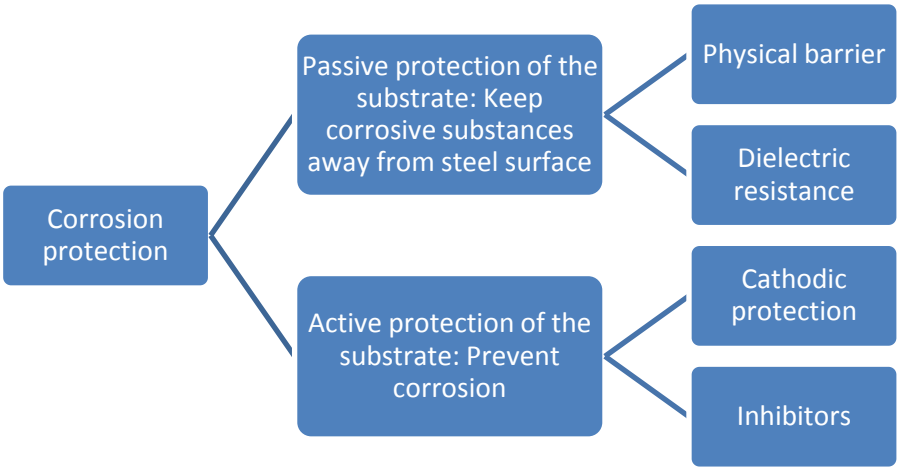

Figure 2.3. Corrosion protection mechanisms.

Barrier protection is possibly the oldest and most widely used method for reducing or preventing corrosion protection. The basic principle is to isolate the base metal from the environment, reducing the diffusion of water and air from the surface. As long as the barrier is intact, the steel is protected and corrosion will not occur, since one of the four conditions would not exist (electrolyte in this case). Two important properties barrier coatings must possess to provide good corrosion resistance are: strong adhesion to the base metal and good mechanical resilience for protection against physical damage of the coating.

Cathodic protection involves connecting an external anode to the metal to be protected and the passing of an electrical dc current so that all areas of the metal surface become cathodic and therefore do not corrode. In

electrochemical terms, the electrical potential between the metal and the electrolyte solution with which it is in contact is made more negative, by the supply of negative charged electrons, to a value at which the corroding (anodic) reactions are stifled and only cathodic reactions can take place [10].

A corrosion inhibitor is a chemical additive which when added to a corrosive aqueous environment inhibits, prevents or reduces the rate of corrosion [10]. This inhibitor can function in one of the following ways:

a) Anodic inhibitors: These block anodic sites, forming a protective layer of oxide film on the surface of metal causing resistance to corrosion. If an anodic inhibitor is not present at a concentration level sufficient to block off all the anodic sites, localised attack such as pitting corrosion can become a serious problem due to the oxidising nature of the inhibitor which raises the metal potential and encourages the anodic reaction.
b) Cathodic inhibitors: they function by reducing the available area for the cathodic reaction which is often achieved by precipitating an insoluble species onto the cathodic sites. Cathodic inhibitors are considered more effective than anodic inhibitors [10].

There is also a common practice of incorporating a cathodic inhibitor because of the danger of pitting when using anodic inhibitors alone; these are called mixed inhibitors. This type of inhibitors works by forming a film that causes the formation of precipitates on the surface, blocking both the anodic and cathodic sites.

Chromates, silicates, and organic amines are common inhibitors. The use of inhibitors is favoured in closed systems where the necessary concentration of inhibitor is more readily maintained.

2.3 Coatings

2.3.1 General introduction

Generally, coatings are used for three primary reasons: to provide aesthetic appearance to surfaces and products, to provide protection from damage by the external environment, and to provide specific attributes to the product. Many coatings are expected to address more than one of these reasons.

Since there are a huge variety of material surfaces with an extensive range of chemical and physical characteristics and applications, there is also a diverse range of coatings to protect them. Depending on the need and requirements of the application, coatings are formulated to provide specific attributes (e.g., antimicrobial, anti-fouling, anticorrosion, etc). In the context of corrosion protection, as discussed above, coatings can provide a physical barrier between the surfaces and the environment to stop the electrochemical processes that lead to corrosion and thus offer long-term protection of assets. However, corrosion protection is also possible via some other mechanisms as discussed next.

2.3.2 Classification of coatings

Anticorrosion coatings are generally classified in accordance with the mechanisms by which they protect the metal against corrosion: as barriers

between the substrate material and its environment, to inhibit the corrosion process, and to act as sacrificial materials.

- Barrier coatings: corrosion protection is obtained by impeding the transport of aggressive species into the substrate by application of a coating system. This coating forms an insulating and physical barrier stopping the contact of corrosive elements.
- Inhibitive coating: this relies on the passivation of the substrate, building up a protective layer which impedes the transport of aggressive species.
- Sacrificial coating: the coating acts as a sacrificial material which means that the substrate is protected by a metal or alloy that is electrochemically more active. One example is the use of zinc for cathodic protection of steel due to its lower electropotential when compared to iron. In this case, the electrode potential of zinc, calculated as the standard potential with referenced to a standard hydrogen electrode is -0.76 V compared to -0.44 V for iron.

2.3.3 Coating systems and processes

Coatings and films can be fabricated from a wide range of materials using many different processes. One of the main types are the wet film coatings. The advantage of these is that they can be applied onto the surfaces of products in different ways, like brush, roller or spray.

Designing a coating system needs to account for the type of material used and its surface condition. The surface preparation, the coating products used

and the total system thickness will depend mainly on the constructional material to be protected [11].

To protect a metal substrate, surfaces tend to be coated with a multi-layer system as shown in Figure 2.4. First, an anticorrosion primer is applied, which provides corrosion protection via a sacrificial layer and good adhesion to the metal substrate. A mid-coat (or tie-coat) is applied that contributes to the barrier protection effect and acts as a transition to the final topcoat which is usually applied if appearance and/or protection against UV-light are important. Among the typical matrices used as mid-coat are epoxies, polyesters or silicones, while polyurethanes are one of the most frequent choices as topcoat [12]. In relation with primers, the majority of them used are zinc-rich compounds to give galvanic protection although some novel primers that are zinc-free are also currently being introduced to the market.

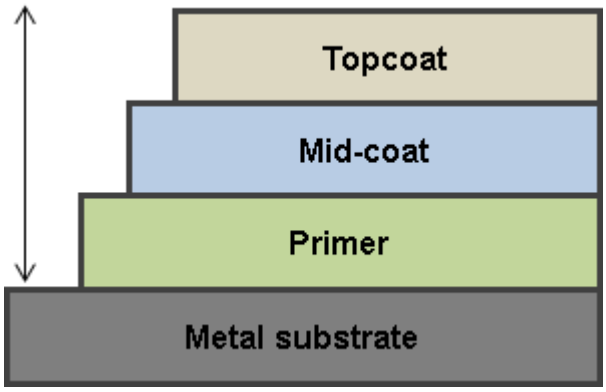

Figure 2.4. Protection of a metal substrate.

A typical coating formulation is constituted of binders, pigments and solvents and diluents. Additional constituents like additives or fillers/extenders can also be added to enhance specific properties. A binder forms the matrix of the coating, the phase in which all other components may be incorporated.

Thus, it is the main constituent material that holds all the ingredients together and plays a vital role in the formation of the protective film. The binder must ensure a number of properties, especially: adhesion to the metal, cohesion within the coating, high mechanical strength, and low permeability. Its main function is to provide protection to the substrate and the other components within the film. The degree of protection of a coating system is highly dependent on the thickness of the coating as well as the type and nature of the binder system.

A pigment is an insoluble substance which is dispersed in the binders and can be used for both decorative, i.e. aesthetic (colour and opacity), properties but in some cases can provide functional benefits (e.g. improving toughness, texture, conductivity, etc.). Pigments can be mica, silicas, TiO_2 and talcs, or organic molecules.

Solvents are added to dissolve or disperse the other constituents of the formulation. They also reduce the viscosity of the formulation in order to enable a homogeneous mixing of the pigments and additives in the binder and allow the material to be easily applied by industrially scalable methods like spraying. Whilst historically organic solvents have been used, there are regulatory drives to reduce the content of these in coatings and to move towards water borne formulations.

Fillers are added to manage the viscosity of the matrix, to increase the volume of the coating through the incorporation of low-cost materials (chalk, wood dust, carbonates, sulphates, silicates), and to improve coating properties such as impact and abrasion resistance and water permeability.

There are a wide variety of functional additives usually added in small amounts to modify the composition and properties of coatings and enhance the desired properties. Some examples include additives to modify surface tension, improve stability to UV, provide anti-graffiti capabilities or improve adhesion.

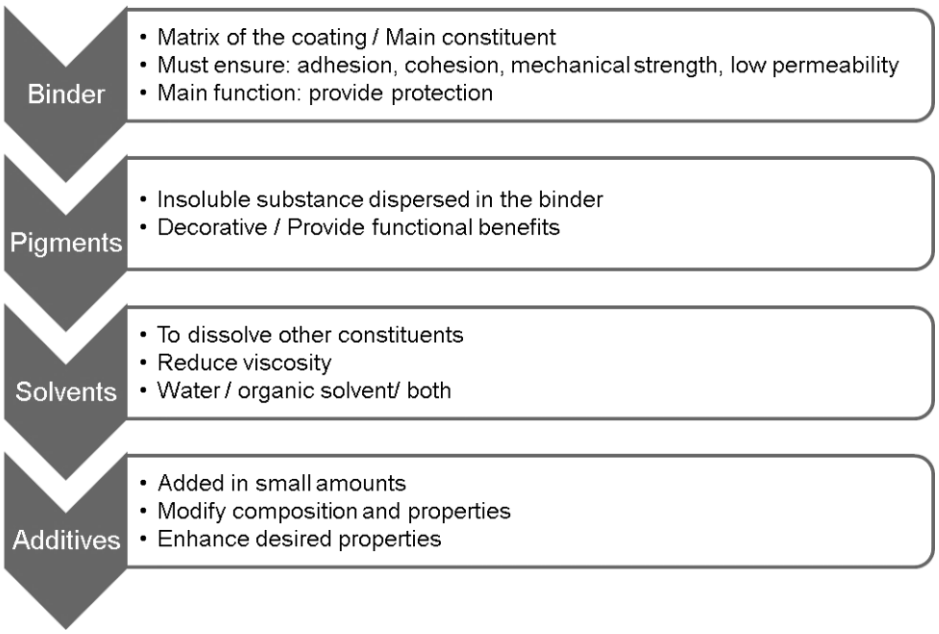

Figure 2.5. Coating constituents.

2.3.4 Binders for anticorrosive coatings

As explained in section 2.2.3., the binders or resins provide the basic structure to a coating. The chemical composition as well as the curing of the binder affects both the aesthetic appearance and the properties of the coating, including anticorrosive performance. There are different binders which can be used for different applications, such as polyesters, vinyl esters, epoxies, polyurethanes, silicones, among others. An overview of these ones is presented below, with special emphasis on silicone binders since it is the main focus of this study.

2.3.4.1 Polyester

Polyesters are made from organic acids, glycols and monomers, all having varying properties. There are two principle types of polyester resin: orthophthalic polyester and isophthalic polyester. Orthophthalic polyesters are based on othophthalic acid, these are the standard economic resins, while isophthalic polyesters have between 42-50 % styrene, provide greater mechanical and corrosion resistance properties but have higher cost [13]. Figure 2.6 shows the idealised chemical structure of a typical polyester:

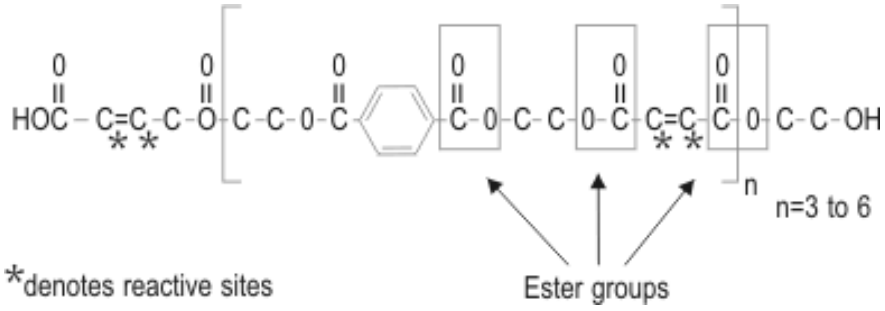

Figure 2.6. Polyester structure adapted from Cripps [14].

Some of the polyester properties are: easy of handling, low viscosity, dimensional stability, as well as good mechanical, chemical-resistance and electrical properties [15].

Polyester resins are the least expensive of the resin options, providing an economical way to incorporate resin, filler and reinforcement. Usually, fillers or extenders are easy to incorporate into the resin and help to reduce the brittleness of polyesters.

Most polyester resins consist of a solution of polymer or oligomer dissolved in a monomer such as styrene. The addition of styrene helps to make the resin easier to handle by reducing its viscosity. The styrene also performs

the vital function of enabling the resin to cure from a liquid to a solid by polymerising with the oligomer chains of the polyester, without the evolution of any by-products. Polyester resins have a limited storage life as they will set or “gel” on their own over a long period of time. Small amounts of inhibitor are usually added during the manufacture process to slow gelation [14].

2.3.4.2 Epoxy

Epoxy resins are widely used as binders for protective coatings in many applications thanks to its versatility in formulation. Epoxy resins are compounds that contain more than one epoxide group, which is the reactive group that enables polymerisation and film formation (Figure 2.7):

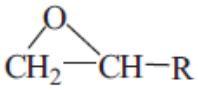

Figure 2.7. Epoxide group adapted from Cripps [16].

Epoxy resins have found extensive use in the coating industry thanks to their excellent adhesion to metals and high resistance to heat, water and chemicals. The corrosion protection provided with epoxy resins is a combination of factors: a crosslinked epoxy polymer matrix with aromatic groups forms a good barrier to corrosion and hydroxyl groups give strong adhesion to metal [17].

Epoxy resins, even though widely used, have a disadvantage since the solvent evaporation in epoxy solvent-borne coatings can produce micro-pores [18]. Liquids can then permeate the coating into the protected substrate via these micro-pores and give rise to crevice corrosion. The use

of nanofillers has been studied trying to toughen the epoxy resins and also improve barrier properties [18-20].

2.3.4.3 Vinyl ester

Vinyl esters are halfway between polyesters and epoxies, combining the best features of both resins. Their double bonded vinyl groups that link the ester groups together contribute a flexible nature to the resin. That flexible nature helps to impart impact resistance and also crack-resistance [21].

Vinyl esters provide excellent chemical resistance (to water, organic solvents and alkalis), but less resistance to acids than polyesters. Vinyl esters are stronger than polyesters and tougher than epoxies. Corrosion resistance of vinyl esters are superior to these of polyesters [22]. As with polyesters, vinyl esters are not practical without additives, reinforcements and fillers [23].

2.3.4.4 Polyurethane

Polyurethanes are a family of resins that have a repeatable group, an urethane bond. The chemistry is the reaction of two or more functional monomers to yield the urethane linkage, as shown in Figure 2.8. Resins based on different molecular weights determine the number of repeated units and the properties of the coating.

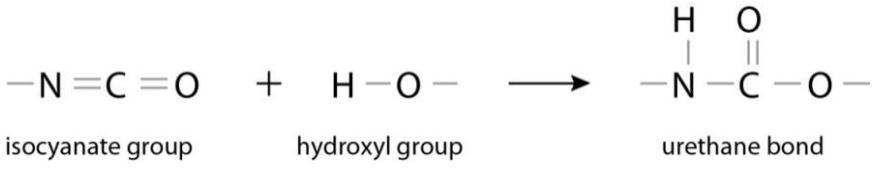

Figure 2.8. Urethane bond [24].

Other resin types are supplied to coating formulators, but for polyurethanes their components (polyols and isocyanates) are supplied. Coating

formulations are made using these components, and in most cases, urethane linkages are produced during the curing process. This gives the possibility for working with different compositions and curing processes [24].

Polyurethanes are very strong and have high shrinkage. The cost of polyurethane material is about 1.5-2 times that of polyester resins [25].

Some of the key benefits of polyurethanes are that they present good abrasion and chemical resistance, good mechanical properties (ruggedness and flexibility), good adhesion to a variety of substrates and reinforcements, UV stability, flexibility or fast cure time, among others [26].

2.3.4.5 Silicone

Silicon is the second most abundant element on earth, exceeded just by oxygen [27]. Silicon is not found in the metallic state in nature, occurring as an oxide and in silicates. Due to this natural abundance of silica as a source of raw materials in combination with its inherent high thermal stability and high mechanical strength, silica and silicon-based research has been carried out widely in the past few decades [28]. Silanes are one of the most commonly used silicon-based chemicals and are used widely for the development of high-performance silicones and advanced functional materials.

A silane that contains at least one Si-C bond structure is known as organosilane and siloxanes are formulations with a Si-O backbone. The structure of an organosilane molecule is represented as:

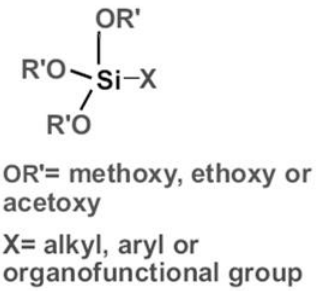

Figure 2.9. Basic organosilane structure adapted from Materne et al. [29]

where X is a non-hydrolysable organic moiety (e.g., amino, vinyl, alkyl…) which can be reactive toward another chemical (amino, epoxy, vinyl…) or non-reactive (e.g., alkyl). OR' is a hydrolysable group that can react with various forms of hydroxyl groups present in fillers or polymers and liberates alcohols or acid on hydrolysis. These groups can provide the linkage with inorganic or organic substrates and thus silane coupling agents have the ability to form a durable bond between organic and inorganic materials. Typically, R': methyl, ethyl, isopropyl… and R is a spacer group, which can be either an aryl or an alkyl chain typically propyl (R: $(CH_2)_n$ with n = 0, 1 or 3) [29].

Organosilanes substituted with only saturated hydrocarbon radicals are called “nonfunctional”, while organosilanes or silanes containing a reactive X group are called “organofunctional” [30]. Organofunctional silanes can carry two different reactive groups (i.e. OR’ and R-X) on their silicon atom, being able to react and couple with different materials.

Organofunctional groups confer their specific reactivities on silane molecules and can serve as bridges between inorganic or organic substrates and organic/polymeric matrices due to the dual reactivity [30]. Thus, they are

often used as coupling agents to modify surfaces and provide good adhesion between inorganic and organic materials as well as other tailored functionalities [29].

Hydrolysis and condensation of silane molecule are the key reactions in applications where organosilanes are involved. Figure 2.10 shows how via these reactions silane molecules can create a good adhesive bond to substrates via hydrogen or covalent bond formation.

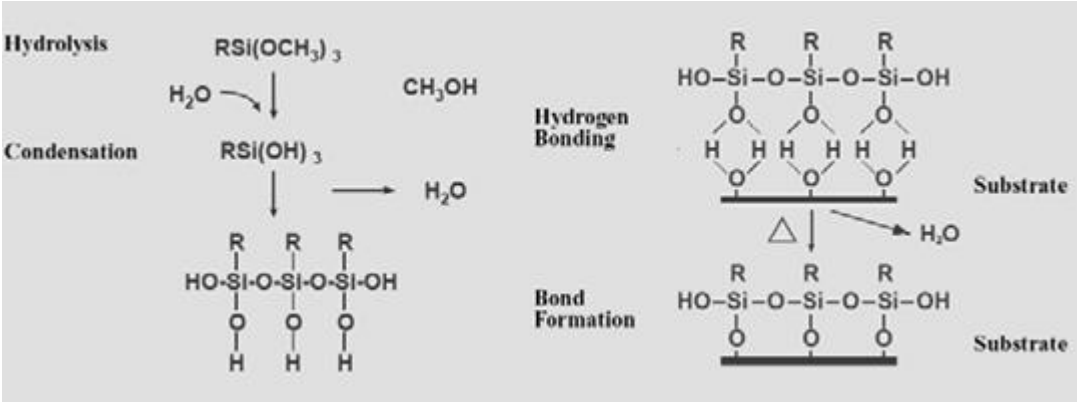

Figure 2.10. The mechanism of hydrolysis, condensation and bonding of organosilanes to an inorganic surface [29].

Depending on the nature of the hydrolysable group (X) attached to the silicon, it can be described as: chlorosilanes, silazanes, alkoxysilanes and acyloxysilanes. These molecules if reacting with moisture or water on a surface, will form silanols, liberating the corresponding by-product (HCl, NH_3, alcohol). These silanols can also react with other silanols to form a stable siloxane bond (-Si-O-Si-) or can react with metals to form a stable M-O-Si bond. This is the key chemistry that allows siloxanes to act as valuable surface-treating or coupling agents. Organosilanes can thus be linked to surfaces directly in different ways.

The unique capability to create covalent bonds between inorganic and organic compounds and the inherent chemical or thermal stability of the siloxane (Si-O-Si) bond make this technology a key component in high-performance paints and coatings [31]. If comparing the chemical properties of the siloxane and typical organic binders, it can be seen that the Si-O bond strength of polysiloxane (443 kJ/mol) is greater than the C-C bond of organic binders (360 kJ/mol), which explains the improved durability of polysiloxane coatings [27, 32]. Polysiloxane coatings exhibit superior gloss and colour retention, but suffer from poor mechanical properties [32]. Moreover, the siloxane coatings are already in an oxidized state, preventing further oxidation [32]. Coating applications that can benefit from polysiloxanes-based technology include primers, heat-resistant coatings, marine biofouling control, and abrasion resistant coatings.

The anticorrosion properties are due to the good barrier effect created by the silane-based coating. The corrosion performance of polysiloxane pre-treated substrate depends upon the polysiloxane layer thickness, uniformity, hydrophobicity and chemical stability. Therefore the polysiloxane-based coatings are effective, but also inert, and are thus not able to play any active role when the corrosion processes start to damage the surface. During corrosion attack the cathodic reactions release hydroxyl ions that increase the pH, inducing the decomposition of the silica network, causing acceleration of the degradation and delamination processes of the polysiloxane coating and the loss of the barrier effect [33]. The modification of the bulk properties of these siloxane-based coatings is thus an interesting

challenge to make the coatings less porous, more mechanically robust, and thus with improved corrosion resistance performance.

2.4 The Sol-Gel process

The term “sol-gel” (solution-gelation) was introduced in the mid-1800s with Ebelmen’s and Graham’s studies on silica gels [34, 35]. During these investigations, it was observed that the hydrolysis of TetraEthyl OrthoSilicate (TEOS), under acidic conditions yielded SiO_2 in the form of a “glass-like material” [36]. Many other researchers continued using sol-gel chemistry. In 1968, the work of Stöber helped to develop silica nanosols. Stöber realised that using ammonia as a catalyst for the TEOS hydrolysis reaction both the morphology and size of the powders could be controlled, leading to the so-called Stöber spherical silica [37].

Generally, the sol-gel process involves hydrolysis and condensation of metal alkoxides (precursors), such as TEOS, in the presence of acid or base as a catalyst [36, 37]. The first stage is the hydrolysis due to the interaction of the alkoxide with water. This is then followed by the condensation of –OH groups or –OH group with –OR group, to produce M-O-M bonds and water or alcohol. Usually, hydrolysis and condensations are competing, and the condensation process starts before the hydrolysis step is completed. The resulting oxide materials present structures varying in range from nanoparticulate sols to continuous polymer gels, depending on the rate of each of these reactions and subsequent drying and processing steps.

Other important factors are the catalyst, which is added to accelerate the processes since alkoxides are not very reactive, and the nature of the co-

solvent, which is necessary because water and metal alkoxides are immiscible liquids.

Many studies have been carried out by using sol-gel methods. A huge variety of coatings with different characteristics and properties have been developed by this process, which shows the potential of the sol-gel chemistry, along with its relatively low cost. During the past decade the development of sol-gel technologies has been remarkable and interest in this type of materials has gone in crescendo, as showed by the growth in publications in the sol-gel materials field (Figure 2.11). This is in line with the interesting properties that silanes can provide, such as adhesion and corrosion resistance.

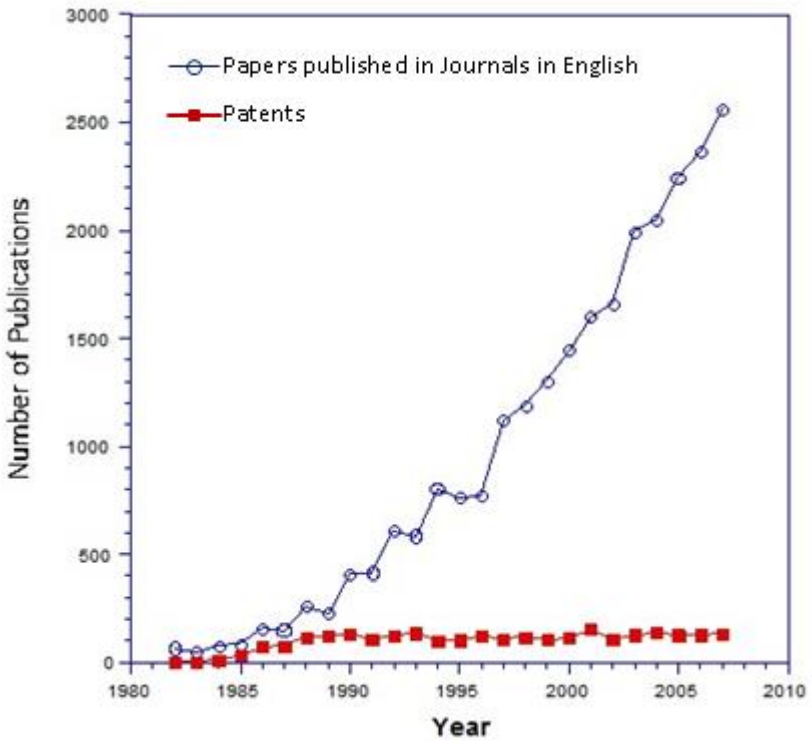

Figure 2.11. Evolution of publications and patents on sol-gel [38].

These coatings are considered a potential replacement for anticorrosion pre-treatments and coatings based on hexavalent chromium. Cr (VI) was widely used due its effective corrosion inhibition properties and low cost. Nevertheless, they are highly toxic and can cause not only environmental impact but also adversely affect human life. Due to this concern, regulations have been put in place intending to eliminate its use. The development of environmentally friendly coating systems is a growing market and silanes are one of the most promising alternatives.

In fact, Boeing has already in the market a sol-gel chromium-free coating that has been commercialised. This coating is used a Cr-replacement on aluminium substrates for corrosion protection [39].

The flexibility of the sol-gel process also permits the incorporation of corrosion inhibiting compounds, thereby providing another mechanism for corrosion protection. These characteristics lead to the possibility of forming environmentally compliant coatings capable of improved corrosion resistance without the use of metal chromates or other hazardous products [40].

2.5 Nanomaterials in coatings

The International Organisation for Standardisation defines the term “nanomaterial” as the material with any external dimensions in the nanoscale or having internal structure or surface structure in the nanoscale; considering “nanoscale” as the size range from approximately 1 nm to 100 nm [41]. Among these nanomaterials there is a subset called “nanoparticles”, having the above size range in all three dimensions.

The synthesis of nanomaterials can be achieved through two approaches, as described in Figure 2.12. While the bottom-up approach involves assembling atom by atom or molecule by molecule into structures, the top-down is the contrary, involving whittling down the size of materials from the bulk to the nanometre scale.

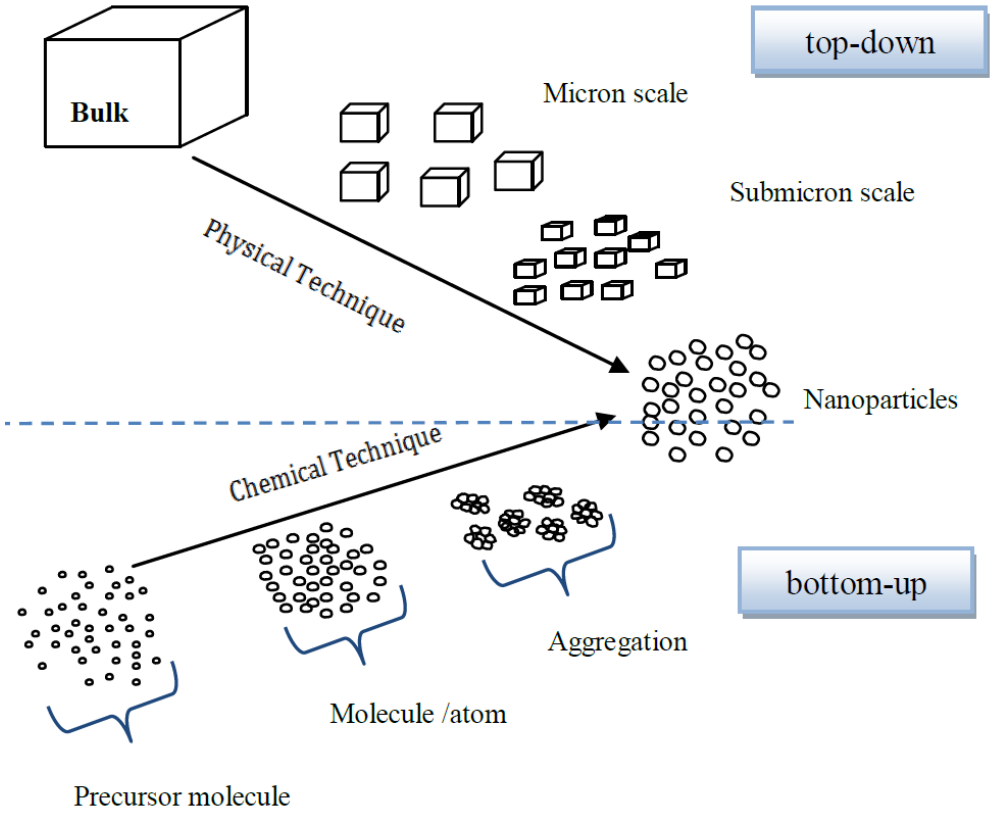

Figure 2.12. Approaches for nanoparticles synthesis [42].

The use of nanomaterials in formulations of coatings has been very promising. Nanoparticle size pigments and fillers, nanopolymer dispersions, and nanoadditives are now commercially available and many more are in the development stage. Nanotechnology aims to discover new properties and behaviours of materials at the nanoscale and has the potential to improve performance and to enable the development of new materials. Nanoparticles

and nanomaterials have been designed as consequence of the current advances in nanotechnology.

Nanomaterials and nanoadditives have the ability to generate new features and perform new functions that are more efficient than or cannot be performed by larger structures. There are lots of available products currently on the market using nanoadditives like cosmetics, medicines or sunscreens among others [43-45].

Due to their distinctive thermal stability and mechanical and molecular barrier properties, a variety of research has been conducted on nanoadditives added to coatings [46, 47]. Nanoparticles can be incorporated into polymer matrices at very low volume and yet have a great impact on coating properties. That is why nanotechnology has also been utilised in preparing nano-sized additives for coatings used to protect steel and other metals from corrosive environments. In addition, coatings incorporating nanoparticles have been developed for specific purposes this being one of the major applications of nanotechnology in construction.

The major challenges facing continued growth of nanotechnology based coatings can be divided into four main categories:

1. Dispersion of nanoparticles to get potential benefits in coatings: nanoparticles have strong tendency to agglomerate and in order to achieve uniform coatings, nanoparticles must be dispersed properly minimizing particle agglomeration.

2. Characterisation: Characterisation and analysis of nanoparticles in a coating may require techniques that are not common in small to mid-size coating manufacturer's research and development laboratories.
3. Health and safety: Although certain nanomaterials have been commercially used for many decades, commercialisation of new nanomaterials has outpaced development of their safe handling methods. The awareness of the need to understand both short- and long-term effects of nanomaterials has increased in recent years [48, 49].
4. Material cost: The cost of nanoadditives has come down in recent years with increasing number of nanoparticles suppliers, improved manufacturing methods, and increased sales volumes.

Nanoparticles can be added to coatings to provide various new functionalities and advantages. The choice of which nanoparticle is used depends on the desired property. For example, calcium carbonate ($CaCO_3$) nanoparticles are selected as reinforcement in polymers due to their low cost, carbon nanotubes (CNT) are chosen because of their enhanced spraying processes [50, 51] and tungsten oxide (WO_3) are used because of their thermochromic effects [52, 53] .

Nanotechnology can be used to manage steel corrosion and some research has been conducted to produce coatings with superior abrasion resistance [54, 55], to enhance the properties of steel in corrosive environments, or to prepare nanoadditives for anticorrosion coatings [31, 47, 54-84]. The potential of nanotechnology in corrosion protection is not fully achieved and it is anticipated that more applications and products will be developed over

the next few years as a better understanding is developed of the interactions of the nanoadditives, the binder systems, and the substrate.

Chapter 3. Literature review

3.1 Introduction

This chapter reviews the current state of the art technology on sol-gel based coatings and additives with the aim of providing a framework to understand the importance of the impact of additives in coatings, the optimum chemistry and structural hierarchy for a target application.

As stated in chapter 2, the use of nanotechnology in coatings is one of the most promising routes to develop high performance and durable anticorrosion systems. For many years, the most effective corrosion systems were based on the use of chromate-rich surface treatments and/or primers and pigments based on chromates. Although chromium is completely benign in its metallic form, hexavalent chromium compounds are in the list of Substances of Very High Concern (SVHC) contained in the REACH (Registration, Evaluation, Authorization and Restriction of Chemicals) regulations, and its use is currently limited in almost all sectors except the aerospace industry [85]. REACH and SVHC considerations are likely to have longer term implications on the supply chains for products containing such substances, impacting commercial viability even where exceptions are allowed. Thus, the development of alternative environmentally friendly systems has been promoted [86-88].

The development of environmentally friendly coating systems is a growing market and sol-gel based coatings are considered as a basis for the development of potential replacement pre-treatments and coatings. The

flexibility of the sol-gel process, which allows the incorporation of corrosion inhibiting compounds and the possibility of obtaining functional materials with tailored properties, is the primary reason it is viewed as a promising technique for the development of alternative coatings. In fact, Boeing has developed a non-hazardous sol-gel coating, Boegel-EPII, which is already in the market and can be applied on a wide range of substrates, such as steel, aluminium or nickel, and using various different methods such as dipping or spraying [89].

While many challenges remain in the commercialisation of these highly inorganic coatings, a material-by-design approach can be adopted to provide new mechanistic insights explaining the improved properties of the siloxane coatings after the addition of suitable nanoparticles.

Inorganic-organic hybrids and novel additives are central to the development of advanced functional materials and coatings. They provide the opportunity to establish compositional and structural hierarchies that have profound implications on behaviour and functional performance and allow the opportunity to envisage metamaterials.

Sol-gel chemistry and techniques have been closely bound to the development of hybrid materials and novel additives. Schmidt et al. [90], Rabinovich et al. [91], Sakka et al. [92], Bernards et al. [93], van Bommel et al. [94], Novac [95], Lichtenhan et al. [96], Brinker et al. [97] and Sanchez et al. [98] are amongst some of the notable contributors to this field. Sanchez et al. in particular has started to frame these material developments from the perspective of a new chemistry “Chimie Douce”. This perspective links the

molecular scale of chemistry to the micro- and macro-scale of materials science and engineering.

There are multiple nano- and micro-scale structures that can be synthesised using chemical methods (as depicted previously in Figure 2.12). The use of these 2-D and 3-D structures form the basis of bottom-up materials chemistry, and is the basis for many attempts to synthesise new functional materials and coatings. The use of these nano- and micro-scale materials is frequently via their incorporation into host matrices, for example the inclusion of silsesquioxanes into composite resins, or nanoparticles as reinforcement for coatings [99]. Much effort has been expended on the synthesis and characterisation of these nano- and micro-scale materials as well as the assessment of their impact on the functional properties of the materials and coatings into which they are included. The number of variations regarding the composition, structure (and structural hierarchy), processing conditions, evaluation methodologies and performance characteristics are so large as to make any global and comprehensive conclusions regarding structure-property relationships impossible.

Furthermore, there are no clearly defined methodologies to build such relationships or to enable a more systematic design approach to accelerate the development of advanced functional materials and coatings.

To more rapidly develop the materials required by industry it is clearly essential to establish design rules that relate synthesis and processing considerations to compositional and structural characteristics and ultimately functional performance. The use of functionalised metal oxide nanoparticles

can be considered as a case study in the development of a design and test methodology.

There are many ways to describe inorganic-organic hybrid composite materials. Novak [95] suggested five major classes based on their macromolecular structures and phase connectivities. These are:

-Type I: Soluble, preformed organic polymers embedded in an inorganic network

- Type II: Embedded preformed organic polymer possessing covalent bonds to the inorganic network.

- Type III: Mutually interpenetrating organic-inorganic networks

- Type IV: Mutually interpenetrating networks with covalent bonds between the organic and inorganic phases

- Type V: “Non-shrinking” sol-gel composite materials.

Sanchez et al. [98] reduced the number of categories to two classes, the first where the only bonding between the inorganic and organic phases was hydrogen bonding or electrostatic bonding. Class 2 materials had strong covalent or iono-covalent bonds.

From the perspective of this project the most simple description is of a film forming matrix incorporating embedded inorganic fillers with the potential of the nanoscale fillers having surface functionalisation. Within this definition therefore there are two primary constituents, the additives and the film forming matrix. There is then the influence of the fabrication and processing methodology. The final functional properties of the material will depend on

not only the global compositional characteristics but also local variations that may be material or process dependant. With regards to the nanoscale filler it is worthwhile summarising some of the key material parameters, Table 3.1:

Table 3.1. Key material parameters for functionalised nanoparticles.

Parameter	**Key variables**	**Comment**
Composition	Metal oxide, alkyl functional metal oxide	Compositional maturity i.e residual hydroxyl, alkoxy groups,
Size	Measurement method, aspect ratio	
Polydispersity	Monomodal, multimodal	
Shape	Spherical, ovoid, raspberry etc	
Porosity	Accessible/non-accessible porosity, micro-/mesopore volume, pore shape distribution	
Crystallinity	Fully or partially amorphous	
Functionalisation level	Fully or partially functionalised	Residual functionalisation agents as monomers/oligomers
Functionalisation type(s)	Single/dual/multi-functionalisation	Residual functionalisation catalyst, retention of target functionality

The details of the fabrication method of integrating these additives into the film-forming matrix are central to the eventual coating structure and morphology. These details include the addition sequence, mixing methodology, temperature, dilution media, the presence of residual chemicals/components, chemical compatibility, viscosity, thermodynamic and kinetic stability.

In addition to these incorporation considerations, the loading level of the additive is one of the key material parameters that can be varied to significantly change the characteristics of the final material.

After final preparation of the formulated system the impact of storage conditions, deposition method, drying and curing on the final material behaviour and functional performance can be assessed.

Whilst there are very many factors which may influence the final morphology, the final cumulative output of these can be monitored by assessing the homogeneity of the coating. Whether the particles are uniformly distributed, clustered, agglomerated or stratified or some combination of these may be dependent on the precise fabrication conditions employed. A full materials by design approach would require a clear understanding of the relative influence of all the above factors and the management tools available to achieve specific outputs. A precise understanding of the influence of each structural and composition variant on the final performance characteristics would also be necessary. The elucidation of the design rules behind such composite materials will be a long term and considerable effort. However, preliminary design rules can be identified by examined the effect and impact of key materials input. Within

this project, these inputs were the presence of a specific nanoparticle type, the loading level of this within a polysiloxane matrix material that had chemical similarity, and the use of and quantity of a functionalising agent. The specific outputs were the surface roughness, corrosion protection provided to the substrate, and key mechanical properties.

3.2 Sol-gel

As mentioned previously in section 2.3, the sol-gel process can be used to obtain functional materials with tailored properties, which has a strong impact on the development of coatings where this process can be of high interest for many applications. Since the mid-1800s, when sol-gel studies started, many works have been carried out using this sol-gel methodology.

The chemistry behind sol-gel processing is based in hydrolysis and condensation reactions, as explained in section 2.4. Through hydrolysis and condensation reactions of molecular precursors (metal alkoxides), the metal oxide-based network is formed.

$$R'Si(OR)_3 + H_2O \rightarrow HO\text{-}SiR'(OR)_2 + ROH \quad (3.1)$$

$$(RO)_2R'Si\text{-}OH + HO\text{-}SiR'(OR)_2 \rightarrow (RO)_2R'Si\text{-}O\text{-}SiR'(OR)_2 + H_2O \quad (3.2)$$

These reactions are strongly affected by the nature of the R-group, the water to alkoxide ratio and the type and amount of catalysts (acid or base catalysts since neutral reaction is very slow). Besides, they are competing which can lead to oxide materials with different structures varying from particulates to polymers, depending on the catalysts and the reactions rates. Hydrolysis results in the replacement of an alkoxy group with a hydroxyl and the release

of the corresponding alcohol molecules. Depending on the conditions and the Si/H_2O ratio, more than one alkoxy group may be hydrolysed: small amount of H_2O leads to slow hydrolysis due to the reduced reactant concentration while a large amount leads to slow hydrolysis due to increased reactant dilution. Condensation reactions involve the silanols groups to produce siloxane bonds and water and alcohol as by-products.

The final microstructure of the metal oxide will depend on the hydrolysis and condensation reactions which are usually controlled by the pH. Under acidic conditions, hydrolysis is favoured and condensation usually starts when hydrolysis is completed, while in alkaline conditions condensation is faster and often occurs on terminal silanols which can result in highly condensed species or chain like structures in the sol and network-like gels. Figure 3.1 shows how pH can affect the growth and structure of silica gels.

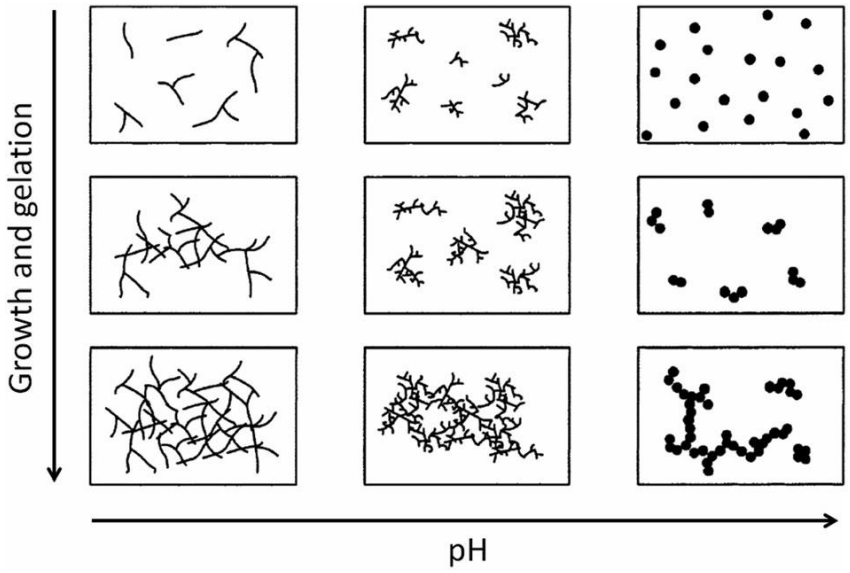

Figure 3.1 pH influence on growth and gelation of a silica gel [100].

The structural evolution of sol-gel materials is quite complex and one way of explaining this can be the matrix showed in Figure 3.2. This matrix was

proposed by Assink and Kay [101] and displays all species of TEOS, from its starting position, $Si(OR)_4(4,0,0)$, to the fully hydrolysed and condensed anhydrous silica, $Si(OSi)_4(0,0,4)$. The “Q” notation has been also used to describe the quatra functionality of silicon: from Q0 when silicon has no siloxane bond, (SiOSi), from Q4 when silicon has for siloxanes bonds. As observed from Figure 3.2, multiple species could be referred as Q0 due to numbers of partially hydrolysed molecules. Therefore, control of the hydrolysis and condensation reactions would determine the chemical evolution of the material during sol-gel synthesis.

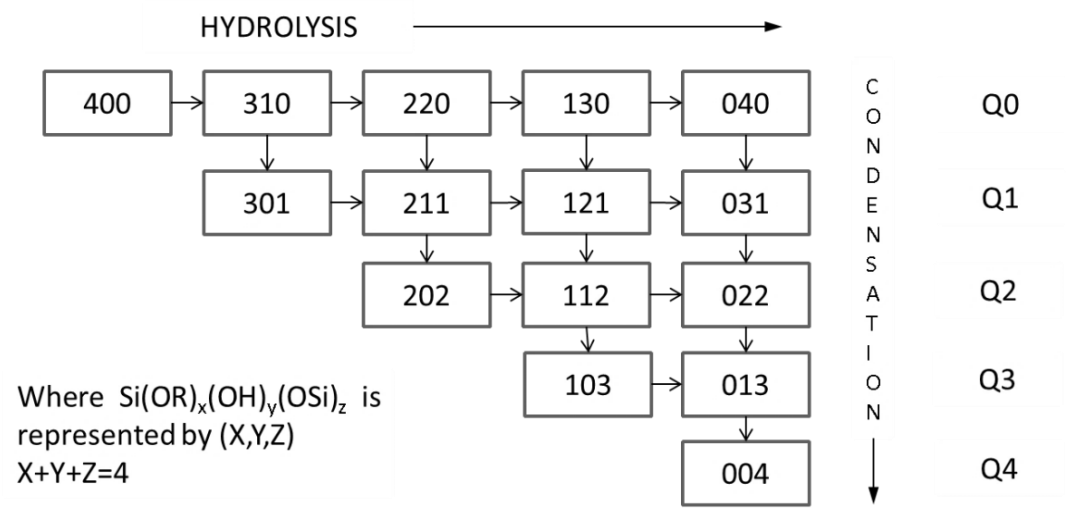

Figure 3.2. Sol-gel structural evolution [101].

Sol-gel coatings can be used for a wide range of applications due to its versatile route but also due to the possibility of being deposited in many different ways such as dipping, spinning or spray, and the possibility of being deposited on many different substrates such as glasses, metals or plastics. Silicates and alkoxy silanes have been also widely used in formulating primers for a variety of substrates and are well known as adhesion promoters. Silicate-based zinc primers have been showed to have superior

long-term economic and environmental performance compared to traditional systems [102], which is probably due to the continuous improvement in the performance and versatility of polysiloxane coatings. This contributes to increase the market research on sol-gel based technologies and the use of polysiloxane as host matrices, an enormous object of interest.

One of the most studied applications using this methodology is the protective sol-gel coatings. The use of sol-gel coatings enable the deposition of a barrier coat that works by insulating the substrate from the aggressive environment. This would allow the coated substrates to extend their durability and resistance to corrosion.

Parameters such as the functional groups in the silane molecule, water and catalyst content, pH of the solution, the nature of the substrate or the curing time, play an important role in the formation of the silane coating. Two groups can be distinguished depending on the nature of the coatings: pure inorganic coatings and organic-inorganic hybrids. Pure inorganic coatings are obtained by hydrolysis and polycondensation of metal alkoxides (SiO_2, ZrO_2, SiO_2-ZrO_2…) but they have some drawbacks since they can be brittle and coatings thicker than 1 µm are difficult to achieve.

In order to overcome this limitation, much work has been put on the development of hybrid coatings, which can be obtained by incorporating organic groups into the inorganic network.

Hybrid sol-gels obtained from organosilane solutions are a very attractive methodology. In general, through the hydrolysis and condensation of organically modified silicates with traditional alkoxide precursors, the hybrid

material is formed. The inorganic components tend to impart durability, scratch resistance, and improved adhesion to the metal substrates, while the organic components contribute to increase flexibility, density, and functional compatibility with organic polymer systems. Then, hybrid films may be designed to have exceptional durability and adhesion, while providing a barrier for permeation of water and corrosion initiators. Much work has been done to develop sol-gel derived hybrid materials going from almost completely inorganic to almost completely organic. Depending on the chemical bond between the inorganic and organic part, the following classification has been established [90, 95, 98]:

- the organic component is directly mixed into the inorganic sol-gel system and there is no chemical bonding between both components

- introducing chemical bonding by using the already existing functional groups to react with the inorganic precursors

- use alkoxysilanes as the only or one of the precursors of the sol–gel process with an organic group (often carried out by either a photochemical or thermal curing following the sol–gel reaction)

The literature on the behaviour of sol-gel coatings is quite extensive. The majority of studies are on sol-gel coatings deposited on stainless steels and aluminium and its alloys, however, studies on carbon steels are not as wide. These studies have demonstrated that coatings using siloxane-based technology are capable of efficiently protecting metals against corrosion. It is worth mentioning that siloxanes are environmentally-compliant chemicals and relatively cheap, so a large variety of cost-effective and eco-friendly

coatings could be developed to be used for corrosion protection instead of the traditional organic coatings.

There are many papers about sol-gel coatings on metal substrates; a good summary of them is described in the paper published in 2009 by Wang et. al [103]. Usually, steel surface can be passivated by using conversion coatings (phosphating, chromating), however these treatments, which works by creating a layer with corrosion products to resist chemical attack, use chemicals which are high toxic.

The use of sol-gel coatings could be a good alternative to conversion coatings, the presence of the metal oxides allows covalent bonding between the siloxanes and the metal, Si-O-metal oxide, which favour the adhesion between coating-substrate, apart from being an environmentally-friend alternative. Despite the increased interest and research on sol-gel coatings, there are still some limitations such as delamination, brittleness and thickness restrictions.

Cracks and defects can negatively affect the anticorrosive performance of the coating in wet media, and thickness limits the applicability of these coatings. It has been showed that the mechanical properties of the coatings are influenced by the nature of the organic substituent but also on the micro- and nanostructures [104, 105]. These hybrid coatings link the properties of inorganic (brittle) materials and organic (flexible) polymers. The introduction of the organic constituent can lead to novel materials with unique synergistic properties. Much attention was put on the abrasion resistance that these coatings poses, which is in fact what first attracted great attention, however

and as with all other properties this will be dependent on the precursors used.

The most commonly utilised sol gel precursor is tetraethyl orthosilicate (TEOS), also known as tetraethoxysilane, with a chemical structure as $Si(OCH_2CH_3)_4$. The main reasons are that this precursor has been studied in detail, their properties are well known and it is cheaper than other alkoxysilanes. Some other alkoxysilane precursors used are tetramethyl orthosilicate (TMOS), methyl triethoxysilane (MTES), methyl trimethoxysilane (MTMS), 3-glycidoxipropyltrimethoxysilane (GPTMS), vinyl trimethoxysilane (VTMS), 3-aminopropyl trimethoxysilane (APS). In a review by Figueira et. al [106], it was showed that for metal substrates the most used precursors are TEOS, GPTMS, MAPTS, MTES and MMA, being TEOS the most widely used.

As mentioned previously, just with minor changes in synthesis parameters is possible to obtain sol-gel coatings with different properties. This also makes more difficult to compare coatings made in different studies since even if the formulations were quite similar, just a minor change (water and catalyst content, pH of the solution, curing time) could have led to dissimilar coating performance. This will also have repercussion on the corrosion performance characteristic of the final coating and its mechanical properties.

One of the hybrids which has attracted much attention is the GPTMS-based system. Basically, these coatings are formed by mixing TEOS with GPTMS. The interest of this combination is the organic part of the GPTMS, which poses an epoxide ring that can be opened to form an organic chain. By using Lewis acids polymerisation can take place which result in the

formation of an organic and inorganic network. The amount of inorganic structures and the extent of organic cross-linking can influence the mechanical properties: high inorganic content usually leads to stiff but brittle materials while a certain amount of organic cross-linking can led to harder but elastic materials.

Thus, sol-gel coatings can be tailored to have specific properties depending as well on the organic substituent: chain length and functionality of the organic precursor.

In a study comparing pure TEOS coating with hybrid coatings containing MTMS, VTMS and GPTMS was shown that an increase in the organic modifier led to greater resistance to cracking and debonding [107]. Other work which studied the effect of increasing the amount of GPTMS led to the conclusion that increased organic content led to thicker coatings, but can compromise the mechanical properties.

In another study about the influence of the nature of the organic substituent (similar chain length and polymerisation) where GPTMS was substituted by n[3-(trimethoxysilyl)propyl]ethylene diamine (TMOSPEDA) and n-octyltrimethoxysilane (OTES), it was found a better network connectivity in the GPTMS structure compared to TMOSPEDA and OTES. This led to the conclusion that mechanical properties can differ depending on the ratio organic/inorganic constituents, going from hard-brittle materials to rubbery-soft.

Mackenzie et.al [108] found that samples could retain their rubbery nature even if the inorganic constituent amount was higher than 70 wt.%. The

balance between mechanical rigidity and adhesion is dependent on the proportion of $Si(OR)_4$ used in the hybrid films.

3.3 Nanomaterials in coatings

The addition of nanomaterials into the organically modified networks or hybrid matrices is aiming to reinforce these nanoenabled coatings. A range of nanoparticles can be selected to provide the desired property or properties aiming to achieve. Nanomaterials can be distinguished in different families: layered nanomaterials, metal-oxide nanoparticles and nanocapsules or nanocontainers. Some of them and their properties will be described in this chapter.

Layered nanomaterials represent an interesting choice to develop materials with controllable functionalities, because of their unique structure which consists in flat layers or piled nanosheets. Multilayers structures are often used where there is a need for advantageous barrier. These barrier properties are important to protect the material inside, impeding the moisture and oxygen to ingress.

The most common naturally occurring layered materials are graphite, graphene, clays and layered hydroxides (LDHs). Layered compounds have been subject of several studies on corrosion protection [109-119] and showed applications in a wide range of areas. This study took into consideration graphene, clays and LDHs. A summary of the properties of these layered nanomaterials can be seen in Table 3.2.

Table 3.2. Properties of some layered materials.

Graphene	Clays	LDHs
Enhance barrier properties [109] High surface area [110] High tensile strength [111] Improve mechanical properties and thermal stability [109]	Hardness [112] UV stabilisation and enhancement of photodegradation [113] Improve thermal and mechanical properties [114] Reinforcing agent [115] Enhance barrier properties [114]	Very flexible [116] Potential as reinforcing nanofillers and as curing agent [116, 117] Enhanced thermal stability [118] Improve mechanical properties [119]

A potential method to enhance corrosion protection is the use of nanocapsules or nanocontainers [120]. These nanocapsules contain healing agents and are embedded in anticorrosion formulations. When the coating is damaged the nearby capsules will be activated, releasing their inhibiting substances into the damaged area and helping to avoid the corrosion attack (Figure 3.3). This provides a self-healing mechanism.

Nanostructures of many oxides have been studied over the years. In this work, the properties of the following oxides were evaluated with special consideration into their possible mode of action for corrosion protection: silica (SiO_2), ceria (CeO_2), zinc oxide (ZnO), titania (TiO_2), zirconia (ZrO_2), and alumina (Al_2O_3), whose properties have been summarised in Table 3.3.

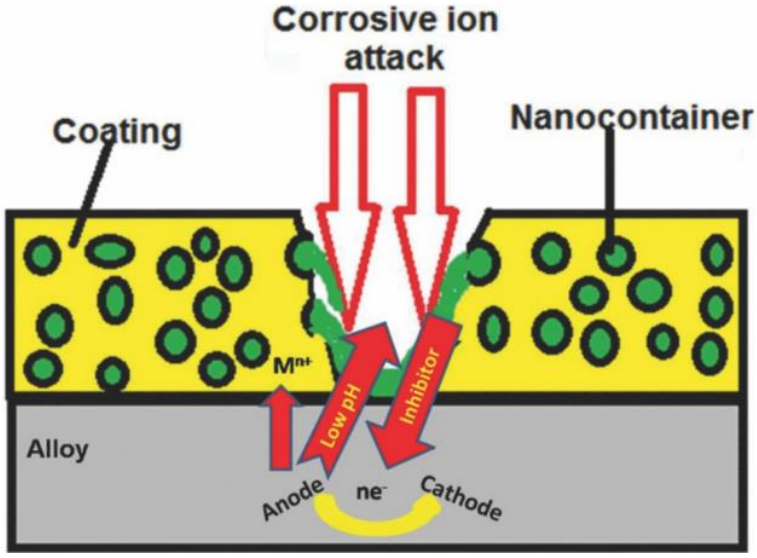

Figure 3.3. Nanocapsules for self-healing materials [121].

Table 3.3. Properties of the metal oxides studied.

Metal oxide	Advantages	Disadvantages	Possible mode of action for corrosion protection
ZnO	Low cost and nontoxicity [56] Photocatalytic activity [57, 59] UV protection [57] Low impact in transparency [56] Increased durability [56] Antibacterial and antifungal properties [58]	Small nanoparticles without capping agents can easily form aggregations, leading to the loss of its active sites and photocatalytic efficiency [59]	Barrier [60]

Metal oxide	**Advantages**	**Disadvantages**	**Possible mode of action for corrosion protection**
TiO_2	Low cost, nontoxicity [61] Photocatalytic activity [61-64] Availability [62] UV resistant material [62] Chemical stability [61]	Does not absorb visible light (to overcome this problem: dye sensitization, doping, coupling and capping TiO_2) [61]	Barrier [63, 64]
ZrO_2	Improve mechanical properties [65] High hardness and strength [65] Enhance thermal stability [66] Good adhesion [67] Antibacterial and photocatalytic effect [66]	Low surface area (could limit its use) [69]	Barrier [65, 68, 70], but could also act as a reservoir for corrosion inhibitors [71]
Al_2O_3	Low cost and light weight Improved durability and mechanical properties [72] Good thermal properties and chemical stability [73] Low thermal conductivity [73]		Barrier [73]

Metal oxide	**Advantages**	**Disadvantages**	**Possible mode of action for corrosion protection**
CeO_2	Hardness and scratch resistance [81] Improvement of water resistance [81] UV protection, non photoactivity [80, 81] Low impact on transparency [81] Storage abilities [82]	Cost	Corrosion inhibitor [81, 82, 83, 84] and barrier properties [83, 84]
SiO_2	Low cost [74] Improve thermal and mechanical properties [54, 75] Scratch resistance [75, 76, 55] Abrasion resistance [54, 55] Low toxicity [77] UV applications [55] Ability to be functionalised with a range of molecules and polymers [54]	Increase system viscosities can alter the curing behaviour of the system [33]	Barrier [47, 78, 79]

After the comparison of the different nanomaterials described and summarised in section 3.3, the one selected for this study were SiO_2 nanoparticles, according to the following reasons:

- could increase the barrier properties of the coating (protection by reducing the diffusion of water and air from the environment to the substrate surface, preventing corrosion from happening) [47, 78],
- provide potentially improved mechanical durability [71, 54-55]
- is one of the lowest cost metal oxides [74].

Therefore, this chapter will continue with the description of the synthesis of this type of nanoparticles, the possibility of surface treatment, the incorporation into polymer matrices and its impact on coating properties.

3.4 SiO_2 nanoparticles

SiO_2 nanoparticles or silicon oxide nanoparticles are typically known as silica. It can be found in its crystalline form in nature (sand) but can also be industrially manufactured (amorphous silica) in various forms: colloidal silica, fumed silica, silica gels. The basic difference is that colloidal silica is in liquid form, it is a suspension of fine amorphous, nonporous and, usually, spherical silica particles in a liquid phase. Its surface area can be quite large and the aggregate size small. One of the widest methods used to prepare silica nanoparticles is the Stöber process, which is further described in 3.4.1.

3.4.1 Stöber synthesis

The Stöber process is used for the synthesis of silica spherical nanoparticles using the sol-gel method. The Stöber method was firstly introduced to produce homogeneous silica nanoparticles using ammonia catalysed hydrolysis and condensation of ethoxysilanes in alcohols as solvent [37].

The process involves hydrolysis and condensation of metal alkoxides (precursors), such as tetraethylorthosilicate (TEOS) in the presence of acid or base as catalyst [36, 37]. Figure 3.4 shows a typical sol-gel process for the production of silica using silicon alkoxides. The hydrolysis of TEOS forms silanols groups:

$$Si\ (OC_2H_5)_4 + xH_2O \rightarrow Si(OC_2H_5)_{4-x}(OH)_x + xC_2H_5OH \quad (3.3)$$

The condensation between silanols groups or between silanols groups and ethoxy groups creates siloxane bridges (Si-O-Si), forming the silica structure.

$$\equiv Si - OC_2H_5 + HO - Si \equiv \rightarrow Si - O - Si + C_2H_5OH \quad (3.4)$$

$$\equiv Si - OH + HO - Si \equiv \rightarrow \equiv Si - O - Si \equiv + H_2O \quad (3.5)$$

Using the Stöber method, the particle size distribution is relatively narrow and can be easily tailored. It has been found that the main parameters governing particle size and distribution are: concentration of catalyst, water and types of solvent and reaction temperature. These factors affect nucleation and growth of silica nanoparticles. For instance, the concentration of catalyst affects particle size, an increase in catalyst addition leads to a bigger size of the particles. Generally, the size of Stöber spheres silica ranges from 20 nm to 1 μm. An interesting advantage of this Stöber silica is

the ability of dispersing them in a liquid phase, such as alcohol, which makes this silica easily manageable for any additional treatment. Other advantages are the retention of primary particle characteristics and the chemically benign environment compared with fumed and colloidal silicas respectively.

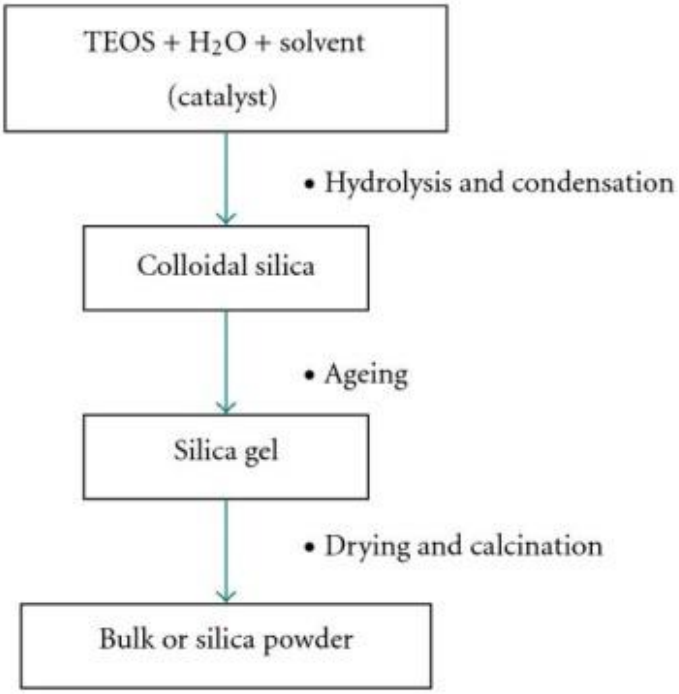

Figure 3.4. Diagram of a typical sol-gel process [54].

3.4.2 Surface treatment or functionalisation

Much research is needed in order to be able to transform functional nanoparticles into commercially available products. Surface chemistry, surface area and degree of aggregation are parameters of importance that can impact significantly the degree of reinforcement independently of the application area.

When nanoparticles are adequately distributed, just a small amount can significantly improve the properties of a material. However, as stated in Chapter 2, nanoparticles have to face some challenges such as problems

with dispersion and agglomeration which are usually the main reason of poor performance. In order to overcome this problem, a chemical modification of the nanoparticle surface is performed. Surface modification or surface treatment of inorganic nanoparticles can lead to a better distribution of nanoparticles and improved nanoparticle-matrix interface leading to enhanced formulations. However, the behaviour of the functionalised nanoparticles will be strongly dependent on the attached groups and the dominating interparticle forces.

3.4.3 Silica functionalisation

Silica poses a large number of silanols groups on its surface, which was determined by Zhuralev to be about 4.6 OH per nm^2 [122]. These silanols groups have a big impact on the surface charge of silica and its stability in solution. They can act as reactive groups to enable chemical grafting, however its affinity to form hydrogen bonding with each other can result in strong filler-filler interaction and lead to agglomerates [123].

In order to obtain coatings with enhanced properties, dispersions with non-aggregated silica are needed, which can impact on properties such as the cross-linking density [123]. A low cross-linking density can lead to porous/defective coatings decreasing the potential of protection they could offered. The size and dispersion of silica nanoparticles will also impact on mechanical durability since hardness and Young's modulus are strongly dependent on this: aggregation will increase the size of silica and lead to decrease mechanical properties of the final formulation [123]. It will also influence the aesthetic appearance since agglomeration can compromise gloss and haze [123].

In order to prevent or reduce agglomeration problems, the silica surface can be modified with the aid of coupling agents. This surface modification can lead to the functionalisation of the particle, improving the chemical interaction between the particle and the coating. This is of high importance since functionalisation can provide the opportunity to control the compatibility nanoparticle-matrix and thus, tune the microstructure of the final material. This ability to control and modify particle interactions and particle-coating interactions can lead in the direction of optimizing nanoparticle processing.

Thus, surface treatment can help to eliminate/reduce this negative effect leading to enhanced coating systems.

3.4.3.1 SiO_2 functionalisation with GPTMS

The functionalisation of nanosilica and its introduction into a polymer matrix can help to reduce stress concentration and enhance interfacial interactions [124]. There are many coupling agents used to do that, however silanes are one of the most used due to their bi-functional nature: they possess one organofunctional group and three hydrolysable groups ($Y\text{-}R\text{-}Si(X)_3$).

From the different hydrolysable groups, one of the most common are the trialkoxysilanes, ($Y\text{-}R\text{-}Si(OR')_3$). By hydrolysis reaction the X group is hydrolysed to silanols, which then condenses to form siloxane bonds. Both reactions are competing and dependent on pH, however, with the right conditions the hydrolysis can go fast while keeping condensation reaction slow.

GPTMS, is one of the preferred types of trialkoxysilanes since it can provide stable pre-hydrolysed solutions with high concentrations of the epoxy-

functional group. If the pH is kept in the range 4 to 7, condensation reaction are kept at minimum.

The reaction between the hydrolysed GPTMS and the silanols groups from silica is a condensation reaction. As mentioned previously, aqueous silica sol has in its surface about 4.6 silanol groups per nm^2, so just a few silane molecules will be required to fully react with the silica surface since each silane may react with three surface groups. Thus, silylation of the silica surface will reduce the number of silanols groups and hence make the sols more stable due to the formation of siloxane bonds between particles. In addition, the epoxide groups from the GPTMS in the silica nanoparticle and the ones from the matrix can react enhancing the nanoparticle-matrix interfacial interaction.

3.5 Silica impact on coating microstructure

As previously mentioned, the addition of nanosilica to a polymer matrix or a resin can have an impact on coating microstructure. However, an enhanced performance can be provided if added in the correct way and amount, since the loading and dispersion of the nanoparticles plays a vital role on the final coating performance. In a study carried out by Shi et al. [125], it was found that modifying an epoxy coating with SiO_2 nanoparticles led to a denser coating with no sign of nanoparticle agglomeration, and silica greatly improved the microstructure of the coating matrix which was attributed to an enhancement of the crosslinking density. Suegama et al. [126, 127] found that an optimum amount of silica added to a silane film led to increased thickness with an uniform distribution of nanoparticles, however exceeding

that certain amount can lead to defects and form porous films [126-130]. This is in line with the studies carried out by Peres et al. [130] where they studied the influence of different amounts of silica (0 to 600 mg/L) into a TEOS-GPTMS hybrid coating and found that the film without nanoparticles showed defects, while coatings with silica depicted different behaviour depending on nanoparticle concentration. Whereas the coating doped with 300 mg/L showed only submicron agglomerates, an increase to 400 mg/L showed higher agglomeration and a further increase up to 600 mg/L led to defects and cracks on the film surface [130].

One of the parameters that is usually dependent on nanoparticle concentration is the thickness of the coatings. In a study carried out by Montemor et al. [131] was found that the addition of silica nanoparticles increased film thickness, decreased the porosity and filled the defects and holes present in a silane film. Same behaviour was noticed by Malzbenger et al. [128], where an increase in coating thickness with filler fraction (from 0 to 0.69 silica volume fraction) was observed, although areas of lower density appears at 0.67 and a further increase to 0.69 resulted in a coating with pores.

However, the most important factor that controls the resulting properties of the final coating is not just the introduction of the correct amount of the nanoparticles but also the interaction between the nanoparticles and the matrix. As stated in 3.4.2, one of the challenges is the dispersion of the nanoparticles and to overcome this, research has been carried out on the surface modification of these nanoparticles and its role on distribution and nanoparticle-matrix interface.

Douce et al. [132] studied the introduction of silica nanoparticles with different sizes and different surface modification into a polysiloxane coating. They use GPTMS to modified the surface of silica and found that the introduction of untreated silica has strongest chemical interaction with the matrix than the epoxy-functionalised silica, which they attributed to decreased interaction fillers-matrix due to epoxy ring opening [132]. Sowntharya et al. [133] studied the introduction of acrylic modified silica into a sol-gel matrix and compared it with in-situ formation of a silica network. They found that the addition of nanosilica led to high stress concentration which made the matrix weak and since the interaction matrix-nanosilica was weak that led to poor mechanical properties compared to the in-situ formation silica network [133]. However, and to the best of my knowledge, these are the only studies reporting strongest interaction of untreated silica against treated silica with a polymer matrix. Usually, the introduction of modified silica to a polymer network led to stronger filler-matrix interaction and a reduction of nanoparticle agglomeration, which has been attributed to the interaction between the functional group on the nanoparticle surface with polymer chains that increase surface change and enhance dispersion.

Dolatzadeh et al. [134] studied the incorporation of various organosilane-modified silica nanoparticles into a polyurethane resin and they found that the modified nanoparticles could be well dispersed within the matrix at level of 6 wt.%. They also found good compatibility even at loadings up to 8 wt.%. However some modified silica showed better dispersion with no aggregations whilst others showed some aggregates what they related with the observation that nanoparticles with lower hydrophobicity or high shear

thinning rheological behaviour could negatively affect dispersion efficiency [134].

Other work carried out by Rostami et al. [135] studied the addition of untreated and modified silica with varying aminosilane functionalities dispersed into a polyurethane coating where they found that the dispersibility of the particles was dependent on the amount of the grafted silane onto the nanosilicas, which also affects the optical properties. Although all films were highly transparent, it was observed that the sample with higher silane grafted had a haze value close to the blank polyurethane resin, which they associated with a better interaction with the resin [135].

The optical properties and visual appearance of the coatings are also affected with the introduction of nanoparticles. Malzbenger et al. [128] found that sol-gel based coatings filled with silica were transparent up to a volume fraction up to 0.67, but at higher filler contents became milky. An increased visual appearance, in terms of light absorbance, was found by Deflorian et al. [136] when they incorporated modified silica nanoparticles with MPTMS into a polymeric matrix. They also found that the presence of MPTMS promoted efficient bonding between silica particles and the polymeric matrix [136]. Same behaviour was observed by Rostami et al. [135]. Chen et al. [137] observed that the incorporation of unmodified or GPTMS-modified silica slightly modified the transparency of an epoxy coating. However, coatings with modified silica had higher gloss and retain transparency more than those containing unmodified silica.

Thus, the introduction of functional groups on the silica surface can lead to a stronger interface between matrix and nanoparticles [54] and the surface

treatment has been proved to supress nanoparticle agglomeration due to enhanced resin-wettability. This is in line with other investigations such as the work carried out by Eslami-Farsani et al. [124] where they compared the influence of the addition of the same amount of untreated silica and GPTMS-modified silica into an epoxy resin. They found that when the epoxy matrix was reinforced with non-treated silica nanoparticles this led to a poor interface filler-matrix, however when GPTMS-silica was added into the epoxy resin the interfacial interaction was enhanced leading to improved properties [124].

In another work carried out by Kang et al. [138], surface modification of silica particles with different functional groups (epoxide, amine and isocyanate groups) was investigated in order to understand how the surface modification could affect dispersity and interfacial properties. They found that the final properties of the composite were highly influenced by the interfacial strength between the matrix and the fillers. Epoxide and $–NH_2$ groups on the silica surface produced very strong interface between matrix and filler compared with the isocyanates [138].

Ghanbary et al. [139] studied the impact of GPTMS-functionalised silica incorporated into an epoxy resin and found that an increment in loading change the surface morphology and can lead to aggregation if exceeding the critical amount, which for their particular study was 4-6 wt.% silica. Nanoparticles were almost homogeneously distributed into the polymeric matrix up to a silica content of 4 wt.%, however an increase up to 8 wt.% led to nanoparticle agglomeration [139].

However, more research needs to be carried out in order to get a proper understanding of all the benefits of surface modification of nanoparticles and its interaction with polymer matrices.

3.6 Silica impact on corrosion performance

Coating adhesion can be affected by the presence of species such as oxygen, water and ions, promoting corrosion. This influences the impedance response of the coating-substrate system when a small ac signal is applied and this response can be analysed with EIS spectra and polarisation curves. Corrosion performance of different coating systems has been investigated using these effective methods. Some relevant corrosion studies on coatings with silica nanoparticles assessed by means of impedance and the interpretation of the data are described below.

Electrochemical studies were carried out by Montemor et al. [82] using EIS and potentiodynamic polarisation to investigate the anticorrosion performance of polysiloxanes-based coatings with CeO_2 and SiO_2 nanoparticles (activated with cerium ions). Figure 3.5.a) shows the EIS results for the different systems studied where a decrease in CPE can be observed (associated with the electrochemical double layer capacitance) from the blank matrix compared with the systems with nanoparticles, which suggest a better prevention of the penetration of species through the coating. This is an indication that the addition of nanoparticles reinforced the barrier properties of the film. In terms of potentiodynamic polarisation, results from Figure 3.5.b) showed that the corrosion potential shift to more positive values showing an improvement due to the nanoparticles addition [82].

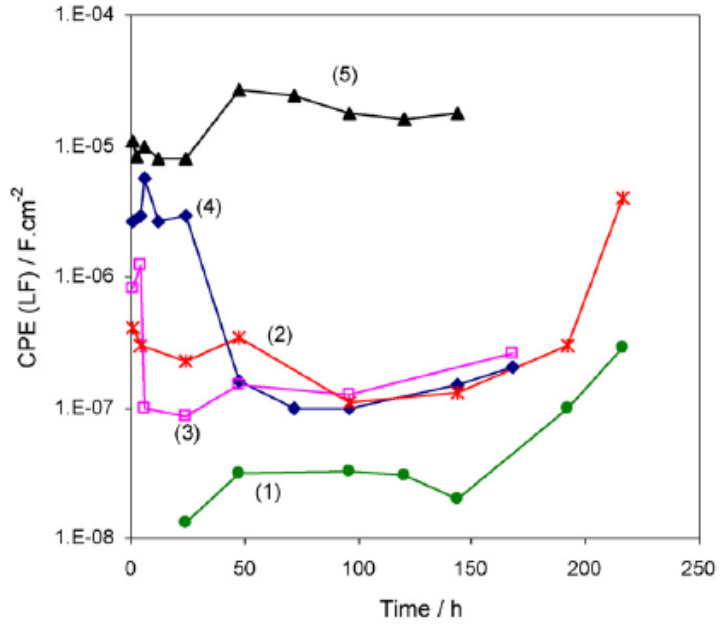

a)

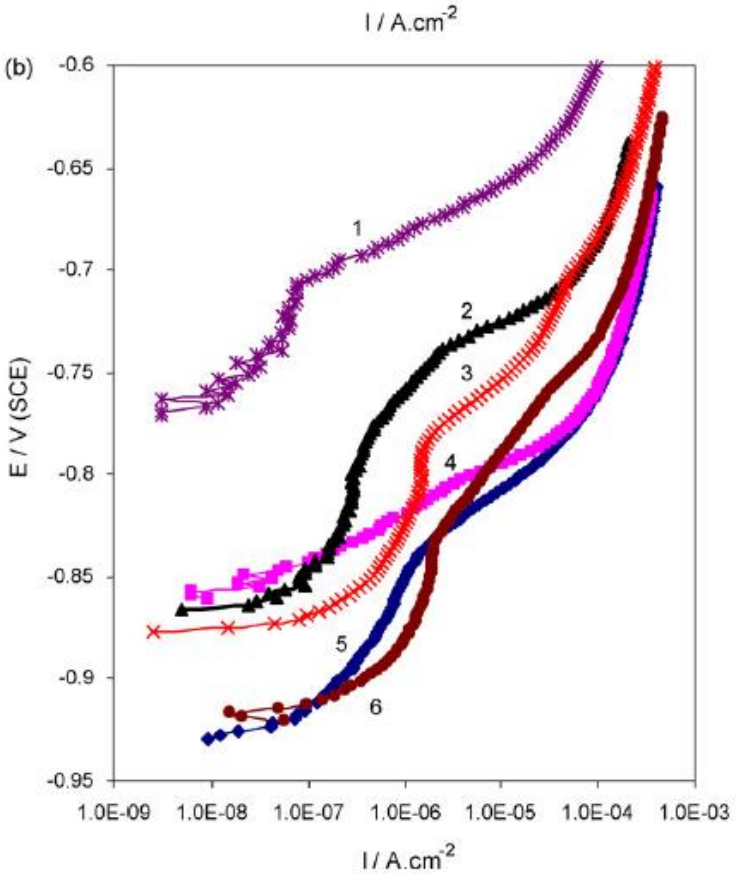

b)

Figure 3.5. a) Evolution of the low frequency fitting parameters obtained for the systems studied, b) Anodic polarisation curves. (1) CeO_2+Ce; (2) CeO_2; (3) SiO_2+Ce; (4) SiO_2; (5) blank matrix [82].

Corrosion resistance of polysiloxane-based coatings containing cerium salts and silica nanoparticles was evaluated by Santana et al. [79] using potentiodynamic polarisation tests and electrochemical impedance spectroscopy measurements. EIS curves are represented in Figure 3.6. After fit the results into an equivalent circuit, it was observed that the two types of coatings have a similar effective capacitance value at the beginning of immersion, which correspond to values of protective coatings. It was also observed that the resistance, both oxide resistance and coating resistance, decrease in time for both coatings due to the ingress of electrolyte through the defects.

In a study carried out by Shi et. a [125], was found that the introduction of silica nanoparticles into an epoxy resin improved the corrosion protection, which they attributed to an improved pore network and the tendency of silica to occupy possible gaps in the coating together with an increased cross-linking density. Improvement on the corrosion protection via the addition of silica nanoparticles was also found by Suegama et al. [126, 127]. They found that there is a critical amount of silica nanoparticles that can be added and will enhance the anticorrosion behaviour of a silane coating, however an excess can led to more porous and defective coating decreasing the corrosion protection [126, 127].

This is showed in Figure 3.7 where the silane filled with 300 ppm of silica presented a higher open circuit potential, indicating a more noble character than the rest of samples, but also in Figure 3.8 where again this formulation showed the highest impedance result, followed by the silane filled with 200

ppm of silica. However, an increase above 300 ppm showed decreased impedance and lower corrosion protection [126].

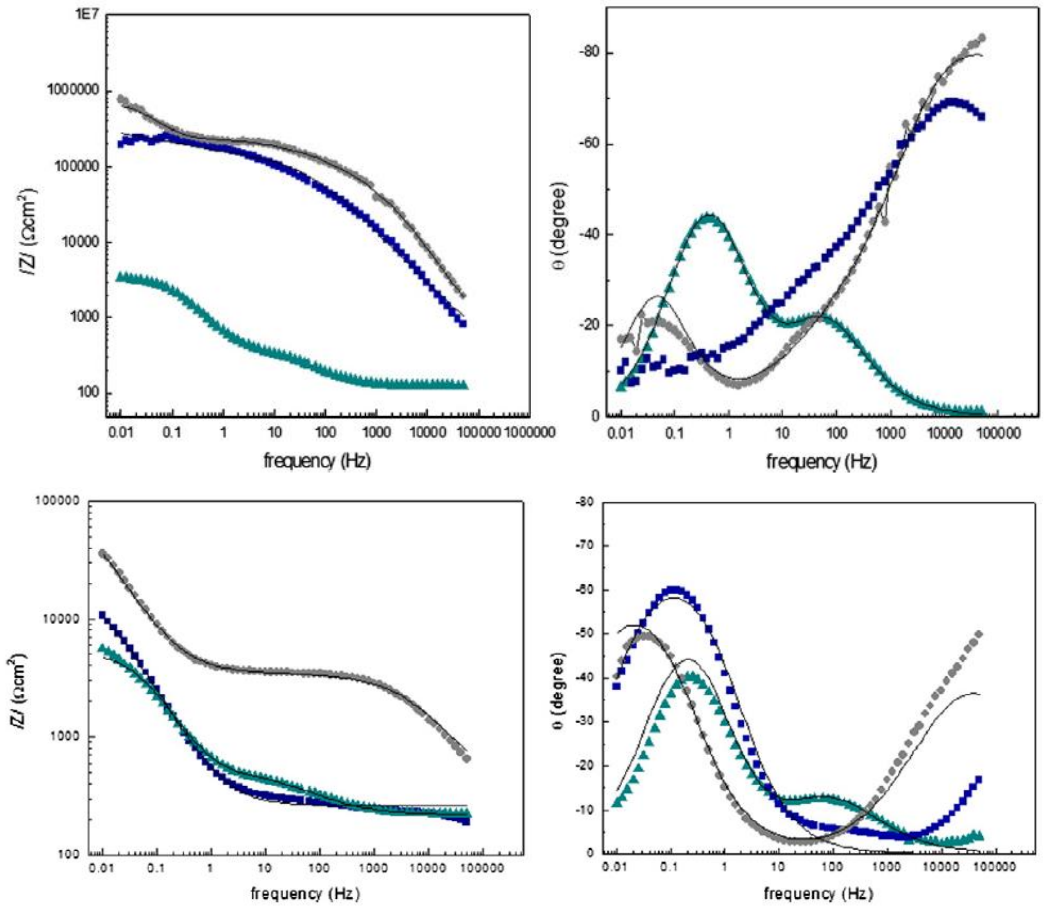

Figure 2.6. EIS curves for coating with lower silica amount (■), coating with higher silica amount (●) and the bare material (▲). Above: immediately after immersion, below: after 24h immersion in NaCl [79].

Same behaviour was shown in a work carried out by Peres et al. [130], where again an optimum amount of silica added into a TEOS-GPTMS led to enhanced corrosion resistant formulations while exceeding that limit made the anticorrosion performance of the coatings decrease.

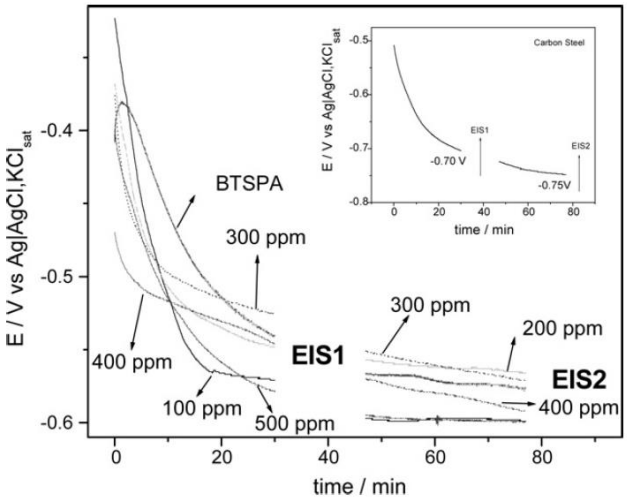

Figure 3.7. OCP values for the steel substrate, silane (BTSPA) sample and silane filled with five different silica nanoparticles concentrations recorded in aerated and unstirred 0.1 mol/L NaCl solution [126].

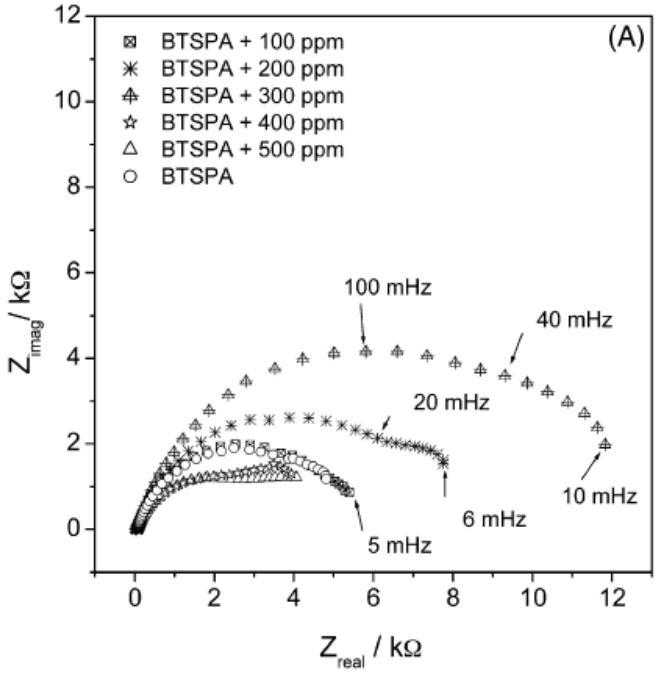

Figure 3.8. Nyquist plots for carbon steel coating with a pure silane coating (BTSPA) and a silane coating filled with five different silica nanoparticle concentrations after 30 min in 0.1 mol/L NaCl solution [126].

Many other studies have been shown to enhance corrosion protection of coatings via the addition of silica nanoparticles. However, not as much effort has been put on understanding the impact of functionalised silica into coating formulations to improve corrosion protection and durability of coatings. Some works using surface treated silica are described below.

In the work carried out by Dolatzadeh et al. [134], where they studied the incorporation of various organosilane-modified silica nanoparticles into a polyurethane resin, was found that the modified nanoparticles generally decreases the corrosion rate, irrespective of the type. They also found that increasing the loading of the nanofillers generally reduce the corrosion rate even further [134]. Similar behaviour was observed in a study carried out by Seo et al. [140] on multi-functional hybrid coatings with modified silica nanoparticles on iron where it was shown that these coatings had excellent corrosion protection.

A study on the anticorrosion performance of epoxy coatings with different functionalised silica nanoparticles percentages, ranging from 0 to 8 wt.% on steel substrate, was carried out by Ghanbari et al. [139]. Usually when one capacitive arc is observed this means that coating behaviour is dominated by the coating capacitance at high frequencies and coating resistance at low frequencies. When increasing immersion time, the resistance used to decrease due to water penetration and movement of species through the coating. If a second semicircle appears in the EIS spectra, this suggest that electrochemical reactions are progressing and the corrosion rate is increasing. In this study, EIS spectra (Figure 3.9) shows how when increasing immersion time, a second semicircle appears in the diagrams for

all the coatings except for the one containing 4% of silica nanoparticles which would mean that at this percentage of silica nanoparticle incorporation, the barrier properties of the coatings were improved enhancing the corrosion resistance of epoxy coating. A loading level of silica nanoparticles up to 4-6 wt.% enhanced the corrosion resistance of the epoxy coating via increasing its barrier properties. However, a further increase in loading led to nanoparticles agglomeration which decreased the corrosion protection ability of these coatings [139].

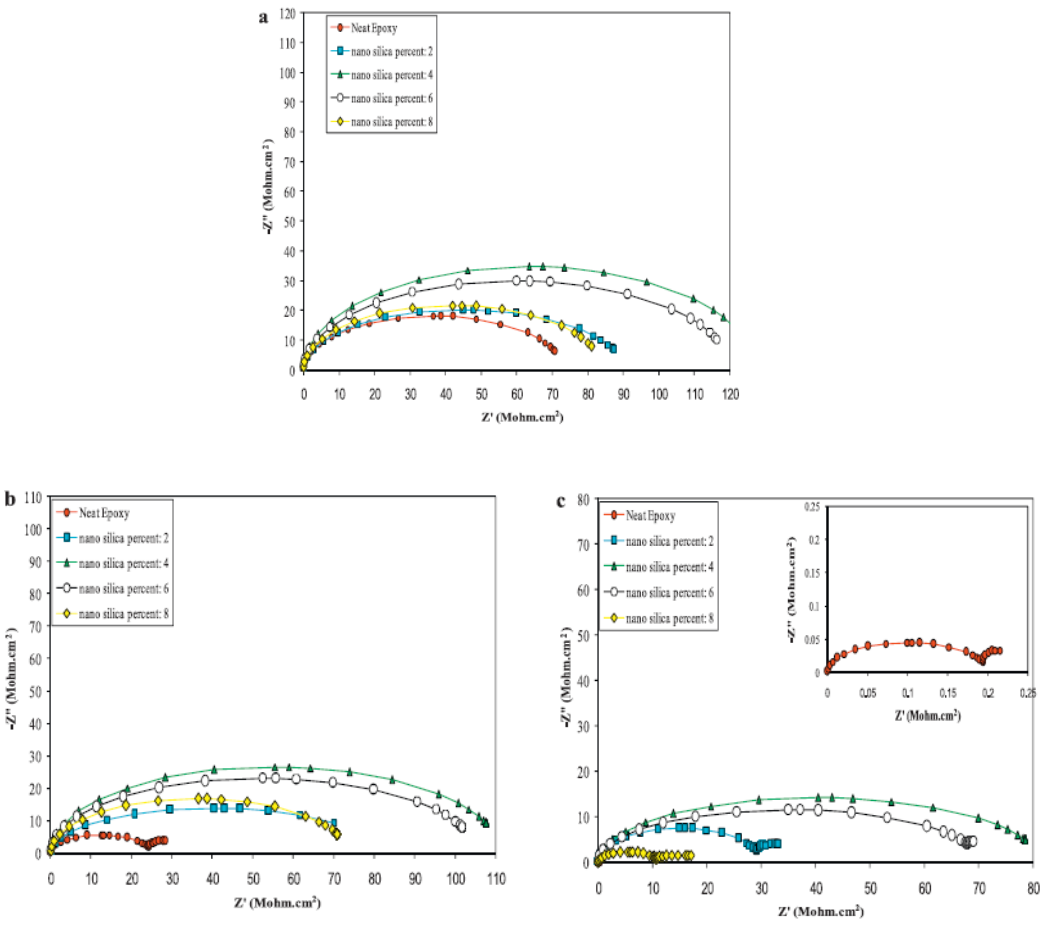

Figure 3.9. EIS spectra of the epoxy coatings containing different nano-silica percentage after: a) 15 days, b) 30 days and c) 60 days immersion me in 3.5 wt% NaCl solution [139].

Deflorian et al. [136] studied the influence of two precursors, MTES and MPTMS, in the preparation of functionalised silica and its incorporation in a polymeric matrix. They found that an appropriate functionalisation of silica is needed to obtain the best performances. The particles which led to improvements of the barrier properties against water and ions permeation with respect to the unfilled resin where the particles which had a 25 mol% MPTMS [136].

3.7 Silica impact on mechanical durability

The incorporation of nanoparticles into a polymer matrix can lead to improved mechanical properties. However, obtaining a uniform dispersion of nanoparticles within the matrix is crucial since as happens with coating microstructure and corrosion performance, the amount of nanoparticles added will impact on its mechanical properties. Wang et al. [141] found that hardness and stiffness were improved with addition of silica into an epoxy matrix and that a proper amount, in this case 8 vol.%, improved scratch resistance and mechanical properties of the epoxy resin.

However, if the amount of nanoparticles exceeds a critical value, nanoparticles will tend to agglomerate which results in the deterioration of the mechanical properties of the coatings: decrease in Young's modulus and wear resistance [142].

One of the most important factors affecting mechanical properties of nanoenabled coatings is the interface between the nanoparticles and the polymer matrix but also the adhesion between the coating and the substrate since this is important when looking at improving the properties of a coating

[143]. Malzbenger et al. [128] studied the mechanical properties of silica-filled sol-gel coatings and found that an increase of filler content led to larger elastic modulus of the coatings. However the hardness increased up to a volume fraction of about 0.58 and then decreased, which they associated it with revealed porosity inside the coating. Regarding the fracture toughness, they found an increase in toughness for the larger volume fractions [128]. Increased elastic modulus, hardness and fracture toughness with increased silica filler has been also reported by Wu et al. [144].

Ballare et al. [129] found that the introduction of silica nanoparticles into a sol-gel hybrid coating enhanced mechanical properties, being the coatings with the highest amount of silica (30 wt.%) presenting the highest elastic modulus and hardness. This is in line with others, where they found that hardness of coatings were proportional to silica filler content [145].

The grafting of nanosized SiO_2 (average particle size 9 nm) with acrylamide and the dispersion in an epoxy matrix via stirring and sonification yielded composites with improved wear properties and reduced friction coefficient relative to the pure polymer and a composite with the untreated SiO_2 even at low nanofiller content (~2 vol %) [146].

Bauer et al. [147] found that the modification of silica and alumina particles led to transparent reinforced polyacrylates with improved scratch and abrasion resistance and increased modulus and heat resistance.

Rostami et al. [135] found that the introduction of amino silane treated silica into a polyurethane resin improved the mechanical performance of the films due to stronger particle-matrix interaction. The mechanical integrity of the

films was improved for the nanosilica with higher grafting amount and decreased with decreasing grafting amount being the resin with untreated silica and the resin itself the samples with lower mechanical properties [135].

Eslami-Farsami et al. [124] used GPTMS to functionalise the surface of silica nanoparticles and incorporate them into E-glass/epoxy panels. They study the flexural response of the samples and reported an effective impact on the flexural properties (stiffness, maximum load and energy absorption) with an addition of 3 wt.% functionalised nanoparticles.

Douce et al. [132] studied the introduction of silica nanoparticles with different sizes and different surface modification into a polysiloxane coating. They found that adding silica increased the Young's modulus but decreases scratch resistance. An increase in filler size also led to large decrease in scratch resistance. Although they found that matrix-filler interactions were weaker for the modified silica, this had no significant effect on Young's modulus, but radically affect the scratch resistance [132].

Bauer et al. [147] studied the modification of nano-sized silica with different trialkoxysilanes as fillers for polymer reinforcement and found that the nanocomposites containing up to 35 wt.% silica presented improved hardness and surface mechanical properties, such as scratch and abrasion resistance, compared with the pure polymers.

As can be observed from literature, authors tend to use hardness to define the wear resistance. However, it has been also shown that the hardness to elastic modulus ratio, H/E, can be a good indicative of wear resistance [148]. This ratio, also called brittleness index, can be used as an indicator of

coating durability since this parameter describes the elastic strain to failure capability of a material [148].

Ranking of materials using this ratio has been recognised by several authors to be in close agreement to the ranking in terms of wear [148]. Furthermore, the fracture toughness can be also described by means of the measured hardness and elastic modulus (which will be further explained in section 8.4). There are no many studies using this ratio that can be used for comparison here, however and thinking that this could be exploited in the future, a couple of them has been put here as examples but also this would be also developed through the work in this thesis.

Hu et al. [149] studied the hardness and elastic modulus profiles of some hybrid coatings (without nanoparticles) and they found that mechanical properties were improved with higher hardness while keeping the brittleness index low.

Sowntharya et al. [133] studied the addition of acrylic functionalised silica into a hybrid sol-gel matrix and they found that an increased weight ratio of nanoparticles to the sol of 1 exhibited the maximum hardness. However they compared with an in-situ generation of –Si-O-Si network which was found to have higher abrasion and scratch resistance [133]. They used the brittleness index ratio to rank the materials in their study, where they found that a coating with high hardness and low brittleness index will have good mechanical properties.

3.8 Conclusions

This chapter has tried to summarise the work carried out on understanding the impact of nanoparticles, and in particular silica nanoparticles into polymer resins, on coating microstructure, corrosion performance and mechanical durability.

Sol-gel based coatings despite decades of research and many potential advantages have not been as widely adopted as they could. Many challenges remain in the commercialisation of these highly inorganic coatings with reservations based on reproducibility and the ability to control sol-gel processing. Improving functional performance requires both understanding and implementation of the technique. The establishment of a clearer understanding of the structure-property relationships of sol-gel based nanocomposite materials using nanoadditives to enhance the performance is needed. A materials by design approach can be adopted to provide new mechanistic insights explaining the improved properties of the siloxane coatings after the addition of suitably functionalised nanoparticles.

The surface of nanoparticles can be functionalised with different coupling agents and at different levels. The degree of functionalisation will affect nanoparticle structure and properties and impact on the final coating performance. Thus, it is important to understand how the functionalisation level will impact on coating microstructure and in what way the final performance will be affected.

The identification of the key design rules governing the behaviour of these nanoenabled coatings will support the development of a knowledge based

selection methodology for future materials design and manufacturing, reducing the time to introduce new materials and helping to expand commercialisation gradually.

This PhD work aims to provide a better understanding of the influence of silica on coating performance and contribute to the development of novel coating technologies in the future for the protection and extended durability of steel infrastructure.

Chapter 4. Evaluation methodology

4.1 Overview

In this chapter different techniques used to characterise the coating films synthesised in this study are described. The evaluation methodology analysis is focused not just on the coating microstructure and surface but also on the electrochemical and mechanical characterisation of the coatings, which provide the ground rules to relate structural aspects and properties for this family of coatings. An illustrative description of the evaluation methodology is depicted in Figure 4.1.

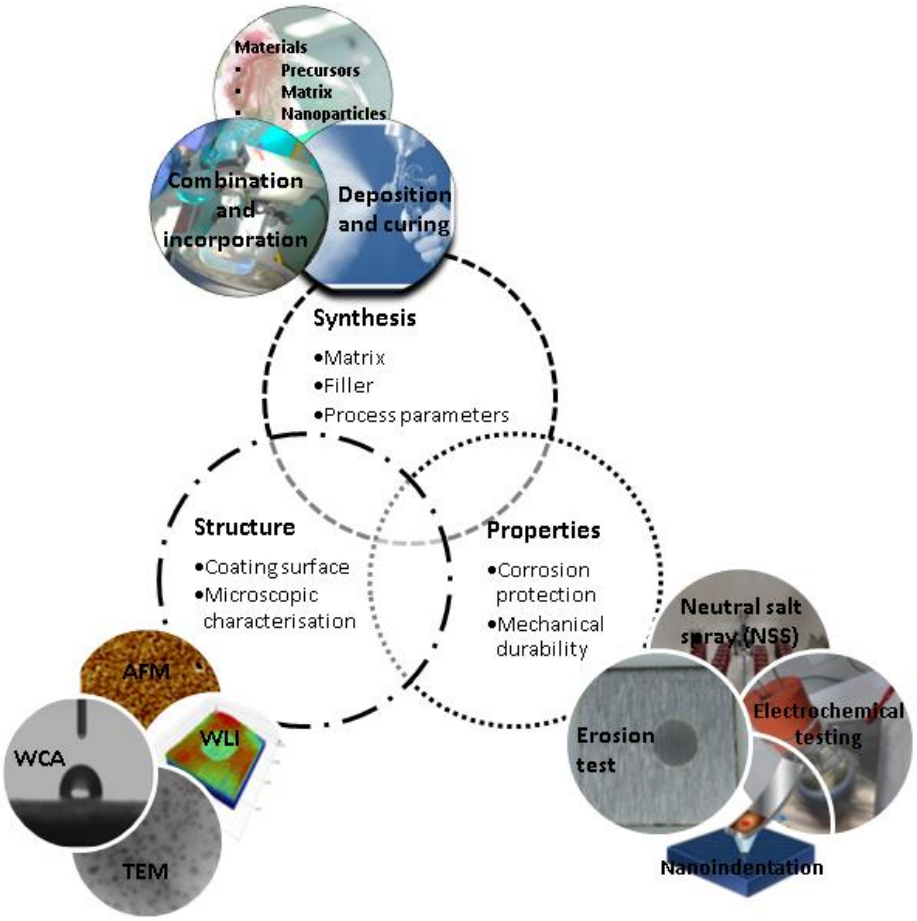

Figure 4.1. Evaluation methodology.

4.2 Coating microstructure characterisation

Characterisation of the coating microstructure and topography was undertaken using a variety of techniques to allow identification of the key features of the coatings and, critically, differences between them.

4.2.1 Thickness measurement

The thickness of coatings is an important parameter which is related to the properties of the films. The method chosen to measure it should be reliable, accurate and simple. Thickness can be measured using either destructive or non-destructive coating thickness measurements. The non-destructive measurements can be carried out on either magnetic or non-magnetic surfaces. Electromagnetic induction is used for non-magnetic coatings on ferrous substrates whilst the eddy current principle is used for non-conductive coatings.

For this study an Elcometer 456 coating thickness gauge was used to measure the dry film thickness on all coating formulations, although Scanning Electron Microscopy (SEM) was also used to look at the cross-sectional areas to assure validity and accuracy with the thickness gauge. The Elcometer 456 uses the Eddy current principle. The uncertainty of measurement is ± 1 µm up to 1500 µm, ± 2 µm 1500-4000 µm, and ± 4 µm up to 4000 µm (with an accuracy of ± 1 %). Since this work was carried out with thicknesses up to 50 µm, it could be said that the uncertainty of any measurement would not be higher than ± 1 µm. This technique works by placing a single coil carrying low voltage current onto the coating specimen, so small currents are induced in opposition to the original field. The field

causes currents to circulate in the substrate which in turn have associated magnetic fields. These fields reduce the voltage across the coil and the voltage variation is dependent upon the distance from the sample and can be related to coating thickness. It is a non-destructive technique which enables to take individual dry film thickness readings quickly without damaging the coating.

For reproducibility, at least five measurements were made at five different locations on each sample. The average and standard deviation of the film thickness for each of the tested coatings were calculated to ensure consistency across the coated surface.

4.2.2 Dynamic Light Scattering

Dynamic Light Scattering (DLS) is a well-established technique for measuring the size and size distribution of molecules and particles typically in the submicron region. It measures the diffusion coefficients of nanoparticles in solution by quantifying dynamic fluctuations in scattered light so the sizes are calculated from the diffusion coefficients in terms of hydrodynamic ratios or diameters.

$$d(H) = \frac{\kappa T}{3\pi\eta D} \qquad (4.1)$$

where d(H) is the hydrodynamic diameter (m), D is the translational diffusion coefficient (m^2/s), κ is the Boltzmann's constant ($1.38 \cdot 10^{-23}$ J/K), T is the absolute temperature (K) and η is the viscosity (Ns/m^2). The temperature needs to be known and stable because knowledge of the viscosity is required.

The diameter obtained with this technique is the diameter of a sphere which has the same translational diffusion coefficient as the particle. Therefore, it will depend not only on the size of the particle core but also on any surface structure, and the concentration and type of ions in the medium.

Any change to the surface of a particle can affect the diffusion velocity which will change the apparent size of the particle. The larger the particle, the slower the movement of particles will be.

The size information that can be obtained from DLS are the mean size (Z-average diameter), an estimate of the width of the distribution (called the polydispersity index), and the distribution of particle sizes. The size distribution obtained as the relative intensity of light scattered by particles in various sizes is known as intensity size distribution. Other size distributions such as volume distribution and number distribution can be also obtained.

For this study, particle sizes and sizes distribution were measured using Malvern Zetasizer Nano ZEN1600 (Malvern, UK).

4.2.3 Contact angle

The contact angle is defined as the angle formed by the intersection of the liquid-solid interface and the liquid-vapour interface. It is a measure of the wettability of a solid by a liquid, and is the angle between the calculated drop shape function and the sample surface (projection in which in Figure 4.2 is referred to as the baseline).

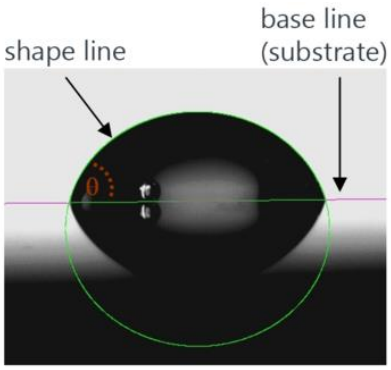

Figure 4.2. Sessile drop for contact angle measurements [150].

Interest in this work is focused on corrosion protection and coating durability, and water is one of the factors that has a major influence on coating degradation. Due to this and since water is the most commonly used liquid used to classify the wettability of solids, the water contact angle was measured to assess coating wettability and water repellence.

According to wetting abilities, a surface with water contact angle less than 90° indicates favourable wetting, while contact angles greater than 90° means that the wetting is unfavourable, meaning that the fluid (in this case, water) will minimize its contact with the surface. If the contact angle is 0° this means complete wetting (spreading), and if this is greater than 150° showing almost no contact between the water drop and the surface, this means that this is a superhydrophobic surface.

The Water Contact Angle (WCA) was determined using the Drop Shape Analyzer – DSA 100 contact angle instrument (Figure 4.3). Sessile drop static contact angles of deionised water were measured in order to provide information about repellency characteristic of coatings. At least three measurements were performed at randomly chosen positions to obtain the mean value of contact angle of each sample on the substrate surface.

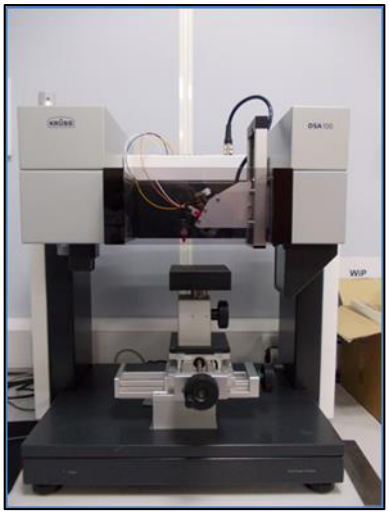

Figure 4.3. Drop shape analyser.

4.2.3 Cross-cut tape test

This test is one of the most commonly used to assess the adhesion of the coatings. It is fast, cheap and easy to perform. The standard followed to rate adhesion by tape test was the ASTM D3359 - 09e2. The procedure is to place the cutting edge on the sample and press down ensuring the cut through the coating to the surface of the substrate. Then, the cutting edge is place on the sample at a 90° angle to the first cut, creating a lattice pattern on the coating, as pictured in Figure 4.4.

Detached flakes of coating are removed by brushing with a soft brush and pressure sensitive tape (Elcometer 99 cross hatch coating adhesion test tape, 25 mm wide semitransparent pressure-sensitive tape, part number T9998894, used in accordance with ASTM D3559) is applied over the crosshatch cut.

Tape is smoothed into place to ensure good adhesion between the tape and the coating and within 90 seconds (± 30 seconds) is removed by pulling it off rapidly.

Adhesion of the coating to the substrate was measured by the Elcometer 1542 cross hatch adhesion tester following ASTM D3359 - 09e2, which specifies a procedure for assessing the adhesion resistance between coatings and substrates when a lattice pattern is cut into the coating.

The adhesion then is rated from 5B (excellent adhesion with no peeling or removal of the coating) to 0B (very poor adhesion, with coating removal greater than 65%).

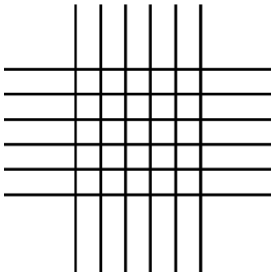

Figure 4.4. Cross-cut tape test lattice pattern.

4.2.4 Atomic Force Microscopy (AFM)

The Atomic Force Microscope (AFM) was used to characterise the coating microstructure and to measure surface roughness of the samples.

The AFM used in this study is showed in Figure 4.5 and was a Dimension Icon (Bruker, Germany). Coating samples were cut in 2 x 1 cm^2 and then placed on the positioning unit. The AFM was used operating in Peakforce Quantitative Nano-mechanical tapping mode using a silicon tip on a nitride cantilever probe (Bruker, nominal spring constant 0.4974 N/m, nominal resonance frequency of 70 kHz).

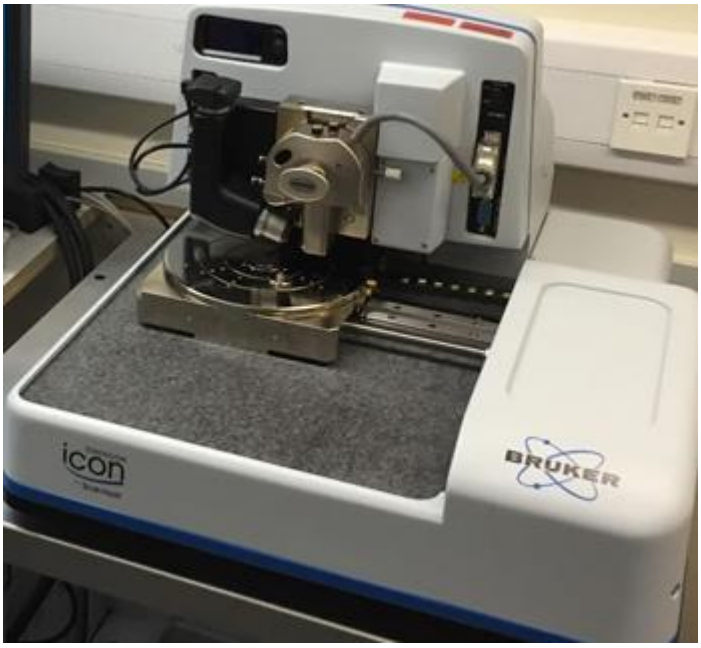

Figure 4.5. AFM device used for this study.

The Atomic Force Microscope (AFM) probes the surface of a sample with a sharp tip, which is located at the free end of a cantilever. The forces between the tip and sample surface cause the cantilever to bend or deflect. The cantilever deflection is then measured by a detector and with this a computer generates a map or surface topography. The basic setup is described in Figure 4.6.a).

The AFM operates by measuring the attractive or repulsive forces between the tip and the sample. AFM can be used in several modes depending on the interaction forces between the probe-sample distance. The three modes are: contact mode, tapping mode and non-contact mode. Moving from contact mode to non-contact mode as the distance increases (Figure 4.6.b). Contact mode imaging is heavily influenced by frictional and adhesive forces, which can damage samples and distort image data. Non-contact mode generally provides low resolution and can be hampered by any

contaminant layer interfering with oscillation. And tapping mode overcomes problems associated with friction, adhesion and contaminants by intermittently placing the tip in contact with the surface and oscillating with sufficient amplitude. Therefore, tapping mode allows high resolution topographic imaging of samples surfaces without inducing damage.

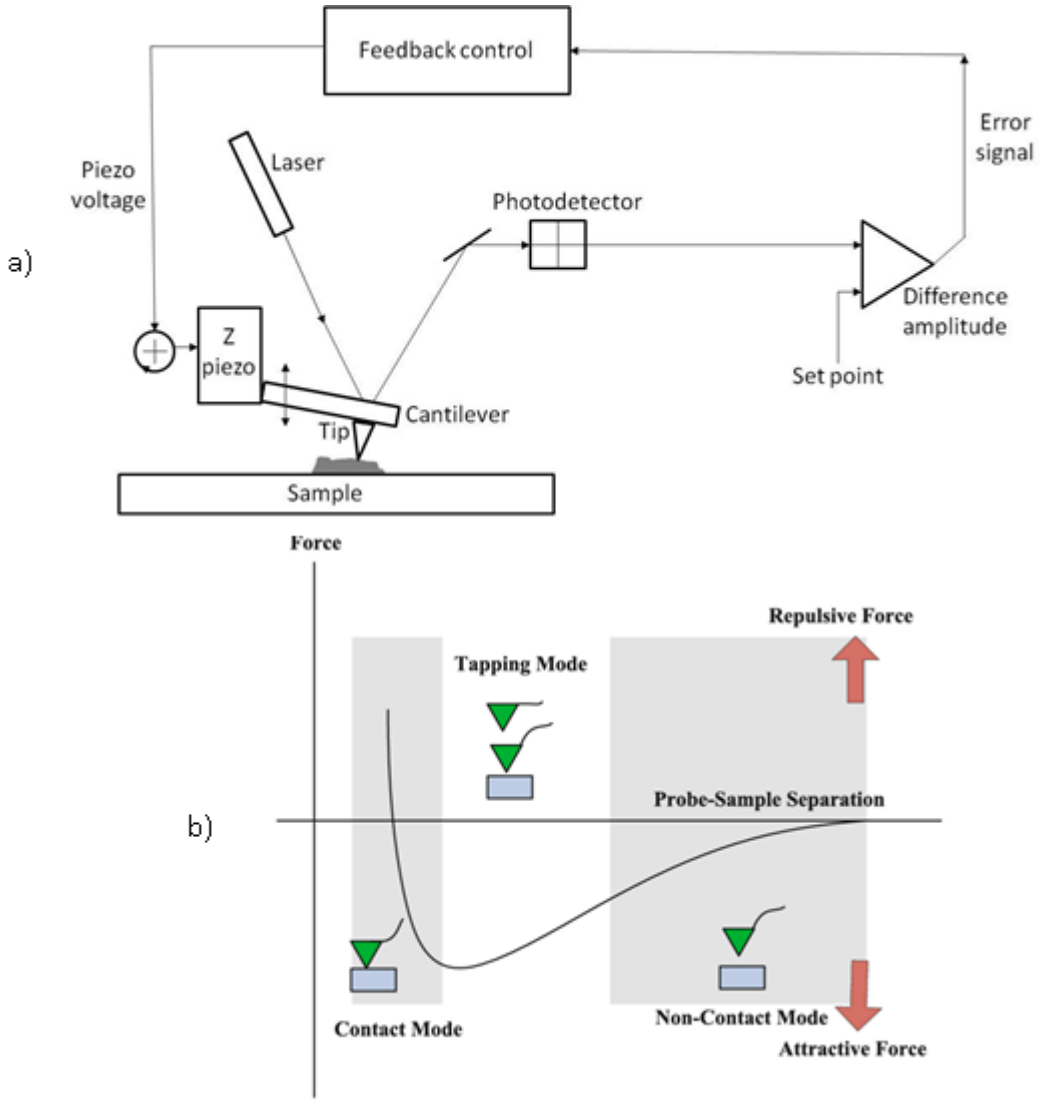

Figure 4.6. AFM basic set up (a) and forces according to the distance sample-probe (b) [151, 152].

4.2.5 White Light Interferometry (WLI)

The White Light Interferometer is a non-contact optical instrument capable of very sensitive 3D surface profilometry and surface roughness characterisation. It is a convenient and fast technique, with no need of sample preparation. The interferometer divides a beam of light exiting a single source into two beams. The object beam which reflects from the sample and the reference beam which reflects off a reference mirror. These two beams are then recombined by the beamsplitter and imaged by a CCD camera to create an interference pattern.

For this work, 3D White Light Interferometer (WLI, Bruker Contour GT-K 3D Optical Microscope) was used to record three-dimensional surface topographies of coatings.

4.2.6 Microscopy

4.2.6.1 Differential Interference Contrast (DIC)

Differential Interference Contrast (DIC) microscopy is an optical microscopy technique used to gain images of unstained or transparent specimens. DIC works on the interferometry principle converting gradients in specimen optical path length into amplitude differences that can be visualized. The optical path difference is defined by the product of the refractive index difference and the thickness between two points on the optical path. Image formation takes place due to phase shift differences of adjacent points and then, depending on the refracting indexes or thickness gradients, the details of the specimen are imagined.

For this work, Differential Interference Contrast microscopy (DIC, Nikon Optiphot Microscope) was used to study the surface of the coating samples and gather information about small scale features in the coatings.

4.2.6.2 Scanning electron microscope (SEM)

The Scanning Electron Microscope (SEM) is an instrument used to observe the morphology of samples at higher magnification and higher resolution compared to an optical microscope. The SEM works by scanning a focused beam of electrons on the surface of a sample. Signals derived from electron-sample interactions contain information about the surface topography and composition of the sample. The data collected over the selected surface area of the sample is used to generate the 2-dimensional image.

Topography of the samples was observed with a Carl Zeiss EVOMA 15 VP SEM. As preparation, samples were coated with gold in order to improve electrical conductivity.

4.2.6.3 Focused Ion Beam – Transmission Electron Microscopy (FIB-TEM)

The Focused Ion Beam (FIB) was used to prepare the samples for Transmission Electron Microscopy (TEM). FIB operates in a similar way to SEM but uses a focused beam of ions, usually gallium (Ga+), instead of a beam of electrons. FIB can be operated for imaging (at low beam) or for sputtering or milling (at high beam). By carefully controlling the energy and intensity of the ion beam, it is possible to produce minute components or to remove unwanted material. For the propose of this work, FIB was used to

produce minute coating sample which were further thinner to the required dimension to be later on suspended on a grid and imaged under the TEM.

Transmission Electron Microscopy (TEM) is an electron microscopy technique in which a beam of electrons is transmitted through a very thin specimen. The image is formed from the electron-sample interactions as the beam is transmitted through the specimen. TEM can be used to obtain higher magnification and resolution images than an optical microscope and a scanning electron microscope.

The FIB preparation was carried out using the FEI Nova 200 Nano Lab High Resolution Field Emission Gun Scanning Electron Microscope (FEGSEM) with precise Focused Ion Beam (FIB). The TEM used was a FEGTEM Field Emission Gun TEM/STEM (FEI Company, Hillsbrow Oregon, USA). The instrument was fitted with HAADF detector and Oxford instrument INCA 350 EDX system and 80 mm X-max SDD detector and Gatan Orius SC600A CCD camera.

4.3 Corrosion testing

4.3.1 Neutral Salt Spray (NSS)

The Neutral Salt Spray (NSS) test is an accelerated corrosion test whose purpose is trying to duplicate in the laboratory in a quick way the corrosion performance that a product would have in the field. Although this type of test has been used for many years, it is difficult to correlate the results with the performance in real environment. However, despite of that, this test is widely used in the literature or in customer specifications.

The NSS test was used in this work as a rapid screening test to evaluate and rank the corrosion protection of the coatings. The test was run in a salt spray chamber (Ascott CC1000ip, Ascott, UK) following the ASTM B 117 Standard Practice for Operating Salt Spray (Fog) Apparatus.

The salt spray cabinet can be seen in Figure 4.7. The coating samples were exposed to a salt fog atmosphere generated by spraying a 5 wt.% aqueous NaCl solution at a constant temperature of 35 ± 2 °C. Prior to exposure, the back and the edges of the samples were covered with lacquer. Specimens were inspected and imaged after exposure to assess performance.

Figure 4.7. Coating samples in the salt spray cabinet.

4.3.2 Electrochemical characterisation

A typical electrochemical corrosion test cell is formed by: the metal specimen (called working electrode), the solution in which the specimen is to be tested, the reference electrode which is in contact with the solution via the bridge tube (a compartment filled with test solution that provides optimum positioning of the reference electrode) and a counter electrode used to supply the current flowing at the working electrode during the test.

The most common electrochemical corrosion measurement device is a potentiostat. A potentiostat performs two main functions: it controls the potential difference between the reference electrode and the working electrode and measures the current flow between the working electrode and the counter electrode.

The setup used to perform the electrochemical characterisation is shown in Figure 4.8. The testing was carried out using a conventional three-electrode cell with 3.5 wt.% NaCl electrolyte at ambient conditions. The working electrode was the coated sample with an exposed area 15.2 cm^2, the reference electrode was Ag/AgCl (4 M KCl) type and the counter electrode was a Pt/Ti wire. The corrosion potential, electrochemical impedance spectroscopy (EIS) and polarisation curves were measured using either an Ivium pocketSTAT (Ivium, Netherlands) or Bio-Logic equipment.

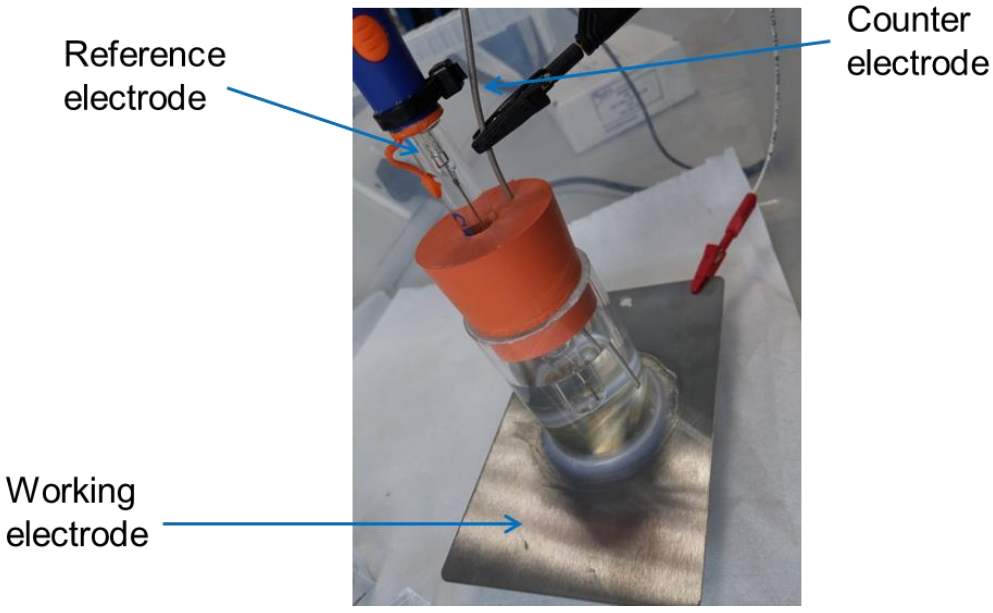

Figure 4.8. Setup used to carry out electrochemical testing.

4.3.2.1 Open-Circuit Potential (OCP)

Open Circuit Potential (OCP) is the difference existing in electrochemical potential between a material and a stable reference potential submerged in an electrolyte, when no electrical current flows between them.

It is the potential in a working electrode comparative to the reference electrode when there is no external current or potential existing in the cell. Once a potential relative to the open circuit is made present, the entire system gauges the potential of the open circuit prior to turning on the cell. And this will be followed by the application of potential relative to the existing measurement.

4.3.2.2 Electrochemical Impedance Spectroscopy (EIS)

Electrochemical Impedance Spectroscopy (EIS) has been commonly used for studying performance and deterioration of coatings. The impedance of a coating is its electrical resistance, as measured by alternating current (AC). EIS uses a range of low magnitude polarising voltages, cycling from peak anodic to cathodic magnitudes, and vice versa, using a spectrum of AC voltage frequencies. Resistance and capacitance values are obtained from each frequency, and these quantities can provide information on corrosion behaviour and rates, diffusion, and coating properties.

The ability of EIS spectra to measure separate processes occurring on the same electrode, is perhaps one of the most powerful features of EIS corrosion measurements. Parameters obtained from EIS spectra are used to: characterise corrosion and coating behaviour, and estimate or predict

equipment service life. Parameters can be extracted either graphically, or through the use of computer software.

However, the most technically rigorous way to obtain parameters that characterise corrosion or coating behaviour is to build a mathematical equation from test electrode corrosion reaction kinetics and fit this equation around experimental EIS data. To do this, EIS parameters can be estimated by using mathematical equations for simple electrical circuits. Once the electrical circuit is known, software can be used to regress an equation around experimental data, by iteratively adjusting parameters until the closest fit of an equation to experimental data is obtained.

Corrosion processes under coatings have their own response in an impedance measurement, so if corrosion occurs, electrons are transferred between molecules and metals in the corroding system. This transfer of electrons can be studied with the help of the impedance Z as the ratio between a small sinusoidal potential perturbation, $V = V_0 \sin(\omega t)$, and the current resulting from this perturbation, $I = I_0 \sin(\omega t + \varphi)$, as [153]:

$$Z = \frac{V_0 \sin(\omega t)}{I_0 \sin(\omega t + \varphi)} \qquad (4.2)$$

The impedance, Z, is frequency dependent and is characteristic of the system that is measured. Z is usually measured for many frequencies in order to create an impedance spectrum. There are also non-electrochemical parameters contributing to the total impedance (like the resistance of the electrolyte and dielectric behaviour of an intact coating). The impedance modulus $|Z|$ can be expressed using complex number:

$$|Z| = Z_{re} + Z_{im} \qquad (4.3)$$

where Z_{re} and Z_{im} are the real part and the imaginary part of the impedance, respectively.

If the reaction mechanism is known, a transfer function may be calculated. Having this, a physical model is then transformed into an equivalent electrical circuit. One difficult part is that more than one circuit is possible and circuits might also be rewritten in a different configuration without changing the response, which makes more difficult the interpretation in terms of chemical and physical parameters.

For bare metals and conversion coated metals, the interfacial capacitance is shorted at frequencies ranging from 5-20 kHz, while for coatings it can range from 50 to 100 kHz. Although electrochemical and diffusional processes, which are associated with corrosion, are detected at frequencies between 10 and 10^{-6} Hz, it is unusual to made the measurements below about 10^{-3} Hz due to instability of corroding metal surfaces [3]. The amplitude signal voltage is usually in the range of 5-50 mV, and is strongly dependent on the system studied. For scratched samples, a maximum value of 5 mV is usually used while for electrocoatings the classical value is 20 mV [154]. Thus, The EIS measurements in this work were performed at the OCP in the frequency range 100 kHz-0.001 Hz with perturbation amplitude of ± 20 mV. The data was analysed using ZView software (Scribner, USA). Constant phase elements (Q) were used in all fittings instead of capacitances considering the non-ideal capacitance behaviour of the system. The impedance of Q is defined by the following equation [155]:

$$Z(j\omega) = (Y_0)^{-1}(j\omega)^{-n} \qquad (4.4)$$

where, ω is the angular frequency, Y_0 is the Q constant and n is a value which represents the deviation from purely capacitive behaviour ($0 \leq n \leq 1$). In the case of an ideal resistor or capacitor, n = 0 or 1 respectively.

The equivalent circuit used in this work to fit the EIS data presents the following parameters: R_s, R_{corr}, Q_{dl}, R_{pore} and Q_{coat}, where R_s represents the solution resistance, R_{corr} is the resistance of the charge transfer, Q_{dl} is the capacitance of the double layer in the electrolyte solution interface, R_{pore} is the resistance of ion-conducting paths/pores in the coating, and Q_{coat} is the capacitance related to the intact part of the coatings. This will be further developed in chapter 7.

4.3.2.3 Polarisation curves

The potentiodynamic polarisation measurement methods enable the determination of instantaneous corrosion rates. The total polarisation curve in a corrosion system is composed from an anodic curve (metal oxidation) and a cathodic curve (reduction of an oxidant from solution).

At the corrosion potential, E_{corr}, anodic and cathodic rates are equal, meaning that the current is zero: all electrons generated by oxidation of the metal are consumed by oxidant reduction reaction on the same metal surface. This leads to the Tafel slopes extrapolation method. As shown in Figure 4.9, the intersection of Tafel lines with the point of coordinates gives E_{corr} and log i_{corr}, which can be used to estimate the corrosion penetration rate (mm/year):

$$CR = K_1 \frac{i_{corr}}{\rho} EW \qquad (4.5)$$

where the corrosion rate, CR, is given in mm/year, i_{corr} in μA/cm^2, K_1 is 3.27x10^{-3} mm g/μA cm year, ρ is the density in g/cm^3 and EW is the equivalent weight (Eq 4.6).

$$EW = \frac{molecular\ mass}{no.of\ electrons\ in\ ch\ arge\ transfer\ reaction} \qquad (4.6)$$

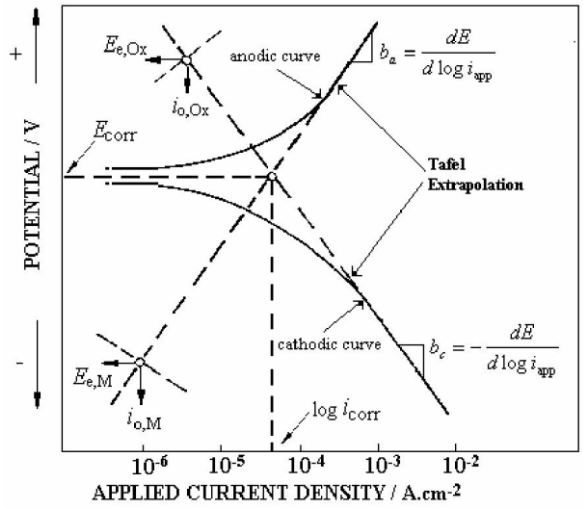

Figure 4.9. Polarisation curves (Tafel behaviour) [156].

Although the polarisation resistance, R_p, is usually obtained from linear polarisation resistance (± 10-20 mV vs OCP), it can be also obtained from Tafel slopes. To do this, the Stern-Geary constant B has to be calculated from anodic and cathodic slopes:

$$B = \frac{\beta_a \beta_c}{2.303\ (\beta_a + \beta_c)} \qquad (4.7)$$

where β_a and β_c are the slope of the anodic and cathodic Tafel reaction, respectively, in V/decade.

Once B is known, the polarisation resistance can be easily calculated from Eq 4.8:

$$R_p = \frac{B}{I_{corr}} \qquad (4.8)$$

4.4 Mechanical properties

4.4.1 Nanoindentation

One of the most widely methods used to measure the mechanical properties of coatings is nanoindentation, which is used to measure the elastic, plastic and time-dependent mechanical properties of many materials. The most common use of nanoindentation is for the measurement of hardness and elastic modulus, although it can be also used to measure other mechanical parameters such us creep parameters or residual stresses.

In nanoindentation tests, a specified load is applied to an indenter of known geometry in contact with the sample. The load is applied through the use of a hard indenter tip (usually diamond) and the penetration depth is measured. The shape and angle of the indenter tip and the penetration depth provide an indirect measurement of the contact area between the tip and the surface of the sample at a specific load, and as a result the hardness can be determined by [157]:

$$H = \frac{P_{max}}{A_c} \qquad (4.9)$$

where P_{max} is the maximum applied load and $A_{c\ is}$ the measured contact area.

Nanoindentation tests were performed using the Nano Test (Micro Materials Ltd., UK) on 1 cm x 1 cm sectioned flat samples, using a Berkovich diamond indenter tip. The indenter has an angle of 65.3° between the tip axis and the faces of a triangular pyramid. Before testing, the machine was calibrated according to ISO-14577. Indentation was load controlled to a maximum load of 1 mN. Experiments were performed at a constant loading and unloading rate equal to 0.01 mN/s and to a maximum load of 0.1 mN/s. The data was analysed using a power law fitting procedure by Oliver and Pharr [158], to derive the hardness and modulus values. Since this analytical technique just provides the reduced modulus, E_r, the following equation (4.10) was used to obtain the Young's modulus, E:

$$\frac{1}{E_r} = \frac{(1-\nu_i^2)}{E_i} + \frac{(1-\nu^2)}{E} \qquad (4.10)$$

where v_i is the indenter Poisson's ratio and has a value of 0.07, E_i is the indenter modulus and is equal to 1140 for diamond and v is the Poisson's ratio associated with the sol-gel coating which is estimated to be 0.225 [104, 128, 149].

4.4.2 Erosion tests

Erosion can be defined as the mechanical removal of material from a target by the cutting action of particles moving at high velocity. The factors that affect erosion are the solid particles (erodent), the target material and the nature of the fluid carrying the erodent. Mechanical properties of the material, such as hardness, fracture toughness or surface roughness, need to be considered since the erosion test result will depend on how mechanically durable the material is.

For this study, the candidate coatings have been exposed to sand erosion by using a submerged impingement jet [159]. The submerged impingement jet reservoir was filled with 50 L of water and 1000 mg/L of sand that was recirculated through a dual nozzle arrangement onto the flat specimens at an angle of 90°, positioned 5 mm from the exit of the nozzle. Sand particles were used with an average particle diameter of 250 µm. The solution was sparged with nitrogen (N_2) during the test and for a minimum of 12 hours prior to starting the test, to reduce the dissolved oxygen concentration in the solution to below 50 ppb. Tests were conducted at a free stream fluid flow velocity of 15 m/s and a temperature of 25 °C. The mass of the samples was measured before and after the test using a mass balance accurate to 1 µg. After the erosion tests, samples were profiled using a Bruker NPFLEX 3D optical profiler.

Chapter 5. Formulation development

5.1 Introduction

The literature review (chapter 3) describes the current state of the art technology on sol-gel coatings and nanoadditives, with more emphasis on understanding the impact of silica nanoparticles in corrosion performance and mechanical durability of coatings. This provides a framework for the development of new coatings with enhanced properties that could be used to protect steel structures. For this PhD the focus is on the marine environment. A literature survey of various nanoparticles used in coatings (as described in Chapters 2 and 3) was done to narrow the options to those which will be explored during this project. This information was used in order to try to develop a coating that meets current industrial practices and fulfils the standards and regulations in the marine industry.

In order to choose the optimal protection system, the following factors were taken into account to ensure the most economical and best technical solution was achieved:

Atmospheric corrosion is the primary form of corrosion for structures which are neither buried nor submerged in a liquid (usually water). The risk of atmospheric corrosion and the rate at which this corrosion occurs are primarily dependent on the relative humidity of where the steel structure is located, the risk of condensation and the concentration of corrosive pollutants, such as sulphur dioxide, acids, alkalis or salts [139].

Designing a coating system needs to account for the type of material used and its surface condition. In this case, carbon steel is the surface sought to be protected from corrosion. The surface preparation, the coating products used and the total system thickness will depend mainly on the constructional material to be protected [11].

To protect a metal substrate, surfaces tend to be coated with a multi-layer system: an anticorrosion primer, a mid-coat and a topcoat, as presented previously in Figure 2.4. Typical matrices used as mid-coat are epoxies, polyesters or silicones, while polyurethanes are one of the most frequent choices as topcoat (A more detailed review on matrices can be found in Chapter 2). With respect to the primer layers, the majority are zinc-rich compounds although some novel primers that are zinc-free are also recently being introduced to the market.

Some substrates normally used for the offshore marine environment are: LR grade A, S-355, S-420, S-460. Understanding that a proper selection of the substrate is one key step, mild steel Q-panels (grade S-46, A1008 steel) were selected for this project because of its availability and use as a matrix in many primers.

Once the substrate was selected, the next step was to make an appropriate selection of matrices taking into account the corrosive environment under study. Thus, the mid-coat as well as the topcoat contribute to the durability of the coating system. In the case of the primer, it is often zinc-loaded for galvanic protection although it may be possible to not use a zinc-based primer if the mid-coat alone can provide good corrosion protection via the use of nanoadditives. This basis will be the focus of study in this PhD.

Typically, in the marine industry, epoxy, silicones and epoxy-silicones are used as mid-coat and polyurethane for the aesthetic topcoat. Polysiloxanes as a matrix for primers are also well known. Hence, when there is a requirement for good adhesion and water resistance as well as high gloss and colour stability, epoxy and polyurethane systems are used in combination. The industry typically uses a polyurethane topcoat if they require an aesthetic enhancement, but this PhD will focus on improving corrosion resistance and mechanical durability via addition of nanoadditives to the mid-coat. Properties such as thermal stability, weather and UV resistance or colour stability among others, could help to make an anticorrosion coating suitable for this harsh environment. The use of a polysiloxane-based matrix can in some cases thus avoid the need for a polyurethane topcoat and hence was selected as the preferred matrix to be studied during this PhD.

Furthermore a proper literature search to-date on various nano-metal oxides and layered compounds was done in order to select the best candidates. Based on the criteria selection for offshore environment and the needed properties for this type of coatings, SiO_2 was selected as the preferred nanoparticle. Some of the reasons of this choice were the potential to increase barrier properties of the coatings (protection by reducing the diffusion of water and air from the environment to the substrate surface, preventing corrosion from happening) [47, 78], improve scratch resistance [71, 76] and because is one of the lowest cost metal oxides [74].

5.2 Materials

5.2.1 Polysiloxane-based matrix

The sol-gel process, which was previously described in Chapter 2, was used to create the polysiloxane-based matrix object of this study. Since there are many ways to create a sol-gel coating, the different precursors and methodology used is described below.

5.2.1.1 Precursors

As previously explained in chapter 2, the sol-gel process involves hydrolysis and condensation of metal alkoxides, which act as precursors for the formation of an inorganic polymer network. Typically this is done in the presence of acid or base as catalyst. For this work, tetraethylorthosilicate (TEOS), one of its widely available oligomeric forms (TES40) and 3-glycidoxypropyltrimethoxysilane (GPTMS) have been used as precursors to create the coating matrix. All precursors (TEOS, TES40 and GPTMS) were supplied by Silanes and Silicones Manufacturing, UK.

Using the sol-gel process, pure inorganic as well as inorganic-organic hybrid materials can be formulated. TEOS has been widely used as a precursor of silica for both pure inorganic and hybrid sol-gel coatings. On the contrary, and for the best of our knowledge, coatings using TES40 as precursor have not been commonly produced. On the other hand, GPTMS has two components: one non-hydrolysable glycidyl ligand (organic) and three hydrolysable methoxy ligands, with all ligands being attached to a central silicon atom.

The schematic description of the precursors is described in Figure 5.1.

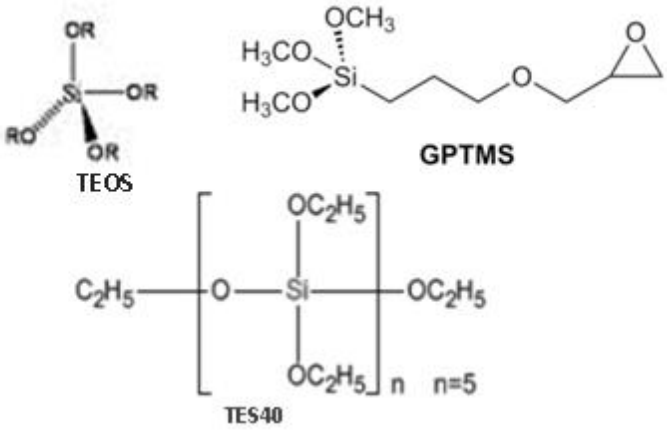

Figure 5.1. Schematic description of the precursors.

5.2.1.2 Synthesis

Pure inorganic polysiloxane coating

The first experiments started with a mix of TES40, solvent blend (isopropanol, methoxy propanol, Industrial Methylated Spirit or IMS), catalyst (acetic acid) and deionized water. It was noticed that the thickness of the coatings were less than 1 µm, which was not sufficient for the purpose of this work.

The next step was to change some reaction parameters in order to increase the coating thickness. These parameters can be: amount of water, amount of catalyst and type, and temperature and duration of reaction.

Some of the parameters changed included: the quantity of water, an increase in the time of reaction, the use of just one solvent (IMS) instead of the solvent blend, and an increase/decrease of the catalyst amount and type (HCl and acetic acid). In addition, some experiments were tried with TEOS (the monomeric form) while others were started with TES40 (the oligomeric form). However, all of these experiments didn't result in an increase of the

coating thickness meaning that when this precursor was used alone it was difficult to create a film-forming coating. Pure inorganic films with thickness higher than a few microns are usually not easily formed using sol-gel chemistry and are fragile and crack easily [160]. This led to a change in formulation via inclusion of a second silane, as explained below.

Hybrid coating

At this point, a second silane with a R- group was introduced to help with the formation of the matrix. This second silane was GPTMS. This precursor has two components: an organic group (non-hydrolysable glydicyl ligand) and an inorganic group (three hydrolysable methoxy ligands).

The combination of these precursors in the presence of acidic catalyst of HCl and with water and IMS as solvents was used to develop the coating matrix. Some of the formulations tried are described in Table 5.1. The addition of this second silane, GPTMS, in three different TES40/GPTMS molar ratios was studied (1:0.6, 1:0.9 and 1:1.8). This quite narrow range was taken in order to understand any small impact of the GPTMS on the final matrix formulation.

An increase in organic content introduced via the glycidoxy group led to an increase in coating thickness, being the TES40/GPTMS=1:1.8 the formulation that generated the thickest coating (measured as described in 4.1.1) with around 30 µm coating thickness, as can be seen from Table 5.2. This is in line with other investigations where it was found that an increase in organic content leads to an increase in thickness [104, 128, 161]. All the coating thicknesses are compiled in Table 5.2, where WFT is the wet film

thickness (as done with a 20, 50 or 100 µm bar), NVC is the non-volatile content of the formulation and DFT is the dry film thickness (measure as explained in 4.1.1).

IMS was used as solvent for this work to facilitate the compatibility matrix-nanoparticles since the silica nanoparticles which were then incorporated into the matrix were dispersed in this solvent. In terms of the choice of catalyst, an acid was chosen instead of a base. This was because the catalyst influences the rate of condensation and higher condensation rates usually results in higher porosity, which is the case for base catalysts. While the reaction rate of hydrolysis is usually increased according to the strength of the acid which makes HCl and HNO_3 as the more common catalysts.

Table 5.1. Molar ratios combination for matrix development.

Formulation	TES40	GPTMS	IMS	HCl	H_2O
1	1	0.6	1.35	0.18	3.07
2	1	0.6	1.35	0.08	3.07
3	1	0.9	1.35	0.08	3.07
4	1	0.9	2.67	0.08	3.07
5	1	0.9	2.67	0.08	6.15
6	1	0.9	2.67	0.75	6.15
7	1	1.8	2.67	0.75	6.15
8	1	1.8	2.67	0.75	8.33

Table 5.2. Wet and dry film thicknesses for matrix development.

Formulation	WFT (µm)	NVC (%)	DFT (µm)
1	20	43.0	11.5
	50	43.0	11.8
2	50	43.8	10.8
3	50	42.5	12.3
4	50	35.7	10.1
5	50	38.4	13.2
6	20	38.5	11
	50	38.5	11.2
7	50	42.2	20.3
8	100	44.0	36.4
	50	44.0	25.1

Thus, HCl was chosen as catalyst not just for that reasons but also since in a previous study, which compared a few catalysts (such as H_2SO_4, H_3PO_4, HNO_3, $C_2H_2O_4$, HCl…) the use of HCl as catalyst led to the formation of thicker coatings with reduced film stress [162]. Thus, the final formulation for the coating matrix was prepared using TES40 and GPTMS as precursors in the presence of HCl as catalyst and with water and IMS as solvents. The followed protocol is depicted in Figure 5.2.

First, a separate prehydrolysis was carried out by adding the same amounts of IMS, H_2O and HCl to TES40 and GPTMS (Pot A and Pot B, respectively) which were stirring for 30 minutes. This step was done in order to promote

homogeneity of the solution by achieving a low hydrolysis rate. After this, both mixtures were combined in one pot and left stirring for another 2 h. After this time where hydrolysis and condensation have taken place, the final solution is obtained. The formulation is then deposited onto the mild steel Q-panels (previously cleaned with IMS) by bar coating (using a 50 µm wire wound bar) and then dried and cured at 90°C for 2 h in an oven.

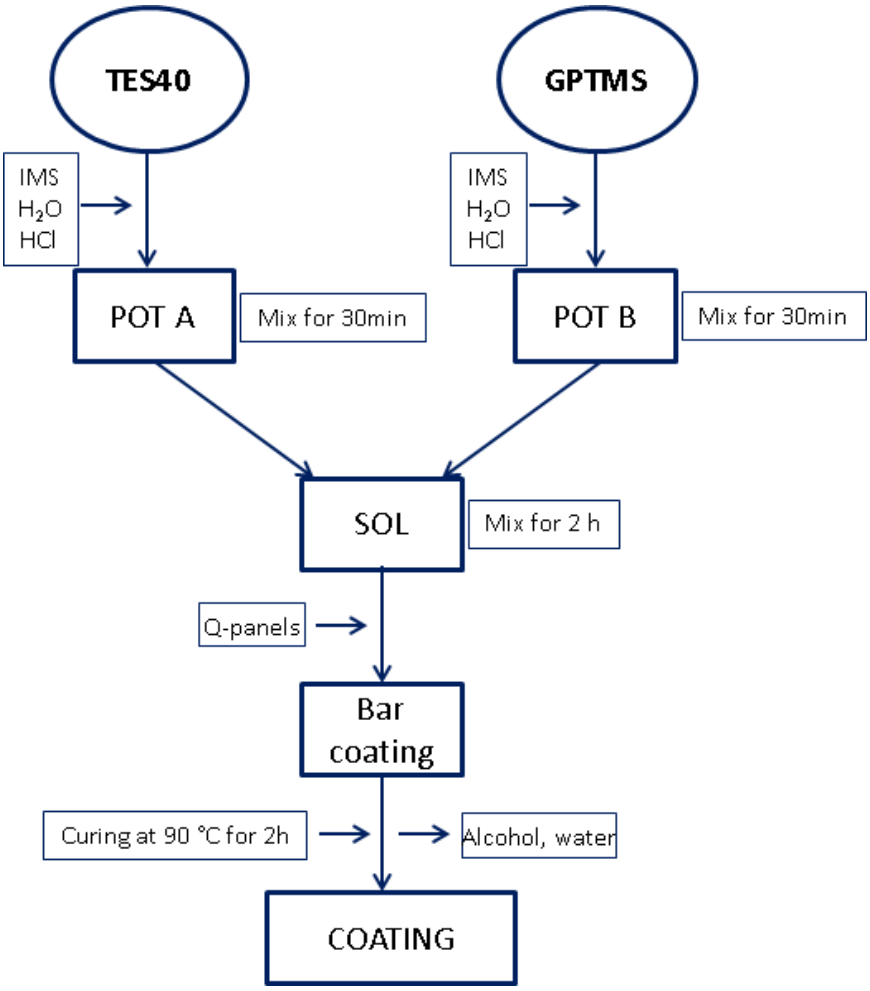

Figure 5.2. Coating matrix development protocol.

5.2.2 Silica nanoparticles

The nanoparticles used in this work are silica nanoparticles. Some of them were surface treated with an organosilane whereas others were used as-synthesised (no surface modification). A more detailed description of the

preparation of both as-synthesised, also termed “unfunctionalised”, and surface treated, also termed “functionalised”, can be found in the following sections.

5.2.2.1 Unfunctionalised silica nanoparticles

Silica nanoparticles for this study were prepared by the Stöber process [37], which produces mono-modal spherical silica nanoparticles by an ammonia catalysed reaction of tetraethoxysilane (TEOS) in alcohols as solvent. The Stöber silica dispersion, which is made at TWI and it is in the process of being commercialised), is a 4.3 wt.% dispersion in IMS (Industrial Methylated Spirit), with the silica nanoparticles having a mono-modal distribution with a mean particle size (Z-average, as measured by dynamic light scattering, DLS, Malvern Zetasizer Nano ZEN1600) of 30 nm. Some more details of these silica nanoparticles are shown in Table 5.3 and Figure 5.3.

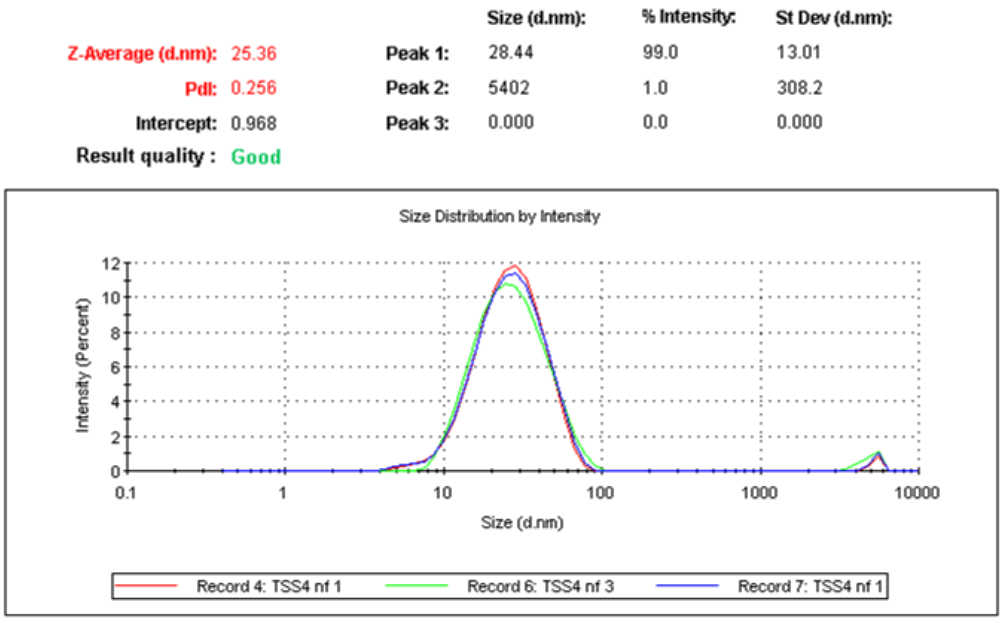

Figure 5.3. Particle size of Stöber silica produced at TWI Ltd.

Table 5.3. Stöber silica nanoparticles made at TWI Ltd.

Property	Measurement method	Target value
Non Volatile Content	Thermogravimetry	4.3 %
Silica content of dried material	TGA	89 %
pH of final solution	pH-metre	8.5 ± 1
Particle size	DLS (Z_{ave})	30 nm
WCA on glass substrate	DSA	< 22°
Appearance	Visual	Single liquid phase. Transparent/ very slight haze

5.2.2.2 Functionalised silica nanoparticles

Silica nanoparticles were surface-treated with GPTMS to make them more compatible with the matrix and to prevent/reduce possible agglomeration of nanoparticles during incorporation into the coating formulation. Surface functionalisation of the synthesised silica nanoparticles with GPTMS was carried out by reacting 0.43 g of GPTMS with 100 g of silica dispersion prepared by the Stöber method, giving a mass ratio of 0.1 g GPTMS/g silica in the dispersion, which is called T0.1 functionalisation level. (The same procedure was followed for synthesising the subsequent functionalisation levels, T0.25 and T0.5). This solution was mixed for a few minutes and then heated to 65°C for 18 h.

In order to facilitate the hydrolysis and subsequent reaction of the GPTMS with the silanols group, the acidity of the solution was adjusted with acetic

acid so that the pH was kept between 3 and 5. This is important since previous research has shown that alkaline conditions (pH 9.0) can lead to the formation of aggregates after surface modification, while surface treated silica at pH 3-5 remains monodisperse with no large aggregation observed [128, 163].

The particle sizes for the functionalisation levels object of this study, going from non-functionalised nanoparticles, T0, to the different functionalisation levels: T0.1, T0.25 and T0.5, are shown in Table 5.4. Particle size measurements were carried out by two different methodologies: dynamic light scattering (DLS) and from TEM images (Figure 5.4).

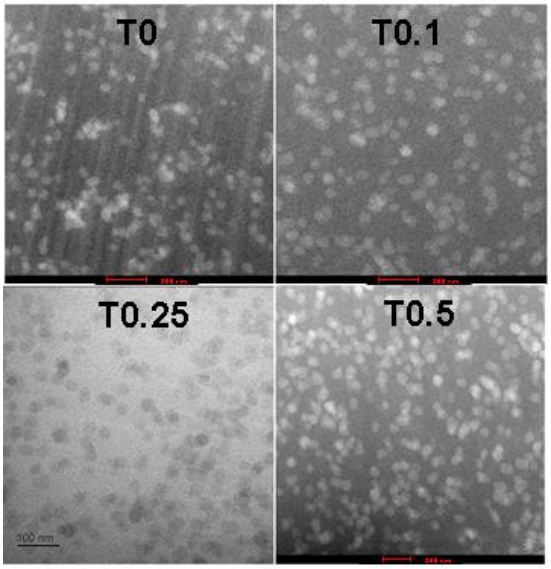

Figure 5.4. TEM images used to calculate particle sizes (scale: 100 nm).

It can be seen from Table 5.4 that the particle sizes from DLS-Number are close to the particle sizes from TEM, with an approximation of 18-26 %. On the contrary, the particle sizes from DLS-Intensity presented a high difference of about the 60 % compared with the particle sizes from TEM. This could be due to the fact that the particle sizes from TEM images where

taken when the silica nanoparticles were already incorporated into the sol-gel based coating and in dry state, while DLS measurements were performed when nanoparticles were in solvent media prior incorporation into the matrix. Therefore, from TEM the diameter of the dried particle is measured while DLS measures diffusivity of the particles to estimate the hydrodynamic size, which is the diameter of the particle and the liquid layer around the particle. As observed from Table 5.4, T0 is smaller than functionalised variants, while the difference in size from T0.1 to T0.5 is not significant. The increase in size may be due to the change in hydrodynamic radius.

Table 5.4. Particle size measured by Zetasizer and from TEM images.

Functionalisation level	Particle size (nm)		
	DLS (Intensity)	DLS (Number)	TEM
T0	~29	~18	~26
T0.1	~47	~35	~30
T0.25	~52	~39.5	~31.5
T0.5	~51	~39	~32

Figure 5.5 shows the hydrolysis of GPTMS and the subsequent functionalisation of the silica surface.

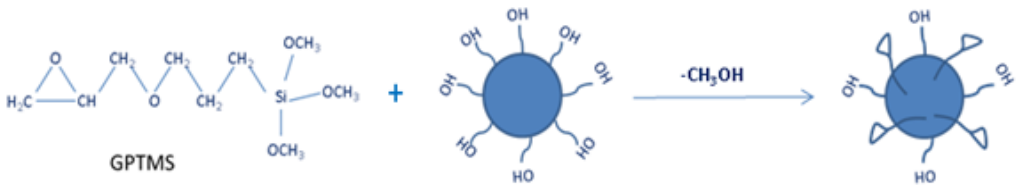

Figure 5.5. Surface functionalisation of silica nanoparticle with GPTMS.

5.3 Nanoparticle incorporation in polymer matrix

The incorporation of nanoparticles into polymeric matrices is of interest for many applications. Specific properties can be obtained with a suitable incorporation of nanoparticles, as it has been described in section 3.3. However, the interface between the matrix and the nanoparticles as well as the nanoparticle loading level can play a critical role. In order to study the impact of silica nanoparticle incorporation into the coating matrix system, the silica nanoparticles were introduced into the matrix formulation. The quantity of nanoparticles added to the formulation was calculated as:

$$wt.\% = \frac{0.043\ x\ Nanosilica\ dispersion(g)}{TES40\ (g) + GPTMS\ (g) + 0.043xNanosilica\ dispersion\ (g)} \quad (5.1)$$

To incorporate the nanosilica, the following protocol, which is also pictured in Figure 5.6, was followed:

- addition of the nanosilica dispersion in IMS to the TES40,

- evaporation of some of the solvent since the nanosilica dispersion, as synthesized, had a large amount of IMS. The removal of approximately 85-90 % of the total solvent contained in the nanosilica dispersion was done with a rotovap at a constant temperature of 65 °C,

- addition of firstly deionised water and then HCl to the solution, which was left stirring for 30 min.

- In parallel, HCl, IMS and DI water was added to GPTMS and left stirring for 30 min

- Both solutions were mixed together and left stirring for 2 h.

Once the incorporation protocol was finished, coating formulations were ready to be deposited onto the substrate (mild steel Q-panels). Prior to coating deposition, steel panels were cleaned with industrial methylated spirit (IMS) to remove grease and/or contaminants. Coatings were applied manually on the steel panels with spiral bar coaters (Elcometer, Manchester, UK) using a 50 µm wire wound bar. The coated samples were then dried and cured at 90°C for 2 h in an oven.

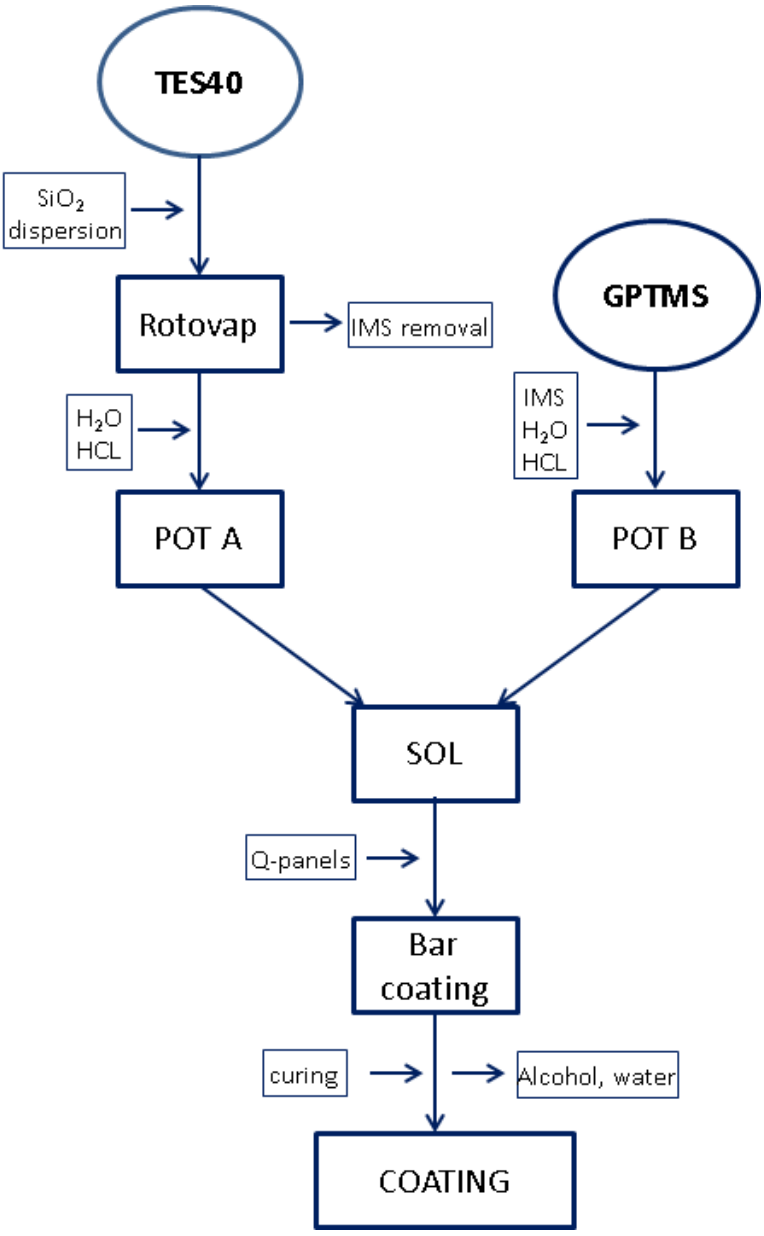

Figure 5.6. Coating procedure diagram.

Chapter 6. Coating microstructure characterisation

6.1 Introduction

Chapter 6 is the first results chapter of this thesis and is focused on understanding the impact on structure and properties of coatings where unfunctionalised and functionalised silica nanoparticles are incorporated into the matrix. As previously mentioned, the incorporation of nanoparticles in a polymer matrix can help to increase thickness [104, 128, 161], improve mechanical properties and corrosion resistance [37, 163-166] (if added to an optimum level) but can also have the opposite effect if not optimised [164]. This chapter starts by describing the impact of the amount of as-synthesised silica nanoparticles into the coating matrix, with experiments conducted at different solid loading levels of 1, 3, 5 and 10 wt.% (as calculated using equation 5.1). Due to the results obtained in these preliminary tests, a more detailed assessment of the coatings with 10 wt.% of unfunctionalised silica nanoparticles and also with 10 wt.% of functionalised silica nanoparticles was carried out. The effect on coating microstructure (thickness, adhesion, morphology) of the different solid loading levels (1-10 wt.%) as well as the more detailed assessment, with 10 wt.% of functionalised and functionalised silica nanoparticles, is described in this chapter.

A further study on the optimisation of both the loading and functionalisation level is also described. In order to do this optimisation, three functionalisation levels and three loading levels were selected. The three functionalisation levels were: T0.1, T0.25 and T0.5.

Surface functionalisation of the as-synthesised silica nanoparticles with GPTMS for the T0.1 functionalisation level was described in 5.2.2.2. T0.25 and T0.5 were produced using the same methodology. The three loading levels selected were 10, 15 and 20 wt.%. All the functionalisation and loading level combinations are summarised in Table 6.1:

Table 6.1. Summary of the functionalisation and loading levels for silica incorporation.

Functionalisation level	**Loading level (wt.%)**		
T0.1	10	15	20
T0.25	10	15	20
T0.5	10	15	20

6.1.1 Thickness measurement

Any mention to “thickness” during this work refers to the dry film thickness of the coatings. As mentioned previously, a preliminary study was carried out to understand the impact of the amount of nanoparticles incorporated into the coating matrix. As-synthesised silica nanoparticles at solid loading levels of 1, 3, 5 and 10 wt.% (as calculated with equation 5.1), were firstly introduced into the optimised formulation with the TES40/GPTMS molar ratio of 1:1.8, which was described in 5.1.1. An increase in coating thickness, measured as described in 4.1.1, was noticed after addition of silica to the coating matrix as can be seen from Figure 6.1.

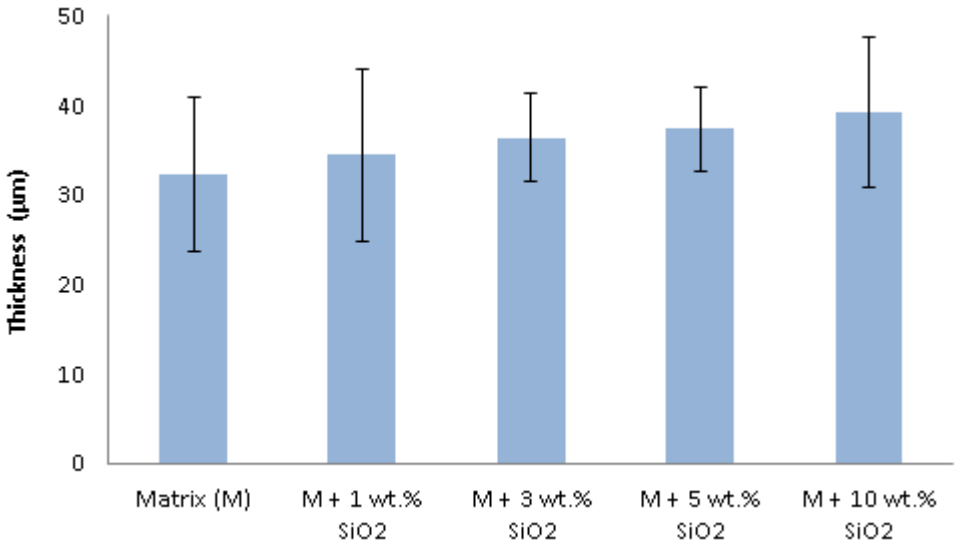

Figure 6.1. Effect of silica loading level on the thickness of the coatings.

However, with the addition of functionalised silica the coating thickness decreased to about 24 µm, also measured as described in 4.1.1, for the set of coatings studied together with the 10 wt.% unfunctionalised silica.

Following the work on understanding the impact of loading and functionalisation level, the thickness results for this study can be seen in Table 6.2. An increase in thickness with increased loading is observed for the T0.1 functionalisation level.

However, for T0.25 and T0.5 there is a small decrease from 10 to 15 wt.%, although it increased again when increasing the loading to 20 wt.%. Looking at each loading level separately, it can also be noticed that increasing the functionalisation level led to increased thickness.

Table 6.2. Effect of loading and functionalisation level on the thickness (μm) of the coatings.

Functionalisation level	Loading level		
	10wt.%	**15wt.%**	**20wt.%**
T0.1	10.3 ± 3.0	11.2 ± 2.6	18.2 ± 3.0
T0.25	14.3 ± 2.9	12.4 ± 1.8	18.9 ± 3.5
T0.5	32.0 ± 4.1	27.0 ± 4.1	38.0 ± 4.2

6.1.2 Adhesion (cross-cut tape test)

The cross-cut tape test method used to measure adhesion of the coating to the substrate rates adhesion from 0B to 5B (no adhesion to well adhered) and gave a 5B rating for all the coating formulations, which indicates the percentage removal of coating during the tape test to be less than 5% which means that all the coatings were well adhered to the substrate. An example is shown in Figure 6.2.

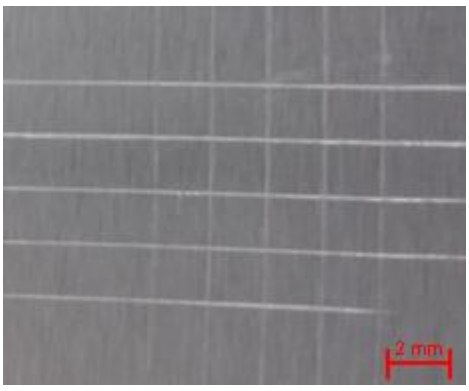

Figure 6.2. Cross-cut tape test example.

6.1.3 Water contact angle (WCA)

Water contact angle was measured for the coating matrix and the coatings with as-synthesised silica and functionalised silica nanoparticles at 10 wt.% solid loading level (as calculated with equation 5.1). An increased WCA, measured as described in 4.1.2, was noticed after addition of silica to the coating matrix which was further enhanced when functionalised silica was added to the same matrix, as can be seen from Table 6.3.

Table 6.3. Effect of silica loading level on WCA of coatings.

	Matrix (M)	**M + 10 wt.% SiO_2**	**M + 10 wt.% Funct-SiO_2**
WCA (°)	80 ± 3.0	83 ± 2.0	90 ± 2.0

Following the work on understanding the impact of loading and functionalisation level, the WCA results for this study can be seen in Table 6.4. An increase in WCA with increased loading is observed at all functionalisation levels. Considering each loading level separately, it can be also noticed that increasing the functionalisation level led to increased WCA.

Table 6.4. Effect of loading and functionalisation level on WCA of coatings.

Thickness (µm)	**10wt.%**	**15wt.%**	**20wt.%**
T0.1	78.4 ± 3.0	79.5 ± 1.6	91.2 ± 1.4
T0.25	78.8 ± 2.1	82.1 ± 4.4	97.5 ± 3.5
T0.5	94.3 ± 4.6	96.5 ± 0.9	101.8 ± 3.3

6.1.4 SEM

The surface microstructure and topography of coated samples were examined with SEM to allow comparison of the homogeneity of the coatings and the distribution of nanoparticles within the coating matrix. It also provided an idea about its impact on the surface roughness of the coating. As can be seen from Figure 6.3, the coating containing 1 wt. % silica nanoparticles shows an inhomogeneous nanoparticles distribution with agglomerations all over the sample while an increase in silica content up to 10 wt. % shows a better distribution of the silica nanoparticles. However, the addition of the functionalised nanoparticles (T0.1 10 wt.%) showed to increase homogeneity and decrease roughness.

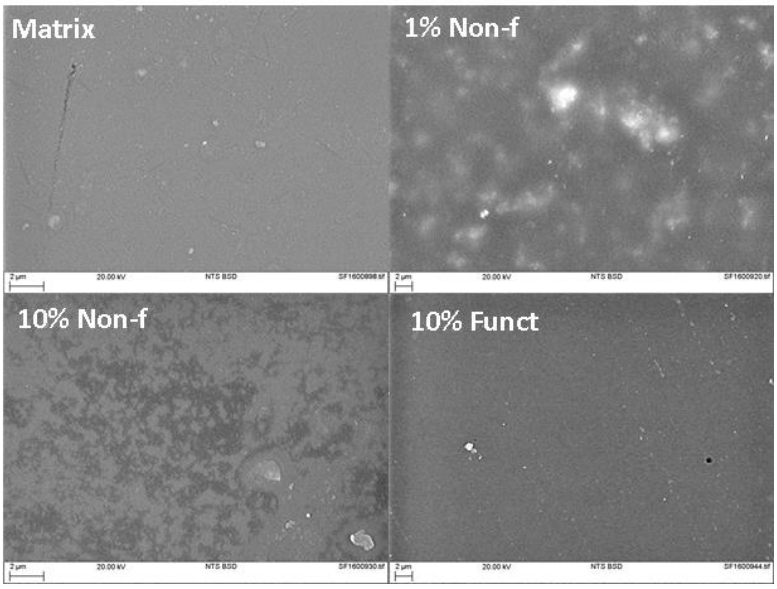

Figure 6.3. SEM images of coating matrix, matrix with 1 and 10 wt.% unfunctionalised silica nanoparticles and with T0.1 10 wt.% functionalised nanoparticles.

SEM was also used to look at the cross-section of the following formulations: coating matrix, matrix with 10 wt.% unfunctionalised silica and matrix with 10

wt.% functionalised silica nanoparticles. Although some damage to the top of the coatings could have been done by doing the cross-section preparation for later SEM imaging, Figure 6.4 provided an indication of the thicknesses for these formulations, which were quite comparable with the measurements addressed in 6.1.1.

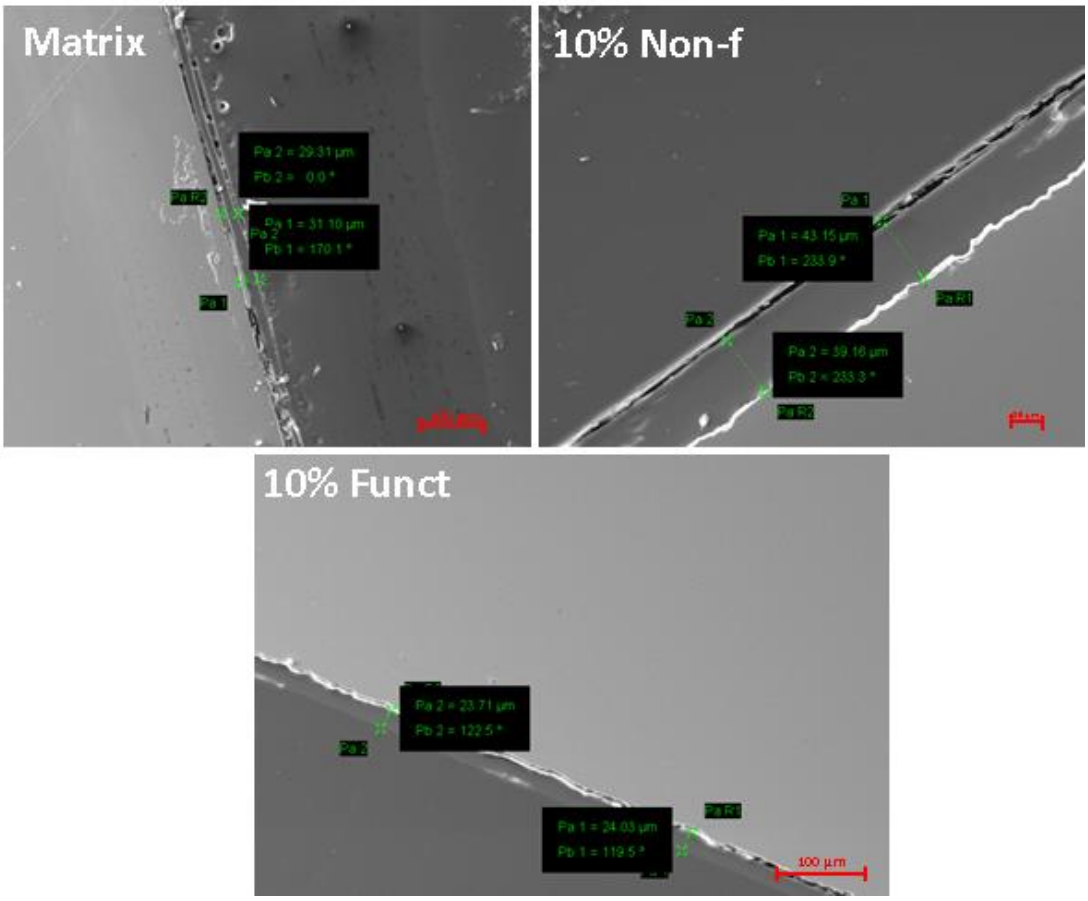

Figure 6.4. SEM cross-section images for the coating matrix, and coatings with 10 wt.% unfunctionalised and functionalised silica (T0.1).

6.1.5 AFM

AFM images for the coatings with non-functionalised and functionalised silica nanoparticles are shown in Figure 6.3. The dark domains are attributed to the silica nanoparticles, which are distributed within the matrix network. As shown with the other imaging techniques, AFM images in Figure 6.5 also

confirmed the better distribution of functionalised silica compared to the non-functionalised.

Some agglomeration can be observed in the coating with non-functionalised silica (Figure 6.5.a), which leads to an irregular and non-homogeneous distribution of these nanoparticles throughout the coating formulation. On the contrary, the silica nanoparticle functionalisation improves nanoparticle dispersion which can be explained as a result of the functionalisation (functionalisation or surface treatment of nanoparticles can cause steric hindrance which helps to avoid nanoparticle agglomeration during the incorporation process) but also due to an increased compatibility between the GPTMS grafted on the silica surface and the GPTMS in the matrix network. The introduction of GPTMS on the silica surface can lead to a stronger interface between matrix and nanoparticles [54] and the surface treatment has been proved to supress nanoparticle agglomeration due to enhanced resin-wettability, which is in line with other investigations [124, 138].

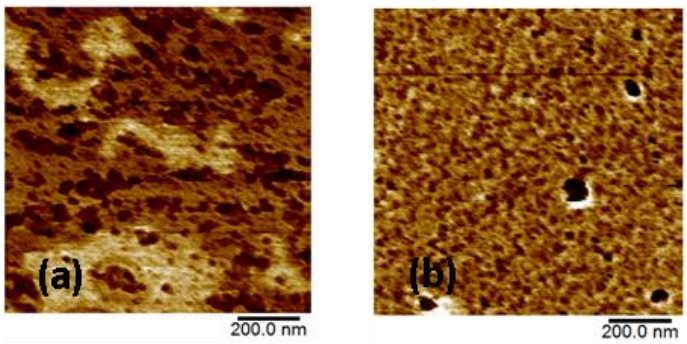

Figure 6.5. AFM images of nanoparticle containing coatings: (a) matrix with 10 wt.% non-functionalised silica, and (b) matrix with 10 wt.% functionalised-silica.

AFM images in Figure 6.6, show that increasing the loading level for the T0.1 functionalisation level, also showed a good dispersion of the functionalised nanoparticles within the coating matrix. Good dispersion is also observed at all loading levels for the T0.25, while for the T0.5 functionalisation level at highest loading, although well dispersed, did not show as good distribution as for 10 and 15 wt.% (Figure 6.4). This would confirm that surface treatment can help to increase compatibility between matrix and nanoparticles, supress agglomeration within the coating matrix and hence, provide coatings with enhanced performance.

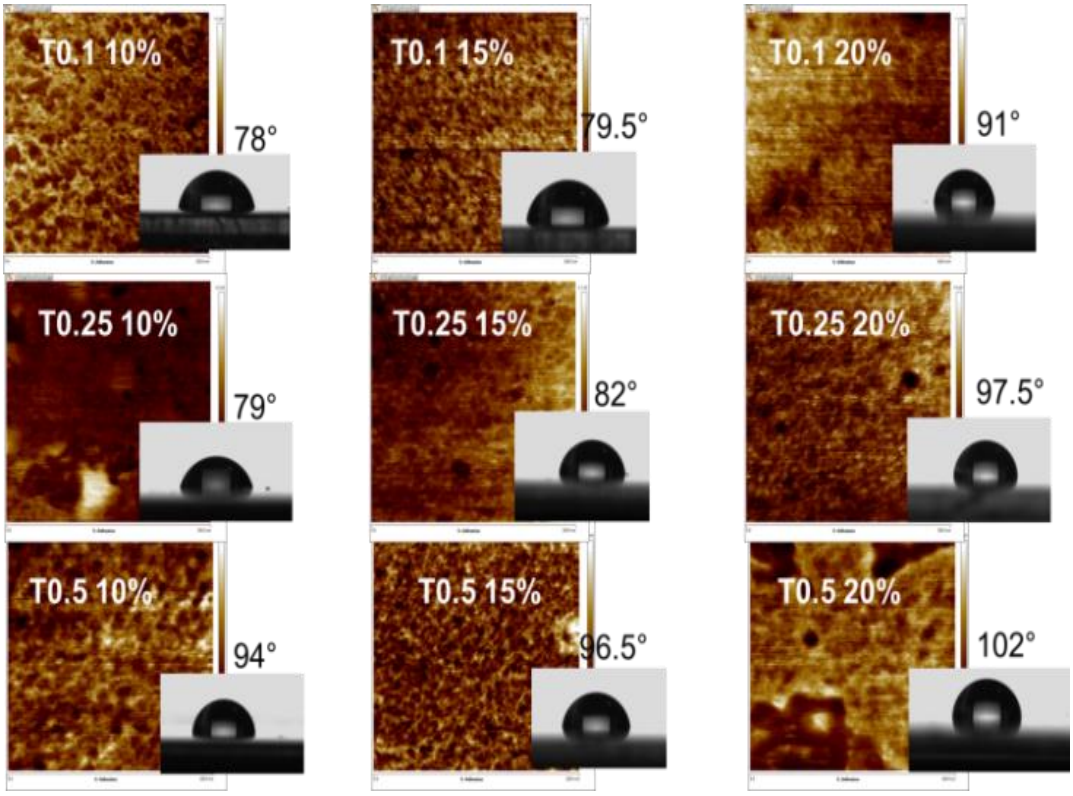

Figure 6.6. AFM images of nanoparticle containing coatings at different loadings and functionalisation levels.

6.1.6 WLI and DIC

White Light Interferometry (WLI) and Differential Interference Contrast (DIC) microscopy, which were described in 4.2.5 and 4.2.6.1, were used to image surface topography and look in detail to identify key features in the coatings as shown in Figures 6.7 and 6.8.

It can be observed from the WLI images in Figure 6.7 that the polysiloxane only coating presents a complex and rough topography, the substrate is apparently visible beneath the coating (represented by blue colour). When non-functionalised silica is added to the polysiloxane formulation (which now acts as a matrix) the resultant coating appears to provide far more uniform coverage with lower but still appreciable roughness. When functionalised silica nanoparticles are incorporated into the polysiloxane matrix further increase in homogeneity and uniformity is observed with the result of a lower level of roughness.

DIC images are in agreement with WLI images. Figure 6.8 shows DIC images where some cracks and areas of apparent disbondment are observed for the sol-gel based matrix, and also some small droplets present throughout the coating which can be possibly due to solvent evaporation during curing process.

In the case of the coating with non-functionalised nanoparticles, even though an increase in homogeneity was observed, there are still some cracks and irregularity of this coating formulation. However the addition of functionalised silica nanoparticles led to a less porous and more homogenous coating formulation. This could be due to the influence of the surface treatment of

silica nanoparticles which possibly helps to increase the flexibility and reduce internal stress, leading to a more homogeneous coating.

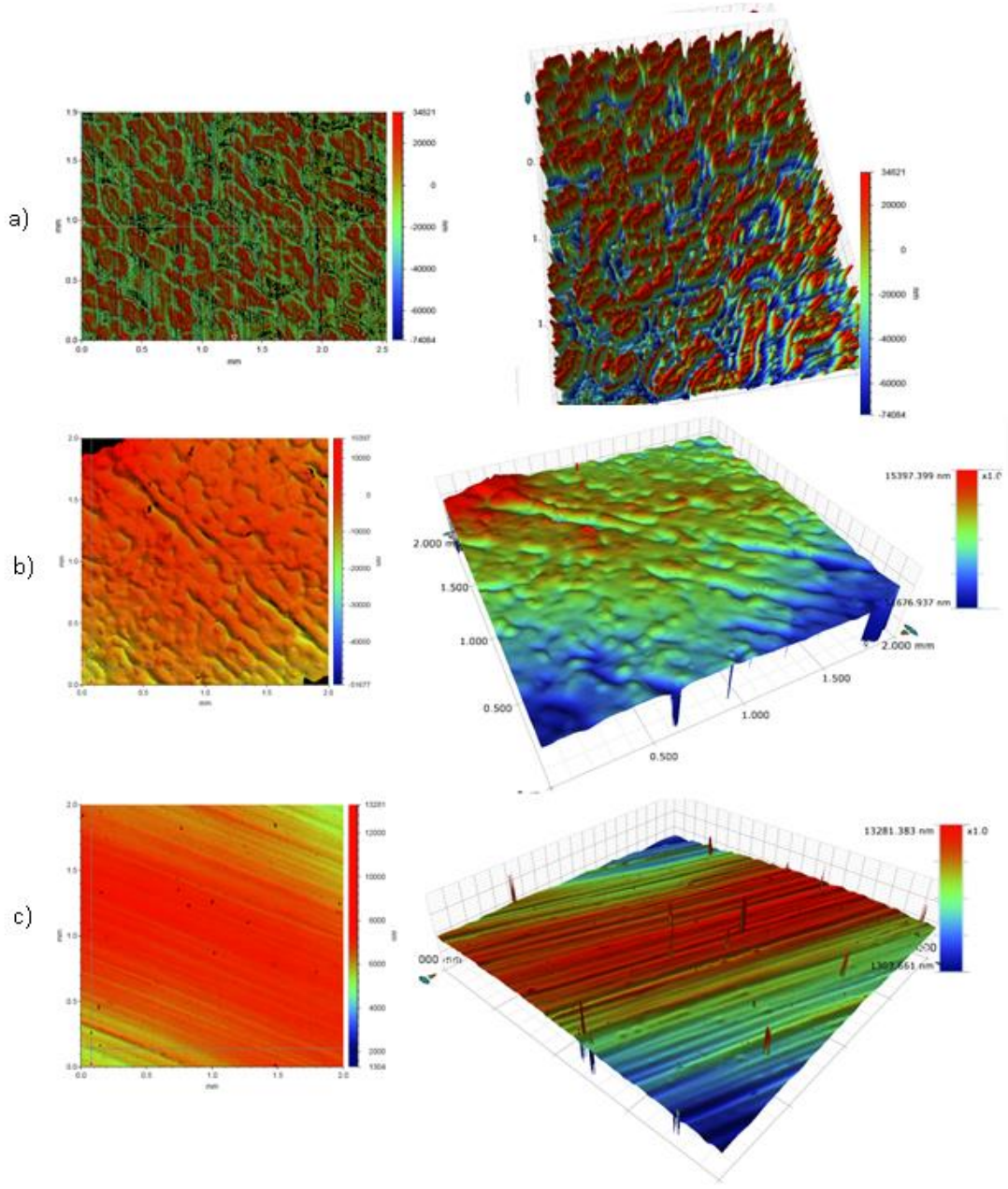

Figure 6.7. 2D and 3D WLI images of all coating formulations. a) Polysiloxane-based matrix, b) matrix with 10 wt.% non-functionalised silica and c) matrix with T0.1 10 wt.% functionalised silica.

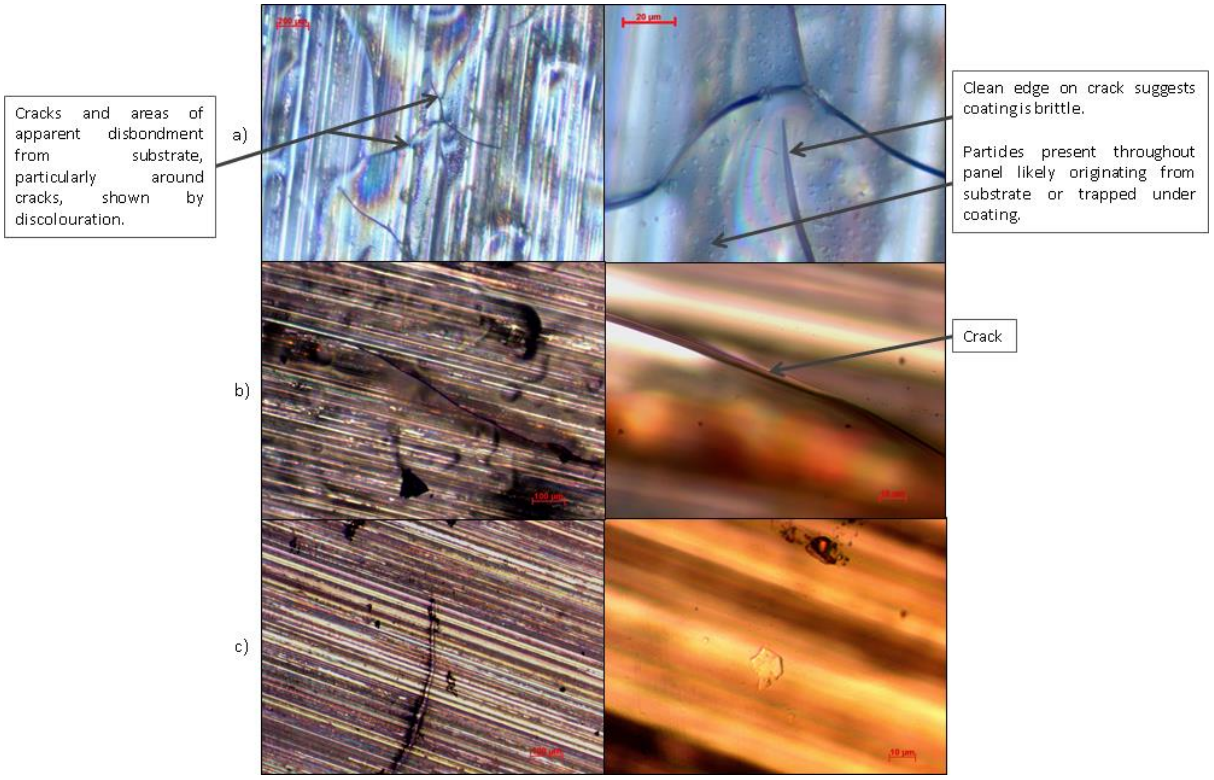

Figure 6.8. DIC images of all coating formulations. a) Polysiloxane-based matrix, b) matrix with 10 wt.% non-functionalised silica and c) matrix with T0.1 10 wt.% functionalised silica.

The surface topography of coating formulations with functionalisation level T0.1 at the three different loading levels (10 wt.%, 15 wt.% and 20 wt.%) are shown in Figure 6.9. There is no wrinkling apparent in these formulations and nanoparticles appear to be uniformly distributed within the matrix. There is a low level of roughness for all loading levels, however increasing the loading appears to have a positive effect which is reflected in the increased uniformity of the T0.1 20wt.%.

Increasing the functionalisation level from T0.1 to T0.25 did not appear to have the same behaviour. At 10 wt.% the T0.25 coating formulations showed some defects, while increasing the loading to 15 wt.% appeared to have a more uniform distribution, as observed from Figure 6.10. A further

increase up to 20 wt.% led to rougher coatings, not homogeneously distributed with parts of the substrate not completely covered by the coating.

WLI images from Figure 6.11 showed the surface topography for the T0.5 formulations. Although there is not apparent wrinkling of the coatings, T0.5 10 wt.% and T0.5 15 wt.% showed similar coating distribution and rough surface, while the T0.5 20% formulation showed higher roughness.

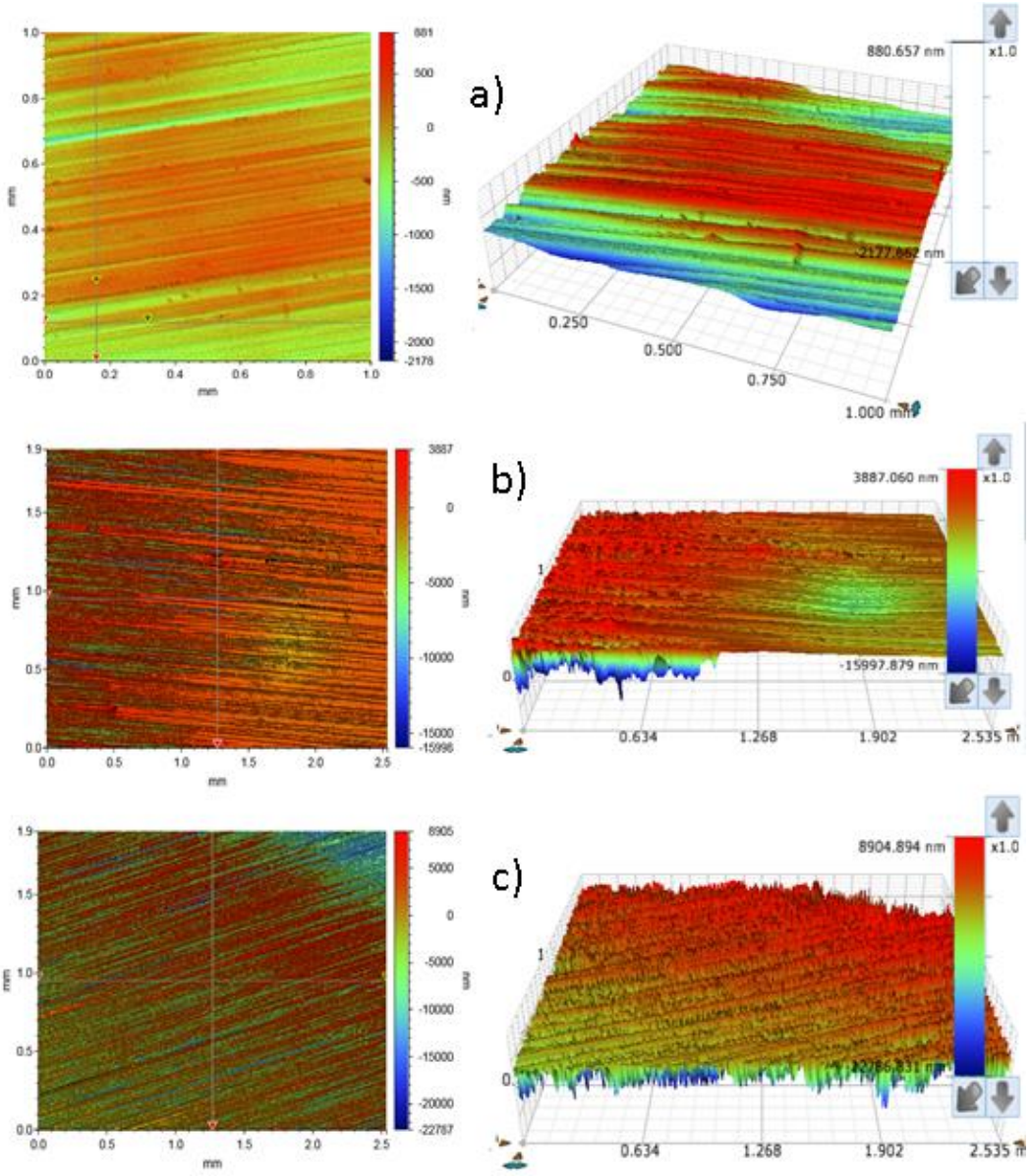

Figure 6.9. WLI images for T0.1: a) 10wt.%, b) 15 wt.% and c) 20 wt.%.

DIC images for the loading and functionalisation study were in agreement with WLI showing homogeneous formulations without areas of disbondment. Since these were mainly the same as the ones presented in Figure 6.8.c), they are not presented here to avoid duplication.

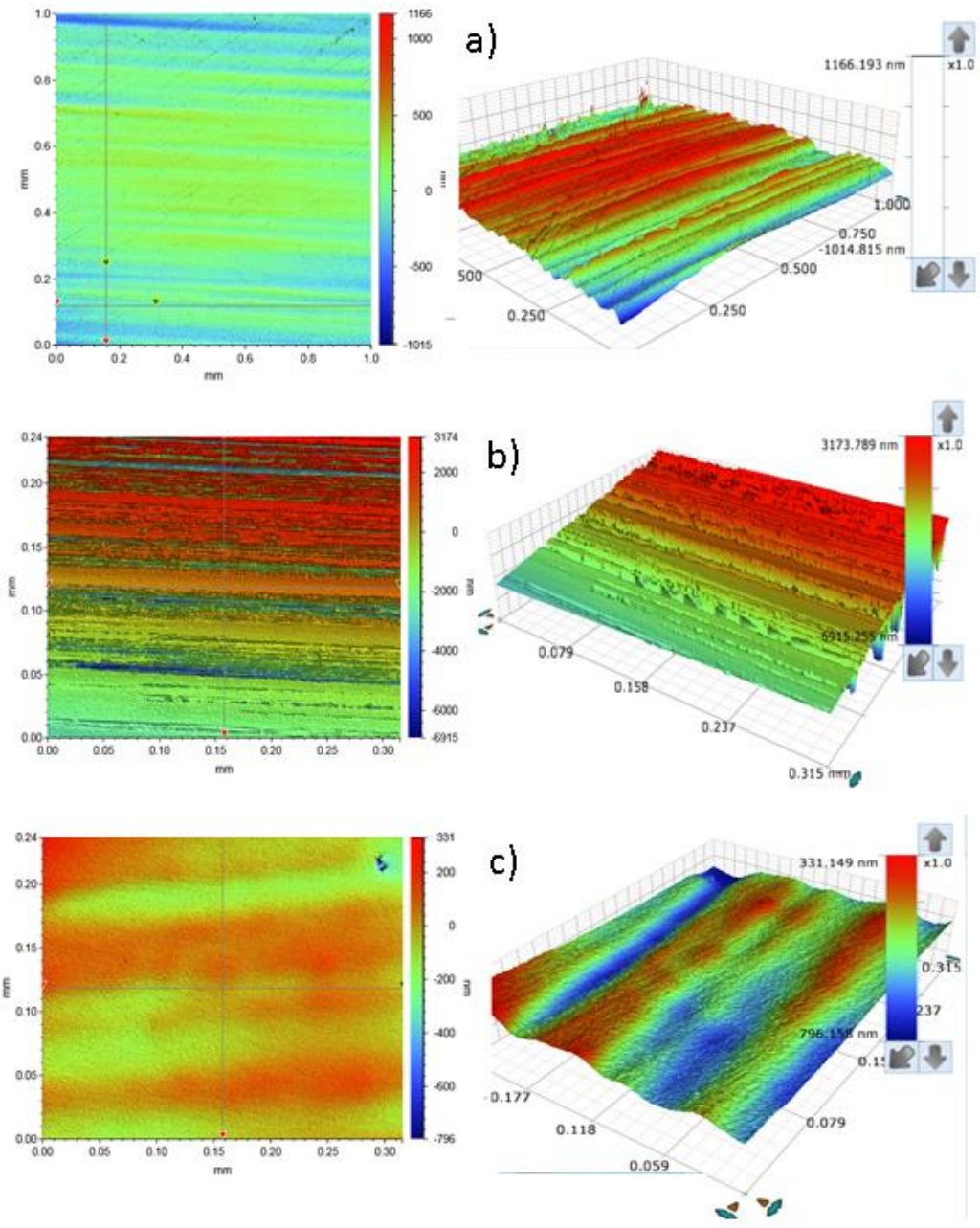

Figure 6.10. WLI images for T0.25: a) 10%, b) 15 % and c) 20%.

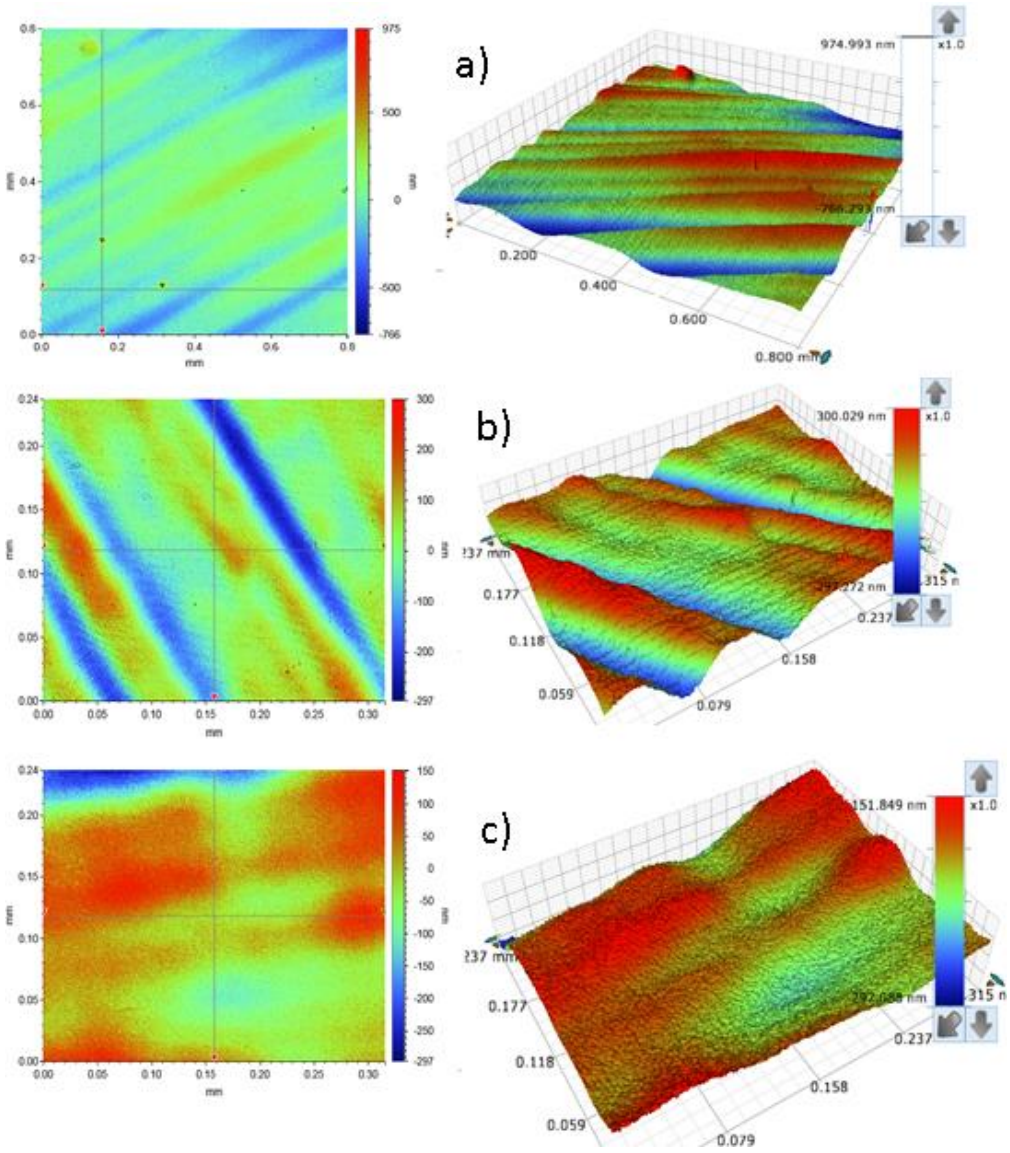

Figure 6.11. WLI images for T0.5: a) 10%, b) 15 % and c) 20%.

6.1.7 FIB-TEM

A more illustrative depiction of the silica nanoparticle distribution can be observed from the TEM images. Due to the complexity and laborious work needed to carried out this analysis, just the most relevant formulations were imaged. Figure 6.12 shows the TEM images for the coatings with non-functionalised silica, T0 10wt.%, and functionalised silica at the lowest functionalisation level, T0.1 10 wt.% and T0.1 20 wt.%, respectively.

As seen from AFM pictures, when the nanoparticles are non-functionalised they tend to agglomerate, however, a small degree of functionalisation (T0.1) led to a higher degree of homogeneity which is even kept when doubling the loading level. It can be observed that the coating with 20 wt.% functionalised silica at T0.1 showed a denser nanoparticulate coating with nanoparticles homogeneously distributed.

An increase in functionalisation level from T0.1 to T0.25 and T0.5 is shown in Figure 6.13. An increase in functionalisation appeared to lead to a small degree of agglomeration, although nanoparticles are still quite well distributed throughout the coating, they started to agglomerate and were not as equally distributed as for the lower functionalisation level (T0.1). However, in agreement with AFM images, the functionalised silica nanoparticles even at higher functionalisation levels were still more homogenously distributed than the non-functionalised nanoparticles even for highest loading levels.

In order to have a clearer picture of the distribution of nanoparticles, TEM images at higher resolution are represented in Figure 6.14. It can be observed that the coating with non-functionalised silica (T0) presented the highest degree of agglomeration, while just a low functionalisation (T0.1) showed a better distribution even at double loading level with nanoparticles homogeneously dispersed through the coating (from 10 wt.% to 20wt.%).

When increasing the functionalisation level, a short degree of agglomeration started to appear although these nanoparticles were still more homogeneously distributed than the nanoparticles without any functionalisation.

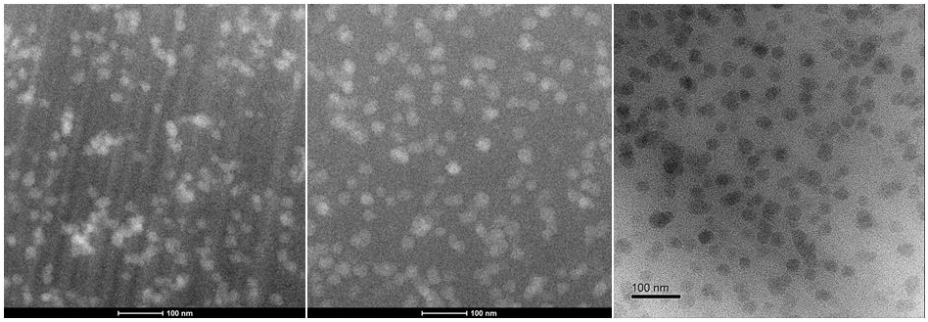

Figure 6.12. TEM images. From left to right: T0 10wt.%, T0.1 10 wt.% and T0.1 20 wt.%.

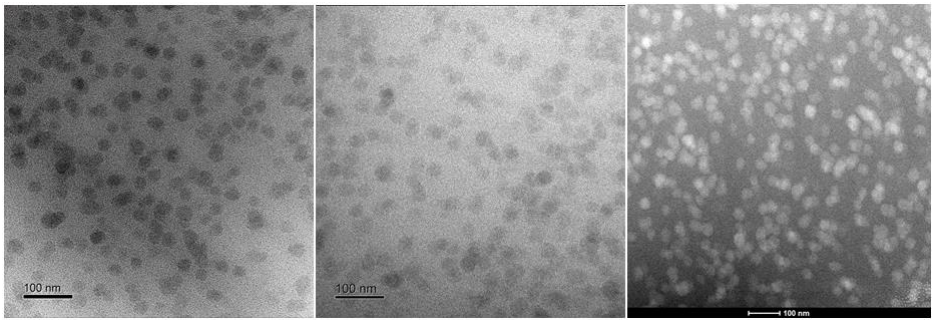

Figure 6.13. TEM images. From left to right: T0.1 20%, T0.25 20% and T0.5 20%.

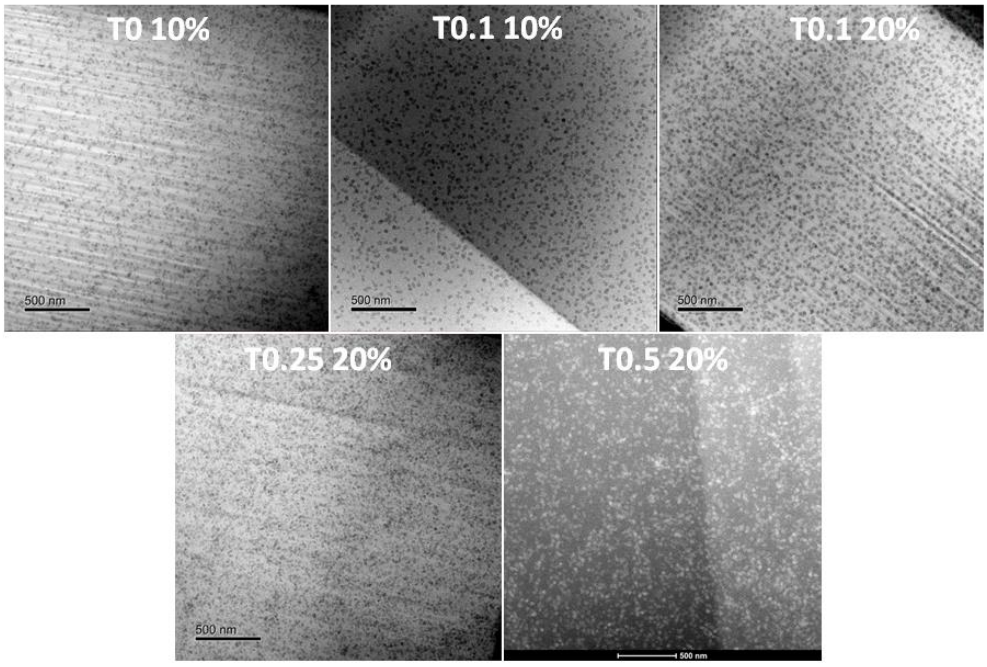

Figure 6.14. TEM images of all formulations.

6.2 Conclusions

The first loading study done with unfunctionalised silica showed that the addition of these nanoparticles led to an increase in coating thickness compared to the base matrix and also indicated that an increase in the loading level from 1 to 10 wt.% led to more resistant coatings. As a result of this, the study of the coating with 10 wt.% unfunctionalised silica nanoparticles was further addressed and the impact of these nanoparticles was also compared with the impact of functionalised silica added to the same sol-gel based matrix at the same loading level.

The sol-gel based matrix finally used in these work although appearing well adhered to the substrate, it was shown to be brittle, which could make the water goes through possible pores or pathways presented in the coating leading to rapidly coating degradation. Microscopy images showed that the introduction of silica led to less porous coatings. However when the nanoparticles were functionalised, the resultant coating showed increased homogeneity and uniformity. This is in line with what is shown on the AFM images, where the coating with unfunctionalised silica showed some agglomeration while the coating with functionalised silica offered a good distribution of nanoparticles. A small increase in water repellence was also observed from the coating matrix to the coating with unfunctionalised silica, which was further enhanced when the coating had functionalised silica incorporated.

This enhanced nanoparticle distribution and enhanced water repellence was due to the functionalisation, since the surface treatment of nanoparticles can

cause steric hindrance and help to avoid nanoparticle agglomeration during incorporation, but also due to the increased compatibility between the matrix and the functionalised nanoparticles as the GPTMS grafted on the silica surface is also present in the matrix network.

The study on loading and functionalisation level led to the following conclusions:

- Increased thickness and enhanced water repellence has been observed with increased loading levels

- Increase in functionalisation level from T0.1 to T0.5 led to thicker coatings with higher WCA

- The functionalised coatings have not shown wrinkling or disbondment

- TEM images have shown improved dispersion for the coatings with functionalised silica nanoparticles. However, although all the functionalisation levels showed enhanced nanoparticle dispersion compared with the coatings with non-functionalised silica, the coatings at T0.25 and T0.5 showed a small degree of agglomeration. On the contrary, the coatings at T0.1 showed silica nanoparticles homogeneously distributed through the sol-gel based matrix

Chapter 7. Corrosion performance

7.1 Introduction

This chapter is focused on understanding the impact on the corrosion performance of coatings of silica nanoparticles incorporated into a polysiloxane matrix. The focus of this chapter is initially to describe the impact on the corrosion behaviour of a polysiloxane based coating incorporating either unfunctionalised or functionalised silica (T0.1) nanoparticles at a loading level of 10 wt.% . Then, the focus is related to the examination of the influence on coating corrosion protection performance of the loading level of these particles and effect of the degree of their functionalisation.

7.2 Neutral Salt Spray (NSS)

The salt spray test, which has been described in 4.3.1, was used to assess the corrosion performance of the coatings over a short period of time. Inspection of the samples was carried out after 24 h, 48 h and 72 h of exposure, with images of the specimens taken at those specific times.

Figure 7.1 shows images of the coating formulations (coating matrix, and matrix with 10 wt.% of either unfunctionalised or functionalised silica T0.1) after exposure at the different interval times. It can be observed that the addition of non-functionalised silica nanoparticles to the sol-gel based matrix improved coating performance (Figure 7.1.b, e) compared to the matrix itself (Figure 7.1.a, d), but corrosion is evident after 72 h.

However an improvement of the corrosion resistance was observed when silica nanoparticles were surface treated with GPTMS and added to the matrix, showing very little corrosion even up to 72 h of exposure (Fig. 4.1. c, f).

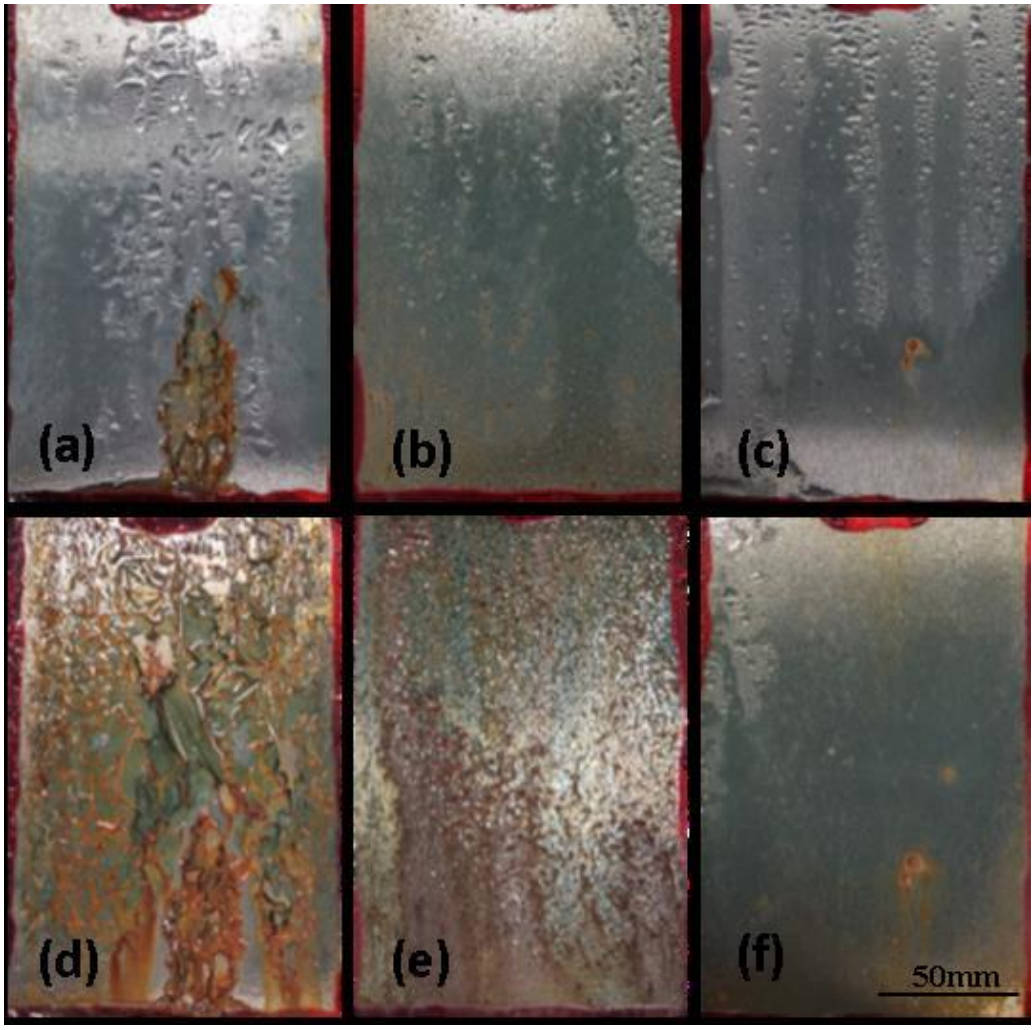

Figure 7.1. Salt spray results after 24 h (above; a, b, and c) and 72 h (below; d, e, and f). From left to right: sol-gel based matrix (a, d), matrix with 10% non-functionalised silica (b, e), matrix with T0.1 10% functionalised-silica (c, f).

Since these initial samples showed promise, a more detailed examination of the behaviour was undertaken in order to identify key factors from the

synthesis and composition of these coatings. Such an approach would assist in determining both structure property relationships but may also facilitate in the design of future coating compositions.

Therefore, the next study examined the influence of loading and functionalisation levels on samples exposed to salt spray testing. This time the exposure was increased by 24 h, to reach 96 h. Results after 96 h of salt spray are shown in Figure 7.2.

There is a notable decrease in corrosion product when increasing loading level of the silica additive at a functionalisation level of T0.1, as observed from Figure 7.2. At the T0.25 functionalisation level, the same behaviour appears to be followed. However, there is no much difference for all the loadings in the case of the highest functionalisation level (T0.5).

When considering the 10 wt.% and 15 wt.% loading levels, the samples with the highest functionalisation level (T0.5) showed very little corrosion. However when increasing the loading up to 20 wt.% the corrosion product decreased quite a lot for all functionalisation levels, showing almost no sample degradation.

Although it is quite difficult to rank the coatings with this test and decide which one performs better after salt spray testing, it can be observed that the coating with functionalised silica at T0.1 and a loading level of 20 wt.% presented almost no corrosion product after reaching 96 h.

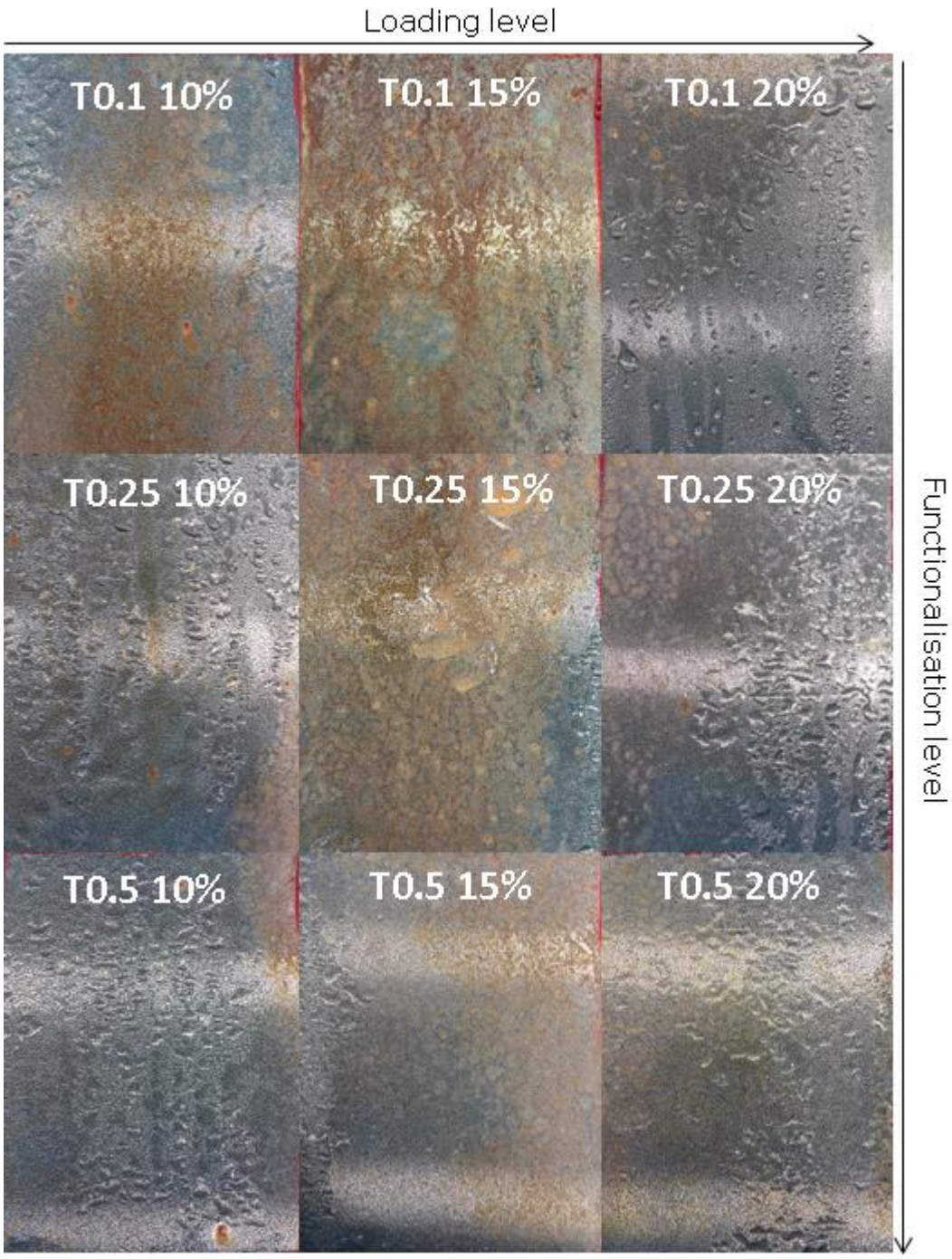

Figure 7.2. Salt spray results for the loading and functionalisation study after 96h.

7.3 Electrochemical characterisation

In order to carry out a quantitative assessment of the corrosion performance, electrochemical testing was also performed for all coating formulations. The setup used to carry out the electrochemical characterisation is described in section 4.3.

7.3.1 Open Circuit Potential (OCP)

The change in the corrosion potential, OCP, as a function of time for the mild steel substrate (Q-panel) and all the coating formulations is given in Figure 7.3. As can be observed all the formulations present a corrosion potential higher than the bare substrate, which could be an indication that these coatings provide a barrier effect. Such a trend has been observed previously in other works [167, 168].

When the experiment started, the coating with non-functionalised silica nanoparticles presented a slightly higher potential than the rest of the coatings. Then, a clear drop can be observed for all coatings up to 24 h.

After that, the potential for both the polysiloxane coating and the coating with non-functionalised silica continues to drop which suggests an increase in defect density and thus, in coating damage and corrosion. An increased anodic activity would shift the corrosion potential in the negative potential direction. On the other hand, the potential for the coating with functionalised silica nanoparticles tends to stabilise after the 24 h, possibly suggesting a higher corrosion resistance of this coating formulation. Similar trends have been observed by other authors looking at coating resistance where

changes in OCP where noticed as corrosion progresses through the coating [169].

It is also worthy to note that even if the potential for all the coating formulations decreased with time, all of them presented higher potential values compared with the bare steel substrate, which suggests that although coating degradation is occurring it is not reaching the substrate.

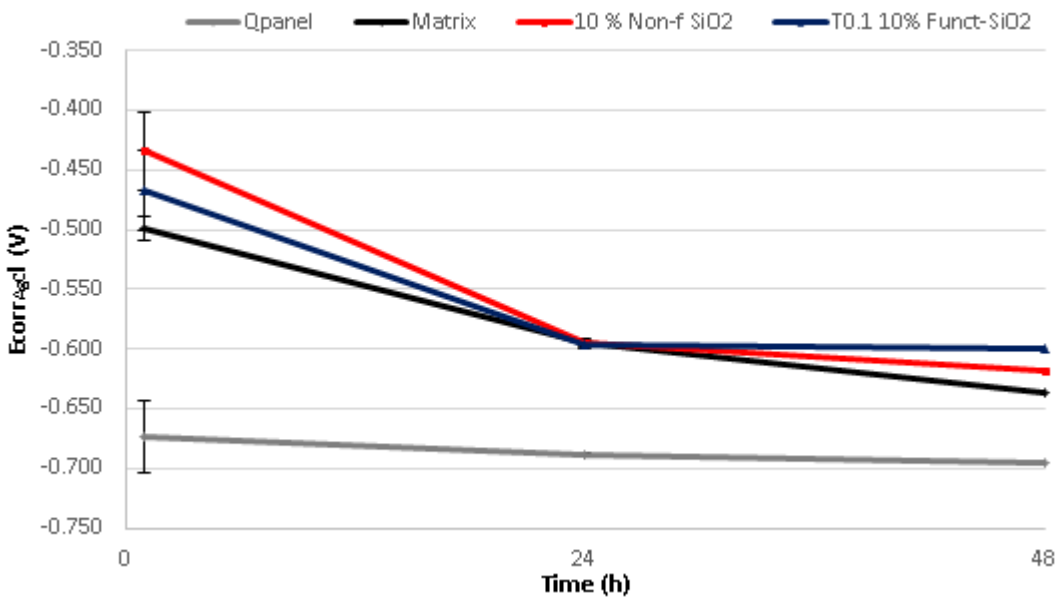

Figure 7.3. Corrosion potential as a function of time.

7.3.2 Electrochemical Impedance Spectroscopy (EIS)

Electrochemical Impedance Spectroscopy (EIS) measurements were carried out for 48 h with the setup as described in Figure 4.8 and the parameters described in section 4.3.2.2.

EIS data obtained during testing needs to be fitted using equivalent circuit models. These models allow a detailed analysis to be carried out that can describe the physicochemical and electrochemical processes associated with the corrosion processes underway.

The equivalent circuit used to fit the EIS data of this work is displayed in Figure 7.4. This circuit is a modified Randles cell where R_s represents the solution resistance, R_{corr} is the resistance of the charge transfer, Q_{dl} is the capacitance of the double layer in the electrolyte solution interface, R_{pore} is the resistance of ion-conducting paths/pores in the coating, and Q_{coat} is the capacitance related to the intact part of the coatings. Constant phase elements (Q) were used in all fittings instead of capacitances, taking into account the fact that the coating is an imperfect dielectric. This is mandatory when the phase angle of capacitor is different from -90° [170].

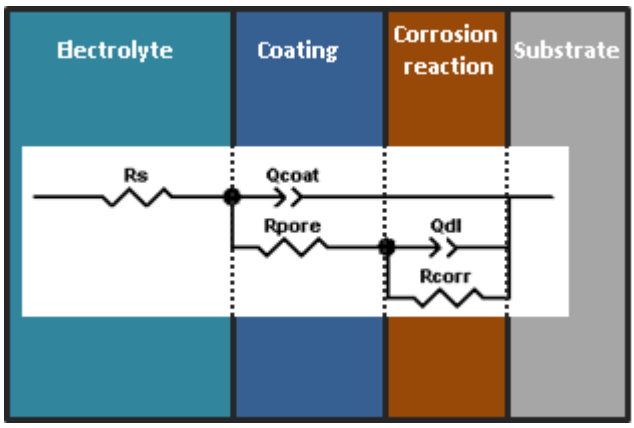

Figure 7.4. Equivalent circuit used to fit EIS data.

Figure 7.5 displays an example of the equivalent circuit and the data fitting for the coating matrix at 48 h. The same procedure was followed for the impedance values for all coating formulations at different times of exposure.

Once the fitting is done with a low fitting error (with χ^2 in the order of 10^{-3}), the different parameters can be calculated and normalised according to the thickness of each coating and the cell exposure area, and the evolution of the parameters can be plotted to monitor coating degradation as a function of time. Normalisation of the parameters to area of exposure and coating

thickness can be done since nanoparticles were homogenously dispersed through the coating matrix, as observed in section 4.2.6.

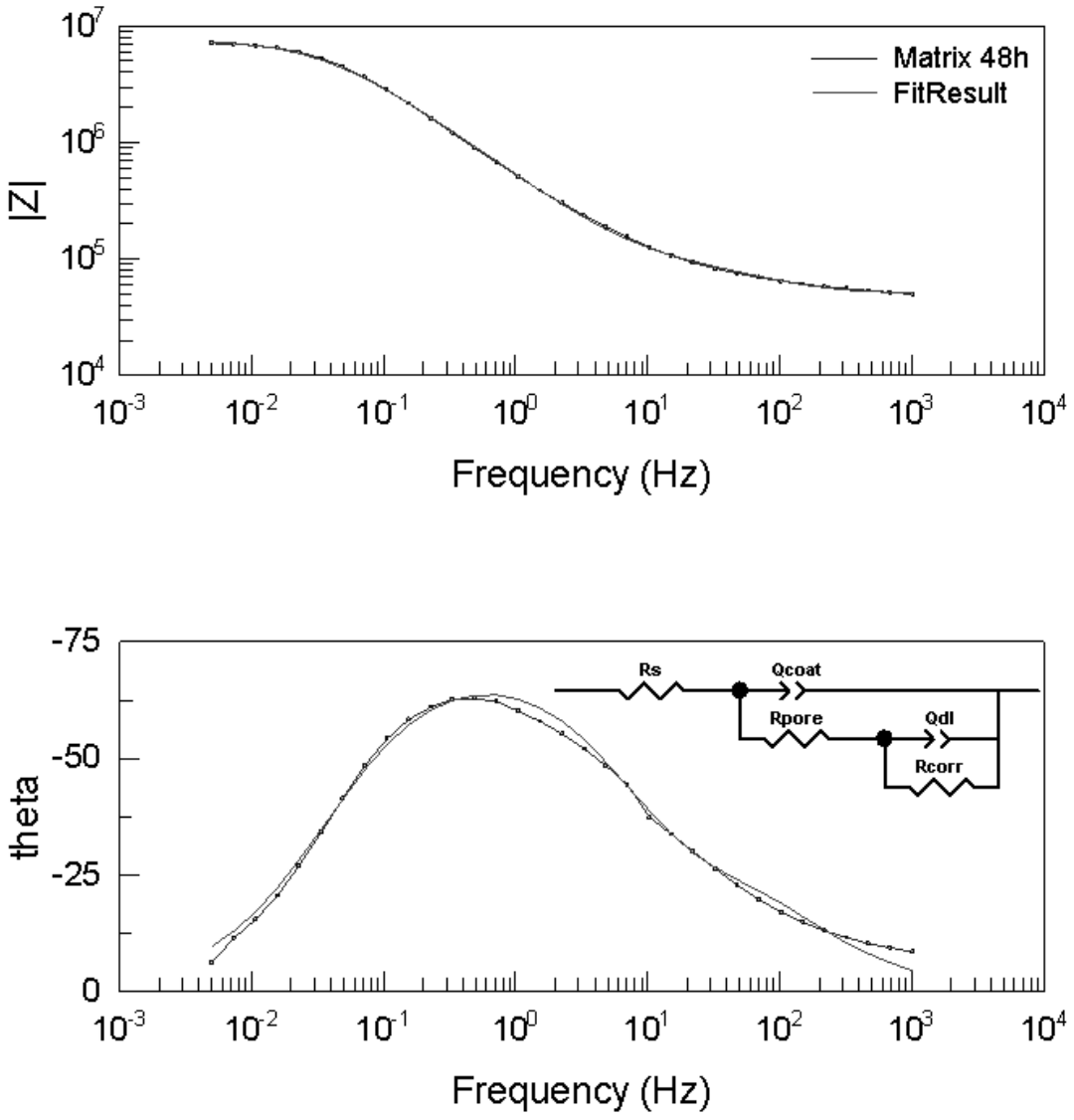

Figure 7.5. Fitting of the EIS Bode plots for the matrix without nanoparticles and equivalent circuit used. R_s= 2.16x10^4 Ω.cm; R_{pore}= 3.02x10^{4}Ω.cm; Q_{coat}= 2.97x10^{-7}F/cm; n_{coat}= 0.86; R_{corr}= 3.35x10^6 Ω.cm; Q_{dl}= 6.85x10^{-7}F/cm; n_{dl}= 0.81; χ^2= 2.64E-3.

Evolution of coating capacitance (Q_{coat}), corrosion resistance (R_{corr}) and pore resistance (R_{pore}) as a function of time is represented in Figures 7.6, 7.7 and

7.8. According to some authors, the coating capacitance can be associated with water uptake or entry of the electrolyte into the coating [154, 171]. As can be seen from Figure 7.6, there is a decrease in coating capacitance from the matrix to the coatings with silica nanoparticles, indicating less water uptake for these nanocoatings. Nevertheless, all samples showed an increase in Q_{coat} with immersion time and thus, in coating degradation. However, the coatings with functionalised silica nanoparticles showed Q_{coat} values about one order of magnitude lower than the matrix and the coating with non-functionalised silica. This indicates a significant improvement in the protective performance of these coatings.

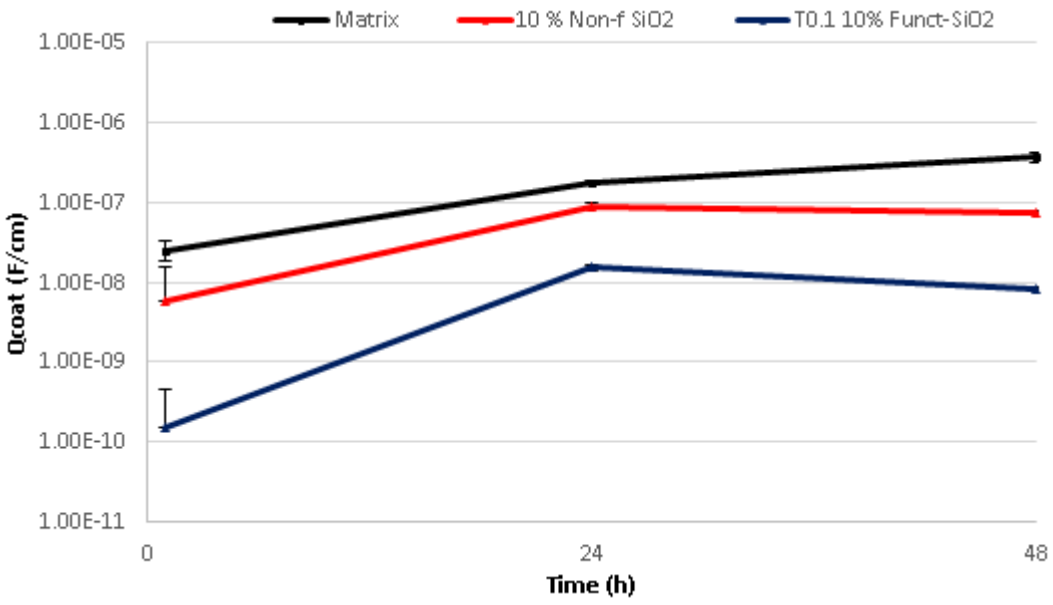

Figure 7.6. Time dependence of coating capacitance (Q_{coat}) up to 48 h.

The evolution of R_{pore} is represented in Figure 7.7. R_{pore} is associated to the existence or absence of ion-conducting paths/pores in the coating and can give an indication of the coating porosity. As can be seen from Figure 7.7, the addition of silica nanoparticles led to an increase in the initial pore resistance, R_{pore}, which could mean that the nanoparticles helped reducing

the number of defects present in the coating and formed during coating deposition and curing. Reduced defects/porosity would lead to a reduction in the ion-conducting pathways, and potentially more homogenous coatings. It can be also observed that the coating with functionalised silica nanoparticles possess the highest pore resistance, which indicates that this coating is less porous than the other formulations and thus, it has the most effective barrier properties.

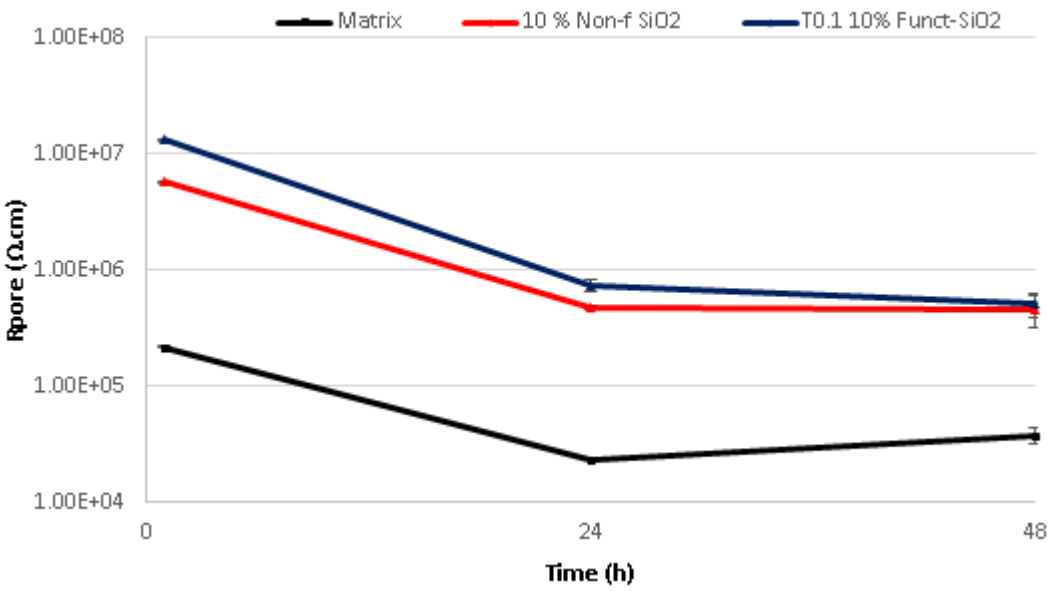

Figure 7.7. Time dependence of pore resistance (R_{pore}) up to 48 h.

When the electrolyte comes in contact with the substrate surface, electrochemical reactions occur which can cause the initiation of corrosion processes leading to the formation of corrosion products at the interface. These processes are described by the resistance at the interface or corrosion resistance, R_{corr}, and the double layer capacitance, Q_{dl}. The evolution of R_{corr} is shown in Figure 7.8. As happened previously with the pore resistance, the corrosion resistance, $R_{corr,}$ is also increased with the addition of silica nanoparticles. It is observed as well that the coating with

functionalised silica nanoparticles possess the highest resistance to corrosion over all formulations. This is in line with other studies where some authors have reported enhanced corrosion protection with the addition of functionalised silica nanoparticles into coating formulations [136, 139].

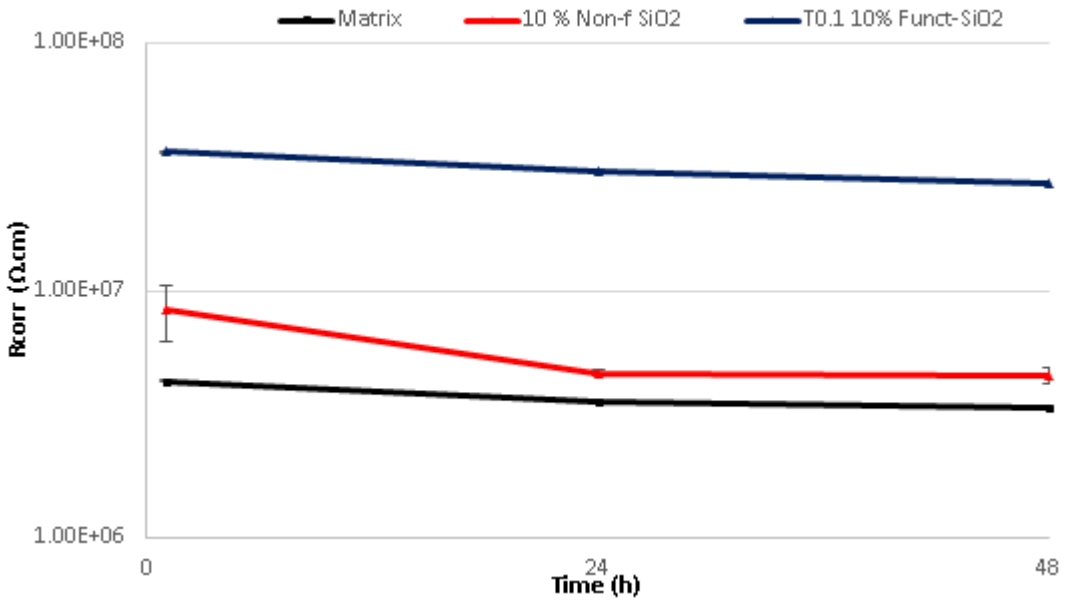

Figure 7.8. Time dependence of corrosion resistance (R_{corr}) up to 48 h.

Electrochemical Impedance Spectroscopy (EIS) measurements were also performed for the loading and functionalisation coatings samples. The test was carried out up to 144 h with the setup as described in section 4.3 and using the equivalent circuit depicted in Figure 7.4 to model the output. The different parameters obtained after fitting EIS data were calculated and normalised according to the thickness of each coating and the cell exposure area as done previously. The evolution of these parameters have been plotted to monitor coating degradation as a function of time. Figures 7.9, 7.10 and 7.11, show the evolution of coating capacitance (Q_{coat}), corrosion resistance (R_{corr}) and pore resistance (R_{pore}) as a function of time for each

functionalisation level (T0.1, T0.25 and T0.5) and at the three loading levels (10 wt.%, 15 wt.% and 20 wt.%).

Figure 7.9 shows the $Q_{coat,}$ R_{corr} and R_{pore} values for all loadings at T0.1 functionalisation level. The coating capacitance, Q_{coat}, which has been already mentioned to be associated with water uptake presents lower values with increased loading. The T0.1 20 % coating formulation shows less water penetration. It is also worth mentioning that at the beginning the coatings presented a rapid increase in coating capacitance. This could be related to the water uptake start point where the electrolyte found the pathway to the substrate and started to penetrate through the coating. Later, it was observed that the coating capacitance tends to stabilise potentially meaning that the coating was absorbing the same amount of water during the rest of the experiment.

The evolution of R_{pore} can be seen in Figure 7.9, where a similar decrease in pore resistance is observed for all loading levels. An increase in loading level could have led to an increase in pore resistance and this could be related with the lower values observed for the water uptake.

The evolution of the corrosion resistance is presented in Figure 7.9. The highest R_{corr} values are observed for the T0.1 20 % coating formulation. These results are in agreement with the salt spray test, where it was shown that the coating which provided the most resistance to the salt spray corrosion test was the coating with highest loading. Thus, it can be postulated that for the T0.1 functionalisation level, an increase in loading level would lead to more resistant coatings.

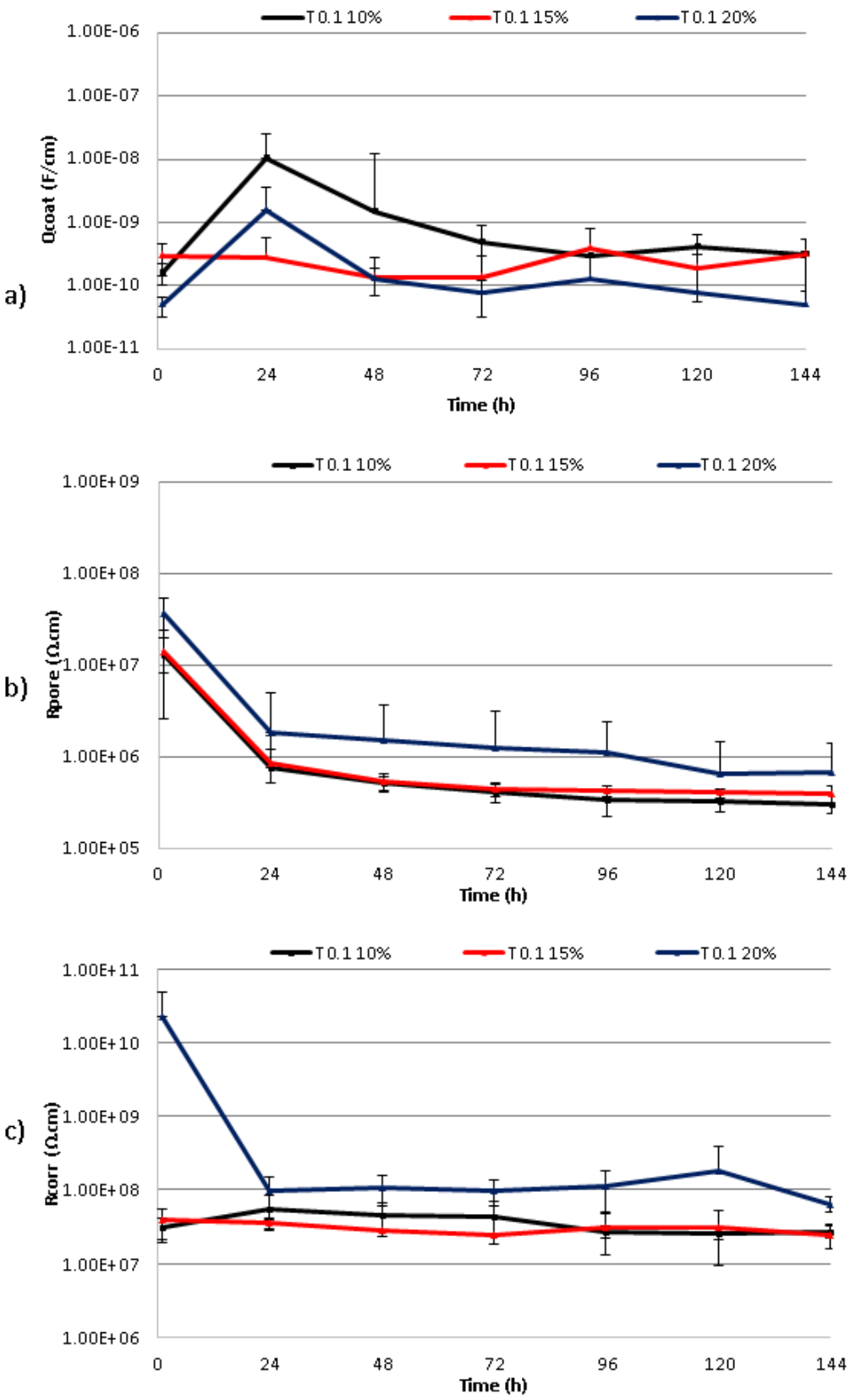

Figure 7.9. Q_{coat}, R_{corr} and R_{pore} (normalised values to cell exposure area and each thickness) for loadings at T0.1 functionalisation level.

Figure 7.10 shows the $Q_{coat,}$ R_{corr} and R_{pore} values for all loadings at T0.25 functionalisation level. In this case, all the formulations showed similar trend for water penetration. The evolution of R_{pore} can be seen in Figure 7.10, where again all the formulations showed similar values for pore resistance. There is a substantial drop at the beginning of the test however, all coating formulations tend to stabilise and at the end there is almost no change in pore resistance.

In terms of corrosion resistance evolution, which can be seen in Figure 7.10, the coating which offered highest corrosion resistance was the T0.25 15%, which also had the least water uptake (lower Q_{coat}) and highest pore resistance. Similar values were shown for T0.25 10 wt.% and T0.25 20 wt%.

Figure 7.11 shows the $Q_{coat,}$ R_{corr} and R_{pore} values for all loadings at T0.5 functionalisation level. All loading levels showed similar coating capacitance values at the end of experiment, while R_{pore} (Figure 7.11) showed similar values for the 10 wt.% and 15 wt.% but the coating at 20 wt.% showed increased pore resistance compared to the lowest loading levels.

Regarding the change on R_{corr}, these samples showed similar tendencies. Initially, the sample with the highest functionalised silica loading level had the highest corrosion resistance values. After 24 h, all the coatings experienced a dramatical reduction followed by a stabilisation in value.

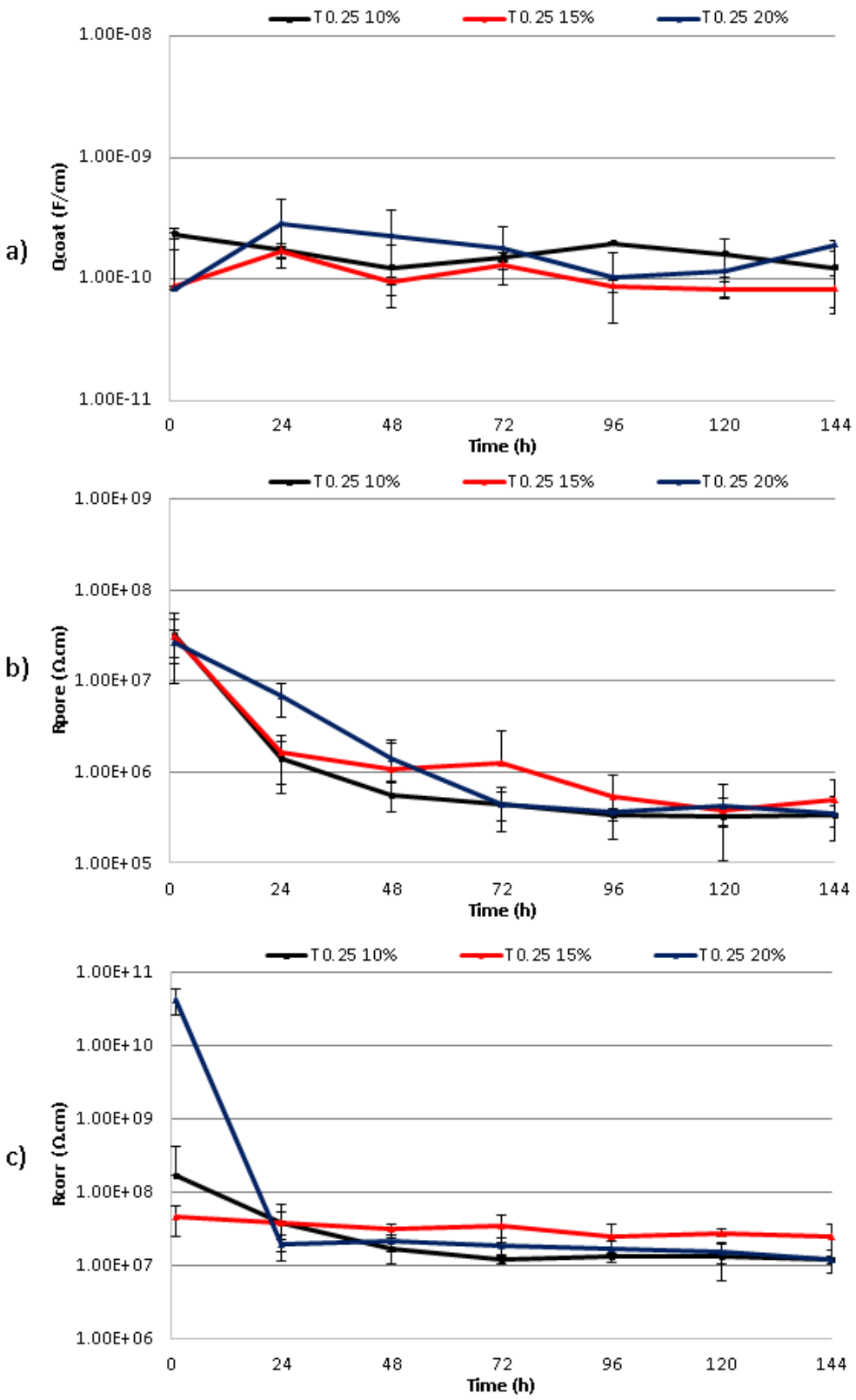

Figure 7.10. Q_{coat}, R_{corr} and R_{pore} (normalised values to cell exposure area and each thickness) for loadings at T0.25 functionalisation level.

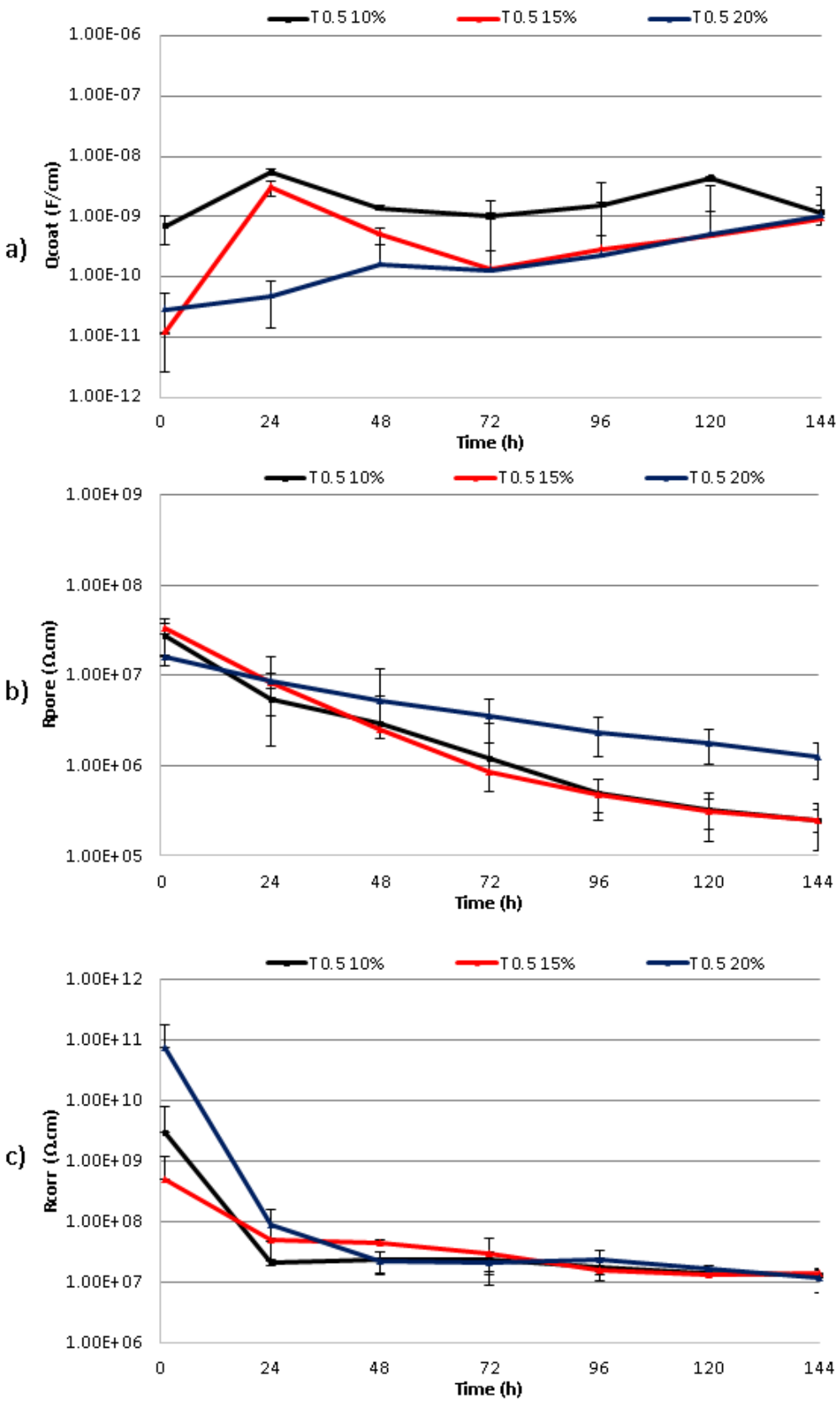

Figure 7.11. Q_{coat}, R_{corr} and R_{pore} (normalised values to cell exposure area and each thickness) for loadings at T0.5 functionalisation level.

Following the analysis on the impact of loading level (increase from 10 wt.% to 20 wt.%) on each functionalisation level, the next step was to look at the impact of functionalisation level (increase from T0.1 to T0.5) on coating corrosion performance. Figure 7.12 shows the $Q_{coat,}$ R_{corr} and R_{pore} values for all functionalisation levels at 10 wt.% loading level. It can be seen that at the same 10 wt.% loading level, the T0.25 presented the lowest water uptake, closely followed by the T.01. However, and although the tendency is very similar, T0.1 had a slightly higher pore resistance, which is in line with R_{corr} tendency and where again this formulation presented higher corrosion resistance over the other formulations loaded at 10 wt.%.

The $Q_{coat,}$ R_{pore} and R_{corr} values for all functionalisation levels at 15 wt.% loading level are shown in Figure 7.13. The T0.25 functionalisation level showed lowest values of Q_{coat} (less water uptake), and higher values of pore resistance and corrosion resistance, although these two were quite similar to T0.1. Thus, it can be said that at 15 wt.%, the formulation which performed best was the T0.25 (which also had the better performance when comparing different loading levels for T0.25).

At the highest loading level (20 wt.%), the functionalisation level T0.1 presented less water uptake than the formulations with higher functionalisation levels, as shown in Figure 7.14, which also offered the highest corrosion resistance over all: about 4 times higher than the T0.5 and more than 5 times higher than the T0.25.

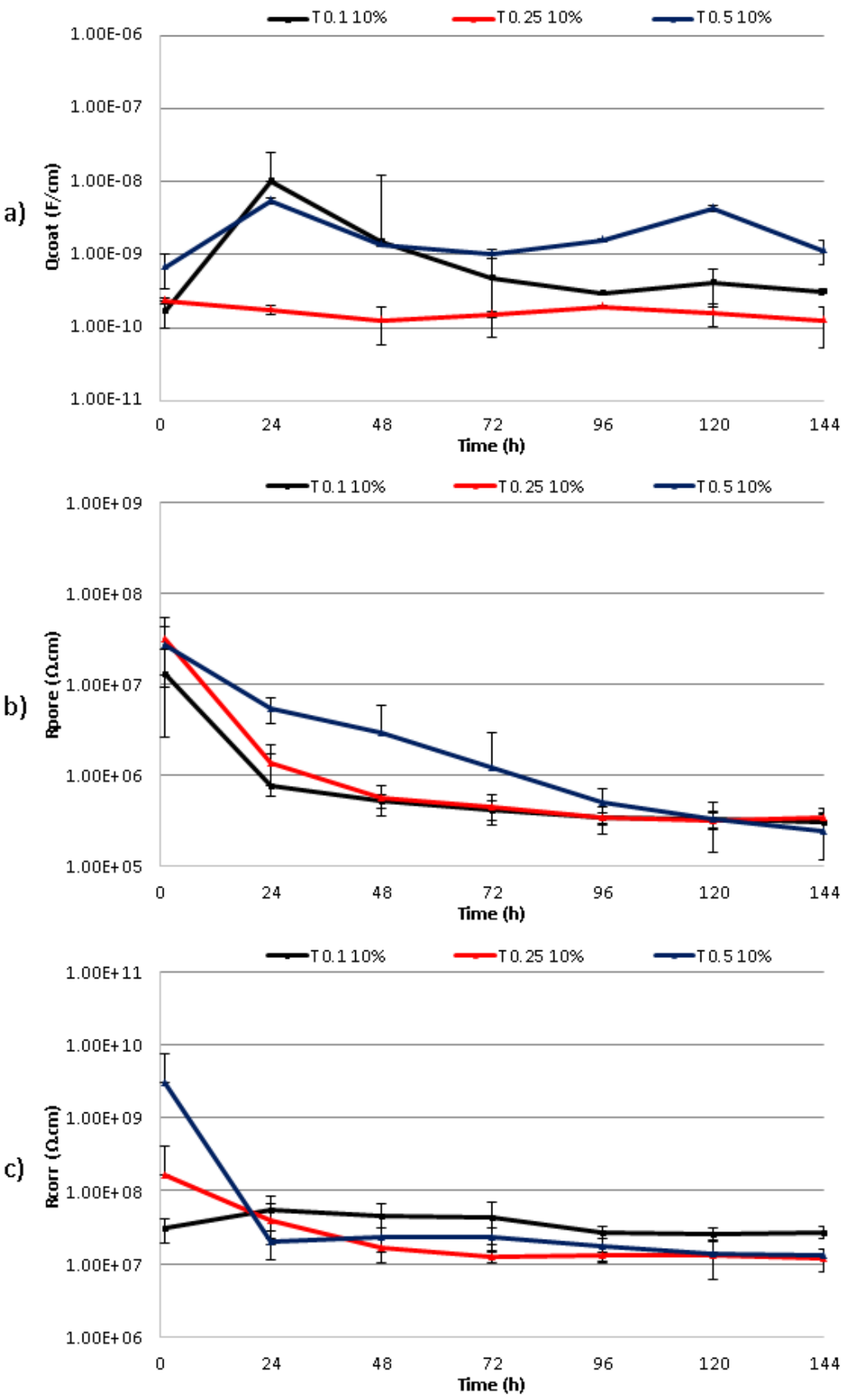

Figure 7.12. Q_{coat}, R_{corr} and R_{pore} (normalised values to cell exposure area and each thickness) for functionalisation levels at 10 wt.%.

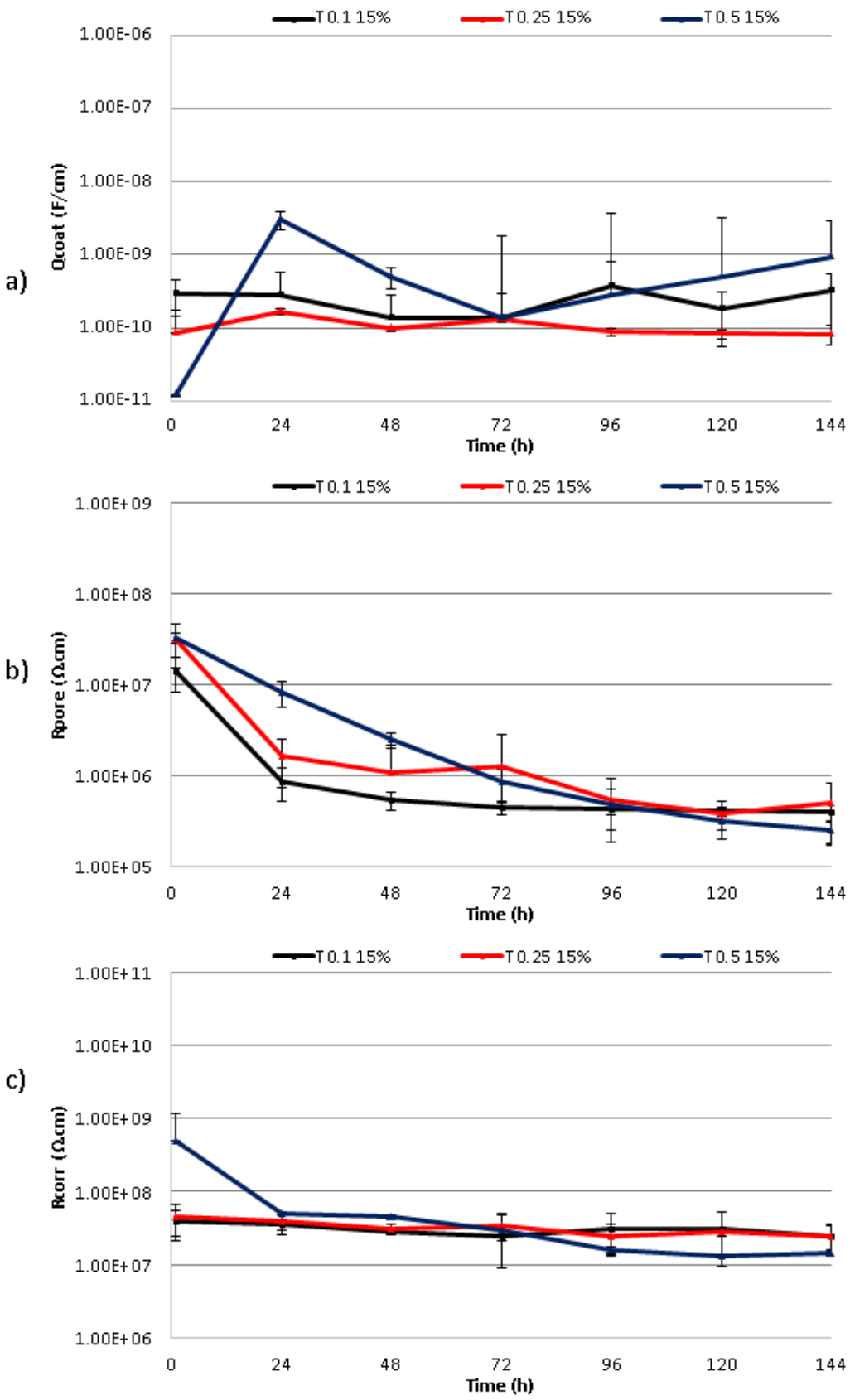

Figure 7.13. Q_{coat}, R_{corr} and R_{pore} (normalised values to cell exposure area and each thickness) for functionalisation levels at 15 wt.%.

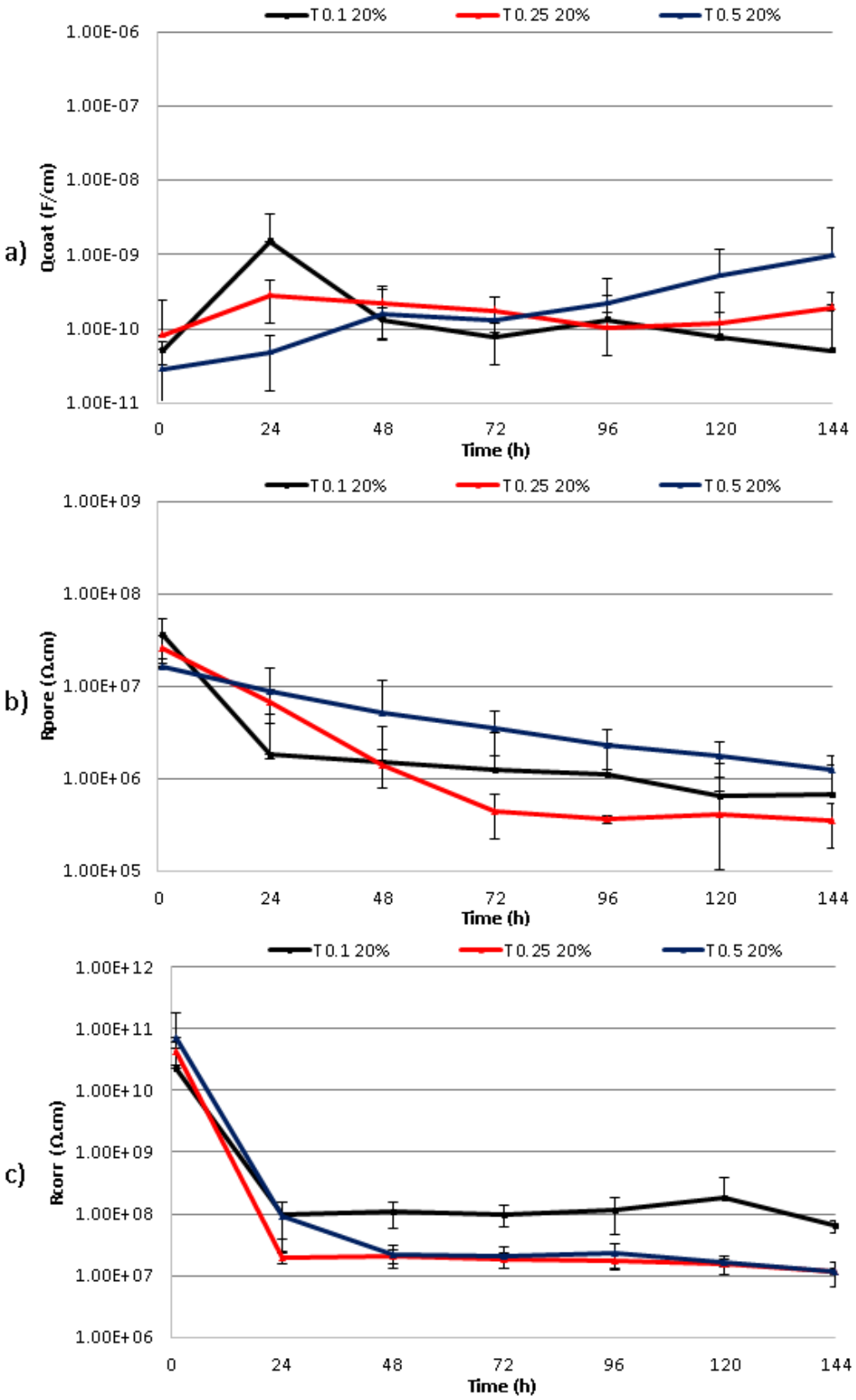

Figure 7.14. Q_{coat}, R_{corr} and R_{pore} (normalised values to cell exposure area and each thickness) for functionalisation levels at 20 wt.%.

Therefore, the coatings which performed better under electrochemical testing were:

According to loading level:

- At 10 wt% loading level: T.01 functionalisation level (T0.1 10wt.%)

- At 15 wt% loading level: T0.25 functionalisation level (T0.25 15wt.%)

- At 20 wt% loading level: T0.1 functionalisation level (T0.1 20wt.%)

According to functionalisation level:

- At T0.1 functionalisation level: 20 wt.% loading level (T0.1 20wt.%)

- At T0.25 functionalisation level: 15 wt% loading level (T0.25 15wt.%)

- At T0.5 functionalisation level: all very similar

In order to check which coating performed best overall, T0.1 20wt.% and T0.25 15 wt.% were compared. T0.1 10wt.% and T0.5 fallen from this comparison since T0.1 20wt.% performed better than T0.1 10wt.% at the same functionalisation level and also better than any coating with T0.5.

$Q_{coat,}$ R_{pore} and R_{corr} for T0.1 20wt.% and T0.25 15 wt.% are represented in Figure 7.15. It can be appreciated that the T0.1 20wt.% presented similar values of water uptake compared to T0.25 15 wt.%. However, in terms of pore resistance, R_{pore}, and corrosion resistance, R_{corr}, T0.1 20wt.% presented the highest values and thus, it can be postulated as the coating formulation with best corrosion performance over all the formulations studied.

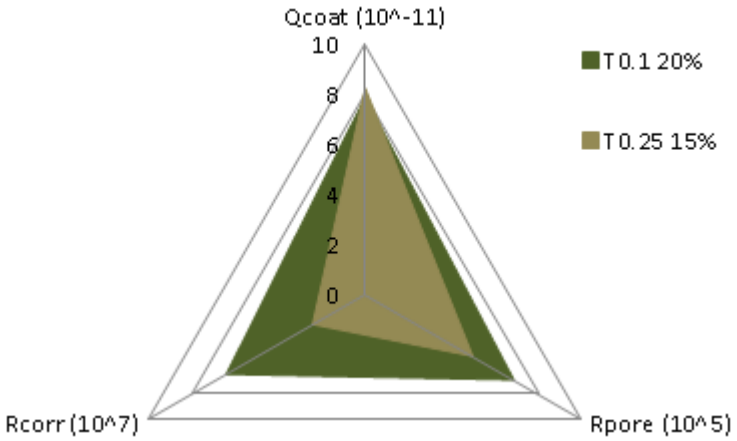

Figure 7.15. Q_{coat}, R_{pore} and R_{corr} values for T0.1 20 wt.% and T0.25 15 wt.%.

7.3.3 Polarisation curves

Potentiodynamic polarisation was carried out once the 48 h EIS test was finished. Figure 7.16 shows the potentiodynamic polarisation diagram for all coatings in 3.5 wt.% NaCl solution at ambient temperature. There is a change in potential to more active or positive values from the substrate to the matrix and from the matrix to the nanoenabled coatings. However the change is more noticeable when functionalised silica nanoparticles were added to the matrix. There is also a change in anodic current which increases by one order of magnitude from the matrix to the coating with unfunctionalised silica and from the last one to the coating with functionalised silica nanoparticles (T0.1).

Corrosion current density is commonly associated with defect density of the coatings, which is related to the pinholes or imperfections which can be form during coating deposition and curing. It basically represents the area of the substrate exposed to the corrosive environment as a result of through-

thickness porosity of the coating and can be calculated using the following relation [176]:

$$P = \frac{R_{ps}}{R_p} \times 10^{-\frac{|\Delta E_{corr}|}{\beta_a}} \qquad (7.1)$$

where P is the defect density (in %), R_{ps} is the polarisation resistance of the substrate without any coating (in Ω.cm^2), R_p is the polarisation resistance for each coating (in Ω.cm^2), ΔE_{corr} is the corrosion potential difference between the substrate and the coating layer, and β_a is the anodic Tafel slope. As can be observed from Figure 7.17, the addition of silica nanoparticles and specifically functionalised silica led to a decrease in defect density, which is related with the improvement in corrosion protective characteristics of this coating formulation. This is in agreement with the results from EIS tests, where the addition of functionalised silica led to decreased pore resistance and water uptake of the coatings and thus, increased corrosion protection.

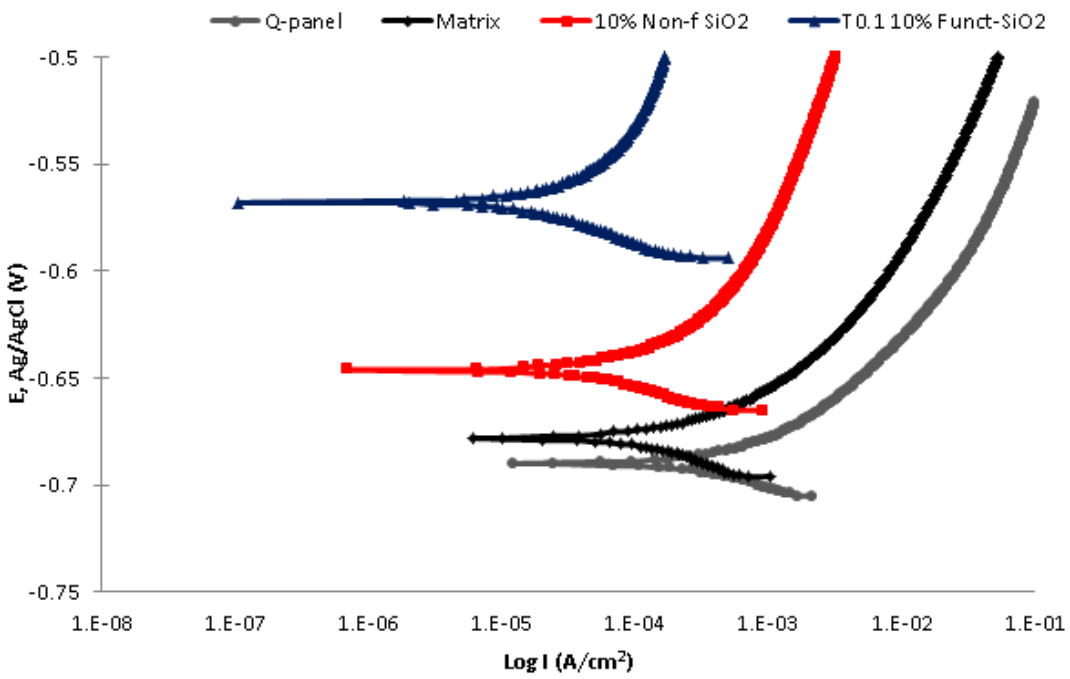

Figure 7.16. Potentiodynamic polarisation curves after 48 h.

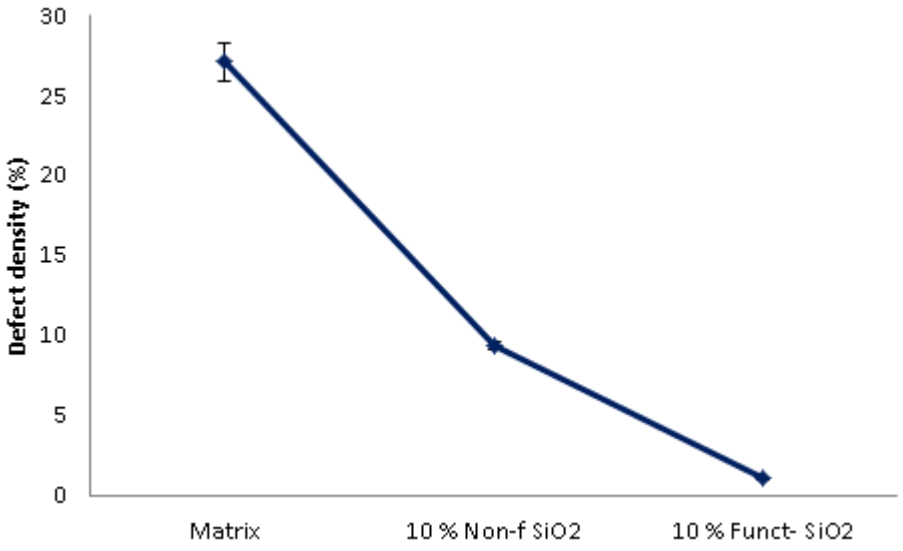

Figure 7.17. Defect density values after potentiodynamic polarisation for the coating matrix, matrix with 1 wt.% unfunctionalised silica and matrix with T0.1 10wt.% functionalised silica.

Potentiodynamic polarisation measurements were also performed for the loading and functionalisation study following the same procedure used above for the unfunctionalised/functionalised previous study, however for this study polarisation was carried out after 144 h, when the EIS was finished.

Defect density results for these coatings are represented in Figure 7.18, where can be observed that the coatings which had the lowest defect density are the T0.1 20wt.% and T0.25 15wt.%. This is in line with the EIS results where these two formulations presented the least water uptake and highest pore resistance which finally led to coatings with higher resistance to corrosion.

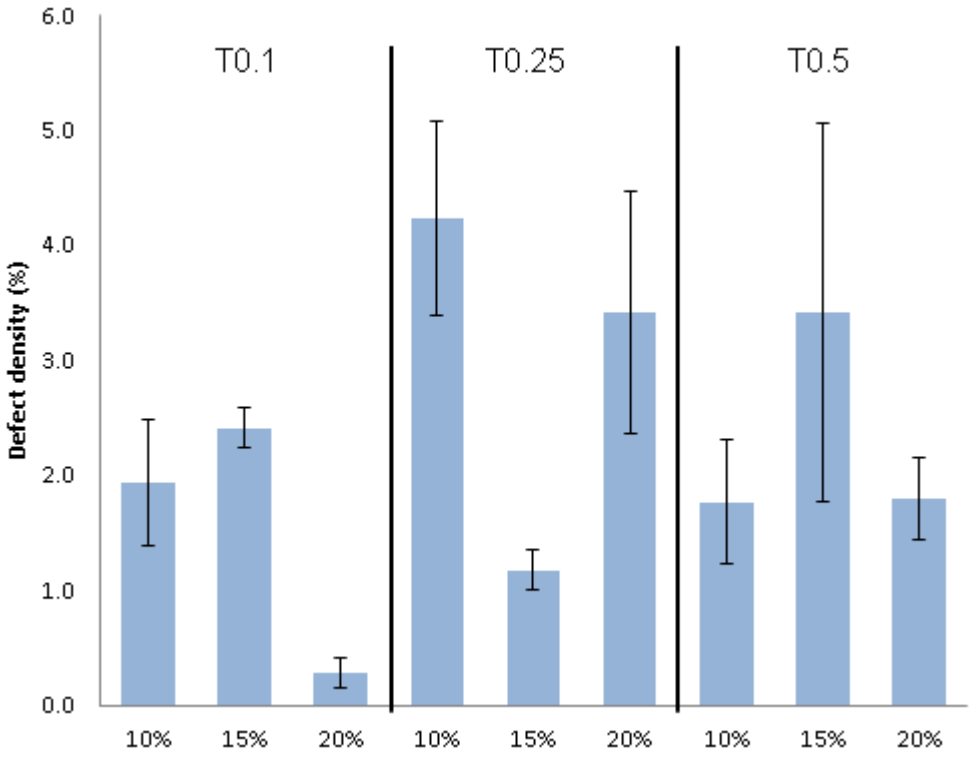

Figure 7.18. Defect density values after potentiodynamic polarisation for the functionalisation and loading study.

7.4 Conclusions

Electrochemical testing revealed that the addition of silica nanoparticles and particularly functionalised silica nanoparticles, correlated with a decrease in coating capacitance and thus, a decrease in water uptake. This is in line with pore resistance evaluation, which presented the highest resistance for the coating with functionalised nanoparticles (T0.1 10wt.%). This indicates that this coating is less porous and has less water uptake which indicates that is the most effective barrier, which is in agreement with the evolution of corrosion resistance. It has been also shown that addition of silica nanoparticles to the coating matrix correlated to increased corrosion resistance, however the addition of functionalised silica led to enhanced

corrosion resistance with values above 10^7 Ω.cm. This suggest a good correlation between the incorporation of silica nanoparticles and the improvement on corrosion protection of the nanoenabled coatings, however this behaviour is dependent on the composition and structural differences in the different coating formulations as can be postulated from the loading and functionalisation study.

The study in loading level and functionalisation level evaluation led to the major conclusions:

An increase in loading level from 10 wt.% to 20 wt.% at T0.1 functionalisation level led to samples which showed decreased defect density. Reduce defect level also correlated with reduce water uptake, and highest corrosion resistance values.

At the 10 wt.% silica loading level, T0.1 functionalisation performed better in corrosion testing (higher corrosion resistance values and lower defect density) than either the T0.25 or the T0.5 levels. At a loading level of 15 wt.% silica, the functionalisation level which performed best was T0.25. And for the highest loading level of 20 wt.% silica, the coating formulation presenting highest degree of protection was the T0.1 20 wt.%.

The coatings with less defect density (T0.1 20 wt.%. and T0.25 15 wt.%.) were found to be the coatings with less water uptake and highest corrosion resistance.

Chapter 8. Mechanical durability

8.1 Introduction

This chapter is focused on understanding the impact of silica nanoparticles on the mechanical properties of the polysiloxane-based matrix. Understanding the consequences of the incorporation of nanoparticles on coating durability and mechanical properties is important since coatings need to provide not only effective corrosion protection but also be robust.

Some important parameters influencing mechanical durability of coatings are adhesion, roughness, hardness, elastic modulus and fracture toughness. The evaluation of these parameters on the study of the influence of unfunctionalised and functionalised silica nanoparticle incorporation as well as the study on the loading and functionalisation level is explained through this chapter.

8.2 Adhesion

An important parameter influencing mechanical properties and durability of any coating is the adhesion of the coating to the substrate. As discussed in 6.1.2, all the coating formulations were rated as 5B (measured by cross-cut tape test). The cross hatch squares on the coating matrix showed no cracking or chipping, and the introduction of nanoparticles both non-functionalised as well as functionalised, did not show any cracking neither.

8.3 Roughness

Another parameter of importance is the coating roughness. Surface roughness analysis was carried out with AFM, as described in 4.2.4.

The average roughness, R_a, and the root mean square roughness, R_q, are two of the key terms used to characterise surface topography: R_a gives an overall description of the height variations and R_q denotes the standard deviation of the distribution of the surface height.

The polysiloxane-based matrix and the coating with non-functionalised silica showed no meaningful difference in surface roughness as can be observed from Figure 8.1, while a remarkable decrease is presented by the coating containing functionalised silica nanoparticles. This could be an indication that roughness is related with nanoparticle distribution: the agglomerates presented in the coating with non-functionalised silica nanoparticles could have contributed to make this coating rougher.

On the contrary, the coating with functionalised silica showed lower roughness on both measures which may be explained by greater coating homogeneity due to the uniform distribution of these nanoparticles.

This decrease in roughness was also observed in the AFM images shown in Figure 8.2. The coating with unfunctionalised silica shows some agglomerates while the coating with functionalised silica nanoparticles shows a more homogeneous and less rough surface, which supports the previous statement.

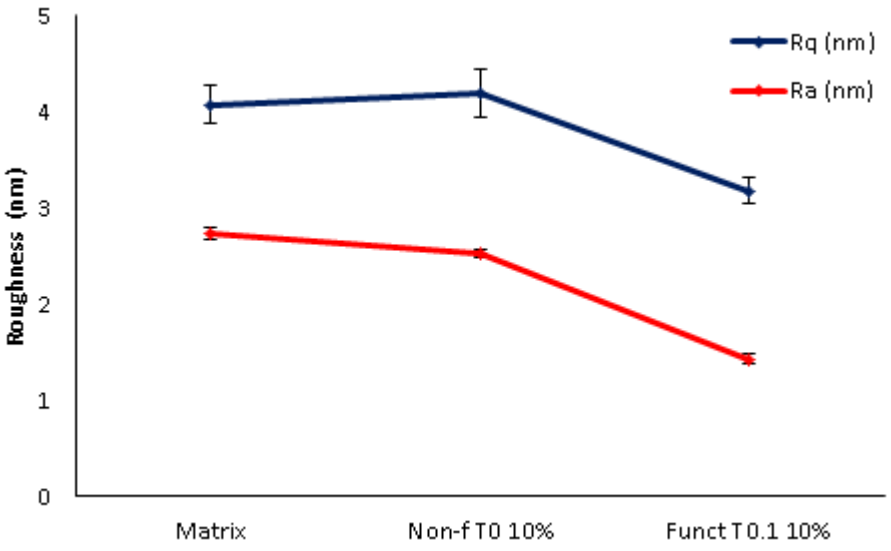

Figure 8.1. Surface roughness parameters, R_a and R_q.

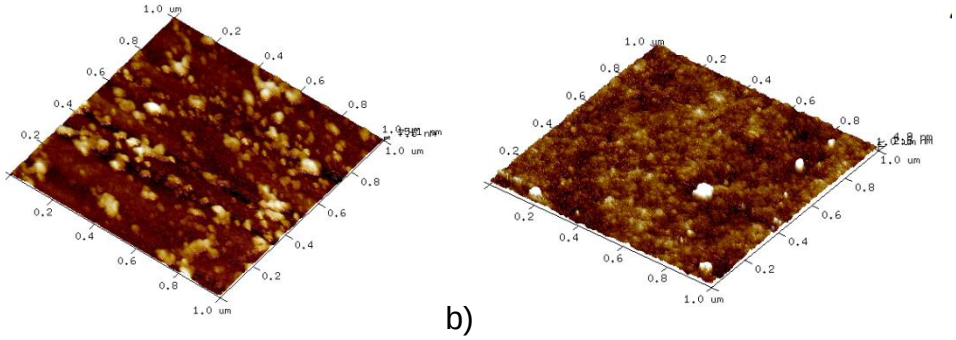

b)

Figure 8.2. Topography images of coating matrix with a) 10 wt.% unfunctionalised SiO_2 and b) T0.1 10 wt.% functionalised SiO_2.

Surface roughness of the samples at different loading and functionalisation levels (description of these formulations is in Table 6.1.) was also studied and the average roughness, R_a, and the root mean square roughness, R_q, for all these coatings are represented in Figure 8.3.

A decrease in surface roughness was observed with increasing loading levels for the T0.1, as observed from Figure 8.3. However, when increasing the functionalisation from T0.1 to T0.25, the roughness increased. This

increase was more noticeable at the 10 wt.% loading level but it decreased at highest loadings being the T0.25 15 wt.% the coating with less rougher surface at this functionalisation level.

When increasing the functionalisation level to T0.5, the values for the roughness started to look quite similar, although the greatest roughness was noticed at 20 wt.%. Thus, among all the formulations studied the coatings with T0.1 20 wt.% and T0.25 15 wt.% showed to have the least rough surface. This could be explained by the silica nanoparticle distribution in these coating formulations. As seen in the TEM pictures from section 6.1.7, these formulations showed an homogeneous nanoparticle distribution through the coatings which, as explained earlier, could have led to less rough surfaces.

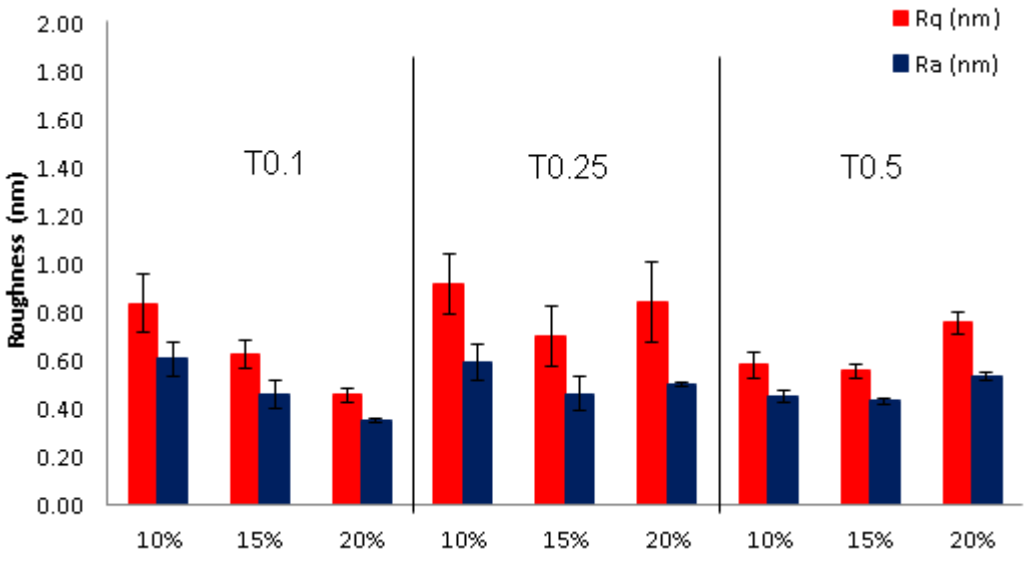

Figure 8.3. Surface roughness parameters, R_a and R_q (measured using AFM) for the loading and functionalisation study.

8.4 Nanoindentation

In order to do a proper study on the mechanical characterisation of these coatings, nanoindentation was used to quantify mechanical properties at submicron scale. The two basic properties obtained directly from nanoindentation are hardness (H) and Young's modulus (E). Hardness is a measure of the material to resist plastic deformation while Young's modulus is related to the resistance of the material to elastic deformation.

The results from the tests are shown in Figure 8.4, where an increase in hardness from the coating matrix to the coatings with silica nanoparticles can be observed. The coating with functionalised silica presents higher hardness values. A similar trend is observed for the Young's modulus, appearing that the addition of silica produces both an increase in hardness as well as an increase in elasticity for this sol-gel based matrix. This trend is expected and it is in agreement with other studies where it was found that the addition of silica increased hardness and elastic modulus [129, 135, 173]. The enhanced compatibility between the matrix and the functionalised nanoparticles and the greater nanoparticle distribution would have led to a more resistant material to elastic deformation. This improved compatibility is due to the surface functionalisation which would favour crosslinking and enhance the network density of the final material [174].

Mechanical properties in nanoenabled coatings depend greatly on the reliability and internal properties of the coating surface. Under mechanical stresses, the cavities or defects between nanoparticles or between nanoparticles and matrix can be the starting point for crack initiation. From

these results, it seems that a better compatibility between organic and inorganic network helps to create a more resistant material to both elastic and plastic deformation due possibly to the improved flexibility due to reduced crosslink density which prevented the defects from being formed in the first place. However, another parameter of importance to achieve suitable mechanical properties is the dispersion of the nanoparticles. It has been shown in other studies that agglomerates in a nanoenabled coating can result in cracks on the coating surface, which will weaken the coating and lead to decrease mechanical properties [135]. This could be the reason why the coating with functionalised nanoparticles presents the highest increment in Young's modulus with relation to the matrix. The aggregates present in the coating with unfunctionalised silica could have led to cracks which would have weakened the coating, showing lower Young's modulus values. This is consistent with the GPTMS reducing crosslink density as the functionalisation effectively shields the particles from each other.

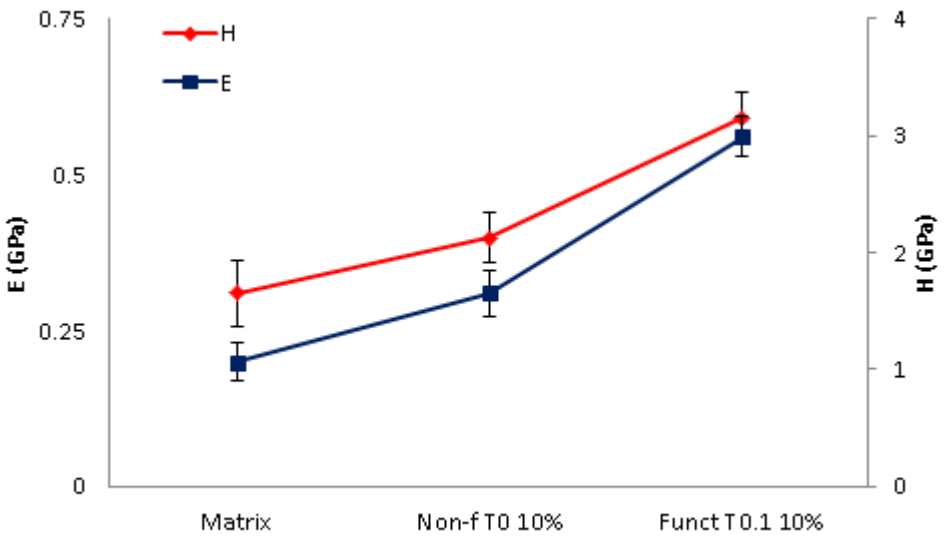

Figure 8.4. Hardness and Young's modulus.

Hardness and Young's modulus of the samples at different loading and functionalisation levels was also studied and the H and E values for all these coatings are represented in Figure 8.5.

It can be observed that the coatings at T0.1 functionalisation level presented the highest values for both hardness and Young's modulus compared with T0.25 and T0.5. There was a small decrease in H and E when increasing the nanoparticle loading from 10 to 15 wt.% that then remain practically the same when further increasing to 20 wt.%.

However, T0.25 did not have the same behaviour, an increase in nanoparticle loading led to increased hardness but in terms of Young's modulus then it decreased for the 20 wt.%.

For the coatings with silica at T0.5 functionalisation level, the values of hardness and Young's modulus remain practically the same for all the loadings.

Although, the expectation would be that an increase in nanoparticle loading would lead to more rigid coatings, this did not occur for the T0.1. This could be explained by the enhanced network compatibility and crosslinking density: if the nanoparticles are homogeneously dispersed through the coating, increasing the loading level would not lead to more rigid coatings.

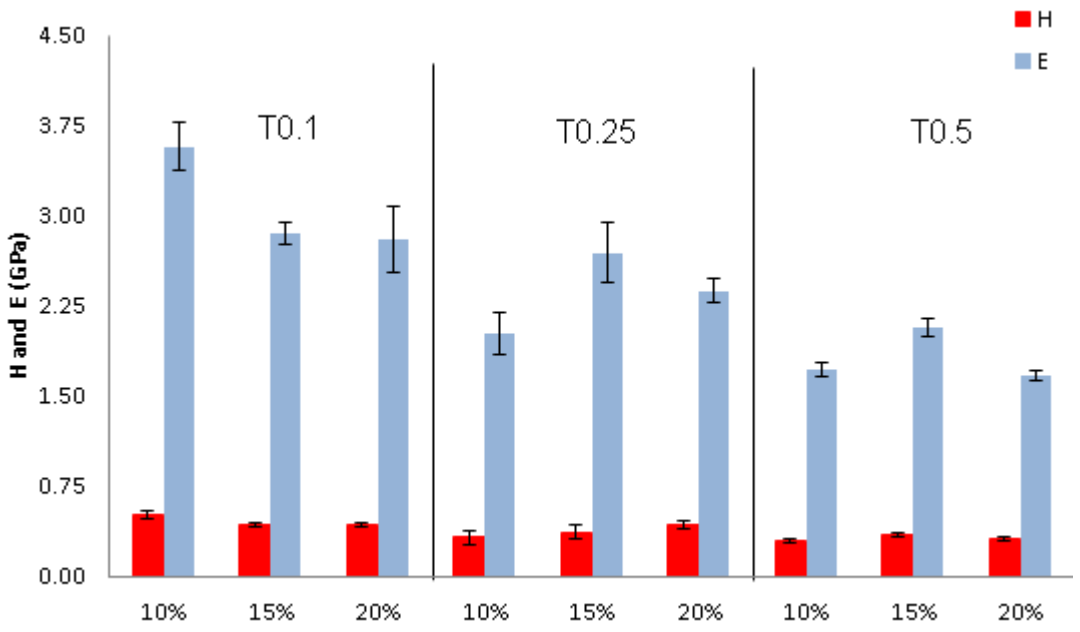

Figure 8.5. Hardness and Young's modulus values for the loading and functionalisation study.

However, hardness and Young's modulus are not the only information which can be extracted from nanoindentation. The combination of these two parameters can give place to different indexes related to material characteristics, like the brittleness index and the fracture toughness.

The brittleness index, H/E, is the ratio of hardness to Young's modulus and it is proportional to the resistance of wear [133, 148, 175]. The evolution of this parameter from the coating matrix to the coating with nanoparticles is represented in Figure 8.6. A decrease in H/E can be observed with the addition of silica nanoparticles to the coating matrix, which is even more noticeable for the coating containing functionalised silica nanoparticles. This decrease in brittleness is in line with the increase in elastic and plastic deformation resistance, as shown previously. This would mean that the addition of silica and particularly, functionalised silica nanoparticles, creates

a less brittle and more durable coating which is in agreement with previous results.

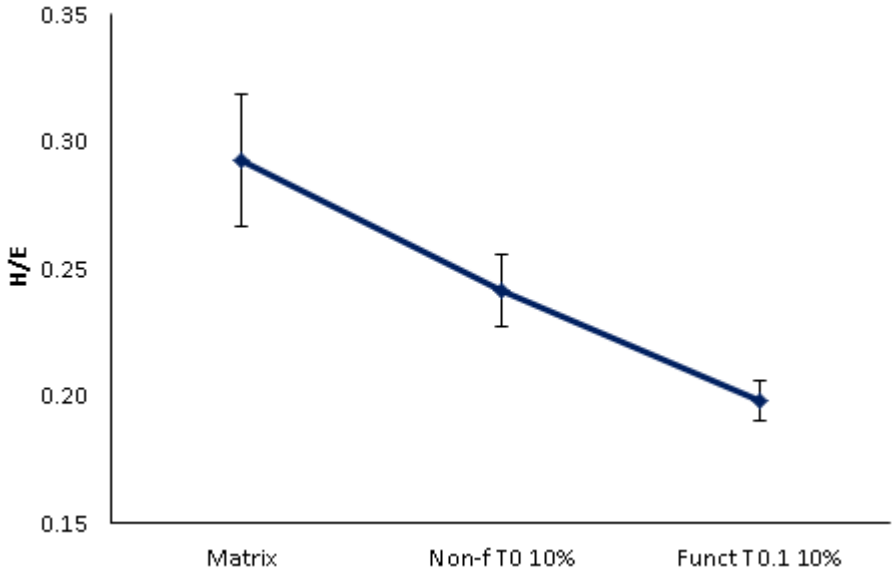

Figure 8.6. Brittleness indexes, H/E.

The brittleness indixes for the loading and functionalisation study are represented in Figure 8.7, where the coatings with silica at T0.1 functionalisation level showed to have less brittleness than the other functionalisation levels. However there was one formulation, T0.25 15 wt.%, which showed to have a decreased brittleness index that could be compared with the values for T0.1 formulations. This is also in line with the hardness and Young's modulus tendency where this formulation presented values in line with T0.1 formulations.

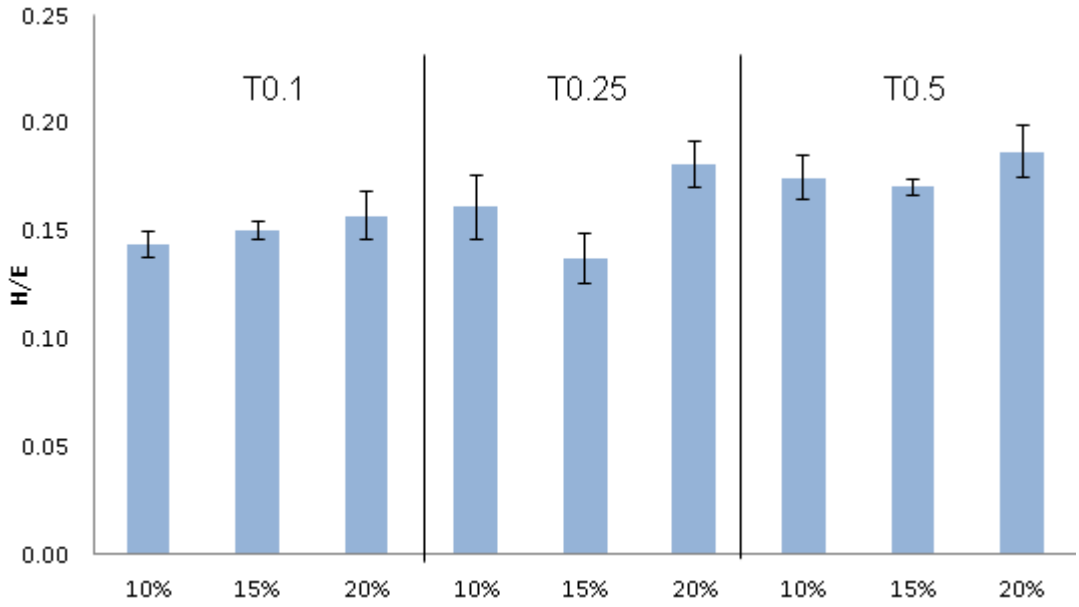

Figure 8.7. Brittleness indexes for the loading and functionalisation study.

Another important parameter used to characterise the mechanical properties of coatings is the fracture toughness of the material. Fracture toughness, K_c, which is defined as the resistance of a material to crack propagation, can be estimated by using the following relation [176]:

$$K_c = \alpha(P/c^{3/2})(E/H)^{(1/2)} \qquad (8.1)$$

where α is a constant which depends on the geometry of the indenter (0.016 for a Berkovich type indenter), P is the peak indentation load and c is crack length. In this equation (8.1), $(P/c)^{3/2}$ refers to the ability of the materials to resist crack propagation and $(E/H)^{1/2}$ refers to the potential to resist a possible fracture [177]. In this work, the ratio $(E/H)^{1/2}$ will be used to indicate the comparative fracture toughness of the coatings. Figure 8.8 shows the evolution of this parameter expressed as $(E/H)^{1/2}$. An increase in fracture toughness can be observed when the sol-gel based matrix is doped with

silica nanoparticles. As expected, the coating formulation with functionalised silica nanoparticles presents the higher $(E/H)^{1/2}$ value, which could be due to the increased compatibility between the matrix and the functionalised nanoparticles and the enhanced nanoparticle distribution which made this coating more resistant to a possible fracture.

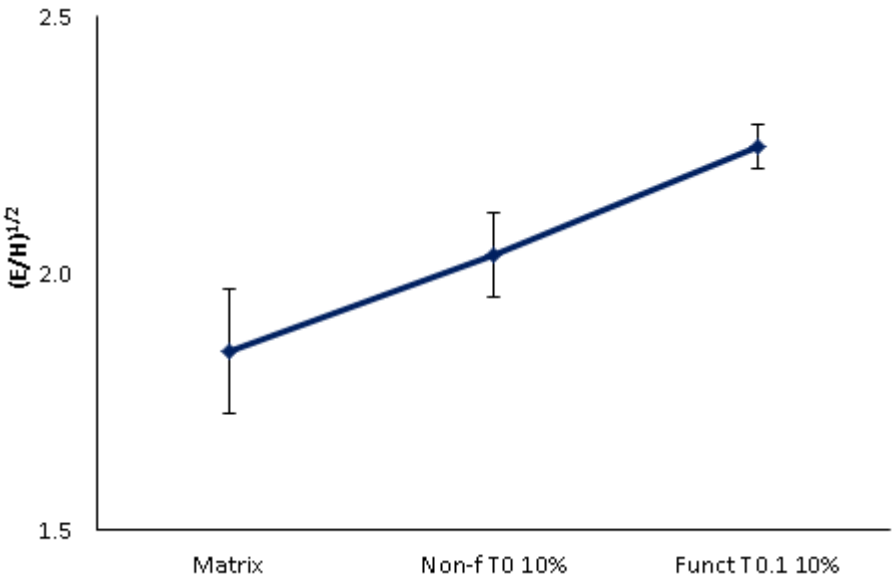

Figure 8.8. Evolution of the potential to resist fracture.

The evolution of the potential to resist fracture for the functionalisation and loading study is represented in Figure 8.9, where the coatings with silica at T0.1 displayed the higher values compared with the higher functionalisation levels, with exception only of the T0.25 15 wt.% formulation. As happened with the brittleness indexes, the T0.25 15 wt.% formulation showed similar values to the coatings with T0.1. On the other side, the coatings at T0.5 functionalisation level showed to have the lower resistance to fracture, which is in line with previous results showing that these coatings were more brittle as well.

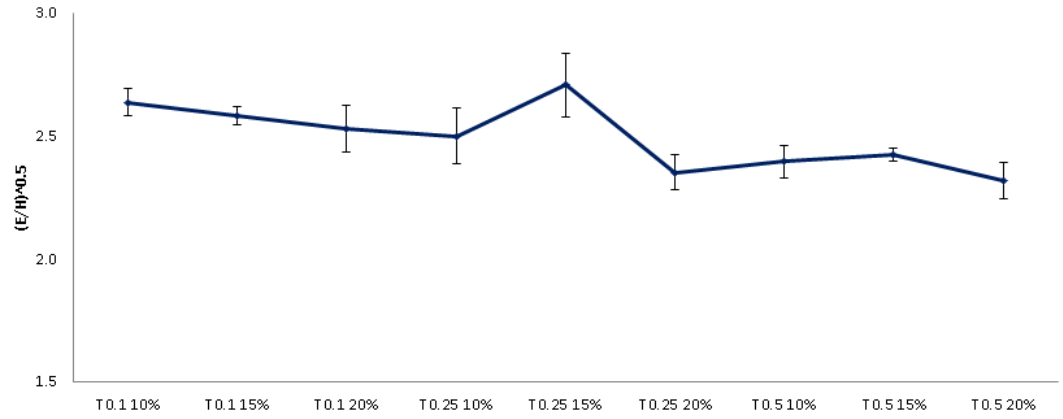

Figure 8.9. Evolution of the potential to resist fracture for the loading and functionalisation study.

8.5 Erosion

An increase in hardness while keeping a convenient low value of the brittleness index, H/E has been related to enhanced abrasion/wear resistance [133, 147, 175]. So in order to be able to correlate brittleness and wear resistance of the coatings, erosion tests were carried out to evaluate wear when studying the influence of unfunctionalised and functionalised silica to the coating matrix. This is important when looking at industrial applications since environmental factors such as sand or rain can cause erosion of coatings and reduce the lifetime.

Figure 8.10 shows the mass loss after sand erosion testing as a measure of the wear resistance of the coatings. A decrease in mass loss can be observed from the matrix to the coatings with silica nanoparticles, which means an improved impact resistance of the coatings with unfunctionalised and functionalised silica nanoparticles. The greatest erosion resistance was

observed by the coating with functionalised silica, reducing the mass loss by approximately the 80 % compared to the base matrix.

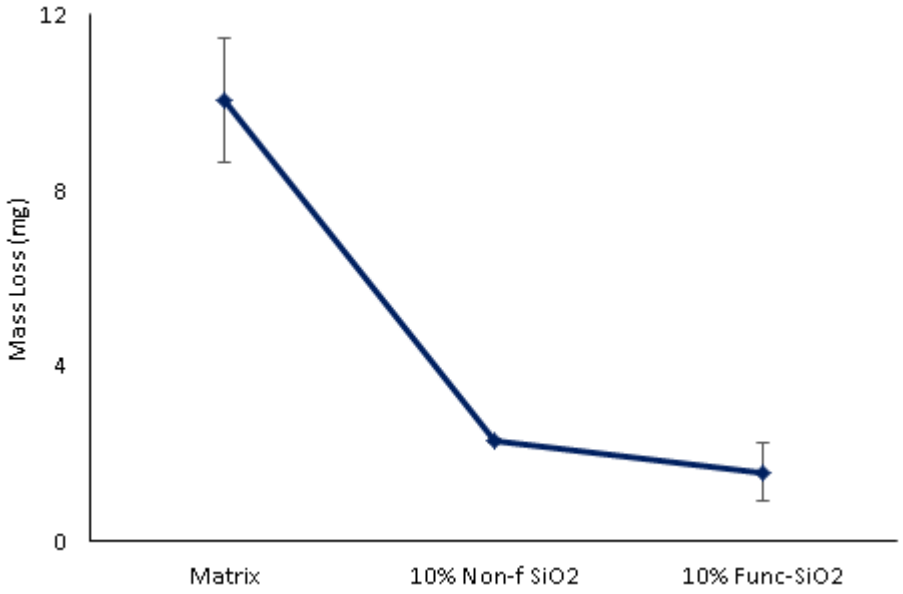

Figure 8.10. Erosion resistance of all formulations after 4-hour submerged impingement jet erosion tests at 15 m/s with a sand concentration of 1000 mg/l.

Images after erosion tests are shown in Figure 8.11. The sand impacted in a circular region of the surface of the samples. The surface morphology images shown that damage extended beyond the primary impacting area resulting a larger wear area with a poorly defined wear scar. This extended damage may be due to the brittleness of the coating matrix which could also have led to greatest rate of removal and subsequent deterioration of the substrate.

On the other hand, the addition of silica nanoparticles appear to have improved the coating formulation and these samples showed similar removal of the coating which was concentrated at the impact area.

Another important and noticeable aspect when looking at Figure 8.11 is the difference in colour in the samples. While the polysiloxane matrix and the coating with non-functionalised silica tended to lose transparency after the erosion tests, the coating with functionalised silica remained transparent after completion of the tests.

Transparency of organic-inorganic nanoenabled coatings depends on the size of the dispersed phase, coating thickness and the refractive index difference between the matrix and the nanoparticles [178]. This type of coating has a high transparency because the size of the nanoparticles as well as the roughness are significantly smaller than the wavelength of light (400 nm).

The transparency of coatings used to decrease with increasing surface roughness, however, the coatings studied in this work were all transparent before testing because their surface roughnesses were far from the minimum wavelength of visible light (400 nm).

However, transparency can be lost after mechanical damage and also aggregates can contribute to deteriorate the mechanical properties and transparency. This may be the reason why the coating with functionalised silica was the only coating which remains transparent after completion of the erosion test.

The drop in transparency may be due to the increase of the defect density when the mass loss increased, which may produce a diffusion of the light at the points of impact generated by the sand particles [179]. On the contrary, the improved hardness and stiffness with the addition of functionalised silica

could have assisted the nanoenabled coating in absorbing and dissipating the impact energy which could have led not only to improve the erosion resistance but also to retain the transparency of this formulation.

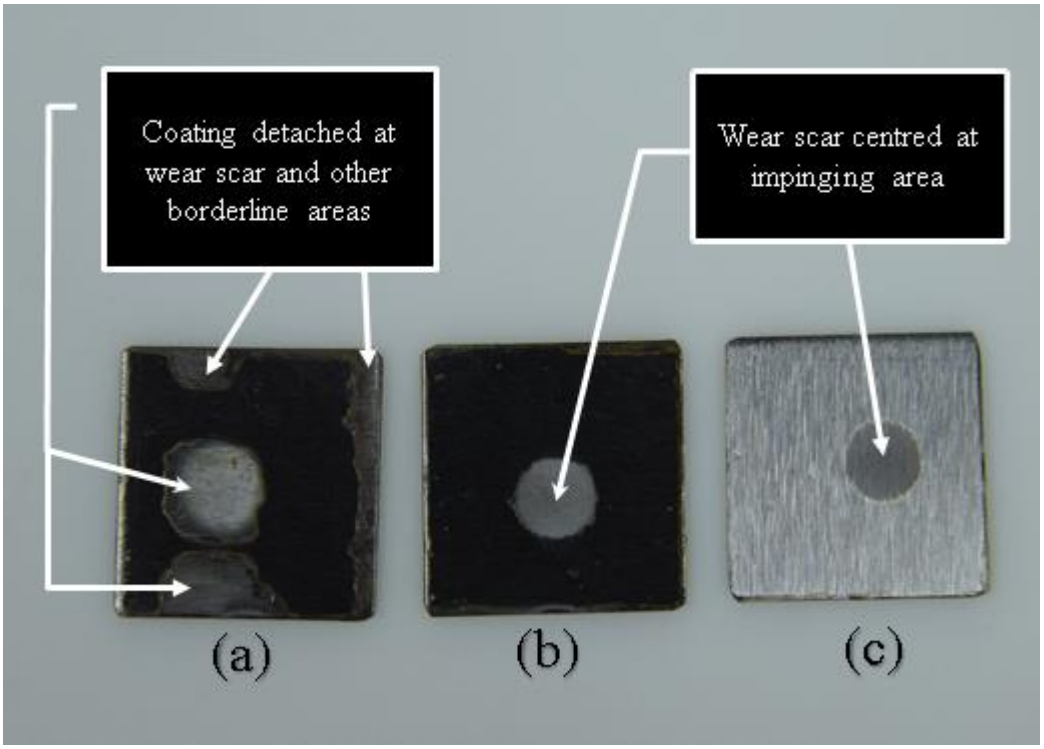

Figure 8.11. Surface morphology images after 4 h submerged impingement jet erosion tests at 15 m/s flow velocity, 1000 mg/L sand loading in a N_2 saturated environment for (a) polysiloxane based matrix (b) matrix with 10 wt.% non-functionalised silica and (c) matrix with T0.1 10 wt.% functionalised silica. (1 x 1 cm^2 samples).

To check the surface morphology, profilometry was carried out after completion of the erosion tests. Surface profilometry images are shown in Figure 8.12.

As seen previously in Figure 8.11, significant removal of the coating matrix is also observed from the surface profiles images in Figure 8.12. In contrast, the coatings with silica nanoparticles just showed removal of the coating at

the impinging area, which can be explained by the improved mechanical properties of these coatings compared to the parent matrix. The nanoenabled coatings did not present any further damage apart from the area where the erosion test was undertaken. This can potentially be related to the increased hardness and elasticity of these coating formulations after the addition of silica nanoparticles, but also with the decrease in brittleness index.

The cumulative effect of these changes in properties could be related to the enhancement in wear resistance. However the coating which exhibited the lowest mass loss and which showed the least surface damage after erosion tests was the coating with functionalised silica, indicating that this coating formulation was more resistant to elastic and plastic deformation, more resistant to wear and thus, more durable.

The edge of the wear scar is very well defined for the coating with functionalised silica which is an indication that this coating is very well adhered to the substrate and that even if erosion damage occurs it will remain at the impinging area and will not go underneath.

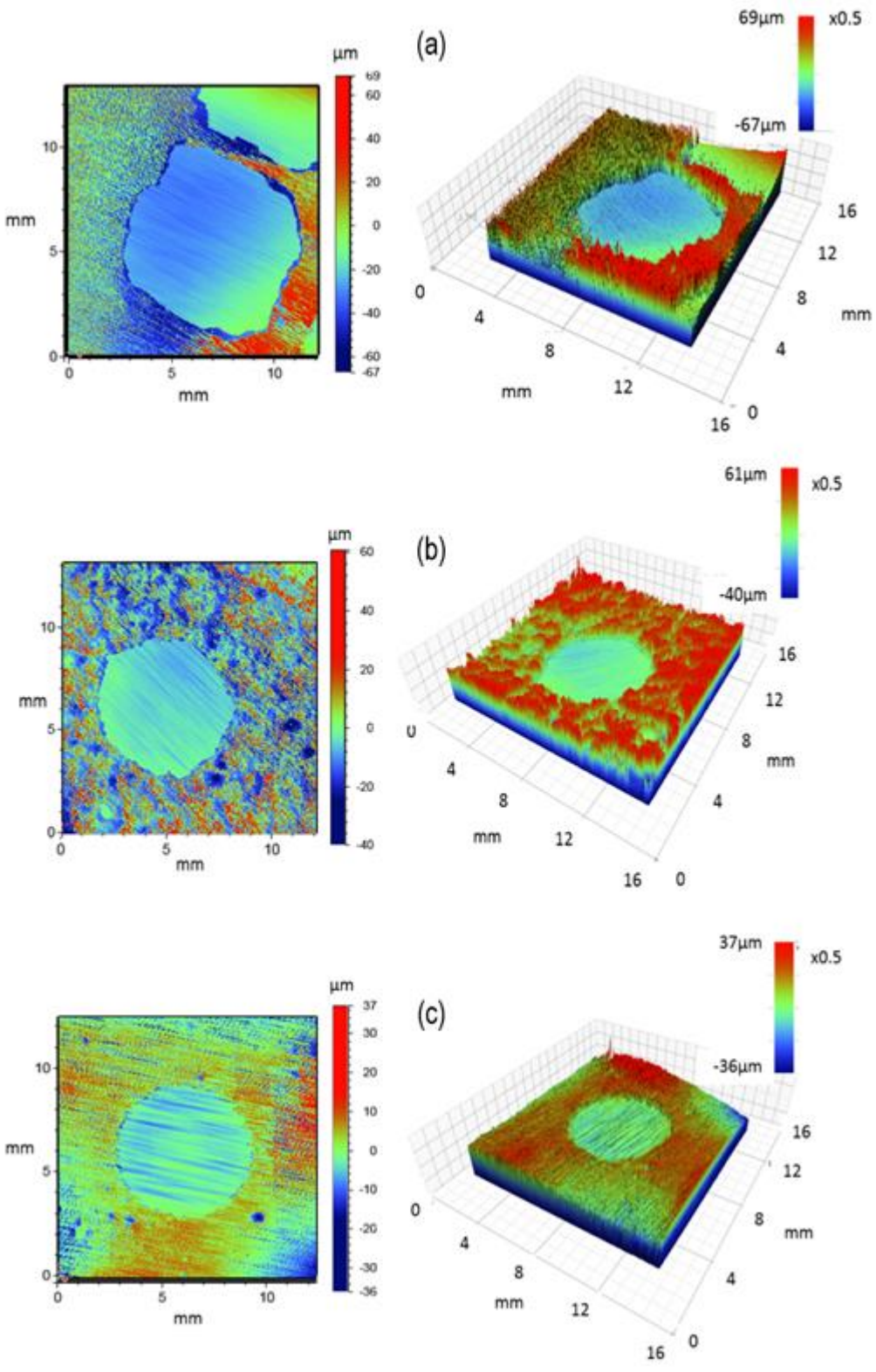

Figure 8.12. 2D and 3D surface profiles images after 4 h erosion tests: (a) sol-gel based matrix (b) matrix with 10 wt.% non-functionalised silica and (c) matrix with T0.1 10 wt.% functionalised silica.

8.6 Conclusions

This chapter has summarised different parameters which could affect the mechanical properties of the coatings under investigation. Surface roughness is an important parameter on coating quality which can influence both mechanical properties and corrosion resistance. Firstly, when non-functionalised silica and functionalised silica were added to the polysiloxane matrix, it was observed that the matrix presents higher roughness which decreased with the addition of silica nanoparticles, being the coating with functionalised silica (T0.1 10 wt.%) the coating presenting the lower roughness. This decrease in roughness may be explained by the greater homogeneity due to the functionalisation with GPTMS which reduced crosslink density effectively shielding the nanoparticles from each other and leading to uniform nanoparticle distribution.

In the study of loading and functionalisation level, a decrease in surface roughness was observed when increasing the loading level for the T0.1 functionalisation level which could be due to the enhanced nanoparticle distribution and decreased defect density. However, T0.25 and T0.5 did not follow the same behaviour. T0.25 presented similar roughness values at 10 and 20 wt.% loading but decreased for the coating at 15 wt.%. In the case of T0.5 coatings, the lowest loadings showed similar roughness values which then increased when incorporating 20 wt.%. The all above formulations, the coating which presented the less rough surface was the T0.1 20 wt.%.

Mechanical properties were also found to be improved with the addition of unfunctionalised silica to the base matrix. The increase in hardness and

elastic modulus can be explained due to the harder and stiffer coating with the silica nanoparticles. It was also found a decrease in brittleness and an increase in the possible resistance to fracture as well as enhanced wear resistance, which is a sign of increased mechanical durability. Nevertheless, there is a further improvement when the nanoparticles are functionalised. The greater homogeneity and the reduced crosslink density presented by this formulation could have led to a decrease in roughness as well as an increase in hardness and elastic modulus, decrease in brittleness, improvement on the resistance to fracture and increased flexibility due to the use of the silane.

The loading and functionalisation level study led to the following conclusions:

- T0.1 coatings exhibited the highest hardness and Young's modulus values compared with T0.25 and T0.5, with the exception of T0.25 15 wt.% whose values of H and E were comparable with those of T0.1.

- In terms of brittleness, T0.5 coatings showed the highest values followed by T0.25, with the exception again of T0.25 15 wt.% which presented lower values which could be comparable with those of T0.1.

- Looking then at the resistance to fracture, the T0.1 coatings appeared to be the most resistant coatings to fracture together with T0.25 15 wt.%, while all the other formulations displayed lower values and thus, lower resistance to fracture.

These results are in-line with results from the roughness evaluation, where the coatings with lower roughness were the coatings at T0.1 functionalisation level and the T0.25 15 wt.%. This could be an indication of

the enhanced nanoparticle distribution of these coatings which led to less rough coatings with enhanced mechanical properties.

Chapter 9. Discussion

The results from the formulation development described in Chapter 5 and the tests conducted in Chapters 6, 7 and 8 involving coating microstructure, corrosion performance and mechanical durability will be analysed and discussed in this chapter.

The focus will be firstly on the influence of incorporating unfunctionalised versus functionalised silica nanoparticles into the polysiloxane-based matrix, in order to understand the impact of the functionalisation of nanoparticles and its effect in coating properties and performance.

Using this study as a starting point, the work will continue by conducting a functionalisation and loading study where the influence of three functionalisation levels (T0.1, T0.25 and T0.5) and three loading levels (10, 15 and 20 wt.%) will be examined.

A comparison between the results gathered with all the tests described in Chapters 6, 7 and 8 could establish the key factors relating macro-scale performance to nano-scale morphology.

Clear understanding of this relationship is expected to contribute towards the elucidation of key design rules which can then be used as the basis for a materials by design methodology capable of the underpinning a new knowledge based technology which can create an excellent opportunity to achieve significant industrial impact.

9.1 Silica impact on coating microstructure

One of the parameters observed while looking at coating microstructure was the thickness. As can be seen in section 6.1.1, the addition of non-functionalised silica nanoparticles to the sol-gel based matrix led to increased coating thickness. This was expected and is in line with other works where the addition of nanoparticles led to increased coating thickness [104, 128, 161]. An increase in loading level also led to increase the coating thickness, which is also in agreement with literature [128, 129, 133].

However, the coating containing functionalised silica for the same loading level was thinner. On the other side, the loading and functionalisation study had two different results: for T0.1 an increased loading led to increased thickness while for T0.25 and T0.5 the thickness decreased at 15 wt.% and increased at 20 wt.% (as can be seen in Figure 6.1 and Table 6.2). It is a possibility that the thickness is influenced by the distribution of nanoparticles. If nanoparticles are not homogeneously distributed, agglomerates could lead to increase the coating thickness in some areas.

Particle size of silica is another parameter of importance, since the functionalisation process lead to changes in the size of the silica particle by introducing functional groups. While the size of unfunctionalised silica remain around 26 nm, the sizes of functionalised silica changed after the different surface functionalisations, however, these sizes were quite similar. Results from Table 5.4, showed that the particle sizes from DLS-Number are close to the particle sizes from TEM, with an approximation of 18-26 %.

On the contrary, the particle sizes from DLS-Intensity presented a high difference of about the 60 % compared with the particle sizes from TEM. This could be due to the fact that the particle sizes from TEM images where taken when the silica nanoparticles were already incorporated into the sol-gel based coating and in dry state, while DLS measurements were performed when nanoparticles were in solvent media prior incorporation into the matrix.

Therefore, from TEM the diameter of the dried particle is measured while DLS measures diffusivity of the particles to estimate the hydrodynamic size, which is the diameter of the particle and the liquid layer around the particle. Since DLS measures the hydrodynamic size, it could be a tendency of aggregate which can influence the value obtained for particle size: if nanoparticles agglomerate, DLS values would appear larger.

In a study where different techniques were used to determine particle sizes was found that diameters obtained from DLS were consistently higher than the other techniques and larger than what was expected based upon the sample characteristics [180]. This is also in line with another study where a comparison between TEM and DLS methods to characterise size distribution led to the conclusion that although DLS-Intensity presented values five times larger than TEM, DLS-number showed a better approximation to the size obtained by TEM: app. 20 % higher than TEM [181], which is quite similar to the results reported here.

Regarding the water repellence, the introduction of nanoparticles to the polymer matrix led to enhanced water repellence, which was more noticeable for the coatings with functionalised nanoparticles (as seen in

Table 6.3). This is in agreement with other works where higher water contact angles have been reported with the addition of nanoparticles which then were further enhanced when the nanoparticles were functionalised [182, 183].

When then looking at increasing the functionalisation levels, it was observed that an increase in functionalisation level led to increased water repellence (Table 6.4). This could be explained by the decrease in OH groups from the silica surface due to the grafting, which led to a decrease in hydrogen bonds between water and nanoparticles [132]. Increased water repellence when increasing nanoparticle loading has been also previously reported [184].

Nanoparticle distribution appears to be an important factor affecting coating performance. Microscopy images and AFM images in sections 6.1.5 showed that the introduction of silica led to less porous coatings, although with some nanoparticle agglomerates. However when the nanoparticles were functionalised, there was an increase in coating homogeneity and uniformity, due to enhanced nanoparticle distribution.

TEM images in section 6.1.7 also confirmed the positive effect provided by surface functionalisation of silica. Independently of the functionalisation level, all the coatings with functionalised silica showed enhanced nanoparticle distribution compared with the coating with unfunctionalised silica. However, coatings with a functionalisation level of T0.1 showed no agglomeration and good nanoparticle dispersion even at highest loadings, while coatings containing silica functionalised at T0.25 and T0.5, whilst still well dispersed throughout, did show some evidence of a small degree of agglomeration.

This enhanced nanoparticle distribution and enhanced water repellence was due to the functionalisation, since the surface treatment of nanoparticles can cause steric hindrance and help to avoid nanoparticle agglomeration during incorporation [54, 185]. But also due to the increased compatibility between the matrix and the functionalised nanoparticles as the GPTMS grafted on the silica surface is also present in the matrix network. This can lead to stronger interface between the matrix and the nanoparticles [54, 124, 138, 142, 146].

9.2 Silica impact on corrosion performance

With respect to corrosion resistance, one of the first tests performed was the neutral salt spray that, whilst not comparable with real life, can be used as a screening test when used to assess initial performance. This test showed that the introduction of functionalised silica led to coatings with higher corrosion resistance compared with both the matrix itself and the coating with non-functionalised silica.

The loading and functionalisation study showed that increasing loading increased the corrosion performance for the T0.1 and T0.25, while coatings containing functionalised silica at T0.5 performed all quite similarly, irrespective of the loading level. Of all the coatings with functionalised nanoparticles, the coating with T0.1 20 wt.% was the coating which showed highest corrosion protection after the salt spray test.

Open circuit potential measurements obtained for the bare substrate, the polysiloxane matrix and the coatings with unfunctionalised and functionalised silica (T0.1) at 10 wt.%, which can be observed in Figure 7.3, showed a strong correlation with the water contact angle measurements

presented in Table 6.3. If comparing the E_{OCP} and WCA values, as done in Figure 9.1, it can be observed that the higher the contact angle, the less negative is the potential. This was also observed by Suegama et. al [126, 127] where they attributed this decrease in the potential to electrolyte penetration during the experiment.

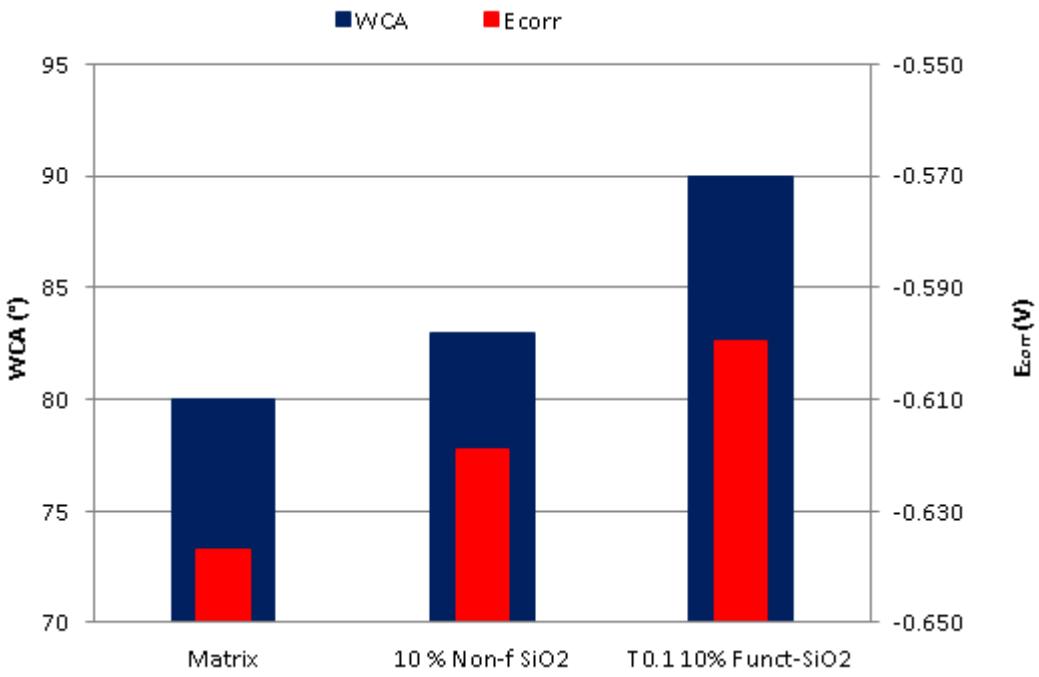

Figure 9.1. Comparison of WCA and corrosion potential.

With the purpose of obtaining a more detailed picture of the parameters influencing coating properties due to the addition of silica nanoparticles, both non-functionalised and functionalised, some properties were studied in combination. Firstly, the influence of silica incorporation in coating roughness (R_a), defect density, water uptake and corrosion resistance is represented in Figure 9.2, where R_{corr} is the corrosion resistance of the coatings (in Ω.cm) and Q_{coat} is the coating capacitance (in F/cm), which can be associated with water uptake or entry of the electrolyte into the coating [154, 171].

As can be observed from Figure 9.2, the coating matrix alone had the highest roughness and highest defect density and the lowest corrosion resistance. It is possible that there is some correlation between these characteristics. Increasing defects in the coating may lead to increased permeability which would then result in an increased propensity to corrosion. Also, surface defects would impact on the overall topographic character of the coating leading to higher levels of roughness. It is also well known, that higher roughness levels can lead to enhanced wetting which itself would lead to improved conditions for corrosion.

Silica particles reduce the shrinkage the coating is capable of undergoing during curing. Reduced shrinkage leads to lower stress generation and lower levels of cracking and defect generation. Since the polysiloxane matrix is brittle, any localised tensile or shear stresses would increase the potential for cracking and defect formation. Thus, the addition of silica nanoparticles led to lower roughness and decreased defect density and would have led to reduce the water uptake and consequently, to increase the corrosion resistance of these coatings.

However, when the silica nanoparticles were surface treated with GPTMS and added to the sol-gel based matrix, there was a further enhancement: the presence of the GPTMS would have provided a more flexible network more able to withstand drying stresses. Thus, the coating formulation with functionalised silica presented the highest corrosion resistance values, which could be related with the decreased roughness due to enhanced nanoparticle distribution. Nanoparticle distribution appears to be an important parameter affecting coating properties, which is in line with other

investigations where it was shown that the anticorrosion performance of the coatings decreased due to increased silica agglomeration [130].

The nanoparticles are preformed and so would represent a barrier to permeation meaning that a more tortuous pathway (lower water uptake) within the coating would be presented leading to reduced defect density and reduced corrosion. In an attempt to understand the possible relation between these parameters, an evaluation of the influence of defect density on coating capacitance (as a measured of water uptake) can be seen in Figure 9.3.

A clear reduction in water uptake with decreased defect density can be observed. This tendency is expected since lowering the defects within the coating will lower the pathways for the entry of electrolyte and thus, decreased the water uptake. This is in line with other works where nanoparticles has been found to fill cavities or pinholes reducing the total free volume of defects and acting as barrier to electrolyte penetration [125, 126, 168, 183-185].

In the same line of thoughts, a decreased water uptake should lead to reduced corrosion. This expected tendency can be also seen in Figure 9.4. Improved corrosion resistance by a decreased water uptake due to decreased defect density is expected and is in line with other reported works where it was also found an improvement in corrosion resistance due to reduced coating capacitance [130, 183, 184].

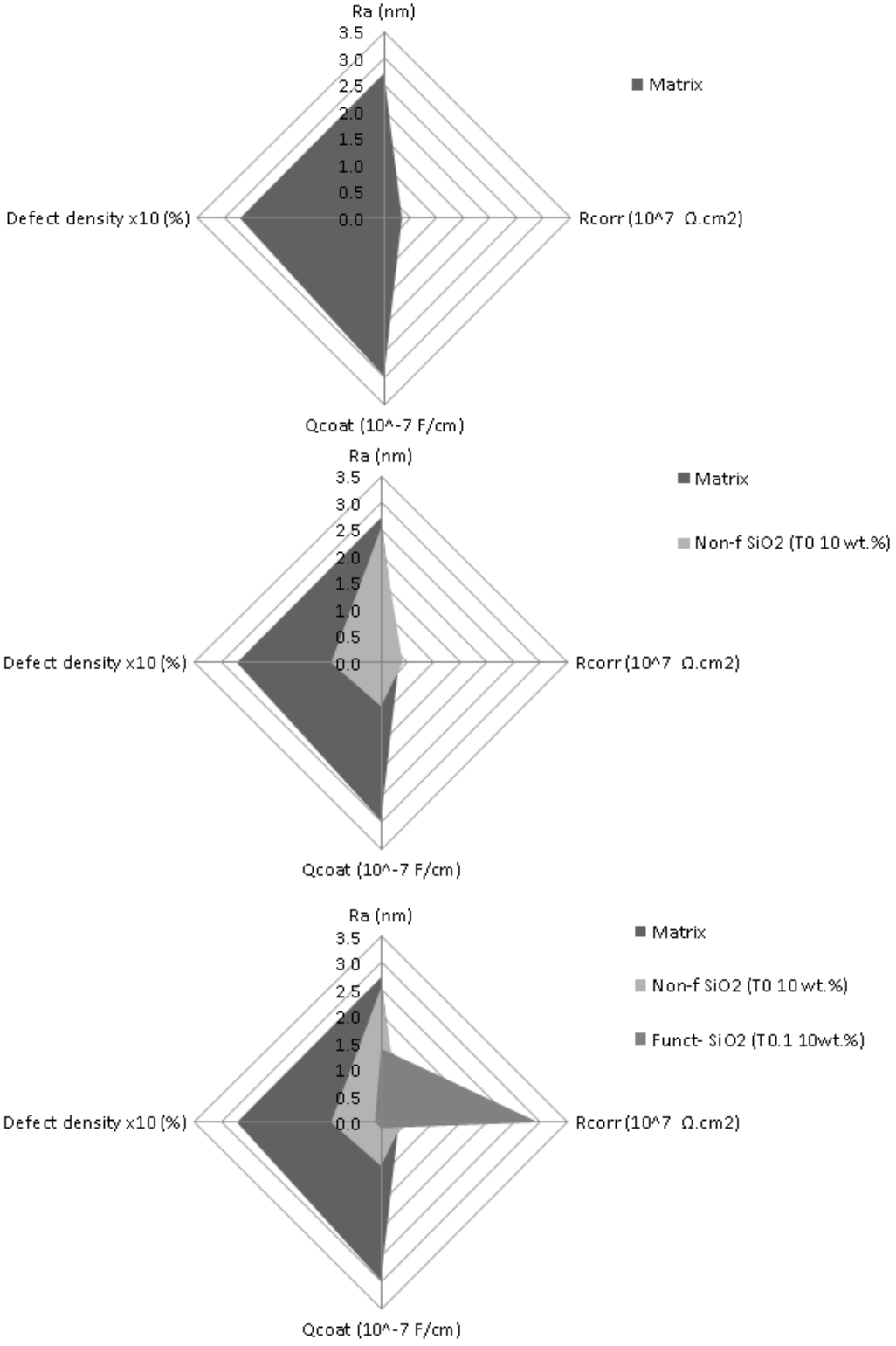

Figure 9.2. Evaluation of roughness, defect density, water uptake and corrosion resistance.

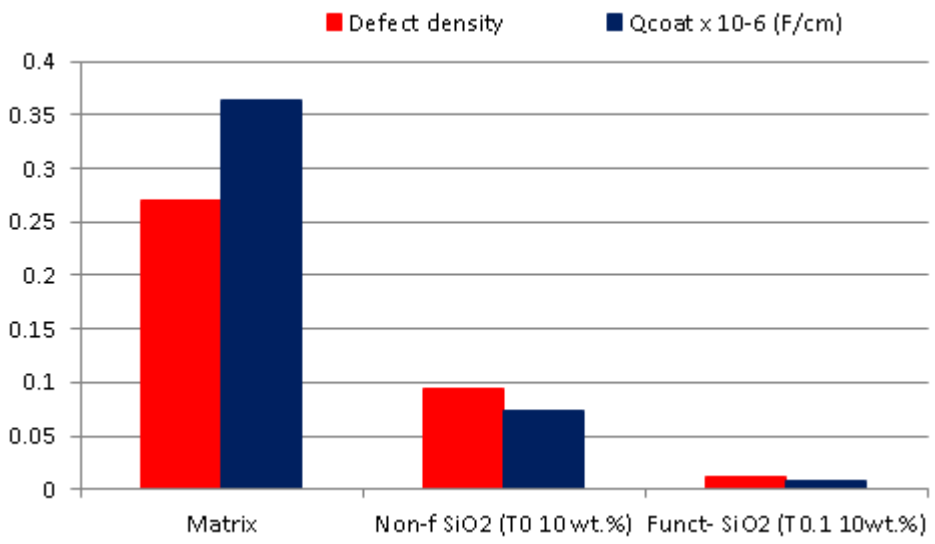

Figure 9.3. Influence of defect density on coating capacitance.

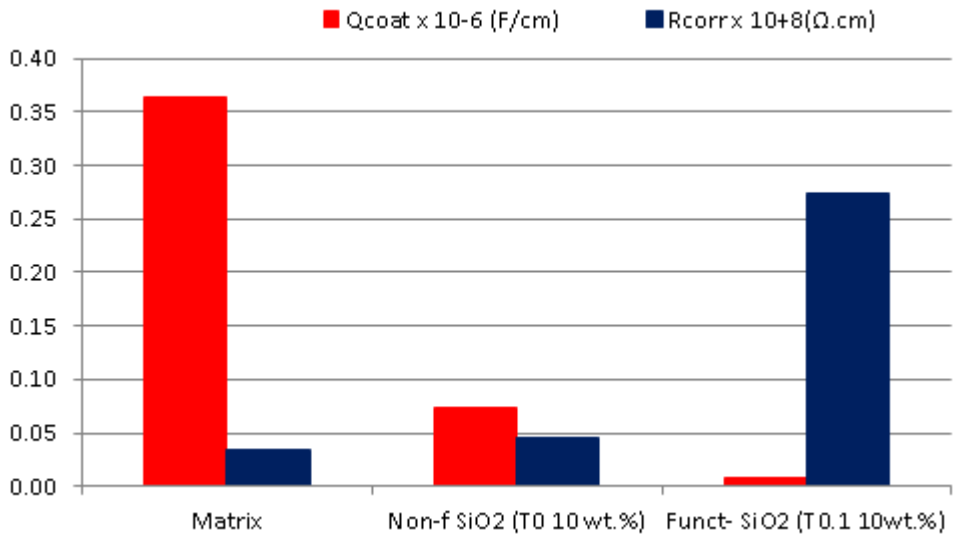

Figure 9.4. Influence of coating capacitance on corrosion resistance.

A similar evaluation has been done for the loading and functionalisation study and the influence of the incorporation of silica at different loadings and functionalisation levels on roughness, defect density, corrosion resistance and water uptake is depicted in Figure 9.5. As seen from Figure 9.5, an increase in loading level for the T0.1 coatings led to decreased roughness as well as lower defect density. The increase in loading while keeping a suitable nanoparticle distribution would have contributed to decrease the

roughness and lower the defect density of these formulations. This positive impact was also reflected on the water uptake since the possible paths for water entrance would be lowered due to the decreased defect density leading to lower electrolyte entrance and thus, leading to enhanced corrosion resistance being the coating with T0.1 20 wt.% the coating with higher resistance to corrosion. Increasing the functionalisation level up to T0.25 led to increased roughness compared with T0.1 as observed from Figure 9.5, with exception of T0.25 15 wt.% which has a similar roughness to T0.1 coatings. Similar trends can be observed for the rest of parameters, the defect density and the water uptake appeared to be lower for T0.25 15 wt.%, which also has the higher corrosion resistance of all T0.25 formulations. The impact of T0.5 functionalisation level is also depicted in Figure 9.5, where an increase in loading level led to a small increase in roughness, however the rest of parameters looked quite similar. If comparing this functionalisation level with the others, it can be observed that the increase in functionalisation level did not improve corrosion resistance and the coatings which presented enhanced corrosion resistance were T0.1 20 wt.% and T0.25 15 wt.%.

A correlation between defect density and coating capacitance and coating capacitance and corrosion resistance was previously found. Therefore, same parameters has been plotted in Figures 9.7 and 9.8 to see if the same tendency was followed. As expected, the samples which showed lower defect density also presented a reduction in water uptake. This decrease in water uptake again led to reduced corrosion, being the samples with T0.1 20 wt.% and T0.25 15 wt.% the coatings with minor defect density and lower water penetration leading to enhanced corrosion resistance.

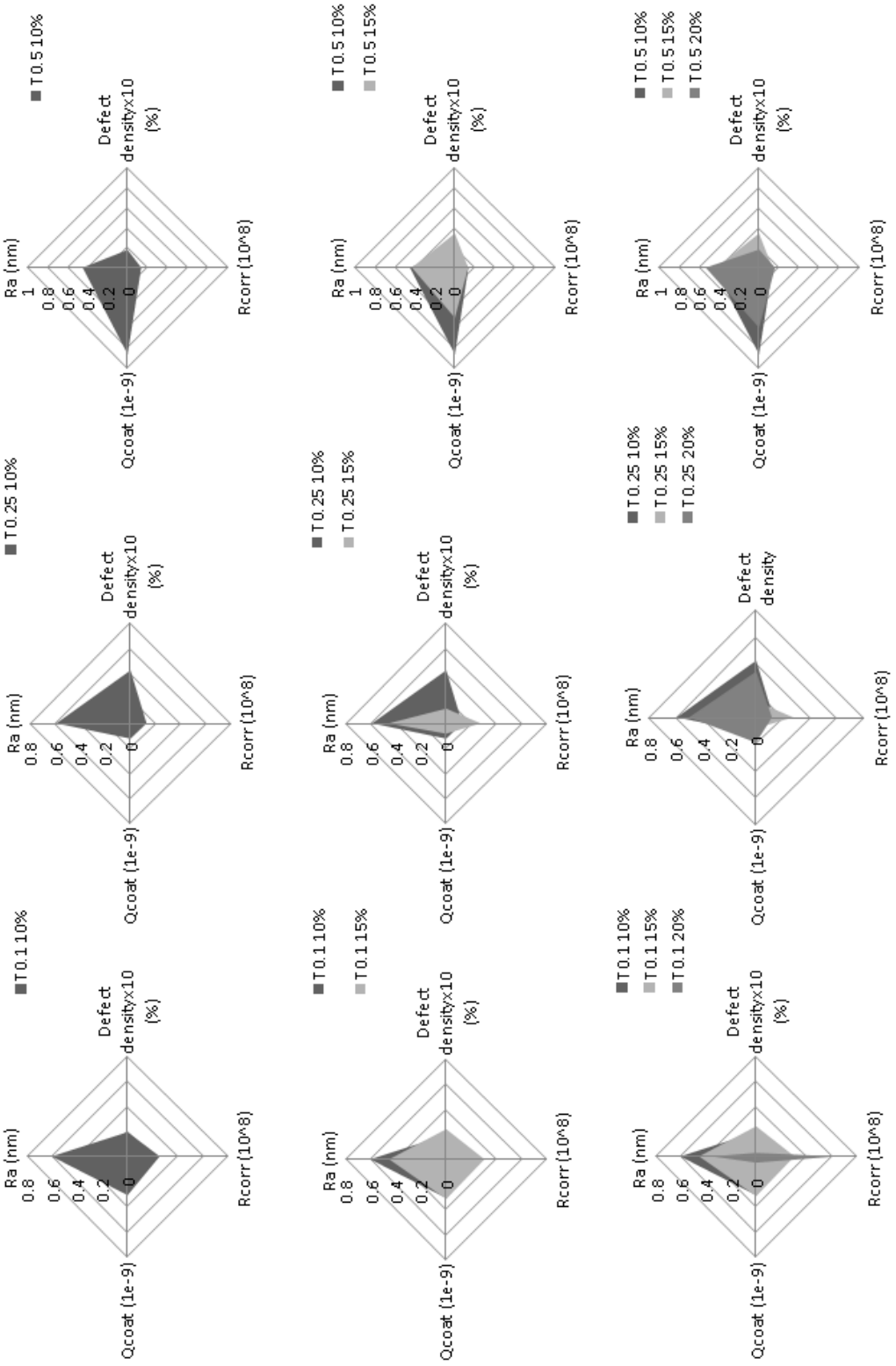

Figure 9.5. Influence of roughness, defect density, water uptake and corrosion resistance (loading and functionalisation study).

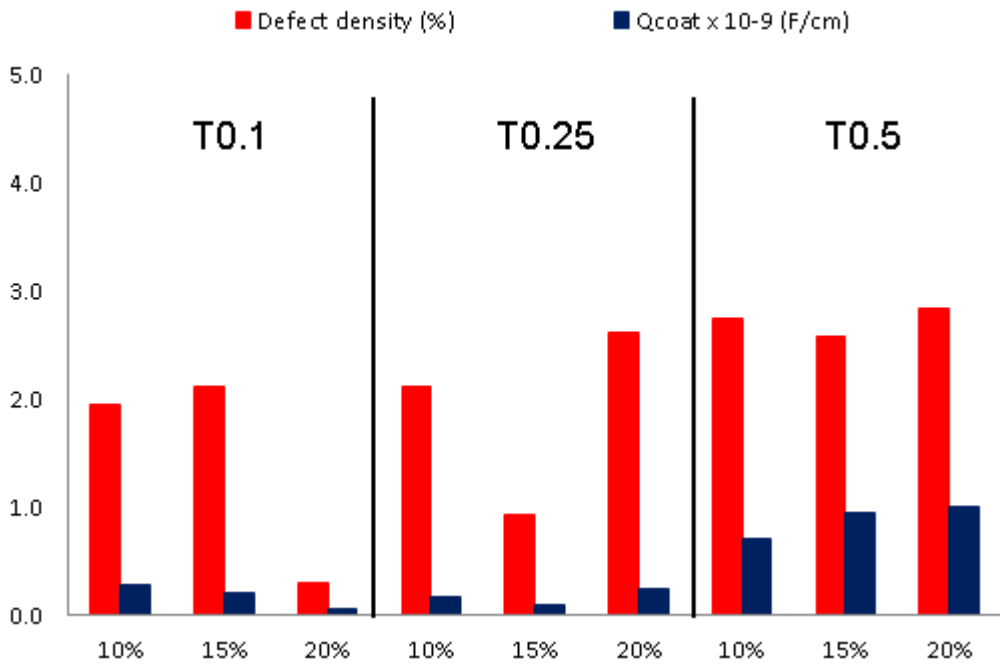

Figure 9.6. Influence of defect density on coating capacitance.

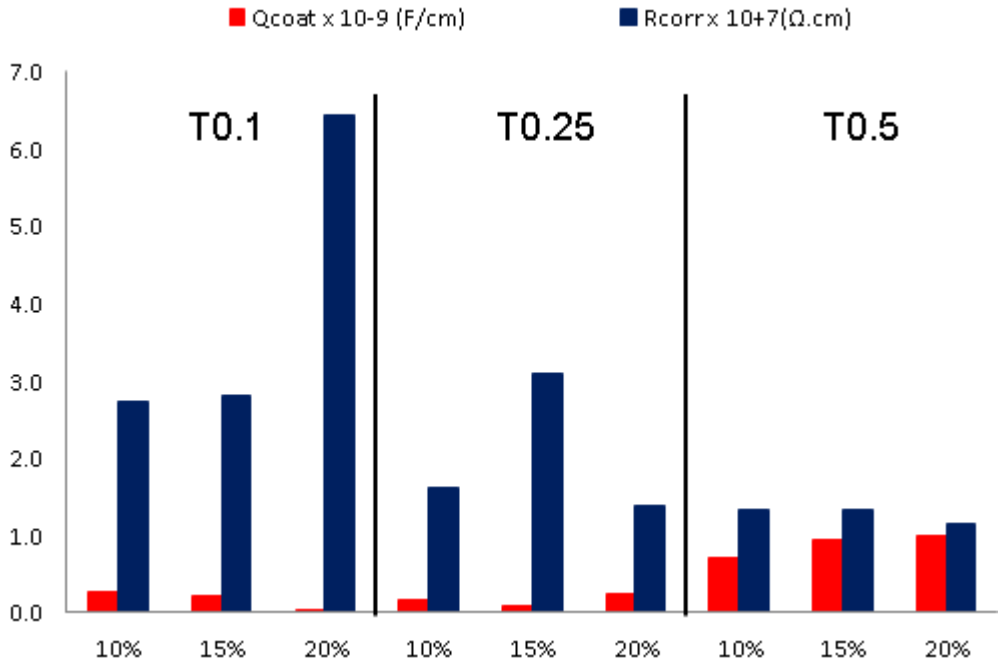

Figure 9.7. Influence of coating capacitance on corrosion resistance.

Although benefits of modifying coatings with nanoadditives are resin specific, a comparison between coatings with incorporated silica is in Table 9.1.

Table 9.1. Comparison of silica incorporation.

N°	Formulation	Electrolyte (immersion time)	R_{corr} ($\Omega.cm^2$)	Improved by	Ref.
1	Epoxy + SiO_2	3 wt.% NaCl (7 days)	7.28×10^5 (2.42×10^4)	30	[125]
2	Silane (BTSPA) + SiO_2	0.1 mol/L (3 h)	3.28×10^5 (5.6×10^4)	6	[127]
3	TEOS-GPTMS + SiO_2	0.1 mol/L (48 h)	1.8×10^4 (2.0×10^4)	1	[130]
4	Polyurethane + octylsilane-SiO_2	0.62 M NaCl (7 days)	8.4×10^8 (2.23×10^7)	38	[134]
5	Epoxy + GPTMS-SiO_2	3.5 wt.% NaCl (15 days)	1.28×10^8 (7.3×10^7)	2	[139]
6	Polysiloxane + GPTMS-SiO_2 (T0.1 10 wt.%)	3.5 wt.% NaCl (48 h)	6.58×10^5 (1.01×10^5)	7	This work
7	Polysiloxane + GPTMS-SiO_2 (T0.1 20 wt.%)	3.5 wt.% NaCl (48 h)	3.25×10^6 (1.01×10^5)	32	This work
8	Polysiloxane + GPTMS-SiO_2 (T0.1 20 wt.%)	3.5 wt.% NaCl (7 days)	1.17×10^6 (3.06×10^5)	4	This work

R_{corr} values in brackets corresponding to R_{corr} of the resin without additives, with exception of N°8 which value corresponds to R_{corr} for T0.1 10 wt.%.

It can be seen that the incorporation of silica tends to enhance the corrosion performance of the coating resins. Looking at results from this work, it can be seen that the introduction of functionalised silica T0.1 at 10 wt.% improved the corrosion resistance of the polysiloxane resin by a factor of 7. Furthermore, if increasing the loading up to 20 wt.%, the corrosion resistance is improved 32 times. A longer immersion period led to the same result, increasing the loading of T0.1 from 10 to 20 wt.% led to enhanced corrosion resistance (4 times higher R_{corr}).

9.3 Silica impact on mechanical durability

There are many parameters affecting coating durability since nanoparticles not only influence corrosion resistance but also the mechanical properties. A diagram combining different parameters studied through Chapters 7 and 8 has been constructed to understand the influence of silica incorporation on mechanical durability. The parameters depicted in Figure 9.8 are roughness (R_a), hardness, Young's modulus, brittleness index, resistance to fracture and defect density.

A comparison between the diagrams for the polysiloxane matrix and the coating with non-functionalised silica shows that the addition of silica reduced the roughness, increased the hardness and elastic modulus of the coatings and decreased the brittleness while increasing the potential to resist fracture. This improvement in mechanical properties was expected and is in agreement with other works where the incorporation of silica led to increased hardness and Young's modulus [129, 135, 173] and decreased brittleness [133]. The higher degree of roughness and defect density

presented by the coating matrix would have affected negatively the mechanical properties of this formulation since pores /defects can act as points of stress concentration and lowering fracture resistance. This is expected and has been reported in other works where an increased porosity or defect density inside the coating has been related to decreased hardness [128].

However, the incorporation of functionalised silica nanoparticles reduced both roughness and defect density. The prevention of the establishment of defects and the improved nanoparticle distribution would have contributed to improve mechanical properties of this nanoenabled coating. This coating seems to be more resistance to elastic deformation, with higher potential to resist fracture and more durable.

Linking these results to literature, a correlation between defect density and hardness can be expected, as presented in Figure 9.9 and also described in [128]. An increased hardness is expected with decreased defect density, as seen from Figure 9.9. However, hardness is not the only parameter affected by the defect density. Young's modulus tends to increase as well when decreasing defects, as also observed from Figure 9.10.

If improvements on hardness and elasticity are seen by decreasing the defect density, it would be expected that the brittleness index (and thus, the wear resistance) should be improved. Figure 9.11 shows how a decreased defect density impacts positively on the brittleness index. These results correlates with results obtained after erosion testing (described in section 8.5), therefore it can be said that a decrease in defect density lead to more durable coatings, with enhanced hardness, elasticity and wear resistance.

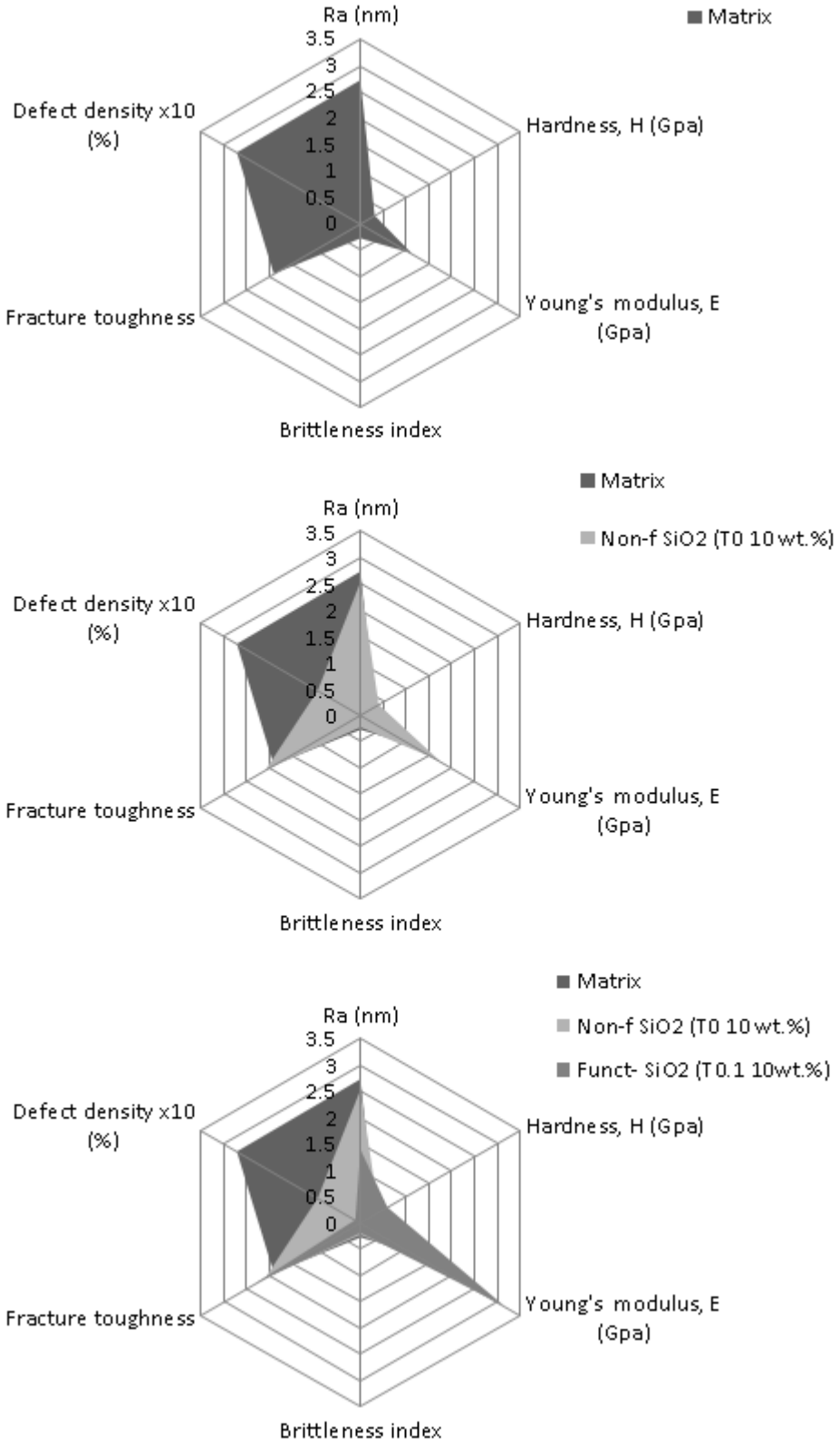

Figure 9.8. Evaluation of mechanical durability and corrosion resistance.

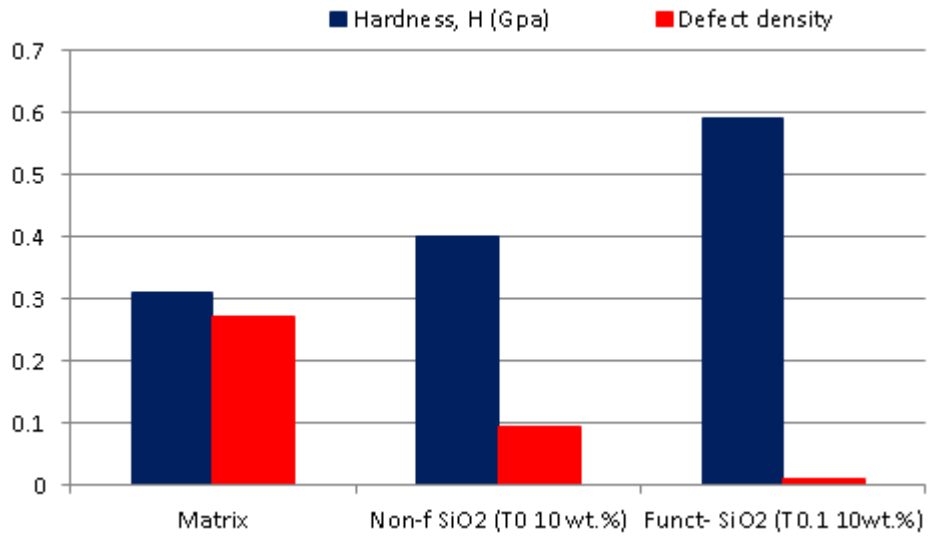

Figure 9.9. Correlation between hardness and defect density.

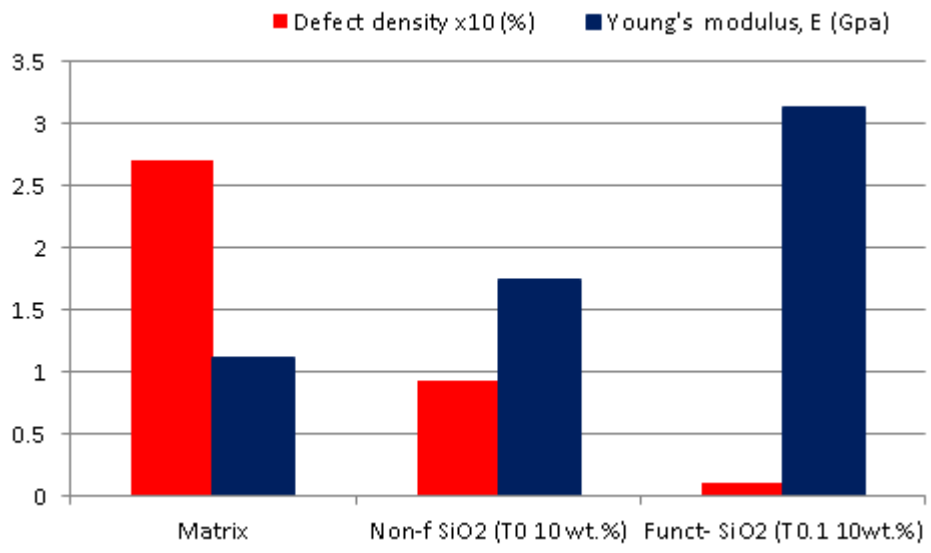

Figure 9.10. Correlation between Young's modulus and defect density.

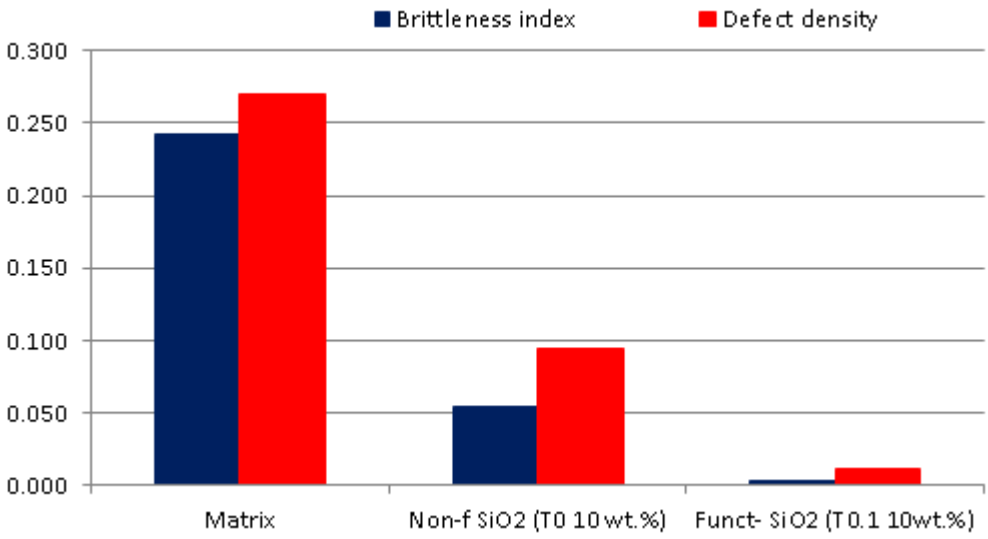

Figure 9.11. Correlation between the brittleness index and defect density.

To further understand the impact of silica loading and functionalisation on coating properties, an evaluation on the effect on mechanical properties is shown in Figure 9.12. Roughness, defect density, hardness, Young's modulus, brittleness index and resistance to fracture are the parameters used to study its influence on mechanical durability, as depicted in the diagrams in Figure 9.12.

As observed from Figure 9.12, an increase in loading level for the T0.1 functionalisation level led to a small decrease in hardness and elasticity, although the brittleness and resistance to fracture showed similar values for all loadings. It is worthwhile to note that if looking at all parameters in combination and due to the similarities in mechanical properties, it appears that the coating with higher loading (T0.1 20 wt.%) presented lower roughness and defect density which could mean that this coating formulation could have the key characteristics to improve coating properties.

When increasing the functionalisation level to T0.25, it can be observed that the coating which presented now lower roughness and defect density is the T0.25 15 wt.%, which is also the coating with increased hardness, Young's modulus and fracture toughness while presenting the lower brittleness.

In the case of further increase to T0.5 functionalisation level, all parameters were quite similar for all formulations and none of the coatings showed improved properties overall.

As seen in the previous study, hardness, elasticity and brittleness were directly correlated with defect density. Therefore, the same parameters have been depicted in Figure 9.13 for further evaluation. Although the difference between these functionalised nanoparticles did not lead to huge changes in mechanical properties as happened before with unfunctionalised silica, it appears that coatings with silica nanoparticles at T0.1 20 wt.% and T0.25 15 wt.% showed improved mechanical properties. These coatings presented decreased defect density and good mechanical properties.

It can be also said that thickness is not a determining factor since the coatings with T0.1 20 wt.% and T0.25 15 wt.% were not the thicker coatings but they presented superior degree of nanoparticle distribution which together with the improved compatibility between the matrix and nanoparticles due to the surface functionalisation made these coatings more durable, as stated previously.

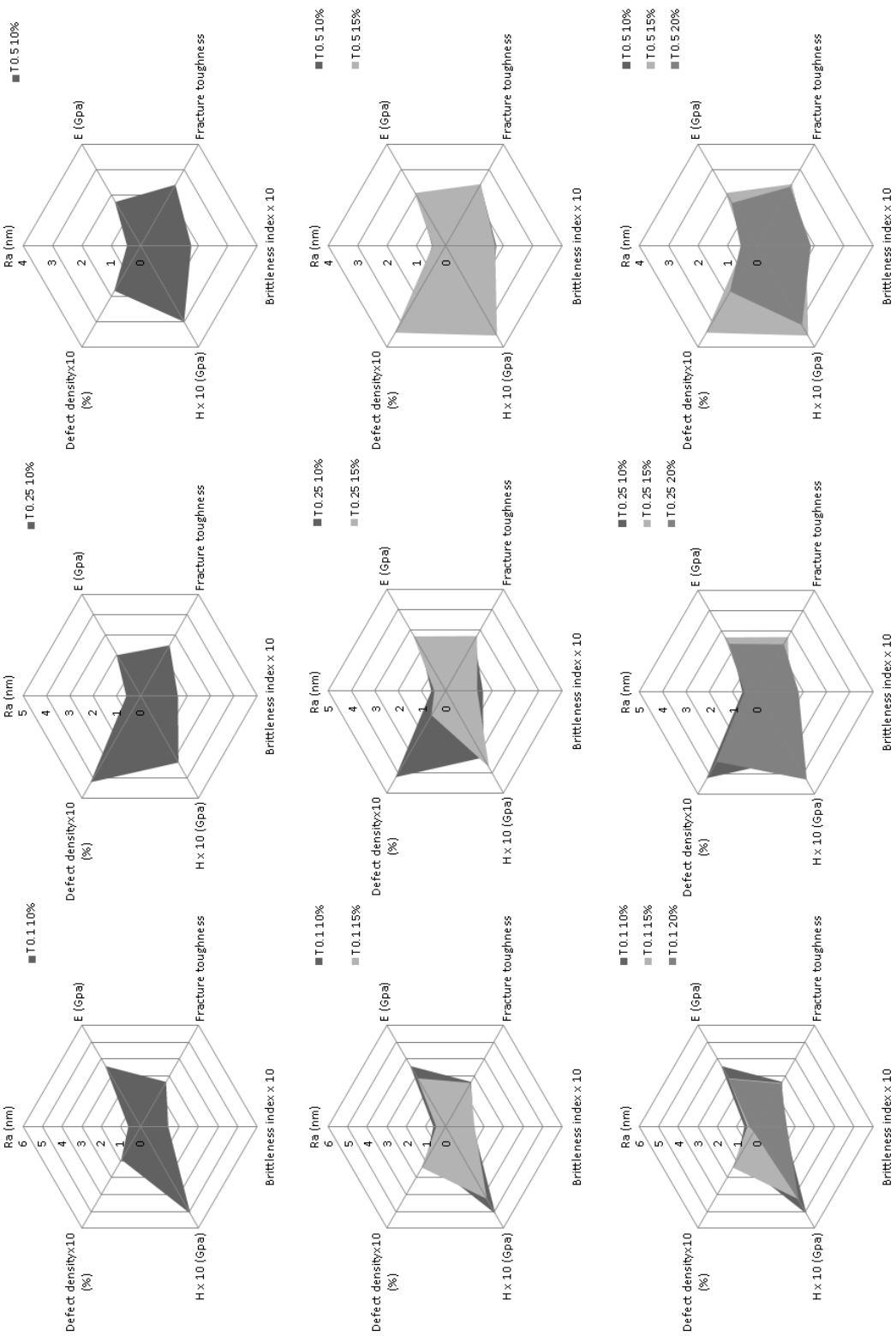

Figure 9.12. Evaluation of mechanical durability (loading and functionalisation study).

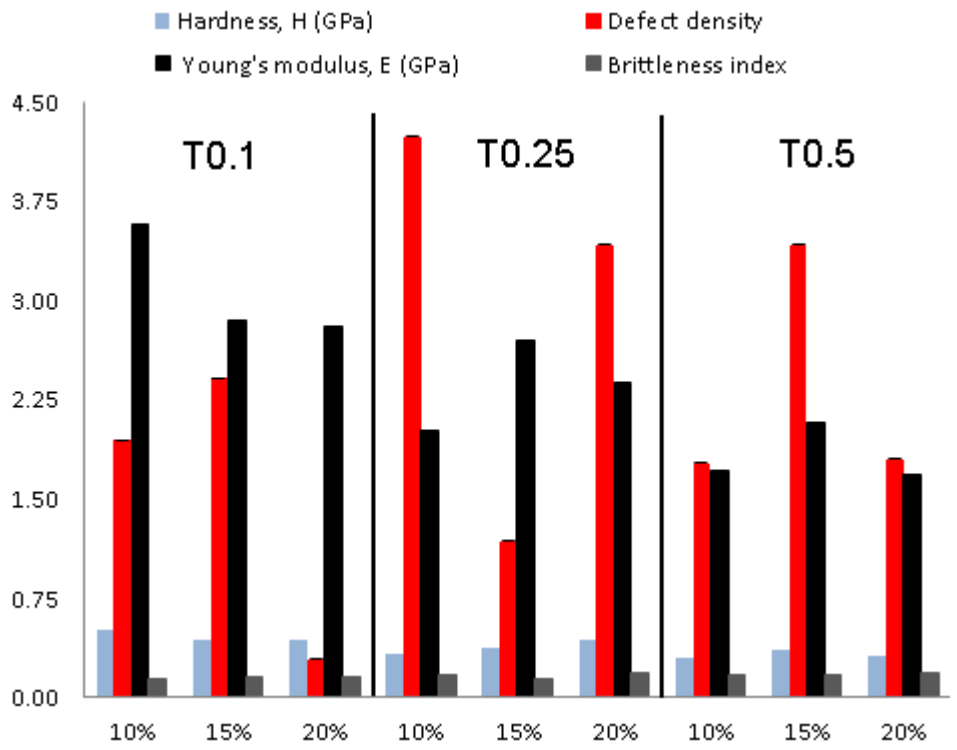

Figure 9.13. Correlation between defect density, hardness, Young's modulus and brittleness index.

From the comparison between the different results gathered during these studies, it can be said that some of the key factors to improve coating performance are the relation between the nanoparticles and the polymer matrix and the distribution of these nanoparticles through the coating. Surface functionalisation helped to do both, improving the nanoparticle-matrix interface as well as enhance nanoparticle distribution. These studies led to the conclusion that just a small degree of functionalisation, T0.1, led to coatings with improved durability. One of the problems associated with the incorporation of nanoparticles is its addition at highest loadings, and this work has demonstrated that with an appropiate functionalisation, silica can be added at loadings as high as 20 wt.% and most probably even at higher loadings since at 20 wt.% this coating formulation showed very good dispersion.

Chapter 10. Conclusions and future work

This final chapter summarises the main findings from this work and proposes additional lines of research that can be followed after this study.

The aim of this work was to create a siloxane based coating compatible with a ferrous substrate and to then modify it with silica nanoparticles to study the interaction of these and their functionalisation state with the coating matrix and their influence on coating morphology and durability.

Preliminary design rules were identified by investigating the effect and impact of key materials input which within this project were: the presence of a specific nanoparticle type, the loading level of this within a polysiloxane matrix material that had chemical similarity, and the use of and quantity of a functionalising agent. The specific outputs were the surface roughness, corrosion protection provided to the substrate, and key mechanical properties.

10.1 Conclusions

It has been found that the incorporation of non-functionalised silica nanoparticles led to an improvement of barrier properties and mechanical durability of the sol-gel derived matrix. However, when the silica nanoparticles were surface treated with GPTMS, the corrosion resistance and the mechanical properties of the coatings were further enhanced, even at equivalent loading levels. This improvement was related to the surface functionalisation with GPTMS which provides a more flexible network. In

addition, this treatment led to enhanced nanoparticle distribution creating an improved barrier to permeation by reducing the defect density and decreasing corrosion rate of the underlying substrate, all of which led to increased coating durability.

To explore this line of investigation, three functionalisation levels (T0.1, T0.25 and T0.5) and three loading levels of the functionalised silica (10, 15 and 20 wt.%) were examined.

When considering the corrosion resistance and mechanical properties, the coatings which showed the most improved coating properties and thus, improved durability, were those with silica nanoparticles at T0.1 20 wt.% followed by the T0.25 15 wt.%.

The relation between the silica nanoparticles, the sol-gel matrix and the distribution of these nanoparticles through the coating appears to be one of the key factors to improve coating performance. In fact, the lowest functionalisation level, T0.1, was the one which gave coatings with the best properties overall. Furthermore, at this functionalisation level coatings did not show any agglomeration which is one of the main problems when increasing the loading levels. This work has demonstrated that with an appropriate nanoparticle functionalisation, silica can be added at loadings up to at least 20 wt.% and be homogenously and uniformly distributed. According to these results, we believe that silica at T0.1 could be added at even higher loadings showing still good dispersion.

It is hoped that this work has helped to provide fundamental understanding about some of the key factors relating macro-scale performance to nano-scale structures, which is hoped to make significant impact.

Sol-gel based coatings despite decades of research and many potential advantages have not been as widely adopted as they could. While many challenges remain in the commercialisation of these highly inorganic coatings, a materials by design approach identifying the key design rules governing behaviour can lead to provide new mechanistic insights explaining the improved properties of the siloxane coatings after the addition of suitably functionalised nanoparticles. Thus, it is hoped that by providing a better understanding of the influence of nanoadditives on coating microstructure, corrosion performance and mechanical durability, this study will contribute to the establishment of a materials by design approach which can be further developed and take it forward. This will facilitate the emergence of novel materials with structural and compositional hierarchies which could be integrated into industrial applications, allowing the discovery-to-deployment challenge to be overcome.

10.2 Future work

This investigation has revealed a strong connection between composition, structure and properties. There are a number of possible directions for taking forward this work:

- Increase the loading level for T0.1 silica and look at its influence on microstructure which then will be related with corrosion resistance and mechanical durability

- Incorporation of T0.1 silica into different matrices including state-of-the-art epoxy and polyurethane coatings
- A more detailed investigation into the functionalisation process and subsequent impact on behaviour
- A survey of functionalisation levels centred on T0.1 but extending the granularity of the data to allow the optimum level to be identified.
- Extend the concept to different particle sizes and size distributions.
- Study the changes in surface morphology after nanoparticle incorporation and try to find a way to control surface roughness.
- Establish clearer relationships between surface morphology and topography and functional performance to enable processing, composition, structure, property guidelines to be developed.
- Investigate dual- and multi-functionalisation of the silica particles which apart from improving corrosion resistance and mechanical durability of a coating formulation may add another desirable characteristic such as anti-fouling, self-cleaning or anti-icing

Although this work would have contributed to initiate a materials by design methodology, there is still an incomplete understanding of the underpinning science, the relationship between design and synthesis and more importantly the integration into industrial application. Thus, a continuation of this work would enable the transition from combinatorial approaches to an effective materials by design methodology which will facilitate the development of novel materials with tailored properties.

List of References

1. Codner, K., Alala, K., Sharma, N., *NAC-10 – Phase II Analysis*, Youngstown State University. WinTec Security, 2011. [Online] Available from: http://www.pb2au.biz/5-6-11_NAC-10_Phase_II_Final_Submittal.pdf

2. International measures of prevention, application, and economics of corrosion technologies study, USA. *NACE International*, 2016. [Online] Available from: http://impact.nace.org/documents/Nace-International-Report.pdf

3. Kelly, R. G., Scully, J. R., Shoesmith, D. W., Buchheit, R. G. 2003. *Electrochemical techniques in corrosion science and engineering*. Marcel Dekker, Inc.

4. Bardal, E. 2007. *Corrosion and protection.* Springer Science and Business Media.

5. Tan, Y. 2013. *Heterogeneous electrode processes and localized corrosion*. Wiley.

6. Schweitzer, P. A. 2010. *Fundamentals of corrosion: Mechanisms, causes and preventive methods*. Taylor and Francis Group.

7. Davis, J. R. 2000. *Corrosion: Understanding the basics*. ASM International.

8. Corrosion protection, U. S. 2015. *Environmental Protection Agency*. [Online] Available from: http://www.epa.gov/region07/underground_storage_tanks/corp.htm

9. Wright, J. 2012. Inhibiting rust and corrosion to prevent machine failures. *Machinery Lubrication*. [Online] Available from: http://www.machinerylubrication.com/Read/29116/inhibiting-rust-corrosion

10. Dariva, C. G., and Galio, A. F. 2014. Corrosion inhibitors – Principles, mechanisms and applications. In: Aliofkhazraei, M. ed. *Developments in Corrosion Protection.* [Online] Available from: https://www.intechopen.com/books/developments-in-corrosion-protection/corrosion-inhibitors-principles-mechanisms-and-applications

11. Hempel. *How to select the right paint system. Guidelines for coating protection in accordance with ISO 12944*. Hempel.

12. Weiss, K. D. 1997. Paints and Coatings: A mature industry in transition. *Progress in Polymer Science*. **22**(2), pp. 203-245.

13. AKeson. 2009. The different polyester resins. *Fiberglassblog.com* [Online] Available from: http://fiberglassblog.com/2009/02/16/the-different-polyester-resins/

14. Cripps, D. Polyester resins. *NetComposites*. [Online] Available from: https://netcomposites.com/guide-tools/guide/resin-systems/polyester-resins/

15. Resins. *Exel Composites*. [Online] Available from: http://www.exelcomposites.com/fifi/english/composites/rawmaterials/resins.aspx

16. Cripps, D. Epoxy resins. *NetComposites*. [Online] Available from: https://netcomposites.com/guide-tools/guide/resin-systems/epoxy-resins/

17. Rouw, A. C., 1998. Model epoxy powder coatings and their adhesion to steel. *Progress in Organic Coatings.* **34**, pp.181-192.

18. Chen, L., Chai, S., Liu, K., Ning, N., Gao, J., Liu, Q., Chen, F., Fu, Q., 2012. Enhanced epoxy/silica composites mechanical properties by introducing graphene oxide to the interface. Appli*ed Materials and Interfaces.* **4**(8), pp.4398-4404.

19. Khmenko, A., Koricho, E. G., Haq, M., 2015. Monitoring the effect of micro-/nanofillers on curing-induced shrinkage in epoxy resins. In:

Fillers and Reinforcements for Advanced Nanocomposites. Elsevier, pp. 461-475.

20. Delucci, M., Ricotti, R., Cerisola, G., 2011. Influence of micro- and nano-fillers on chemico-physical properties of epoxy-based materials. *Progress in Organic Coatings*. **72**, pp. 58-64.

21. Vinyl ester resins. *Composite Materials from MFG*. [Online] Available from: http://www.moldedfiberglass.com/materials/vinyl-ester-resins

22. Advanced composite materials. [Online] Available from: http://www.faa.gov/regulations_policies/handbooks_manuals/aircraft/amt_airframe_handbook/media/ama_ch07.pdf

23. Slama, W. R., 1996.Polyester and vinyl ester coatings. *Journal of protective coatings and linings*. [Online] Available from: http://www.paintsquare.com/library/articles/Polyester_and_Vinyl_Ester_Coatings.pdf

24. What is a polyurethane. *Tosoh Europe*. [Online] Available from: http://www.tosoheurope.com/our-products/polyurethanes

25. Mannari, V., Patel, J. 2015. *Understanding coating raw materials*. Germany: Vincentz Network.

26. Polyurethane resins. *Composite Materials from MFG.* [Online] Available from: http://www.moldedfiberglass.com/materials/polyurethane-resins

27. Lide, D. R. 2007. *Handbook of Chemistry and physics*. Taylor & Francis.

28. Young, S. K. 2002. Overview of sol-gel science and technology, *U. S. Army Research.* Laboratory Report No. OMB 0704-0188.

29. Materne, T., de Buyl, F., Witucki, G. L. 2006. Organosilane technology in coating applications: review and perspectives. *Dow Corning*. [Online] Available from: http://www.dowcorning.com/content/publishedlit/26-1402-01.pdf

30. Noll, W. 1968. *Chemistry and Technology of Silicones*. Academic Press.

31. Vincentz. 2007. Using the Si-O strength. *European Coatings Journal*, **6**, pp.54-61.

32. Sorensen, P. A., Kiil, S., Dam-Johensen, K. 2009. Anticorrosive coatings: a review. *Journal of Coatings Technology and Research*. **6**(2), pp.135-176.

33. Montemor, M. F., Ferreira, M. G. S. 2011. A review on the use of nanostructured and functional organosilane coatings modified with corrosion inhibitors as environmentally friendly pre-treatments for metallic substrates. *European Federation of Corrosion Publications.* 58, pp.39-64

34. Ebelmen, J. J. 1846. *Annales de Chimie et de Physique*. **16**, pp.129.

35. Graham, T., 1864. *Journal of Chemical Society*. **17**, pp.318-327.

36. Hench, L. L., West, J. K. 1990. The Sol-Gel process. *Chemical Reviews*. **90**(1), pp33-72.

37. Stöber, W., Fink, A., and Bohn, E. 1968. Controlled growth of monodisperse silica spheres in the micron size range, *Journal of Colloid and Interface Science.* **26**, pp.62-69.

38. Barbe, C. Who is doing Sol-Gel? A snapshot. [Online] Available from: https://www.isgs.org/index.php/papers-and-articles/48-who-is-doing-solgel

39. Spadafora, S. J., Pepe, F. R. 1993. A comparison of sulfuric acid/boric acid anodize and chromic acid anodize processes. *The Boeing Co*. Seattle. Report No. NADC-93042-60.

40. Metroke, T. L., Parkhill, R. L., Knobbe, E. T. 2001. Passivation of metal alloys using sol-gel derived materials. *Progress in Organic Coatings.* **41**, pp.233-238.

41. The European Commission. 2011. Commission's recommendation of 18 October 2011 on the definition of nanomaterials. *Official Journal of the European Union.* [Online] Available from: https://ec.europa.eu/research/industrial_technologies/pdf/policy/commission-recommendation-on-the-definition-of-nanomater-18102011_en.pdf

42. Yaya, A., Agyei-Tuffour, B., Dodoo-Arhin, D., Nyankson, E., Annan, E., Konadu, D. S., Sinayobye, E., Baryeh, E. A., Ewels, C. P. 2012. Layered nanomaterials- A review, Global Journal of Engineering, *Design and Technology.* **1**(2), pp.32-41.

43. McNeil, S.E. 2011. Unique benefits of nanotechnology to drug delivery and diagnostics, Methods in Molecular Biology. **697**, pp.3-8.

44. Lu, P., Huang, S., Chen, Y., Chiueh, L., Shih, D. Y. 2015. Analysis of titanium dioxide and zinc oxide nanoparticles in cosmetics. *Journal of Food and Drug Analysis*. **23**(3), pp.587-594.

45. Morlando, A., Cardillo, D., Devers, T., Konstantinov, K. 2016. Titanium doped tin dioxide as potential UV filter with low photocatalytic activity for sunscreen products. *Material Letters*. **171**, pp.289-292.

46. Katsoulis, C., Kandare, E., Kandola, B. K. 2011. The effect of nanoparticles on structural morphology, thermal and flammability properties of two epoxy resins with different functionalities. *Polymer Degradation and Stability.* **96**, pp.529-540.

47. Zhu, A., Cai, A., Zhang, J., Jia, H., Wang, J. 2008. PMMA-grafted-silica/PVC Nanocomposites: mechanical performance and barrier properties. *Journal of Applied Polymer Science*. **108**(4), pp.2189-2196.

48. The Royal Society & The Royal Academy of Engineering. 2004. Possible adverse health, environmental and safety impacts. *Nanoscience and Nanotechnology*. [Online] Available from: http://www.nanotec.org.uk/report/chapter5.pdf

49. Warheit, D. B. 2004. Nanoparticles: Health impacts? *Materials Today*. **7**(2), pp.32-35.

50. Taphouse, J. H., Bougher, T. L., Singh, V., Abadi, P. P. S. S., Graham, S., and Cola, B, A. 2013. Carbon nanotube thermal interfaces enhanced with sprayed on nanoscale polymer coatings. *Nanotechnology*, **24**(10):105401.

51. Balani, K., Anderson, R., Laha, T., Andara, M., Tercero, J., Crumpler, E., Agarwal, A. 2007. Plasma-sprayed carbon nanotube reinforced hydroxyapatite coatings and their interaction with human osteoblasts in vitro. *Biomaterials.* **28**, pp.618-624.

52. Leftheriotis, G., Papaefthimiou, S., Yianoulis, P., Siokou, A. 2001. Effect of the tungsten oxidation states in the thermal coloration and bleaching of amorphous WO3 films. *Thin Solid Films*. **384**, pp.298-306.

53. Niklasson, G. A., Norling, A., Possnert, G., Berggren, L. 2008. Optical properties of amorphous tungsten oxide films: Effect of stoichiometry. *Journal of Physics: Conference Series*, **100**, 082023

54. Rahman, I. A., Padavettan, V. 2012. Synthesis of silica nanoparticles by sol-gel: size-dependent properties, surface modification, and applications in silica-polymer nanocomposites –A review. *Journal of Nanomaterials*, Article ID 132424.

55. Myers, M. 2011. Current and impeding developments in silica nanoparticle use in UV-curable systems. *Paints & Coatings Industry*

56. Logothetidis, S., Laskarakis, A., Kassavetis, S., Lousinian, S., Gravalidis, C., Kiriakidis, G. 2008. Optical and structural properties of ZnO for transparent electronics. *Thin Solid Films*. **516** (7), pp.1345-1349.

57. Whang, T., Hsieh, M., Chen, H. 2012. Visible-light photocatalytic degradation of methylene blue with laser-induced Ag/ZnO nanoparticles. *Applied Surface Science*. **258**(7), pp.2796-2801.

58. Renuka, R., and Ramamurthy, S. 2000. Antibacterial and antifungal properties of electrochemically prepared zinc oxide films in presence and absence of light. *Bulletin of Electrochemistry.* **16**(11), pp.500-503.

59. Wang, Y., Liu, J., Sun, D. D. 2012. Enhancing stability and photocatalytic activity of ZnO nanoparticles by surface modification of graphene oxide. *Journal of Nanoscience and Nanotechnology*. **12**(5), pp.3896-3902.

60. Zhou, D., Keller, A. A. 2010. Role of morphology in the aggregation kinetics of ZnO nanoparticles. *Water Research*. **44**(9), pp.2948-2956.

61. Gupta, S. M., Tripathi, M. 2011. A review of TiO2 nanoparticles. *Chinese Science Bulletin*. **56**(16), pp.1639-1657.

62. Fujishima, A., Rao, T. N., Truk, D. A. 2000. Titanium dioxide photocatalysis. Jo*urnal of Photochemistry and Photobiology C: Photochemistry Reviews.* **1**(1), pp.1-21.

63. Shen, G. X., Chen, Y. C., Lin, L., Lin, C. J., Scantlebury, D. 2005. Study on a hydrophobic nano-TiO2 coating and its properties for corrosion protection of metals. *Electrochimica Acta.* **50**, pp.5083-5089.

64. Bamoulid, L., Maurette, M.T., De Caro, D., Guenbour, A., Ben Bachir, A., Aries, L., El Hajjaji, S., Benoit-Marquie, F., Ansart, F. 2008. An efficient protection of stainless steel against corrosion: combination of a conversion layer and titanium dioxide deposit. *Surface and Coatings Technology*. **202**(20), pp.5020-5026.

65. Khorramie, S.A., Baghchesara, M. A., Lotfi, R., Dehagi, S. M. 2012. Synthesis of ZrO2 nanoparticle by combination of sol-gel auto-combustion method-irradiation technique, and preparation of Al-ZrO2 metal matrix composites. *International Journal of Nano Dimension*. **2**(4), pp.261-267.

66. Sultana, S., Rafiudding, Khan, M. Z., Shahadat, M. 2015. Development of ZnO and ZrO2 nanoparticles: Their photocatalytic

and bactericidal activity. *Journal of Environmental Chemical Engineering.* **3**(2), pp.886-891.

67. Borilo, L. P., Spivakova, L. N. 2012. Synthesis and characterization of ZrO2 thin films. *American Journal of Materials Science.* **2**(4), pp.119-124.

68. Gole, J. L., Prokes, S. M., Stout, J. D., Glembocki, O. J., Yang, R. 2006. Unique properties of selectively formed zirconia nanostructures. *Advanced Materials*. **18**(5), pp.664-667.

69. Paek, C., McCormick, A. V., Carr, P. W. 2010. Preparation and evaluation of carbon coated alumina as a high surface area packing material for high performance liquid chromatography. *Journal of Chromatography.* **1217**(42), pp.6475-6483.

70. Wright, P. K., Evans, A. G. 1999. Mechanisms governing the performance of thermal barrier coatings. *Current Opinion in Solid State and Materials Science.* **4**(3), pp.255-265.

71. Zand, R. Z., Flexer, V., De Keersmaecker, M., Verbeken, K., Adriaens, A. 2015. Effects of activated ceria and zirconia nanoparticles on the protective behaviour of silane coatings in chloride solutions. *International Journal of Electrochemical Science.* **10**, pp.997-1014.

72. Clark, M. D., Maschmann, M. R., Patel, R. J., Leever, B. J. 2014. Scratch resistance and durability enhancement of bulk heterojunction organic photovoltaics using ultra-thin alumina layers. S*olar Energy Materials and Solar Cells.* **128**, pp.178-183.

73. Comite, A., Cozza, E. S., Di Tanna, G., Mandolfino, C., Milella, F., Vicini, S. 2015. Thermal barrier coatings based on alumina microparticules. *Progress in Organic Coatings.* **78**, pp.124-132.

74. Kim, M. H., Na, H. K., Kim, Y. K., Ryoo, S. R., Cho, H. S., Lee, K. E., Jeon, H., Ryoo, R., Min, D. H. 2011. Facile synthesis of

monodispersed mesoporous silica nanoparticles with ultralarge pores and their application in gene delivery. *ACS Nano*. **5**(5), pp.3568-3576.

75. Wang, Z. Z., Gu, P., Zhang, Z., Gu, L., Xu, Y. Z. 2011. Mechanical and tribological behaviour of epoxy/silica nanocomposites at the micro/nano scale. *Tribology Letters*. **42**, pp.185-191.

76. Wang, J., Guangming, W., Jun, S., Yang, T., Zhan, Q., Zhou, B., Deng, Z. 2000. Scratch-resistant improvement of sol-gel derived nano-porous silica films. *Journal of Sol-Gel Science and Technology*. **18**(3), pp.219-224.

77. Webster, T. J. 2009. *Safety of nanoparticles: from manufacturing to medical applications*. New York: Springer-Verlag

78. Zhao, Y., Dan, N., Pan, Y., Nitin, N., Tikekar, R. V. 2013. Enhancing the barrier properties of colloidosomes using silica nanoparticle aggregates. *Journal of Food Engineering*. **118**(4), pp.421-425.

79. Santana, I., Pepe, A., Jimenez-Pique, E., Pellice, S., Milosev, I., Cere, S. 2015. Corrosion protection of carbon steel by silica-based hybrid coatings containing cerium salts: Effect of silica nanoparticle content. *Surface and Coatings Technology*. **265**, pp.106-116.

80. Zholoback, N. M., Ivanov, V. K., Shcherbakov, A. B., Shaporev, A. S., Polezhaeva, O. S., Baranchikov, A. Y., Spivak, N. Y., Tretyakov, Y. D. 2011. UV-shielding property, photocatalytic activity and photocytotoxicity of ceria colloid solutions. *Journal of Photochemistry and Photobiology*. **102**(1), pp.32-38.

81. Echalier, B. 2005. Nanoparticles of Cerium Oxide – Application to coatings technologies. In: *Nano and Hybrid Coatings conference, January 2005, Manchester.* [Online] Available from: http://www.pcimag.com/articles/83469-nanoparticles-of-cerium-oxide-application-to-coatings-technologies

82. Montemor, M. F., Ferreira, M. G. S. 2007. Cerium salt activated nanoparticles as fillers for silane films: Evaluation of the corrosion

inhibition performance on galvanised steel substrates. *Electrochimica Acta*. **52**(24), pp.6976-6987.

83. Montemor, M. F., Pinto, R., Ferreira, M. G. S. 2009. Chemical composition and corrosion protection of silane films modified with CeO2 nanoparticles. *Electrochimica Acta*. **59**, pp.5179-5189.

84. Zand, R. Z., Verbeken, K., Adriaens, A. 2013. Evaluation of the corrosion inhibition performance of silane coatings filled with cerium salt-activated nanoparticles on hot-dip galvanized steel substrates. *International Journal of Electrochemical Science*. **8**, pp.4924-494.

85. Montemor, M. F. 2014. Functional and smart coatings for corrosion protection: A review of recent advances. *Surface and Coatings Technology*. **258**, pp.17-37.

86. Bethencourt, M., Botana, F. J., Cano, M. J. and Marcos, M. 2004. Advanced generation of green conversion coatings for aluminium alloys. *Applied Surface Science*. **238**, pp.278-287.

87. Almeida, E., Santos, D., Fragata, F., de la Fuente, D., Morcillo, M. 2006. Anticorrosive painting for a wide spectrum of marine atmospheres: Environmental-friendly versus traditional paint systems. *Progress in Organic Coatings*. **57**, pp.11-22.

88. Hughes, A. E., Cole, I. S., Muster, T. H., Varley, R. J. 2010. Designing green, self-healing coatings for metal protection. *NPG Asia Materials*. **2**(4), pp.143-151.

89. Blohowiak, K. Y., Osborne, J. H., Seebergh, J. E. 2010. Boeing researchers develop 'green' sol-gel coatings. *SAE International*. [Online] Available from: http://articles.sae.org/8318/

90. Schmidt, H., Scholze, H., Kaiser, A. 1984. Principles of hydrolysis and condensation reaction of alkoxysilanes, *Journal of Non-Crystalline Solids*. **63**, pp.1-11.

91. Rabinovich, E. M., Macchesney, J. B., Johnson Jr., D. W., Simpson, J. R., Meagher, B. W., Dimarcello, F. V., Wood, D. L., Sigety, E.

A.1984. Sol-gel preparation of transparent silica glass. *Journal of Non-Crystalline Solids*. **63**(1-2), pp.155-161.

92. Sakka, S., Yoko, T., 1992. Sol-gel-derived coating films and applications. In: Reisfeld, R., Jorgensen, C. K. ed. *Chemistry, Spectroscopy and Applications of Sol-gel Glasses.* **77**, pp.89-118.

93. Bernards, T. N. M., van Bommel, M. J., Boonstra, A. H. 1991. Hydrolysis-condensation processes of the tetra-alkoxysilanes TPOS, TEOS and TMOS in some alcoholic solvents. *Journal of Non-Crystalline Solids*. **134**(1-2), pp. 1-13.

94. Van Bommel, M. J., de Haan, A. B. 1994. Drying of silica gels with supercritical carbon liquid. *Journal of Materials Science*. **29**, pp.943-948.

95. Novac, B. M. 1993. Hybrid nanocomposite materials – between inorganic glasses and organic polymers, *Advanced Materials*. **5**(6), pp.422-433.

96. Lichtenhan, J. D., Vu, N. Q., Carter, J. A., Gilman, J. W., Feher, F. J. 1993. Silsesquioxane-siloxane copolymers from polyhedral silsesquioxanes. *Macromolecules*.**26**(8), pp.2141-2142.

97. Brinker, C. J., Scherer, G. W. 1990. *Sol-Gel Science: The physics and chemistry of sol-gel processing*. London: Academic Press.

98. Sanchez, C., Rozes, L., Ribot, F., Laberty-Rober, C., Grosso, D., Sassoye, C., Boissiere, C., Nicole, L. 2010. “Chimie douce”: A land of oportunities for the designed construction of functional inorganic and hybrid organic-inorganic nanomaterials, *Comptes Rendus Chimie*. **13**, pp.3-39.

99. Vu, C., Laferté, O. 2006. Silica nanoparticles in the optimisation of scratch and abrasion resistance of high performance UV multi-layer coatings, *European Coatings Journal*. **6**, pp.34-40.

100. Danks, A. E., Hall, S. R., Schnepp, Z. 2016. The evolution of 'sol-gel' chemistry as a technique for materials synthesis. *Materials Horizons*. **3**, pp.91-112.

101. Assink, R. A., Kay, B. D. 1984. 1H NMR studies of the sol-gel transition. *MRS Proceedings*. **32**, pp.331.

102. PPG. 2011. Comparing PPG polysiloxane coatings and traditional coating systems. *PPG Protective and Marine Coatings*. [Online] Available from: https://www.cgedwards.com/ameron/PSX%20700SG%20Whitepaper%20Final.pdf

103. Wang, D., Bierwagen, G. P. 2009. Sol-gel coatings on metals for corrosion protection. *Progress in Organic coatings*. **64**, pp.327-338.

104. Latella, B. A., Gan, B. K., Barbe, C. J., Cassidy, D. J. 2008. Nanoindentation hardness, Young's modulus, and creep behaviour of organic-inorganic silica-based sol-gel thin films on copper. *Journal of Material Research*. **23**(9), pp.2357-2365.

105. Mammeri, F., Le Bourhis, E., Rozes, L., Sanchez, C. 2005. Mechanical properties of hybrid organic-inorganic materials. *Journal of Materials Chemistry*. **15**, pp.3787-3811.

106. Figueira, R. B., Silva, C. J. R., Pereira, E. V. 2015. Organic-inorganic hybrid sol-gel coatings for metal corrosion protection: a review of recent progress. *Journal of Coatings Technology and Research.* **12**(1), pp.1-35.

107. Latella, B. A., Ignat, M., Barbe, C. J., Cassidy, D. J., Barlett, J. R. 2003. Adhesion behaviour of organically-modified silicate coatings on stainless steel. *Journal of Sol-gel Science and Technology*. **26**(1-3), pp.765-770.

108. Mackenzie, J. D., Huang, Q., Iwamoto, T. 1996. Mechanical properties of ormosils. *Journal of Sol-gel Science and Technology*. **7**, pp.151-161.

109. Yang, J., Bai, L., Feng, G., Yang, X., Lv, M., Zhang, C., Hu, H., Wang, X. 2013. Thermal reduced graphene based polyethylene vinyl alcohol nanocomposites: enhanced mechanical properties, gas barrier, water resistance, and thermal stability. *Industrial & Engineering Chemistry Research.* **52**(47), pp.16745-16754.

110. Zhang, L., Zhan, F., Yang, X., Long, G., Yingpeng, W., Zhang, T., Huang, Y., Ma, Y., Yu, A., Chen, Y. 2013. Porous 3D graphene-based bulk materials with exceptional high surface area and excellent conductivity for supercapacitors. *Scientific Reports*. **3**, Article n°1408.

111. Lee, C., Wei, X., Kysar, J. W., Hone, J. 2008. Measurement of the elastic properties and intrinsic strength of monolayer graphene. *Science*. **321**(5887), pp.385-388.

112. Lam, C.K., Cheung, H., Lau, K., Zhou, L., Ho, M., Hui, D. 2005. Cluster size effect in hardness of nanoclay/epoxy composites. *Composites Part B: Engineering*. **36**(3), pp.263-269.

113. Araujo, A., Botelho, G. L., Silva, M., Machado, A. V. 2013. UV stability of poly(lactic acid) nanocomposites. *Journal of Materials Science and Engineering: B*. **3**(2), pp.75-83.

114. Burgentzle, D., Duchet, J., Gerard, J. F., Jupin, A., Fillon, B. 2004. Solvent-based nanocomposite coatings: I. Dispersion of organophilic montmorillonite in organic solvents. *Journal of Colloid and Interface Science*, **278**(1), pp.26-39.

115. Deshmane, C., Yuan, Q., Perkins, R. S., Misra, R. D. K. 2007. On striking variation in impact toughness of polyethylene-clay and polypropylene-clay nanocomposite systems: the effect of clay-polymer interaction. *Materials Science and engineering: A*. **458**, pp.150-157.

116. Moyo, L., Focke, W. W., Hedenreich, D., Labuschagne, F. J. W. J., Radusch, H.-J. 2013. Properties of layered double hydroxide micro- and nanocomposites. *Materials Research Bulletin*. **48**, pp.1218-1227.

117. Pradhan, S., Costa, F. R., Wagenknecht, U., Jehnichen, D., Bhowmick, A.K, Heinrich, G. 2008. Elastomer/LDH nanocomposites: Synthesis and studies on nanoparticle dispersion, mechanical properties and interfacial adhesion. *European Polymer Journal*. **44**(10), pp. 3122-3132.

118. Hsueh, H. B., Chen, C. Y. 2003. Preparation and properties of LDHs/epoxy nanocomposites. *Polymer*. **44**, pp.5275-5283.

119. Wang, Z., Han, E., Ke, W. 2005. Influence of nano-LDHs on char formation and fire-resistant properties of flame-retardant coating. *Progress in Organic Coatings*. **53**, pp.29-37.

120. Arunchandran, C., Ramya, S., George, R. P., Mudali, U. K. 2012. Self-healing corrosion resistive coatings based on inhibitor loaded TiO2 nanocontainers. *Journal of The Electrochemical Society.* **159**(11), pp.552-559.

121. Wei, H., Wang, Y., Guo, J., Shen, N. Z., Jiang, D., Zhang, X., Yan, X. 2015. Advanced micro/nanocapsules for self-healing smart anti-corrosion coatings. *Journal of Materials Chemistry*. **3**(2), pp.469-480.

122. Zhuravlev, L. T. 2000. The surface chemistry of amorphous silica. Zhuravlev model. *Colloids and Surfaces A: Physicochemical and Engineering Aspects.* **173**, pp.1-38.

123. Greenwood, P. 2010. *Surface modifications and applications of aqueous silica sols*. Doctoral thesis, Chalmers University of Technology.

124. Eslami-Farsani, R., Khosravi, H., Fayazzadeh, S. 2015. Using-3-glycidoxypropyltrimethoxysilane functionalized SiO2 nanoparticles

to improve flexural properties of glass fibers/epoxy grid-stiffened composite panels. *International Journal of Chemical, Molecular, Nuclear, Materials, Metallurgy and Engineering*. **9**, pp.1377–1380.

125. Shi, X., Nguyen, T. A., suo, Z., Liu, Y., Avci, R. 2009. Effect of nanoparticles on the anticorrosion and mechanical properties of epoxy coating. *Surface and Coatings Technology*. **204**, pp.237-245.

126. Suegama, P. H., Recco, A. A. C., Tschiptschin, A. P., Aoki, I. V. 2007. Influence of silica nanoparticles added to an organosilane film on carbon steel electrochemical and tribological behaviour. *Progress in Organic Coatings*. **60**, pp. 90-98.

127. Suegama, P. H., de Melo, H. G., Recco, A. A. C., Tschiptschin, A. P., Aoki, I. V. 2008. Corrosion behaviour of carbon steel protected with single and bi-layer of silane films filled with silica nanoparticles. *Surface and Coatings Technology*. **202**, pp.2850-2858.

128. Malzbender, J., den Toonder, J. M. J., Balkenende, A. R., de With, G. 2002. Measuring mechanical properties of coatings: a methodology applied to nano-particle-filled sol-gel coatings on glass. *Materials Science and Engineering R*. **36**, pp.47-103.

129. Ballare, J., Jimenez-Pique, E., Anglada, M., Pellice, S. A., Cavalieri, A. L. 2009. Mechanical characterization of nano-reinforced silica based sol-gel hybrid coatings on AISI 316L stainless steel using nanoindentation techniques. *Surface and Coatings Technology*. **203**, pp.3325-3331.

130. Peres, R. N., Cardoso, E. S. F., Montemor, M. F., de Melo, H. G., Benedetti, A. V., Suegama, P. H. 2016. Influence of the addition of SiO2 nanoparticles to a hybrid coating applied on an AZ31 alloy for early corrosion protection. *Surface and Coatings Technology.* **303B**, pp.372-384.

131. Montemor, M. F., Cabral, A. M., Zheludkevich, M. L., Ferreira, M. G. S. 2006. The corrosion resistance of hot dip galvanized steel

pretreated with bis-functional silanes modified with microsilica. *Surface and Coatings Technology*. **200**, pp.2875-2885.

132. Douce, J., Boilot, J., Biteau, J., Scodellaro, L., Jimenez, A. 2004. Effect of filler size and surface condition of nano-sized silica particles in polysiloxane coatings. *Thin Solid Films.* **466**, pp.114-122.

133. Sowntharya, L., Gundakaram, R. C., Soma Raju, K. R. C., Subasri, R. 2013. Effect of addition of surface modified nanosilica into silica-zirconia hybrid sol-gel matrix. *Ceramics International.* **39**, pp.4245-4252.

134. Dolatzadeh, F., Moradian, S., Jalili, M. M. 2011. Influence of various surface treated silica nanoparticles on the electrochemical properties of SiO2/polyurethane nanocoatings. *Corrosion Science.* **53**, pp.4248-4257.

135. Rostami, M., Ranjbar, Z., Mohseni, M. 2010. Investigating the interfacial interaction of different aminosilane treated nanosilicas with a polyurethane coating. *Applied Surface Science*. **257**, pp.899-904.

136. Deflorian, F., Fedel, M., Dirè, S., Tagliazucca, V., Bongiovanni, R., Vescovo, L., Minelli, M., de Angelis, M. G. 2011. Study of the effect of organically functionalised silica nanoparticles on the properties of UV curable acrylic coatings. *Progress in Organic coatings.* **72**, pp.44-51.

137. Chen, S., You, B., Zhou, S., Wu, L. 2009. Preparation and characterization of scratch and mar resistant waterborne epoxy/silica nanocomposite clearcoat. Journal of Applied Polymer Science. 112, pp.3634-3639.

138. Kang, S. Hong, S., Choe, C.R., Park, M., Rim, S., Kim, J. 2001. Preparation and characterization of epoxy composites filled with functionalized nanosilica particles obtained via sol-gel process. *Polymer*. **42**, pp.879–887.

139. Ghanbari, A., Attar, M. M. 2015. A study on the anticorrosion performance of epoxy nanocomposite coatings containing epoxy-silane treated nano-silica on mild steel substrate. *Journal of Industrial and Engineering Chemistry*. **23**, pp.145-153.

140. Seo, J. Y., Han, M. 2011. Multi-functional hybrid coatings containing silica nanoparticles and anti-corrosive acrylate monomer for scratch and corrosion resistance. *Nanotechnology.* **22**, pp.1-9.

141. Wang, Z. Z., Gu, P., Zhang, Z., Gu, L., Xu, Y. Z. 2011. Mechanical and tribological behaviour of epoxy/silica nanocomposites at the micro/nano scale. *Tribology Letters*. **42**, pp.185-191.

142. Guo, D., Xie, G., Luo, J. 2014. Mechanical properties of nanoparticles: basics and applications. *Journal of Physics D: Applied Physics*. **47**, pp.1-25.

143. Subasri, R. 2014. Properties of nanocomposite hard coatings on polycarbonate. In: Vikas Mittal ed. *Polymer nanocomposite coatings*. Taylor and Francis Group.

144. Wu, L. Y. L., Tan, G. H., Zeng, X. T., Li, T. H., Chen, Z. 2006. Synthesis and characterization of transparent hydrophobic sol-gel hard coatings. Journal of Sol-Gel Science and Technology. 38, pp.85-89.

145. Wu, L. Y. L., Chwa, E., Chen, Z., Zeng, X. T. 2008. A study towards improving mechanical properties of sol-gel coatings for polycarbonate. Thin Solid Films. 516, pp.1056-1062.

146. Zhang, M.Q.; Rong, M.Z.; Yu, S.L.; Wetzel, B.; Friedrich, K. 2002. Effect of particle surface treatment on the tribological performance of epoxy based nanocomposites. *Wear.* **253**, pp.1086-1093.

147. Bauer, F., Glasel, H., Decker, U., Ernst, H., Freyer, A., Hartmann, E., Sauerland, V., Mehnert, R. 2003. Trialkoxysilane grafting onto nanoparticles for the preparation of clearcoat

polyacrylate systems with excellent scratch performance. *Progress in Organic Coatings*. **47**, pp.147-53.

148. Leyland, A., Matthews, A. 2000. On the significance of the H/E ratio in wear control: a nanocomposite coating approach to optimised tribological behaviour. *Wear.* **246**, pp.1-11.

149. Hu, L., Zhang, X., Sun, Y., Williams, R. J. J. 2005. Hardness and elastic modulus profiles of hybrid coatings. *Journal of Sol-Gel Science and Technology*. **34**, pp.41-46.

150. Kruss. Drop shape analysis. *Kruss*. [Online] Available from: http://www.kruss.de/services/education-theory/glossary/drop-shape-analysis/

151. Jalili, N., Laxminarayana, K. 2004. A review of atomic force microscopy imaging systems: application to molecular metrology and biological sciences. *Mechatronics*. **14**, pp.907-945.

152. Das, S. K., Pota, H. R., Petersen, I. R. 2014. Intelligent tracking control system for fast image scanning of atomic force microscopes. In: *Computational Intelligence applications in Modelling and Control*. Germany: Springer-Verlag.

153. Cesiulis, H., Tsyntsaru, N., Ramanavicius, A., Ragoisha, G. 2016. The study of thin films by electrochemical impedance spectroscopy. In: *Nanostructures and thin films for multifunctional applications*. Switzerland: Springer.

154. Olivier, M. G., Poelman, M. 2012. Use of Electrochemical Impedance Spectroscopy (EIS) for the Evaluation of Electrocoatings Performances. In: Reza Shoja Razavi ed. *Recent researches in corrosion evaluation and protection*. Intechopen.

155. Orazem, M.E., Tribollet, B. 2008. *Electrochemical Impedance Spectroscopy*. New York: John Wiley & Sons.

156. Badea, G. E., Caraban, A., Sebesan, M., Dzitac, S., Cret, P., Setel, A. 2010. Polarisation measurements used for corrosion rates determination. *Journal of Sustainable energy.* **1**(1).

157. Fisher-Cripps, A. C. 2011. *Nanoindentation*. New York: Spring-Verlag.

158. Oliver, W. C., Pharr, G. M. 1992. An improved technique for determining hardness and elastic modulus using load and displacement sensing indentation experiments. *Journal of Materials Research.* **7**(6), pp.1564.

159. Neville, A., Wang, C. 2009. Erosion-corrosion mitigation by corrosion inhibitors- An assessment of mechanisms. *Wear*. **267**(1-4), pp.195-203.

160. Jianguo, L., Gaoping, G., Chuanwei, Y. 2006. Enhancement of the erosion-corrosion resistance of Dacromet with hybrid SiO2 sol-gel. *Surface and Coatings Technology*. **200**, pp. 4967.

161. Zheng, S., Li, J. 2010. Inorganic-organic sol gel hybrid coatings for corrosion protection of metals. *Journal of Sol-Gel Science and Technology*. **54**, pp.174–187.

162. Fardad, M. A. 2000. Catalysts and structure of SiO2 sol-gel films. *Journal of Materials Science.* **35**, pp.1835-1841

163. He, W., Wu, D., Li, J., Zhang, K., Xiang, Y., Long, L., Qin, S., Yu, J., Zhang, Q. 2013. Surface modification of colloidal silica nanoparticles: Controlling the size and grafting process. *Bulletin of the Korean Chemical Society*. **34**, pp.2747–2752.

164. Rahimi, H., Mozafarinia, R., Razavi, R.S., Paimozd, E., Najafabadi, A.H. 2011. Processing and properties of GPTMS-TEOS hybrid coatings on 5083 aluminum alloy. *Advanced Materials Ressearch*. **239–242**, pp.736–742.

165. Zheludkevich, M.L., Salvado, I.M., Ferreira, M.G.S. 2005. Sol–gel coatings for corrosion protection of metals. *Journal of Materials Chemistry*. **15**, pp.5099–5111.

166. Zheludkevich, M.L., Serra, R., Montemor, M.F., Miranda Salvado, I.M., Ferreira, M.G.S. 2006. Corrosion protective properties of nanostructured sol-gel hybrid coatings to AA2024-T3. *Surface and Coatings Technology*. **200**, pp.3084–3094.

167. Longhi, M., Kunst, S.R., Beltrami, L.V.R., Kerstner, E.K., Filho, C.I.S., Sarmento, V.H.V., Malfatti, C. 2015. Effect of tetraethoxy-silane (TEOS) amounts on the corrosion prevention properties of siloxane-PMMA hybrid coatings on galvanized steel substrates. *Materials Research*. **18**, pp.1140-1155.

168. Kunst, S.R., Cardoso, H.R.P., Beltrani, L.V.R., Oliveira, C.T., Menezes, T.L., Ferreira, J.Z., Malfatti, C.F. 2015. New sol-gel formulations to increase the barrier effect of a protective coating against the corrosion and wear of galvanized steel. *Materials Research*. **18**, pp.38-150.

169. Figueira, R. B., Callone, E., Silva, C. J. R., Pereira, E. V., Dire, S. 2017. Hybrid Coatings Enriched with Tetraethoxysilane for Corrosion Mitigation of Hot-Dip Galvanized Steel in Chloride Contaminated Simulated Concrete Pore Solutions. *Materials*. **10**, pp.306-327.

170. Barsoukov, E., Macdonald, J.R. 2005. *Impedance Spectroscopy: Theory, experimental and applications*. New Jersey: John Wiley & Sons.

171. Zheludkevich, M.L., Serra, R., Montemor, M.F., Yasakau, K.A., Salvado, I.M.M, Ferreira, M.G.S. 2005. Nanostructured sol-gel coatings doped with cerium nitrate as pre-treatments for AA2024-T3 corrosion protection performance. *Electrochimica Acta*. **51**, pp.208–217.

172. Leidheiser, H. 1979. Electrical and electrochemical measurements as predictors of corrosion at the metal—organic coating interface. *Progress in Organic Coatings*. 7, pp.79–104.

173. Bauer, F., Ernst, H., Hirsch, D., Naumov, S., Pelzing, M., Sauerland, V., Mehnert, R. 2004. Preparation of scratch and abrasion resistant polymeric nanocomposites by monomer grafting onto nanoparticles, 5[a] Application of mass spectroscopy and atomic force microscopy to the characterisation of silane-modified silica surface. *Macromolecular Chemistry and Physics*. **205**, pp.1587-1593.

174. Bauer, F., Sauerland, V., Glasel, H., Ernst, H., Findeisen, M., Hartmann, E., Langguth, H., Marquardt, B., Mehnert, R. 2002. Preparation of scratch and abrasion resistant polymeric nanocomposites by monomer grafting onto nanoparticles, 3[a] Effect of filler particles and grafting agents, *Macromolecular Materials and Engineering*. **287**, pp.546-552.

175. Pintaude, G. 2013. Introduction of the Ratio of the Hardness to the Reduced Elastic Modulus for Abrasion, Tribology - Fundamentals and Advancements. In: Gegner, J. ed. *Tribology – Fundamentals and advancements*. InTechopen. [Online] Available from: https://www.intechopen.com/books/tribology-fundamentals-and-advancements/introduction-of-the-ratio-of-the-hardness-to-the-reduced-elastic-modulus-for-abrasion

176. Pharr, G. M. 1998. Measurement of mechanical properties by ultra-low load indentation, *Materials Science and Engineering: A*. **253**(1-2), pp.151-159.

177. Shen, L., Wang. L., Liu, T., He, C. 2006. Nanoindentation and morphological studies of epoxy nanocomposites. *Macromolecular Materials and Engineering*. **291**, pp.1358-1366.

178. Wang, D., Zhang, Z., Li, Y., Xu, C. 2014. Highly transparent and durable superhydrophobic hybrid nanoporous coatings fabricated

from polysiloxane. *Applied Materials and Interfaces*. **6**, pp.10014-10021.

179. Marouani, A., Bouaouadja, N., Castro, Y., Duran, A. 2013. Effect of the sandstorms on the solar panels, *Akademik Platform*, [Online] Available from: http://www.isites.info/PastConferences/ISITES2013/ISITES2013/papers/A1-ISITES13089.pdf

180. Domingos, R. F., Baalousha, M. A., Ju-nam, Y., Reid, M. M., Tufenkji, N., Lead, J. R., Leppard, G. G., Wilkinson, K. J. 2009. Characterizing manufactured nanoparticles in the environment: multimethod determination of particle sizes. *Environmental Science and Technology*. 43, pp. 7277-7284.

181. Souza, T. G. F., Ciminelli, V. S. T., Mohallem, N. D. S. 2016. A comparison of TEM and DLS methods to characterise size distribution of ceramic nanoparticles. *Journal of Physics: Conference Series.* 733, 012039.

182. Sriramulu, D., Reed, E. L., Annamalai, M., Venkatesan, T. V., Valiyaveettil, S. 2016. Superhydrophobic, self-cleaning NIR-reflective silica nanoparticles. *Scientific Reports*. 6, 35993.

183. Lakshmi, R. V., Bera, P., Anandan, C., Basu, B. J. 2014. Effect of the size of silica nanoparticles on wettability and Surface chemistry of sol-gel superhydrophobic and oleophobic nanocomposite coatings. *Applied Surface Science*. 320, pp. 780-786.

184. Huang, K. Y., Weng, C. J., Lin, S. Y.,Yu, Y. H., Yeh, J. M. 2009. Preparation and anticorrosive properties of hybrid coatings based on epoxy-silica hybrid materials. *Journal of Applied Polymer Science*. 112, pp. 1933-1942.

185. Wu, L., Cao, D., Huang, Y., Li, B. 2008. Poly(L-lactic acid)/SiO_2 nanocomposites via in situ melt polycondensation of L-lactic acid in the presence of acidic silica sol: Preparation and characterization. *Polymer*. 49, pp. 742-748.

186. Xiao, X., Wang, D., Li, Y., Jackson, E., Fang, Y., Zhang, Y., Xie, N., Shi, X. 2016. Investigation into the synergistic effect of nano-sized materials on the anti-corrosion properties of a waterborne epoxy coating. *International Journal of Electrochemical Science*. 11, pp. 6023-6042.

187. Rosero-Navarro, N. C., Pellice, S. A., Duran, A., Aparicio, M. 2008. Effects of Ce-containing sol-gel coatings reinforced with SiO2 nanoparticles on the protection of AA2024.*Corrosion Science*. 50, pp. 1283-1291.

188. Zand, R. Z., Verbeken, K., Flexer, V., Adriaens, A. 2014. Effects of ceria nanoparticle concentrations on the morphology and corrosion resistance of cerium-silane hybrid coatings on electro-galvanized steel substrates. *Materials Chemistry and Physics*. 145, pp. 450-460.